Physics-Based Forecasts of Investment Sentiment:
Evidence from Past Boom-and-Bust Periods and the Anticipated Dynamics of 2026

CPM Investing White Paper 2025-01 (Version 5)
Jeffrey A. Hansen
CPM Investing LLC

September 14, 2025 — Version 1 (Initial SSRN submission)
October 22, 2025 — Version 5

For updates and the most recent version, visit the SSRN page:
https://papers.ssrn.com/sol3/papers.cfm?abstract_id=5482086

www.cpminvesting.com

Abstract

This paper describes physics-based forecasts of investment sentiment, drawing on evidence from past boom-and-bust periods and applying the framework to anticipated dynamics in 2026. Conventional explanations view sentiment as a reaction to news or policy events, but our findings indicate that shifts in optimism and pessimism follow predictable physical mechanisms. Specifically, the orbital geometry of the solar system alters solar emissions, which in turn influence the Earth's ionosphere and the stability of global electromagnetic standing waves. Greater stability in these standing waves is associated with higher investor optimism, while instability corresponds to increased pessimism.

Using U.S. stock market data from 1935 to 2024, we test this mechanism across seven studies. An out-of-sample evaluation from 2000 to 2024 shows that orbital geometry predicts 88 percent of turning points in the U.S. stock market's 14-week Relative Strength Index within ±1 week *($p < 0.001$)*. These results demonstrate both historical validity and forward-looking relevance. Based on current astronomical conditions, the model anticipates that the dynamics of 2026 will resemble earlier periods of extreme dislocation, offering investors and researchers a novel framework for understanding and preparing for major sentiment shifts.

Jeffrey Hansen began his career in geophysics and natural resource exploration before pivoting to the investment industry. He has evaluated investment strategies and managers globally with Russell Investments and Nikko AM. Later, as a portfolio manager, he oversaw global multi-asset mutual funds distributed in Japan. His current focus is on asset allocation research.

This document is submitted as part of ongoing scientific research into physics-based drivers of investor sentiment. This report is not intended as investment advice.

Executive Summary

Investor sentiment has long been recognized as a decisive force in financial markets. Economists from John Maynard Keynes to Robert Shiller have emphasized the role of optimism, pessimism, and herd behavior in driving asset prices beyond what fundamentals alone can explain. Yet while sentiment is widely acknowledged, its causes have remained elusive. Conventional explanations treat mood shifts as spontaneous reactions to news, policy changes, or random noise. This white paper offers an alternative: investor sentiment is systematically influenced by predictable astronomical conditions, specifically the orbital geometry of the solar system, meaning the distances and angles among groups of planets, acting through solar emissions. We propose a four-element mechanism:

1. Orbital geometry affects the stability of solar energy emissions.
2. Solar emissions influence the altitude of the Earth's ionosphere.
3. Ionospheric changes alter the stability of global electromagnetic standing waves (commonly called Schumann resonances).
4. Greater stability of electromagnetic standing waves increases investor optimism.

While speculative, this proposed causal mechanism is supported by statistical evidence across our seven studies using U.S. stock market data from 1935 to 2024. The report focuses on a specific orbital geometry, a 90-degree angle between the weighted center points of two groups of planets. The inner group contains Mercury through Saturn, and the center is determined by the standard tidal force formula. The outer group overlaps and contains Jupiter through Neptune, and the center is determined by a mix of factors unrelated to the 90-degree configuration. Investors experience periods of high euphoria, as indicated by high market returns, during the event of a 90-degree configuration of the two centers. These events tend to be clustered in time, and we call the cluster of events and investors' typical reaction to them an Anxiety-Free Period. A key finding in this report is that the electromagnetic standing waves appear to track the 90-degree configuration events, which is described in Study D.

Our first analysis, **Study A**, is a demonstration of the power of orbital geometry in identifying inflection points in stock market price acceleration. We test whether orbital geometry can forecast turning points in the 14-week Welles' RSI, a measure of price acceleration, in the U.S. stock market. Using publicly available NASA orbital data, without recalibration of our calculations, we find that predicted turning points match actual turning points 88 percent of the time within ±1 week during the period 2000–2024. This result is unlikely to have arisen by chance ($p < 0.001$).

Study B examines whether our measure of the strength or intensity of a 90-degree configuration event in affecting investor sentiment is associated with detectable changes in various measures of solar energy from 1964 to 2024. We use the tightness of clustering within the outer planets (Jupiter, Saturn, Uranus, and Neptune) to forecast the intensity of the 90-degree event. We find that tightness of clustering is associated with differences in the correlations among various metrics of solar energy emissions (i.e., sunspot counts, F10.7 solar flux, and the Ap Index), which are significantly higher during tight-cluster periods ($p < 0.001$).

Study C analyzes 11 clusters of the 90-degree configuration events since 1940. On average, the stock market rose 22 percent prior to the market price peak within the cluster, and fell 9 percent afterward, with the difference highly significant ($p < 0.001$). This study reinforces the view that the 90-degree orbital geometry events are systematically linked to stock market booms and then market busts when a cluster of 90-degree events ends.

Study D examines just one cluster of 90-degree configuration events because of limited data on electromagnetic standing waves (commonly referred to as Schumann resonance). During the 2017 Anxiety-Free Period there were three 90-degree configuration events making up the cluster. Distinct patterns appeared in global electromagnetic standing wave frequencies over the course of the three 90-degree events. The 90-degree configuration is significant in explaining the stability of these frequencies ($p < 0.001$). These findings are consistent with the hypothesis that electromagnetic standing waves are part of the transmission pathway from astronomical conditions to human sentiment.

To compensate for Study D's evaluation of a single cluster of three 90-degree events beginning in 2017, **Study E** examines 26 90-degree events since 1933. These events encompass 13 Anxiety-Free Periods. We test whether sunspot counts change just after a 90-degree configuration event ends. Of the 26 90-degree events, 77 percent are followed within four weeks by lower sunspot counts ($p < 0.01$). A second part of this analysis evaluates whether Earth-based readings of solar emissions show an unusual shift around nine clusters of the 90-degree configuration events (the Oulu data begins in 1965, so it is not possible to test the earlier periods). The Oulu neutron monitor readings tracked sunspot readings more closely during and adjacent to the clusters of the 90-degree configuration events ($p < 0.005$). These results support the hypothesis that orbital geometry affects the Sun itself and, in turn, solar energy variation reaching Earth.

Study F examines investor cognition and decision making. In our survey of 831 professional investors, we find a significant bias ($p < 0.001$) toward the Analytical decision-making style, which is associated with brainwave frequencies in the 13–30 Hz range. These overlap with the electromagnetic standing wave frequencies that were shown in Study D to be correlated with orbital geometry, suggesting an interesting link between standing waves and a significant bias of professional investors.

Study G demonstrates four long-term phases in what we call the Mega Sentiment Cycle, determined solely by orbital geometry. We are currently in Phase 1 of a long-term cycle that began in September of 2022. Since 1942, Phase 1 has encompassed only 32 percent of all weeks but accounted for 53 percent of all investment gains. Price-to-earnings ratios are also significantly higher ($p < 0.001$) during Phase 1, even though economic growth as measured by GDP shows no systematic differences across the four phases. This suggests that sentiment, not fundamentals, may be the primary driver of high valuations.

Conclusion: Together, these studies demonstrate a consistent relationship between orbital geometry, solar activity, and measurable shifts in investor sentiment and market performance. They provide evidence that investor sentiment is not merely random or news-driven but reflects predictable variations in the orbital geometry of the solar system. The framework suggests that market direction can be anticipated months in advance, providing investors with a tool to mitigate losses and exploit periods of euphoria. For investors, policymakers and economists, it highlights the importance of accounting for non-economic forces when interpreting market movements. As a result of this research, our view is that the *timing* of major stock market declines is determined by physics-induced shifts in sentiment, while the *magnitude* of the declines is determined by economic and market fundamentals.

The next significant opportunity to test this framework arrives in mid-2026, when a cluster of 90-degree configurations suggests that another Anxiety-Free Period will occur. The first of three 90-degree configuration events begins late April 2026 and ends just a month later. The highest level of euphoria for all 2026 events will be toward the end of this first event in late May. A second 90-degree configuration event begins in early August and ends in the last half of September. The third and final event begins in late November and ends in December. For periods with favorable economic and market conditions, based

on historical patterns, markets will show elevated optimism and tolerance for high valuations across all three 90-degree configuration events in 2026. With favorable economic conditions, the period with the highest risk of dramatic market declines will be in December, after the final 90-degree event.

In the context of unfavorable economic and market conditions, the period with the highest risk of dramatic declines is in late May 2026, just at the end of the first of the three events. Stock market price may decline dramatically at that time. The remaining two events would then be likely periods of price recovery.

If global electromagnetic standing waves are indeed related to Anxiety-Free Periods, they should display greater stability during the 90-degree configuration events. Therefore, the upcoming 2026 Anxiety-Free Period provides a real-time opportunity to test the hypothesized link between orbital geometry and investor sentiment.

By framing sentiment as a physics-based, forecastable phenomenon, this research challenges long-standing assumptions in economics and finance. It suggests that markets are not only efficient aggregators of information but also sensitive to natural rhythms in the solar system.

Table of Contents

Appendices

I. Introduction

Investors, economists, and policymakers have long acknowledged that the stock market is affected by the emotional impulses of investors. These emotional impulses, described broadly as investor sentiment, encompass periods of optimism and pessimism, risk-on and risk-off herding behavior, euphoria and panic, and, more broadly, periods of aspirational and critical thinking. In the 1930s, the phrase "animal spirits" was famously used by John Maynard Keynes to describe the stirring of emotions.[1] In the 1990s, Alan Greenspan warned of "irrational exuberance," referring to extended periods of investor optimism.[2]

These terms describe the biases, positive and negative, that investors have in their reaction to real-world conditions and events. Many see these emotional biases as arising spontaneously, seemingly in response to shared interpretations of news and events. However, our hypothesis is that there are deeper, physically grounded causes rooted in environmental electromagnetic variation determined by the orbital geometry of the solar system. Our findings suggest that many transitions between optimism and pessimism can be forecast months in advance using publicly available NASA orbital data.

Orbital geometry, which describes the clustering and angular relationships of groups of planets, can help anticipate gradual cyclic shifts in investor sentiment.[3] The focus of this report, however, is on the prediction of the more episodic periods of overwhelming optimism and euphoria, which begin and end based on a 90-degree configuration event between two overlapping groups of planets, the inner planets (Mercury through Saturn) and the outer planets (Jupiter through Neptune). For these episodes of euphoria, the important causal relationships in our hypothesized mechanism are:

1. Orbital geometry increases the stability of the Sun's energy emissions.
2. More stable solar emissions increase the stability of the Earth's ionospheric altitude.
3. More stable ionospheric altitude increases the stability of global electromagnetic standing waves (often called Schumann resonances).
4. Greater stability in standing waves increases investor optimism.

This causal sequence is central to our hypothesis and underpins the studies that follow. Elements 1 and 4 are highly speculative. Elements 2 and 3 are extrapolations of recognized physics but remain speculative in this context. We describe these extrapolations and provide statistical support where possible. Because these mechanisms likely operate across all markets, we will next explain why our analysis concentrates on U.S. stocks.

Our Focus is on the Sentiment of Investors in U.S. Stocks

Human emotion affects all capital markets, but we see its effects most clearly in the U.S. stock market. While bonds, commodities, and currencies are also influenced by investor emotion, their price movements are shaped directly by other forces. Bond prices are guided in large part by the decisions of central banks, and the liability needs of large institutions. Commodities are affected by supply and demand dynamics, as

[1] Keynes JM. The general theory of employment, interest and money [Internet]. London: Macmillan; 1936. [cited 2025 Aug 4].
https://www.marxists.org/reference/subject/economics/keynes/general-theory/

[2] Greenspan A. The challenge of central banking in a democratic society [Internet]. Washington (DC): Board of Governors of the Federal Reserve System; 1996 Dec 5 [cited 2025 Aug 4].
https://www.federalreserve.gov/boarddocs/speeches/1996/19961205.htm

[3] Note: Our hypothesized mechanism for gradual cyclic sentiment shifts is different than the one for episodic shifts.

well as transportation and storage costs. Currencies are affected by global trade, relative inflation expectations, and interest rate differentials. These anchors do not remove the influence of emotion, but they tend to dilute and obscure it.

Stocks, by contrast, are residual claims on distant and uncertain future cash flows. Their value depends jointly on beliefs about long-horizon growth and the discount rates used to translate those beliefs into present prices. Small shifts in risk appetite, perceived uncertainty, or the expected path of economic policies can therefore produce large moves in stock prices. This is why, even when concrete fundamentals change little over short periods, the stock market can move sharply when collective expectations change.

In addition, U.S. stocks tend to be informationally efficient, which means that the current price level reflects all positive and negative factors that investors currently perceive. It can quickly move higher or lower based on small shifts in investors' outlook. While individuals may not sense these changes in emotion because they are subtle, we can see the effects in collective behavior because they affect millions of people at the same time. Thus, the stock market is persistently near a tipping point as it balances positive and negative factors, making it a sensitive gauge of collective sentiment. These factors make the stock market highly sensitive to shifting investor expectations about long-term future conditions. For these reasons, our focus is on stock market action.

Misinterpreting Geometry-Driven Market Price Moves

It is common, especially in media commentary, to interpret the level of the stock market as a real-time assessment of current events and economic policy. While this may be true for price changes over a day or two, over horizons of a few weeks to roughly six months, we believe that market moves are influenced more by naturally occurring shifts in human emotion than by rational evaluations of economic and market fundamentals.

Financial economists have recognized that the stock market is dominated by what they describe as noise in the short term, but that over somewhat longer horizons it tends to embed useful information about the real economy. Fischer Black argued that markets are influenced by noise traders, creating short-run mispricing that gradually converges toward fundamentals. Robert Shiller showed that prices fluctuate more than can be justified by dividends in the near term but acknowledged that they do reflect economic reality over time. John Cochrane and others have found that stock returns contain predictive content for future economic activity, especially at horizons of six to twelve months.[4] [5] [6]

Thus, after about six months, the stock market does a reasonable job of assessing economic conditions. But during the noisy and emotional two-week to six-month period, the surprising forces we describe are significant predictors of stock market action. Not only can orbital geometry make sense of this noisy period, but it can also indicate the likely path of the market beyond the six-month horizon.

The Importance of Correcting for the Emotional Biases of Investors

The broader goal of this report is to highlight the impact these emotional non-economic forces have on our economic decision making and, ultimately, to reduce their impact. The emotional biases introduced by orbital geometry distract us from accurately assessing the economic merits of stocks – and, therefore, should be minimized as much as possible. Fortunately, these forces can be systematically addressed

[4] Black F. Noise. J Finance. 1986;41(3):529-43.
[5] Shiller RJ. Irrational exuberance. Princeton (NJ): Princeton University Press; 2000.
[6] Cochrane JH. Asset pricing. Princeton (NJ): Princeton University Press; 2005.

because they are driven by objective variables, are readily forecastable, and exert significant influence on investor behavior. A deeper understanding of sentiment shifts linked to orbital geometry allows us to anticipate them, compensate for them, and lessen their impact on economic and investment decisions.

Purpose of Report

The purpose of this report is to present our hypothesized four-element mechanism explaining how orbital geometry influences human emotion, including investor sentiment, and leads to periods of euphoria. The elements of the mechanism are supported by our statistical analysis of empirical data, through established concepts in physics, and through logical extensions of established concepts. To be clear, the hypothesized mechanism and its elements are speculative and need to be confirmed and revised by others, which is why we describe the details of our calculations.

This report presents seven studies of potential relationships between solar energy variation and investor sentiment. For ease of discussion, we will use measures of price acceleration as proxies for investor sentiment. These include our proprietary measures and the 14-week RSI. The remaining sections of this report are outlined below along with descriptions of our main statistical studies.

[7] Note: RSI is a widely used measure of price acceleration. See Appendix F for more information.
[8] Note: Out-of-sample period from December 1 2000 through April 1 2024
[9] Note: The metrics considered are the Ap Index, F10.7 Radio Flux, sunspot number, and Oulu NM count.

I. Introduction

return prior to the market peak averaged 21.5% and had an 8.8% average loss after the peak. These differences are statistically significant ($p < 0.001$). Since the endpoints of the 90-degree events producing the Anxiety-Free Periods can be predicted, investors can adopt defensive strategies to reduce losses as these periods end.

V. Element 2: Solar Emissions Affect Earth's Ionosphere.

Extrapolation of accepted concepts.

VI. Element 3: Earth's Ionosphere Affects Stability of Global Standing Waves

Study D - Patterns in the Global Electromagnetic Standing Waves Correspond to 90-Degree Configuration Events in 2017 and 2018 (p. 39): Distinct patterns appeared in global electromagnetic standing wave data (commonly called Schumann resonance) during predicted shifts in sentiment associated with the Anxiety-Free Period of 2017. Our metric of the 90-degree configuration was significant ($p < 0.001$) in explaining the stability of the global electromagnetic standing wave frequencies in the range of 14 to 21 Hz.[10] This supports our hypothesis that these standing waves act as a transmission pathway between solar variation and human emotion, although the test is done on only one cluster of 90-degree configuration events because of limited standing wave data availability.

Study E - Anxiety-Free Periods are Correlated with Sunspot Counts and Oulu NM Readings (p. 45): To compensate for the limited global electromagnetic standing wave data in Study D, we analyze the relationships between our sunspot series, the Oulu NM series, and the 90-degree configurations associated with the Anxiety-Free Periods. In Part 1 of the study, the 13 Anxiety-Free Periods from 1935 through 2023 are associated with short-term changes in sunspot counts. The sunspot count is significantly higher ($p < 0.01$) four weeks after the end of a 90-degree configuration event. In Part 2, during the periods adjacent to and during the nine Anxiety-Free Periods from 1964 through 2023, the Oulu NM readings track more closely to the sunspot series. The reduced divergence is significant ($p < 0.005$). These findings suggest that orbital geometry influences the Sun, and that those effects are detected on Earth.

VII. Element 4: Electromagnetic Standing Waves Affect Investor Sentiment

Study F - Professional Investors Have an Analytical Bias (p. 57): In our sample of 831 professional investors, we find that they have a significant ($p < 0.001$) bias toward the Analytical cognitive and decision-making style. Independent electroencephalogram studies suggest that analytical decision making is centered in the brainwave range of 13–30 Hz, which overlaps with the electromagnetic waves displaying similar patterns to the physics-based drivers in Study D.

[10] Note: Period of usable standing wave data was from June 5, 2015 through December 31, 2021.

Distinctive Feature of the Hypothesized Mechanism: Orbital Geometry

A key component of the hypothesized mechanism is how we aggregate and characterize planetary forces. Our research suggests that groups of planets, rather than individual planets, are most relevant; the key is the broad spatial relationships within two planetary groups, not precise planetary alignments. Moreover, the critical factor in understanding the Anxiety-Free Periods is not the alignment of the planets with one another, but the general spatial relationship of two groups of planets. To capture this, we focus on what we call the *orbital geometry* of the solar system. For the purposes of this report, we define orbital geometry as the arrangement of the two groups of planets in the solar system. We explore this concept in Part IV of the report.

Orbital geometry does not forecast specific events; it helps anticipate how groups of investors are likely to respond to whatever events occur. In this way, orbital geometry appears to amplify investor responses to economic conditions and current events. For example, geometry-induced optimism can heighten positive reactions to favorable news. It makes investors more reactive to positive news and events.

Geometry-induced pessimism can intensify the impact of negative developments. It makes investors more reactive to negative news and events. These emotional amplifiers can act as catalysts, triggering larger price changes if there is an economic need for a change. As a result of this research, our view is that the *timing* of major stock market declines is determined by physics-induced shifts in sentiment, while the *magnitude* of the declines is determined by economic and market conditions.

Timing

The timing of this report is significant. In mid-2026, there will be an opportunity to test the connections between orbital geometry, investor sentiment, and electromagnetic standing waves. We anticipate a multi-month period marked by investor euphoria and a seeming absence of critical thinking, conditions that have historically resulted in stock market booms that are often followed by sharp price declines. A striking example of this dynamic occurred in the lead-up to the 1987 Crash. This upcoming Anxiety-Free Period is the focus of this report both because of the upcoming 2026 episode and because these episodes tend to have well-defined beginnings and ends, making them relatively easy to observe in physical and market data and to test statistically.

I. Introduction

To place this hypothesis in an appropriate historical context, the next section reviews the historical and scientific research on solar activity, human behavior, and market sentiment, along with the early our early findings that motivated our continued research.

II. Background Research

This report describes our hypothesized mechanism for how solar energy affects investor sentiment. While elements of our hypothesized mechanism are novel, the topic of solar system dynamics affecting human behavior has been studied for at least 200 years. See Appendix A for a review of key figures in this history.

Solar Energy Variation Affects Investor Sentiment

Our hypothesis is that observed changes in investor sentiment are affected by changes in electromagnetic emissions from the Sun. There are two important causal relationships in this sequence:

Relationship A: The orbital geometry of the solar system affects solar energy emissions.

Relationship B: Solar energy emissions affect human emotion, including investor sentiment.

A wide range of research has investigated the relationship between solar energy emissions and human emotion (Relationship B). Research has established clear relationships between solar energy variation and stress, heart attacks, and suicides. Appendix B provides a list of selected papers on this topic.

Related more specifically to investor sentiment, a 2003 working paper by researchers at the Federal Reserve Bank of Atlanta found that stock returns tend to fall following coronal mass ejections, also supporting Relationship B. They suggested that geomagnetic disturbances may influence mood, leading investors to attribute their bad mood to negative economic prospects rather than environmental conditions.[11]

Relationship A, above, is more controversial. Some studies suggest that the gravitational interactions of the planets affect the Sun. These studies point to correlations between sunspots, solar flares, and planetary positions over many solar cycles. We describe recent studies describing this view by NASA and the Helmholtz-Zentrum Dresden-Rossendorf in Germany in Appendix C.

The view that the gravitational interaction of the planets affects the Sun is, however, far from universally held. The prevailing view among physicists is that planets do not have a material impact on the Sun or the Earth. Physicists point to traditional formulas for tidal and gravitational forces, which are strongly affected by the distance between bodies. Those formulas suggest that the distances between the Sun and the planets are too great for the planets to have an impact on the Sun. They assert that the main factors affecting energy emitted from the Sun and its distribution throughout the solar system are determined by the Sun's internal dynamics. Appendix D has a summary of the prevailing view of physicists about planetary distribution affecting solar energy, along with a discussion of the minority view that planets do affect the Sun.

[11] Krivelyova A, Robotti C. Playing the field: geomagnetic storms and the stock market. Fed Reserve Bank Atl Work Pap. 2003;2003-5.
https://www.atlantafed.org/research/publications/wp/2003/05

The results of our studies align with the minority view, suggesting that planets do indeed affect the Sun and that solar energy variation, in turn, affects investor sentiment, supporting both Relationship A and B above. Broader acceptance of these views has been limited by the absence of a plausible, physically observable mechanism supported by empirical data. We hope this paper presents a plausible mechanism, supported by empirical data, that is sufficient to encourage further research.

Recognizing the Impact of Physics-Based Shifts in Sentiment Is Becoming More Important

The need to understand physics-based sentiment shifts is increasingly important. Because the accuracy and speed of electronic communication about company and economic information have increased since the mid-1980s, the stock market has become more efficient in pricing the stocks of individual companies. Appendix E presents the results of our study suggesting that economic and company-level information likely had a greater impact on market prices prior to 1985 than after. As a result, physics-based shifts in sentiment now likely exert a relatively larger influence on stock prices than they did decades ago.

Our Early Research

In 2007, we developed proprietary indicators of price acceleration that have been useful in identifying short- and long-term inflection points in the U.S. stock market. We call these price-based measures the Market Resilience Index® series and maintain them for a range of market indexes, such as the Standard & Poor's 500 Index (S&P 500®) and the Dow Jones Industrial Average (DJIA®).[12] The three Market Resilience Indexes[13] are:

- Micro Market Resilience Index: indicates the trends of price acceleration lasting approximately three months.
- Macro Market Resilience Index: indicates the trends of price acceleration lasting several quarters.
- Exceptional Macro Market Resilience Index: appears periodically and indicates when the Macro Market Resilience Index is likely to develop a more positive slope. When it ends, the Macro Market Resilience Index is likely to develop a more negative slope.

As an example, Figure 1 below shows these for the U.S stock market[14] from December 2, 2005 to December 30, 2011, a period that encompasses the Global Financial Crisis (see Appendix V for data sources).

[12] STANDARD & POOR'S, S&P 500®, and S&P are registered trademarks of Standard & Poor's Financial Services LLC; DOW JONES®, DJIA®, and DOW JONES INDUSTRIAL AVERAGE® are registered trademarks of Dow Jones Trademark Holdings LLC. These indexes are referenced for informational purposes only. S&P and Dow Jones hold the trademarks, which are licensed for use. CPM Investing LLC is not affiliated with, sponsored by, or endorsed by S&P Dow Jones Indices, Standard & Poor's Financial Services LLC, or Dow Jones Trademark Holdings LLC.

[13] Market Resilience Index® is a registered trademark of CPM Investing LLC. All rights reserved. https://trademarks.justia.com/977/30/market-resilience-index-97730506.html

[14] MeasuringWorth. Dow Jones Industrial Average [Internet]. 1896–present. Charlottesville (VA): MeasuringWorth; c2025 [cited 2025 Sep 15]. https://www.measuringworth.com/datasets/DJA/

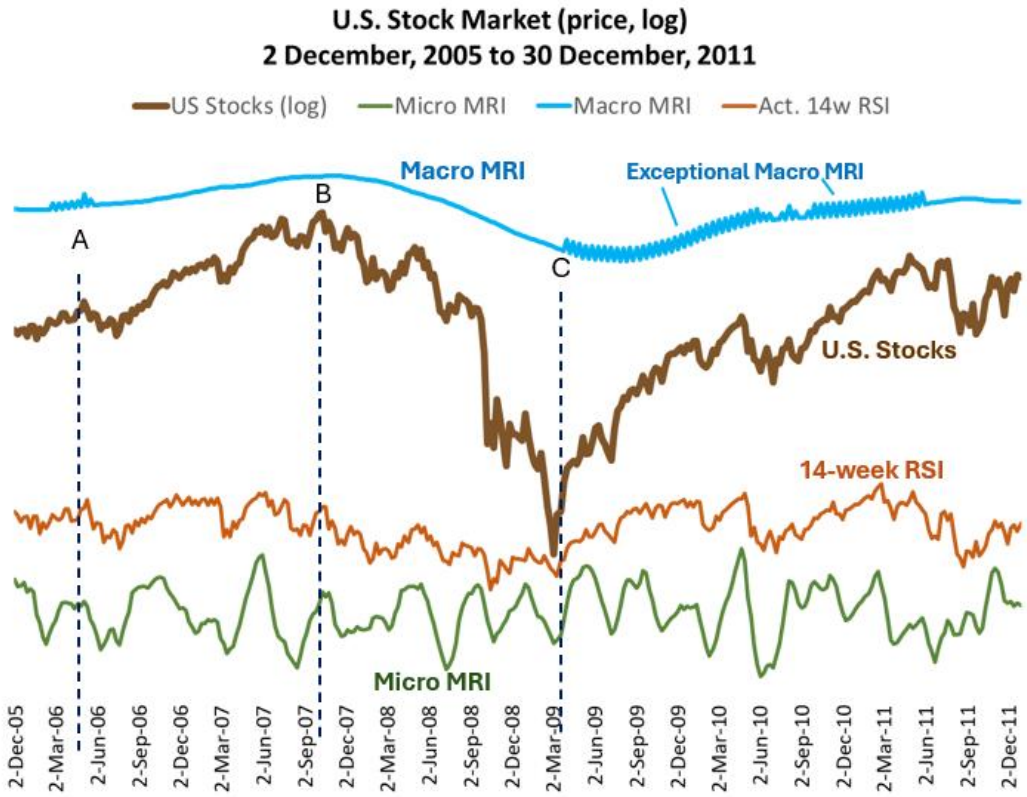

Figure 1. U.S. Stock Market Price (log) Level, Market Resilience Indexes, and the 14-week RSI from December 2, 2005 through December 30, 2011. Sources: CPM Investing LLC calculations using data from MeasuringWorth and public market sources. 'U.S. stocks' and 'U.S. stock market' refer to the DJIA, S&P 500, or related ETFs depending on the period.

The Micro Market Resilience Index is shown as a green line along the bottom of Figure 1. It excels at identifying important short-term trends in sentiment. The Macro Market Resilience Index is shown as the heavy blue line along the top, with the vertical spikes appearing along it indicating the presence of Exceptional Macro Market Resilience Index. The figure also includes the 14-week RSI, which is like the Micro Market Resilience Index, but can be more easily computed and is widely used in the investment industry. These metrics are described in Appendix F.

Observations:

- Point A indicates a period of increased price acceleration, as indicated by the appearance of the Exceptional Macro Market Resilience Index. We later found this period coincides with the 2006 Anxiety-Free Period, which, as we mention later, is one of the mildest Anxiety-Free Periods of the last century.
- Point B shows that the peak in the Macro Market Resilience Index coincides with the peak in market prices, a common pattern historically.
- Point C is the inception of the Exceptional Macro Market Resilience Index, which coincides with the market bottom after the declines of 2007 and 2008 associated with the Global Financial Crisis, which is its intended behavior.

II. Background Research

Observed Correlation between the Market Resilience Indexes and the Oulu NM Series

In 2018, we sought to develop a better understanding of the drivers of shifts in our Market Resilience Indexes. The regularity of shifts from 1920 through 2018 caused us to look at metrics of solar energy and we observed a surprising correlation with the Oulu NM series, a commonly used measure of the net solar energy reaching Earth. We describe this metric along with other solar emission-related series in Appendix G. We show the intriguing visual relationships between our Market Resilience Indexes and the Oulu series in Appendix H. Appendix I shows a statistical analysis of the Macro Market Resilience Index and the Oulu series, which shows a statistically significant relationship between the inflection points of the two series.

In Part III of this report, we present a demonstration of the relationship between orbital geometry and stock market price acceleration, using a simulated 20-year forecast. We used a wide range of physics-based factors or "drivers" to forecast the 14-week RSI, a widely used measure in the investment industry, for the for the U.S. stock market from late 2000 through 2024. Part III also outlines the four elements of our hypothesized mechanism.

III. Orbital Geometry Affects Market Performance

We demonstrate the relationship between orbital geometry and investor sentiment through our forecasts for the U.S. stock market's 14-week price acceleration, specifically the Relative Strength Index developed by J. Welles Wilder Jr., which we believe is a good proxy for investor sentiment.[15] The 14-week RSI is widely used in the investment industry to monitor short-term cyclical price changes. In this report, we will refer to this measure as the 14-week RSI or RSI.

Study A – Physics-Based Forecasts of Price Acceleration for U.S. Stock Market

To generate these forecasts, we used six of our 30+ physical dimensions of solar system orbital geometry, which include clusters of planets, angles and distances among those clusters. Each of these six drivers was selected because of its statistical significance in explaining actual 14-week RSI values from 1940 through late 2000. We then added the predicted Anxiety-Free Periods and M-Spike series and built an eight-driver model calibrated to explain the variability of the actual 14-week RSI over the historical period.

We then held that model constant over the entire forecast window of late 2000 to 2024, changing only the location of the planets, and thus the orbital geometry, for each week using NASA data. This allowed us to generate a Predicted 14-week RSI for the U.S. stock market for the 20-year forecast window without readjusting the parameters of the eight-driver model.

The Predicted 14-week RSI appears as the dotted green line in Figure 2 below. The Actual 14-week RSI is shown as the solid green line. The price of the U.S. stock market (log scale) is shown as the brown line.

[15] Note: RSI is a widely used measure of what the investment industry called price momentum. It was developed by J. Welles Wilder Jr. See: https://en.wikipedia.org/wiki/Relative_strength_index. Although commonly described as a momentum indicator, the RSI more accurately reflects price gradient (or slope), that is, how quickly and consistently prices are changing. For simplicity in this report, we will describe RSI as a measure of price acceleration. Along with the Market Resilience indexes, it is a good indicator of investor sentiment.

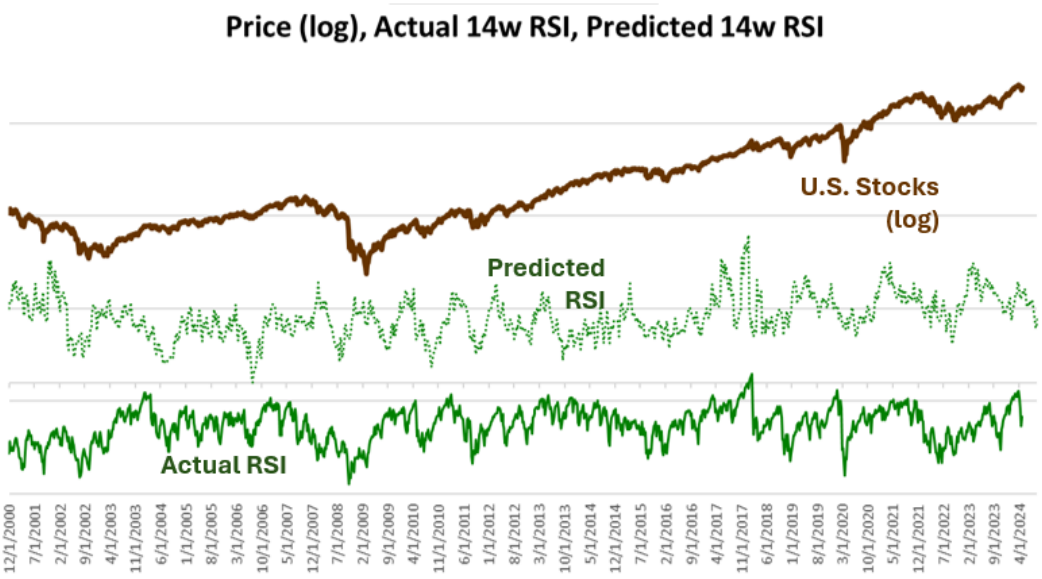

Figure 2. Predicted and Actual 14-week RSI for the U.S. stock market from December 1, 2000 through April 1, 2024. The figure shows the price of the U.S. stock market (log), the predicted 14-week RSI, and the actual 14-week RSI. Sources: CPM Investing LLC calculations using data from NASA, MeasuringWorth, and public market sources. 'U.S. stocks' and 'U.S. stock market' refer to the DJIA, S&P 500, or related ETFs depending on the period.

The peaks and troughs of the Predicted and Actual 14-week RSI generally coincide. The alignment of the inflection points is highlighted in Figure 3, below.

Study A: Forecasting with Orbital Geometry

Purpose: To test the significance of the Predicted RSI's identification of inflection-point timing, we used a peak/trough detection algorithm and a plus and minus 1-week window.

Key Results:

- 88.02% of Predicted RSI turning points were matched by Actual RSI turning points within ±1 week.
- Expected match rate by chance: ~0.25%.
- Binomial test p-value: < 0.001, indicating a very low probability of achieving this alignment by chance.

Interpretation:

- Predicted RSI turning points are effective at anticipating actual sentiment shifts. The high match rate is consistent with the hypothesis that solar system orbital geometry influences investor sentiment. If the relationship were weak, a 20-year forecast based solely on stable physics-based drivers would be unlikely to achieve this level of success.

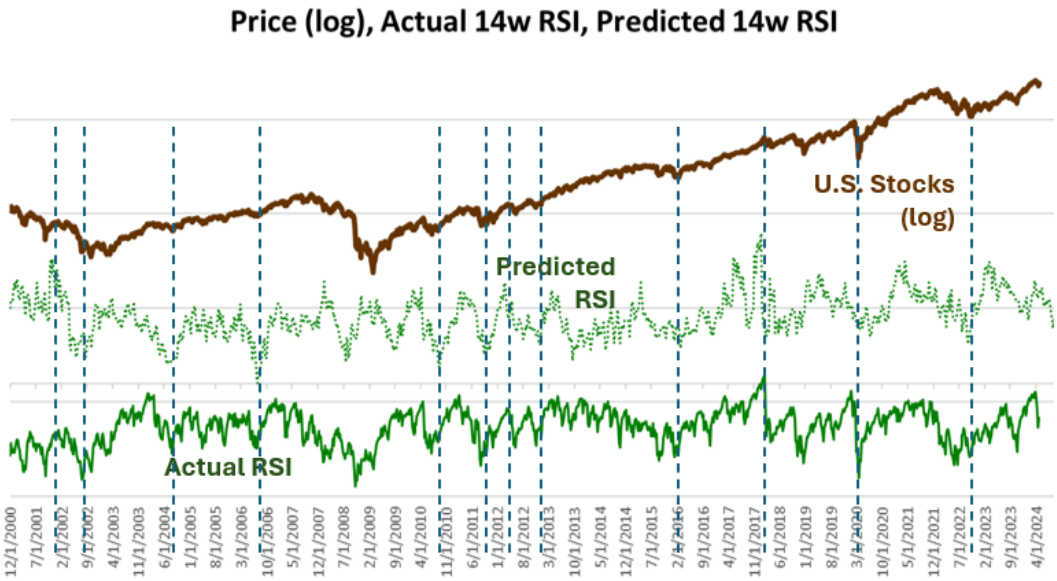

Figure 3. Predicted and Actual 14-week RSI for the U.S. stock market from December 1, 2000 through April 1, 2024. The figure shows the price of the U.S. stock market (log), the predicted 14-week RSI, and the actual 14-week RSI. The alignments of noteworthy inflection points in the predicted RSI, actual RSI, and market prices are highlighted with vertical lines. Sources: CPM Investing LLC calculations using data from NASA, MeasuringWorth, and public market sources. 'U.S. stocks' and 'U.S. stock market' refer to the DJIA, S&P 500, or related ETFs depending on the period.

As described in the grey box, which summarizes objective statistical testing, 88% of the short-term inflection points in the actual 14-week RSI occurred within +/- 1 week of the predicted inflection points. The likelihood of this success rate occurring by chance is low ($p < 0.001$).

Noteworthy Patterns in the Actual and Predicted 14-Week RSI

The first noteworthy pattern is indicated by arrow "A" in Figure 4 below. Note that the Actual 14-week RSI declined in a long-term trend beginning in May of 2007 while the Predicted 14-week RSI maintained a horizontal trend through the end of 2008, reflecting the likely path of the Actual 14-week RSI in the absence of economic and market stress.

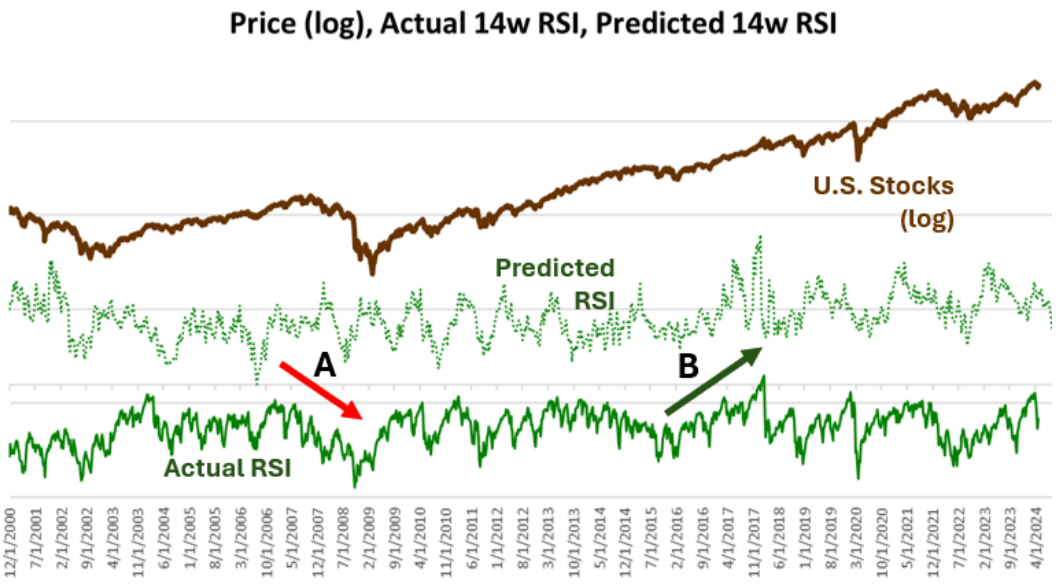

Figure 4. Predicted and Actual 14-week RSI for the U.S. stock market from December 1, 2000 through April 1, 2024. The figure shows the price of U.S. stock market (log), the predicted 14-week RSI, and the actual 14-week RSI. Two noteworthy periods are marked A and B. Sources: CPM Investing LLC calculations using data from NASA, MeasuringWorth, and public market sources. 'U.S. stocks' and 'U.S. stock market' refer to the DJIA, S&P 500, or related ETFs depending on the period.

With the Predicted RSI as a reference, one could determine before the major price decline of late 2008 that the market had a far lower price gradient than expected, which implies that investors had negative sentiment about economic and market conditions. Thus, the underperformance of the Actual 14-week RSI relative to the Predicted 14-week RSI is an effective indicator of negative investor sentiment related to economic and market conditions, even when the stock market is moving higher in absolute terms.

This period also shows that short term trends and cycles may be heavily influenced by current events and physics-induced sentiment shifts, while longer-term trends are affected by economic and market fundamentals. This is consistent with the notion that fundamentals change gradually, not abruptly.

Second, there is a distinct period of strong market performance and strong movements higher by both the Predicted and Actual 14-week RSI, indicated by point "B" in Figure 4 above. This period reflects the presence of an Anxiety-Free Period, which we will discuss after highlighting additional points from Study A:

- We use solar system orbital geometry to predict price acceleration, not stock price level or stock market returns. We focus on price acceleration because it is a better indicator of the emotional stance of investors.
- Our conceptual framework is that orbital geometry does not affect stocks or the stock market directly. Instead, it affects the people who buy and sell stocks. Stock prices move only because of the views of people trading them. Thus, understanding the human response to orbital geometry is an important focus of our work.
- Price acceleration does not have a long-term positive trend like the U.S. stock market has had over the last century. Price acceleration cannot increase (or decrease) indefinitely – it must stop and move in the opposite direction. Because of the long-term positive trend of the market price

and the lack of a long-term trend in the naturally occurring shifts in sentiment, there will be periods when the stock market moves higher, even when the natural shifts in sentiment indicate pessimism.[16]

- The stronger the economy is, the less the stock market follows the patterns established by orbital geometry. Outperforming the path determined by orbital geometry in metrics such as the Predicted 14-week RSI indicates a positive condition for the economy and the market. Underperforming orbital geometry indicates a negative condition. We should hope for positive divergence between the market price and metrics predicted by orbital geometry.

Anxiety-Free Periods and M-Spikes

During the process of developing the more than three dozen physics-based cyclic drivers that help explain the gradual variation seen in our Market Resilience Indexes, we found that there are shifts in sentiment that begin and end abruptly. We have identified two types of episodic shifts, the Anxiety-Free Periods and the M-Spikes. Both are determined solely by orbital geometry and can be seen in both stock market performance and, as shown in Study D, the stability of electromagnetic standing waves.

An Anxiety-Free Period is a period of investor euphoria lasting about half a year. They often occur before major market declines, such as 1987 and 1937. These are prominent episodes in market performance, and all have the same underlying orbital geometry. The calculation of the Anxiety-Free Period – based on the 90-degree configuration of the inner and outer orbital groups – is simple and can be replicated easily by others. We will discuss Anxiety-Free Periods at length in this report.

M-Spikes

An M-Spike is named for its distinctive "M" shape. It lasts several weeks and is characterized by optimism corresponding to the first leg of the "M," a price decline and a strong price recovery corresponding to the middle "V," and a decline in optimism for the final leg of the "M." The M-Spikes are not easily replicated, and their calculation is not described in this report.

Figure 5 below shows the average return profile of all 53 M-Spikes that occurred from 1940 through December 2023. The lower panel shows the average predicted M-Spike over this period centered on the lowest point in the middle "V." It also shows the range of the predicted level driver each week indicated by upper and lower bands representing plus and minus 25% of the cross-sectional standard deviation of range.

The upper panel shows the average price change relative to the price at the trough in the predicted M-Spike. It shows that market prices typically decline into the trough, but there is a sharp rebound in price within about six weeks of the trough. There is then a decline in prices through about week eight.

[16] Note: To create a successful investment process using the naturally occurring shifts in sentiment, one must additionally use a metric for determining the strength of the long-term trend of the US stock market.

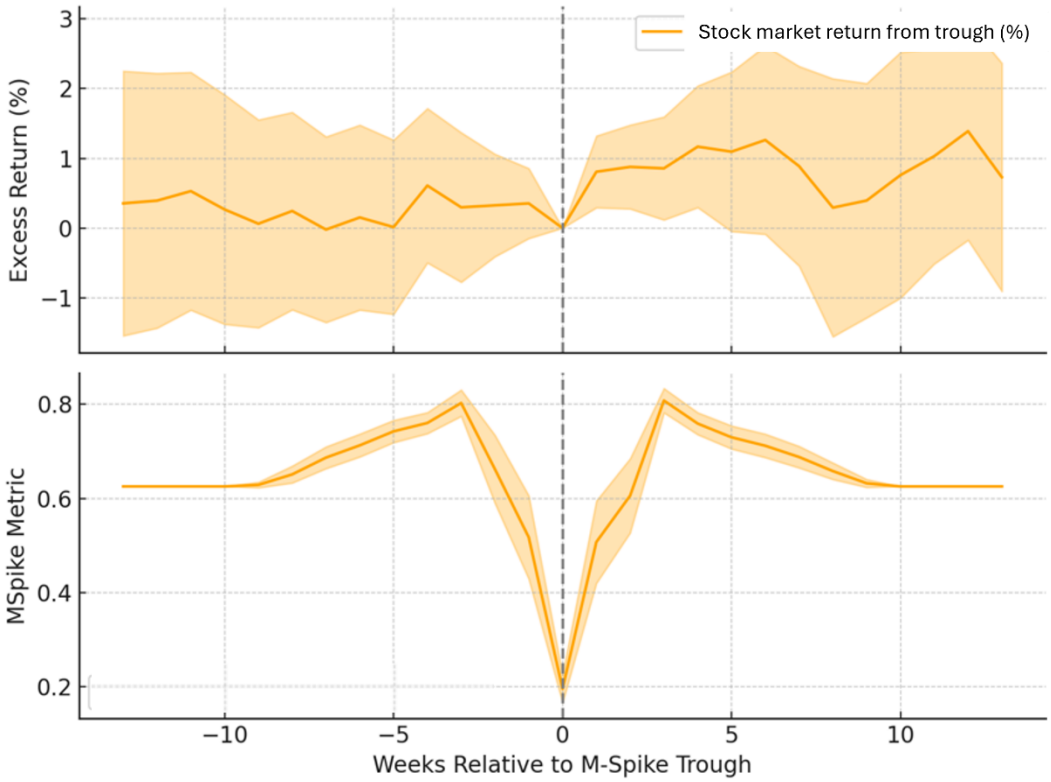

Figure 5. Average Return Profile of 53 M-Spike Episodes From 1940 through December 2023. The lower panel shows the average M-Spike factor over this period centered on the lowest point in the middle "V." It also shows the range of the factor each week indicated by upper and lower bands representing the 25% of the cross-sectional standard deviation of range. The upper panel shows the average return from the lowest point in the price pattern, after adjusting for the long-term average weekly return of 0.13%. Sources: CPM Investing LLC calculations using data from NASA, and MeasuringWorth, and public market sources. 'U.S. stocks' and 'U.S. stock market' refer to the DJIA, S&P 500, or related ETFs depending on the period.

M-Spikes are dramatic when they happen because of the multiple shifts between optimism and pessimism. Sentiment changes direction quickly and the changes are easily misinterpreted by investors as an identification of a new longer-term market trend. M-Spikes appear to cause investors to reassess their conviction about economic and market conditions and sometimes initiate a change in the long-term trend of market prices.

Compared to the Anxiety-Free Periods, M-Spike episodes are much shorter. Their brevity and distinctive central trough complicate statistical testing using weekly data. A regression of our predicted M-Spike levels against weekly stock market returns yields a p-value of 0.18. This means that, assuming the null hypothesis of no true relationship, there is an 18% chance of observing results by chance. While this does not meet conventional significance thresholds (commonly 0.10 or 0.05), the result remains noteworthy, especially because the M-Spike is derived from orbital geometry patterns, not from any financial or economic data. Our ongoing research aims to refine the methodology for identifying and modeling M-Spike episodes, including improvements to their detection and characterization in the predicted M-Spike series.

IV. Element 1: Orbital Geometry Affects the Sun

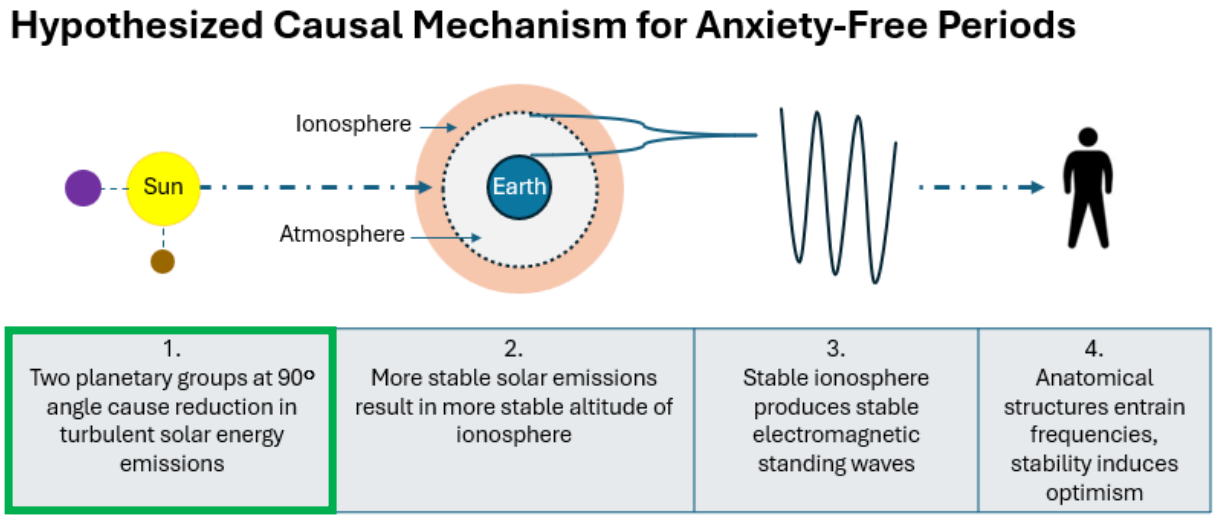

Figure 6. Hypothesized causal mechanism for Anxiety-Free Periods. The diagram outlines the proposed sequence linking solar system geometry, solar emissions, ionospheric stability, global electromagnetic standing waves, and human physiological entrainment. It is repeated at the start of each section to highlight the relevant step. This figure highlights Element 1. Source: CPM Investing LLC.

Overview

This section describes two orbital geometry centers, the Inner Orbital Center (inner and middle planets) and the Outer Orbital Center (middle and outer planets) and explains how their positions, relative to the Sun, can shape solar energy dynamics. The Inner Orbital Center is weighted using tidal force calculations, while the Outer Orbital Center's weights were based on a range of internal studies designed to explain the impact of planetary position on our measures of market price acceleration, the Market Resilience Indexes.

We describe Study B, which supports the validity of the metric we use to forecast the intensity of each Anxiety-Free Period. Intensity is linked to how tightly the members of the Outer Orbital Center are clustered. When the members are clustered tightly, the Anxiety-Free Periods are more intense.

Study C is a two-part analysis of all 13 Anxiety-Free Periods since 1933. Part 1 evaluates the difference between the weekly returns prior to the peak in market prices associated with the Anxiety-Free Period, and also the returns after the peak. It shows they are significantly different. Part 2 assesses the likelihood of obtaining the return profile – the pattern of positive returns before the peak in market prices and negative returns after the peak – in the history of the stock market.

An important feature of our hypothesized mechanism is that it focuses on groups of planets as opposed to individual planets. We use the centers of two overlapping groups of planets to characterize solar system orbital geometry. The inner and middle planets, Mercury through Saturn, comprise the Inner Orbital Group. The middle and outer planets, Jupiter through Neptune, comprise the Outer Orbital Group. These two groups and their calculated center points help us estimate their impact, likely from gravitational and electromagnetic forces, on the Sun.

Development of the Weights of Individual Planets in the Inner and Outer Orbital Centers

We established the weighting schemes of both the inner and outer planets to explain the cyclic changes in sentiment observed in our Market Resilience Indexes. We tested several approaches, including standard gravitational and tidal formulas and variations of these, to assess how well they accounted for variation in both the Micro and Macro Market Resilience Indexes. Our tests included ordinary least squares regression as well as optimization routines. The resulting planetary weights in the two orbital groups were thus determined by fitting orbital geometry to the cycles of the Market Resilience Indexes.

Once these weights were established, we investigated whether these new dimensions of orbital geometry could help explain the 1987 Crash and the period of strong market returns leading up to it. Using the Inner and Outer Orbital Centers, we found that the boom period preceding the Crash coincided with the two centers being 90 degrees apart, with the Sun at the vertex. We then examined more than 100 years of U.S. stock market history to determine whether the 90-degree relationship was connected to other notable market patterns. This investigation led to the identification of the Anxiety-Free Periods.

The Inner Orbital Geometry Center

The Inner Orbital Center consists of the inner and middle planets – Mercury through Saturn – and is essentially determined by the standard formula for tidal attraction. The tidal formula considers the mass of the planet and the distance the planet is from the center of the Sun.

Tidal Force Gradient :

$$T = G \cdot m / r^3$$

Where:

- *T* is the tidal force gradient, or the differential gravitational effect,
- *G* is the gravitational constant,
- *m* is the planet's mass, and
- *r* is the distance between planet and the center of the Sun.

The tidal formula is suited for modeling shape distortions, resonance effects, and mechanical stress in physical systems such as the Sun's plasma layers.

Figure 7 below shows the eight planets, their mass, distance from the Sun, and their final weighting in the Inner Orbital Group.

Planet	Mass of Planet ($x10^{24}$ kg)	Distance from Planet to Sun (AU[17])	Final Weight in Inner Orbital Group
Mercury	0.3	0.4	14%
Venus	4.9	0.7	34%
Earth	6.0	1.0	15%
Mars	0.6	1.5	—
Jupiter	1898	5.2	35%
Saturn	568	9.6	2%
Uranus	87	19.2	—
Neptune	102	30.1	—
Total			100%

Figure 7. Weights for the Inner Orbital Group. The table shows the names of eight planets, their masses, distance from the Sun, and the weights used to calculate the Inner Orbital Group Center.

Jupiter and Venus emerge as the dominant contributors in the Inner Orbital Center. Uranus and Neptune are too far from the Sun to have a tidal impact despite their large masses. While Mars is relatively close to the Sun, its mass is too small for it to have a tidal impact. While Mercury is small, its proximity to the Sun gives it a noteworthy tidal force. Figure 8 below is a diagram of the members of the Inner Orbital Group and the center as of August 1, 2025, calculated using the weights above. Two dashed circles are shown for scale. A circle at about 9 AU from the Sun approximates the orbit of Saturn. A circle at about 1 AU from the Sun approximates the orbit of Earth.

[17] Note: 1 AU (Astronomical Unit) is the average distance between the Sun and Earth

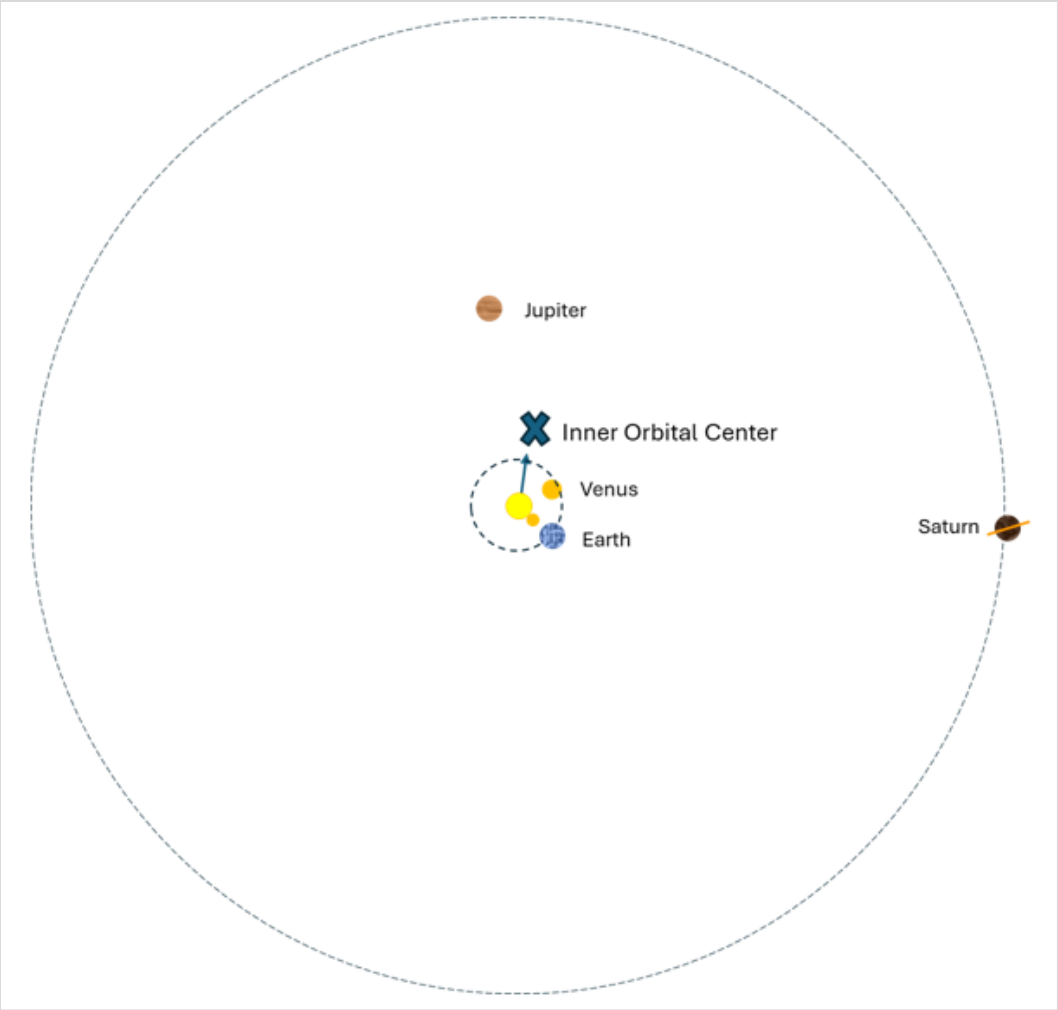

Figure 8. Geometry of the Inner Orbital Group and the Inner Orbital Center as of August 1, 2025. Source: CPM Investing calculations using NASA data.

The weighted average of the coordinates of these five planets represents the Inner Orbital Center and is indicated as a single coordinate, labeled "X" in the figure above. Our studies suggest that, at least in the region of Earth's orbit, this single point in space is the focal point for the tidal attractions on the Sun related to this group of planets.

The Outer Orbital Geometry Center

We sought to identify planetary weights for the Outer Orbital Center that reflect each planet's net influence, potentially arising from a combination of mass, location, and magnetic field strength. The weights are intended to be analogous in function to the tidal weights used for the Inner Orbital Group.

In contrast to a standard regression model that estimates marginal effects of explanatory variables (including an intercept term), our aim was to derive spatial or orbital weights that represent each planet's contribution to the structure and behavior of the Outer Orbital Center itself.

Early in our work on physics-based sentiment drivers, we found that the outer planets have a stronger statistical relationship with price acceleration than expected based on traditional tidal or gravitational

modeling alone. This observation led us to develop a final weighting scheme based on statistical relationships and a final subjective component.

Specifically, we evaluated the relative importance of the four outer planets – Jupiter, Saturn, Uranus, and Neptune – in explaining variation in two different series related to the price acceleration of the stock market from January 1940 through December 2023: the 14-week RSI for short-term price acceleration, and the Macro Market Resilience Index for long-term price acceleration.

We used two methods to develop potential weights for the members of the Outer Orbital Group. First, we ran ordinary least squares regressions using a range of orbital geometry metrics, including alignments and angular relationships associated with all planets.[18]

Second, we used an optimization tool to minimize the root mean squared error (RMSE) between the observed and predicted price acceleration series, subject to the constraint that all planetary weights remain non-negative. This optimization-based approach is widely understood in investment modeling and provided a practical means of evaluating how well different combinations of weights explain movement in the short- and long-term price acceleration series. Figure 9 summarizes the results from both methods.

	Shorter-Term Price Acceleration (14-Week RSI)					**Longer-term (Macro MRI)**	**Average Shorter- and Longer-Term**
	Ordinary Least Squares Regression			RMSE	Avg OLS, RMSE	Ordinary Least Squares Regression	--
	Coefficient	p-Value	Weight[19]	Weight	Weight	Weight	**Contribution**
Jupiter	0.085	6.81 E-10	0.31	0.54	0.43	0.40	**0.42**
Saturn	0.087	2.95 E-11	0.32	0.29	0.31	0.33	**0.32**
Uranus	0.060	0.009	0.22	0.01	0.12	0.27	**0.20**
Neptune	0.042	0.039	0.15	0.16	0.16	0.00	**0.08**
			1.00	1.00	0.56	1.00	**1.00**

Figure 9. Regression and Optimization Statistics Used as Guides for Determining Planetary Weights in the Outer Geometry Center. Sources: CPM Investing calculations using data from NASA, MeasuringWorth, and public market sources. 'U.S. stocks' and 'U.S. stock market' refer to the DJIA, S&P 500, or related ETFs depending on the period.

Comments

- Jupiter emerged as the most influential member of the Outer Orbital Group. This is consistent with expectations based on its size, magnetic field strength, and its position between the inner and outer planetary groups. Because the standard tidal formula assigns 35 percent of the Inner Orbital Group's weight to Jupiter's position, we mirrored that allocation by assigning 35 percent to Jupiter in the Outer Orbital Center.
- The contributions of Uranus and Neptune vary considerably across the analyses, with Uranus having a 22% weight in the ordinary least squares to a 1% weight in the RMSE in the analysis of

[18] Note: We set the intercept to zero. While excluding the intercept is not standard practice in formal econometrics, doing so allowed us to identify relative contributions and align the regression structure with the non-negative optimization process used as the second method. We did not attempt to build a predictive model in the classical sense; rather, the goal was to inform orbital weights that represented the spatial definition of the Outer Orbital Group members regarding mass, location, and magnetic field strength that could reflect the central focal point of the group.
[19] Note: Weights are determined by multiplying the coefficient of the variable by (1 – p-value)

short-term price acceleration. Neptune has a 16% weight in the combined analyses for the short-term price acceleration and a zero weight in explaining long-term price acceleration. In recognition of this variation, we assigned each of those planets a rounded weight of 12.5 percent. We set them to the same weight to avoid implying high precision in the methodology we used.

- The balance was allocated to Saturn.

The final weights for both orbital groups are shown in Figure 10 below.

Planet	Mass of Planet (x10^{24} kg)	Strength of Magnetic Field Relative to Earth's[20]	Distance from Planet to Sun (AU)	Final Weight in Inner Orbital Group	Final Weight in Outer Orbital Group
Mercury	0.3	0.006x	0.4	14%	—
Venus	4.9	0x	0.7	34%	—
Earth	6.0	1x	1.0	15%	—
Mars	0.6	0x	1.5	—	—
Jupiter	1898	9x	5.2	**35%**	**35%**
Saturn	568	0.4x	9.6	2%	40%
Uranus	86.8	0.5x	19.2	—	12.5%
Neptune	102	0.3x	30.1	—	12.5%
Total				100%	100%

Figure 10. Weights for the Inner and Outer Orbital Groups. The table shows the names of eight planets, their masses, distance from the Sun, and the weights used to calculate the two Orbital Group Centers. Sources: CPM Investing LLC calculations using data from NASA.

The prominence in the Outer Orbital Center of the outer planets is not consistent with the prevailing view in physics. But it is consistent with views of a minority of researchers. Both views are summarized in Appendix D, as mentioned earlier. Appendix J presents additional information on why the outer planets may deserve greater weight than the traditional models suggest.

Figure 11 below shows a diagram of the orbital geometry associated with the Outer Orbital Group and its center as of August 1, 2025.

[20] Note: Planetary weights are based on each planet's relative magnetic influence rather than mass alone. Approximate values and field characteristics are drawn from the following sources: Mercury (≈ 0.01× Earth) [a]; Venus (no intrinsic field) [b]; Earth (1×) [c]; Mars (no global field) [d]; Jupiter (≈ 8–9×) [e]; Saturn (≈ 0.4×) [f]; Uranus (≈ 0.5×) [g]; Neptune (≈ 0.3×) [h].

a. Anderson BJ et al. *Science*. 2011;333:1859–62. Available from: https://doi.org/10.1126/science.1211001
b. Russell CT, Vaisberg OL. In: Hunten DM et al., eds. *Venus.* Tucson: Univ Arizona Press; 1983.
c. Merrill RT et al. *The Magnetic Field of the Earth.* San Diego: Academic Press; 1996.
d. Acuña MH et al. *Science*. 1999;284:790–3. Available from: https://doi.org/10.1126/science.284.5415.790
e. Connerney JEP. *J Geophys Res.* 1993;98:18659–79. Available from: https://doi.org/10.1029/93JE00980
f. Dougherty MK et al. *Space Sci Rev.* 2004;114:331–83. Available from: https://doi.org/10.1007/s11214-004-1432-2
g. Ness NF et al. *Science*. 1986;233:85–9. Available from: https://doi.org/10.1126/science.233.4759.85
h. Ness NF et al. *Science*. 1989;246:1473–8. Available from: https://doi.org/10.1126/science.246.4936.1473

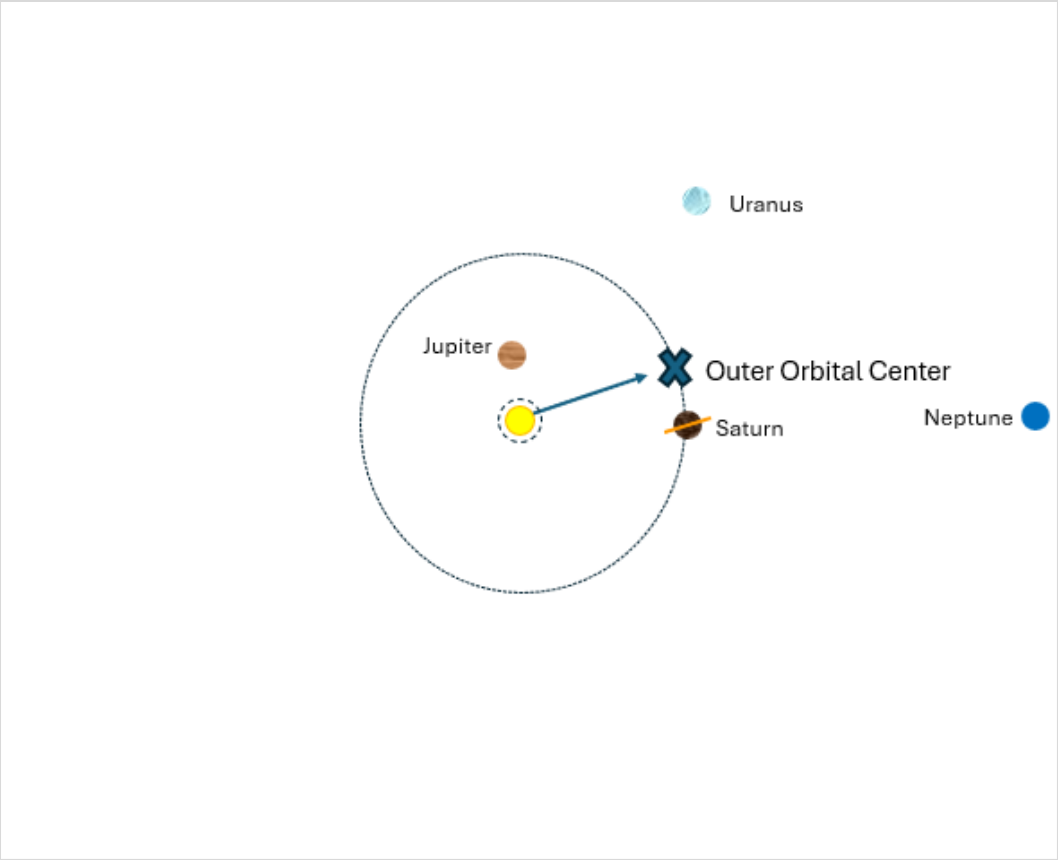

Figure 11. Geometry of the Outer Orbital Group and the Outer Orbital Center as of August 1, 2025. Source: CPM Investing LLC calculations using data from NASA.

Thus, while the Inner Orbital Center is weighted based on an accepted calculation of tidal forces, the Outer Orbital Center has weightings influenced by a range of regressions and optimizations seeking to explain the variability of short-term price acceleration (measured by the 14-week RSI) and long-term price acceleration (measured by the Macro Market Resilience Index).

The result of this investigation are physics-based drivers, which indicate the likely paths of the gradually changing Micro and Macro Market Resilience Indexes and other market price acceleration metrics during times of economic and market stress. Each physics-based driver can consist of several different dimensions of orbital geometry, such as distances and angles between multiple bodies. We maintain over thirty different drivers and sub-drivers that we use to predict the path of several price acceleration metrics. Some of these are used in the studies presented in this report.

Investigation of the 1986/7 Stock Market Boom

After the cyclic metrics of price acceleration were analyzed, we used our analytical tools to investigate the orbital geometry dynamics of the largest boom-and-bust market episode of the last 80 years, commonly referred to as the 1987 Crash. The market declined 35% over the course of two months. While less often discussed, the market moved up 54% over the 11 months prior to the market's peak. We found that the extreme shift in market sentiment in 1987 appeared to relate to a 90-degree angle between the Inner and Outer Orbital Centers with the Sun at the vertex.

Figure 12 below shows the location of the Inner Orbital and Outer Orbital Centers forming a 90-degree angle with the Sun at the vertex. We use the range from 86 degrees to 94 degrees to calculate the Anxiety-Free Period.

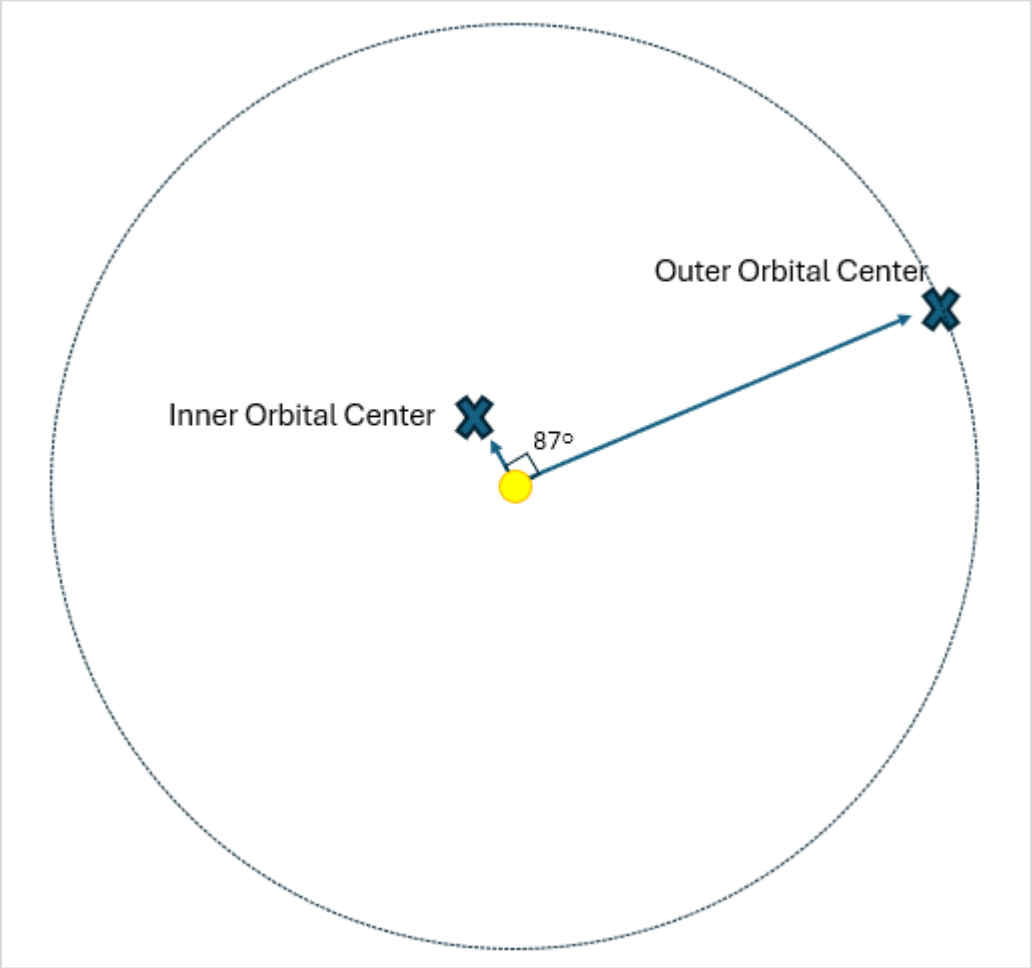

Figure 12. Geometry of the Inner Orbital Center and the Outer Orbital Center. Source: CPM Investing LLC calculations using data from NASA.

In Figure 13 below, we show the predicted Anxiety-Free Period of 1987, determined by the 90-degree configuration between the two Orbital Group Centers, as the dotted yellow line. The beginning of the 90-degree configuration occurs when that line moves abruptly higher from its baseline. The 90-degree configuration ends when the line moves abruptly back to the base line. The height of the column formed by this movement is rough indication of the impact the configuration will have on sentiment.[21] The higher the column, the bigger the likely impact. The final column of the predicted Anxiety-Free Period ends at the time the market begins to decline. A series of six predicted M-Spikes is also shown.

[21] Note: At the top of some columns is an indicator of the predicted maximum investor euphoria. The calculation of the peak indicator is based solely on orbital geometry but is outside the scope of this report. A successful simulated investment strategy for navigating several Anxiety-Free Periods is to stay in the market to the point of maximum euphoria and then exit the market when our measure of short-term price acceleration begins a negative trend.

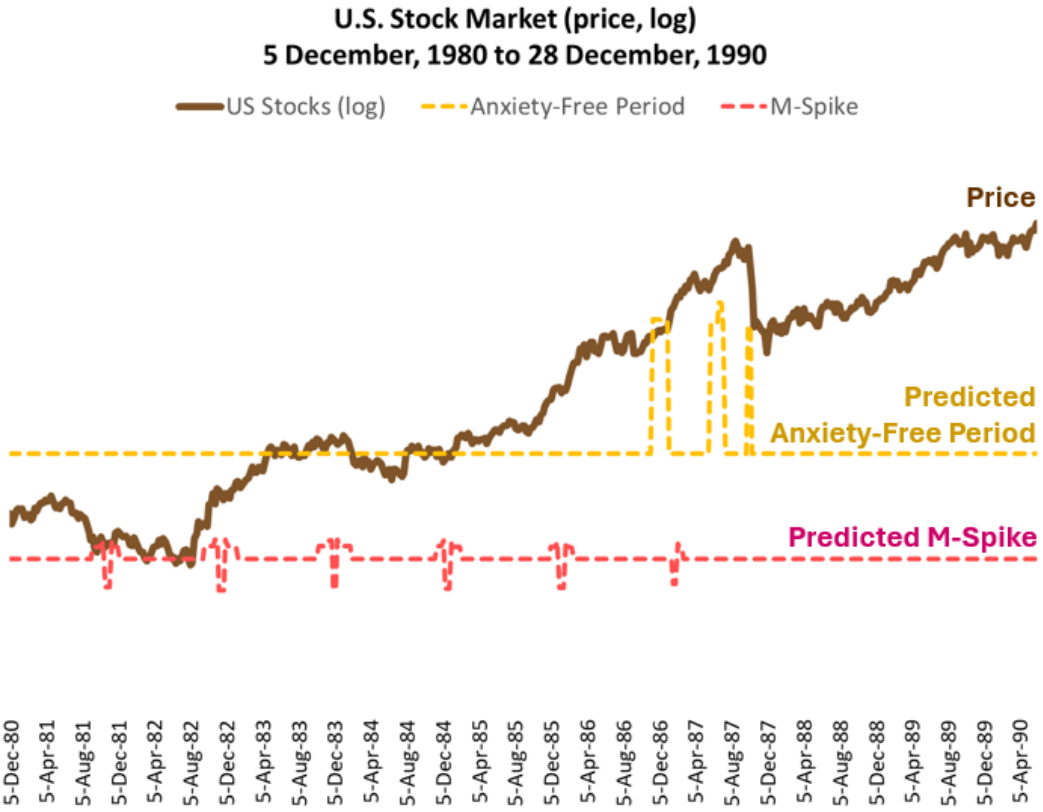

Figure 13. U.S. stock market price level (log) from December 5, 1980 to December 28, 1990. The chart shows the price level of the stock market along with a line marking the Anxiety-Free Period, which spans the strong price appreciation beginning in late 1986 and ending in late 1987 just before the market drops by 35% over the course of two months. It also shows six M-Spike episodes. The Anxiety-Free Period and M-Spike episodes are calculated using our preferred weights for the planets in the inner and outer orbital geometry groups. Sources: CPM Investing LLC calculations using data from NASA, MeasuringWorth, and public market sources. 'U.S. stocks' and 'U.S. stock market' refer to the DJIA, S&P 500, or related ETFs depending on the period.

We then evaluated the entire history of the stock market since 1900 and found other periods of high returns followed by price declines that also coincided with the 90-degree event.

The 90-degree configuration revealed similar and significant dynamics before the 1937 Crash, as shown in Figure 14 below. The highest point in the third column[22] of the Anxiety-Free Period closely corresponds to the top of the market.

[22] Note: This point is based entirely on orbital geometry, but its calculation is not described in this paper.

Figure 14. U.S. stock market price level (log) from December 5, 1930 to December 27, 1940. The chart shows the price level of the stock market along with a line marking the Anxiety-Free Period, which spans the strong price appreciation beginning in late 1936 and ending in early 1937. It also shows nine M-Spike episodes. Sources: CPM Investing LLC calculations using data from NASA, MeasuringWorth, and public market sources. 'U.S. stocks' and 'U.S. stock market' refer to the DJIA, S&P 500, or related ETFs depending on the period.

Figure 15 below shows similar dynamics during the strong stock market of 2017. We will discuss this period in detail in a later section.

Figure 15. U.S. stock market price level (log) from June 15, 2015 to December 31, 2021. The chart shows the price level of the stock market along with a line marking the Anxiety-Free Period, which spans the strong price appreciation beginning in early 2017 and ending in early 2018. It also shows five M-Spike episodes. Sources: CPM Investing LLC calculations using data from NASA, MeasuringWorth, and public market sources. 'U.S. stocks' and 'U.S. stock market' refer to the DJIA, S&P 500, or related ETFs depending on the period.

Our calculations for the 90-degree configurations of the Inner and Outer Orbital Groups identified 15 similar conditions since 1920, as shown in Figure 16 below.

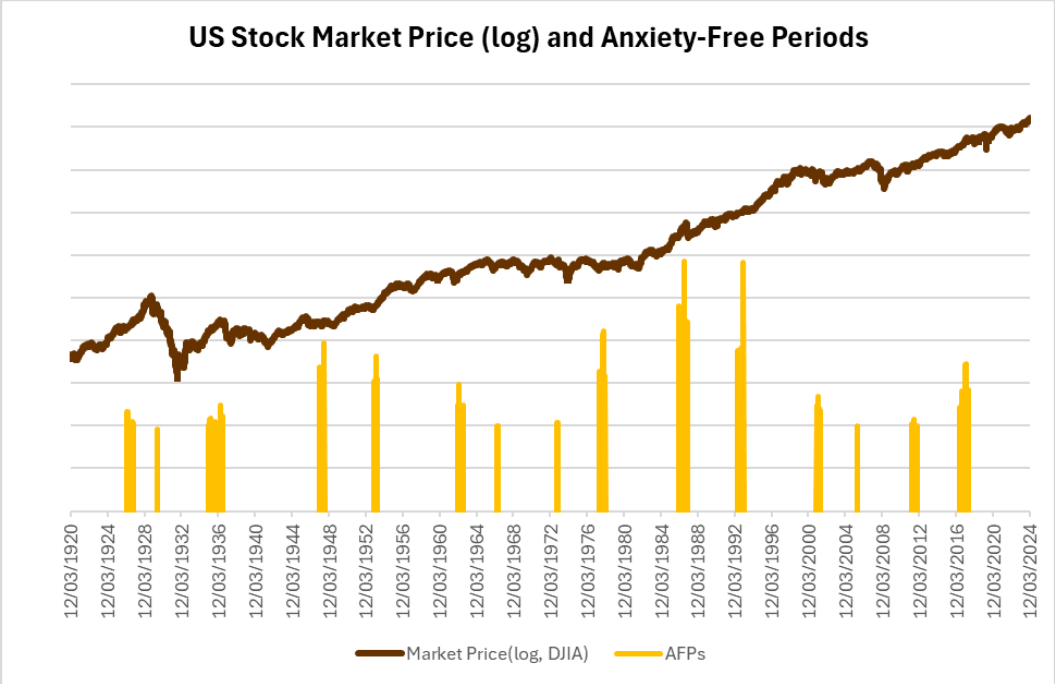

Figure 16. U.S. stock market price level (log) from 1920 through 2024. The chart shows the price level of the stock market along with vertical lines marking 15 Anxiety-Free Periods using our preferred weights for the planets in the inner and outer orbital geometry groups. Sources: CPM Investing LLC calculations using data from NASA, MeasuringWorth, and public market sources. 'U.S. stocks' and 'U.S. stock market' refer to the DJIA, S&P 500, or related ETFs depending on the period.

Each yellow column represents a 90-degree configuration event. Since many events are clustered in time, we group them into a single Anxiety-Free Period.

Fitting to the Market Resilience Indexes, but Not to the Anxiety-Free Periods

In the process described above, we used quantitative tools to fit cyclical measures of orbital geometry to cyclical changes in stock market price acceleration, as measured by the 14-week RSI and our Market Resilience Indexes. It is reasonable to question the future strength of these relationships. In the investment industry, we often face a similar challenge when evaluating a new investment process. A new investment manager may present a backtest showing that their process and its decision rules worked well in the historical period on which it was calibrated. We treat with caution any claims that the same rules will be equally effective in future periods. Almost by definition, we will see strong performance of the decision rules over the period on which they were calibrated.

The case of our fitting process, as described above, is different in important ways. The main fitting exercise was in determining the weights of the planets in the two orbital geometry groups. For the weightings of the Inner Orbital Group members, we began with standard formulas for gravitational and tidal attraction and found that the tidal formula best explained the short-term cyclical shifts in price acceleration as indicated by the Micro Market Resilience Index and the 14-week RSI. Had neither standard formula proven effective, we would have tested additional variations.

A similar process was used for the weighting of the Outer Orbital Group members, where we considered various correlations between the planets and price acceleration metrics. While these steps raise the

possibility of fitting important parameters to a particular environment that we will later test statistically, the concern is not justified in this case. After the calculations for the Inner Orbital Center and the Outer Orbital Center were calculated, we then observed that the 90-degree angle between them corresponded to several market booms that were followed by busts. That observation was not part of the fitting process.

After identifying the 90-degree configuration of the two orbital centers and acknowledging the importance of the two weighting schemes, we conducted sensitivity analyses of the planetary weights and the 90-degree angle itself. We found no compelling evidence that adjustments to the weighting schemes were needed.

While we believe the weights above are sufficiently accurate to forecast the 2026 Anxiety-Free Period, we acknowledge that the weighting schemes will be improved in the future. This remains an area of our ongoing research. Nonetheless, the upcoming 2026 90-degree configuration and its potential associated Anxiety-Free Period will offer a meaningful opportunity to evaluate the robustness of this framework.

Encouraged by the success of orbital geometry analysis, we extended our work to identify the M-Spikes and to develop a method for detecting the physics-based drivers of the 14-week Relative Strength Index (RSI). Figure 17 below shows the variables involved in this research.

	Price Acceleration Metrics	**Predicted Paths Based on Orbital Geometry**
Cyclic Patterns		
Trends Lasting up to Three Months	Micro MRI: Short term price acceleration trends	Micro Physics-Based Driver: Expected path of the Micro MRI during times of economic stress
Trends Lasting Three to Six Months	14-week RSI: Price acceleration trends lasting three to six months	Predicted 14-week RSI series. Expected path of the 14-week RSI in the absence of economic stress
Trends Lasting Several Years	Macro MRI: Price acceleration trends lasting several years	Macro Physics-Based Driver: Expected path of the Macro MRI during times of economic stress
Episodic Patterns		
Episodes of optimism lasting up to one year	--	Predicted Anxiety-Free Period series
Episodes of optimism and pessimism lasting a few months	--	Predicted M-Spike series

Figure 17. Cyclic and Episodic Physics-Based Drivers. Source: CPM Investing LLC.

This report focuses on the episodic patterns because they have abrupt beginnings and ends and are therefore easier to detect in market prices and physical variables.

An Interpretation of the Effects of the Weighting Scheme

First, the standard tidal influence model aligns with our findings for the Inner Orbital Center and supports our view that the inner planets contribute to generating low-frequency electromagnetic turbulence in solar emissions. The standard tidal formula quantifies the differential gravitational pull exerted by one body on another, resulting in a force gradient across the affected body. This spatial variation in gravitational force can induce stretching, deformation, or internal stress—effects that, in stellar environments like the Sun's convective zone, may promote turbulence and complex fluid motions. This dynamic is widely recognized among physicists.

Second, the middle and outer planets, Jupiter through Neptune, which are grouped in the Outer Orbital Center, appear to influence how such turbulence moves across heliospheric distances, potentially preserving it or slowing down its decay. This phenomenon may be related to the more structured electromagnetic environment when these massive planets with expansive magnetic influences are clustered. The more structured environment could allow for the preservation of the low frequency electromagnetic turbulence generated by the Sun, especially at Earth's orbit, just 1 AU from the Sun. Appendix K discusses the concept of what we call an Emission Preservation Zone.

In summary, the inner planets exert tidal forces on the Sun, generating turbulence in its electromagnetic output, while the outer planets act to sustain or extend that turbulence as it propagates outward through electromagnetic interactions. The influence of the Inner Orbital Group on the Sun is likely to be predominantly gravitational, with a secondary electromagnetic component. By contrast, the influence of the Outer Orbital Group is likely to be predominantly electromagnetic, with a secondary gravitational component.

A 90-Degree Angle Between the Inner and Outer Orbital Centers Corresponds to Anxiety-Free Periods

The 90-degree angle formed between the two orbital centers was initially identified through inspection, but statistical testing demonstrates that this configuration exerts a significant influence on both solar energy emissions and investor sentiment. A review of astrophysical research indicates that the importance of 90-degree configurations has been recognized in prior work. Appendix L provides a discussion of this angle in astrophysics, with many of the noted dynamics similar to those described in this report. The reproducibility of our findings regarding the 90-degree configuration, together with the approach of the 2026 Anxiety-Free Period, provides justification for our continued emphasis on these periods and their associated orbital geometry.

Assessing the Intensity of Anxiety-Free Periods

The height of the columns in Figure 16 above reflects the relative intensity of the event, with the higher columns being more intense. Conceptually, our intensity metric is determined by the distance between the members of the Outer Orbital Group and the calculated center of that group. The more tightly arranged the members are, the greater the intensity. The more dispersed the members are, the less effect the 90-degree configuration has on sentiment. Thus, the low height of the 2006 Anxiety-Free Period, for example, indicates it was not an intense episode, which coincides with the absence of a distinct market boom with an abrupt end during that period, although the market did move higher from there and later formed a bubble before the market decline of 2008, associated with the Global Financial Crisis. The tall height of the 1987 Anxiety-Free Period compared to others represents the intensity of the period.

In practice, we use the distance between the Sun and the Outer Orbital Center as a proxy for the tightness of clustering. The greater the distance, the tighter the cluster of Outer Orbital Group members around the center. We do this as a simplifying step and explain the rationale in Appendix M.

We hypothesize that the tight clustering of the members of the Outer Orbital Group creates what we call an Emission Preservation Zone in the region between the Sun and the Outer Orbital Center, and that this zone affects a range of solar energy metrics in the region of Earth's orbit. To test this hypothesis, we analyzed the correlations of weekly readings of various measures of solar activity during two periods, a higher intensity period and a low intensity period. Our hypothesis is that a higher intensity reading provides a defined path of delayed damping as the emissions move out from the Sun through the Emission Preservation Zone, and we should see higher correlations among the solar energy metrics. In contrast, a low intensity reading creates more damping of various forms of solar energy emissions, which results in a low correlation among the various metrics.

Study B – Estimating the Intensity of Geometry-Induced Sentiment Shifts

We analyzed four solar energy-related metrics, described in Appendix G, with data from April 1964 to May 2024:

- Sunspot number (magnetic activity on solar surface)
- Ap Index (geomagnetic activity)
- F10.7 cm solar flux (a proxy for solar radiation)
- Oulu NM Count Rate Pressure Adjusted (proxy for net electromagnetic activity affecting Earth)

Weekly values of these four measures were separated into two groups:

- **Low Intensity Weeks**: Weeks in which the Outer Orbital Center was closer than its midpoint of all weeks evaluated. After removing weeks with missing data, the number of weeks included is 1,467.
- **High Intensity Weeks**: Weeks in which Outer Orbital Center was farther than its midpoint. After removing weeks with missing data, the number of weeks included is 1,569.

Correlation matrices were computed among the four solar energy metrics for each group. The overall level of correlation was quantified by averaging the six off-diagonal correlation values within each matrix. Figure 18 below shows the correlations.

High Intensity – Outer Orbital Group is Far from Sun				
	Ap	F10.7	SN	Oulu NM
Ap Index	1			
F10.7	0.41	1		
SN	0.41	0.97	1	
Oulu NM	0.50	0.63	0.62	1

Low Intensity – Outer Orbital Group is Close to Sun				
	Ap	F10.7	SN	Oulu NM
Ap Index	1			
F10.7	0.16	1		
SN	0.18	0.95	1	
Oulu NM	0.34	0.55	0.58	1

Figure 18. Correlations of Solar Energy Metrics by High Intensity and Low Intensity Weeks. Sources: CPM Investing LLC calculations using data sources listed in Appendix G.

In all pairs, the correlations are higher in the "High Intensity" group. The results of the statistical analysis are:

- **Mean Correlation (Far):** 0.591
- **Mean Correlation (Close):** 0.462
- **T-Statistic:** 4.92
- **P-Value:** < 0.001

These findings indicate that the solar energy metrics are significantly more synchronized when our intensity readings are high (Outer Orbital Groups members are more tightly clustered and the center is farther from the Sun). When the members of the Outer Orbital Center are more spread out, the previously stable energy pathway may become fragmented into far weaker zones, allowing the interplanetary medium to introduce dispersion among the metrics.

Measurements like sunspot number, which reflect the solar surface activity directly, remain largely unaffected. In contrast, metrics such as the Ap index (geomagnetic activity), F10.7 flux (radio emissions), and Oulu NM counts (modulated cosmic rays) require propagation through the interplanetary medium and may be differentially disrupted by its varying structure and stability. When the planets are more evenly distributed, they lose their combined strength and their net effect on the Sun and, in turn, the effect on the Earth moves toward zero.

These results are important because they:

- Support our view that solar emissions are indeed affected by orbital geometry.
- Suggest that the intensity of orbital geometry changes over time, which adds a layer of complexity to studies of orbital geometry and other variables, including human emotion. There are times when planetary influences are minimal due to the time-varying nature of orbital geometries.
- Support using the Sun-Outer Orbital Center distance as a metric when forecasting the intensity of the Anxiety-Free Periods.

Study B: Intensity of Physics-Induced Sentiment Shifts

Purpose:
To test whether the synchronization of solar energy-related metrics varies with the position of the Outer Orbital Center relative to the Sun, and whether greater distance corresponds to stronger emission preservation.

Key Results:
– Data from April 1964 to May 2024 on sunspot number, Ap Index, F10.7 cm solar flux, and Oulu neutron counts
– Weeks divided into "High Intensity" (Outer Orbital Center far from Sun; n=1,569) and "Low Intensity" (close to Sun; n=1,467)
– Average correlation among solar metrics: 0.591 (far) vs. 0.462 (close)
– T-statistic: 4.92; $p < 0.001$
– All metric pairs showed stronger correlation in the High Intensity group

Interpretation:
When the Outer Orbital Center is far from the Sun, its member planets are tightly clustered, strengthening the Emission Preservation Zone and leading to more synchronized solar energy outputs. When the center is closer, the planets are more dispersed, weakening this pathway and allowing greater dispersion of solar signals. These results support the hypothesis that orbital geometry modulates solar emissions, and they justify using the Sun–Outer Orbital Center distance as a measure of intensity when forecasting Anxiety-Free Periods.

Study C – Detailed Performance Analysis of All Anxiety-Free Periods Since 1933

The 13 Anxiety-Free Periods since 1933 determined by the 90-degree configuration between the two orbital centers are associated with stock market booms and busts, as shown in Figure 19 below. Because there is no universally accepted quantitative rule for identifying local peaks and troughs in long-term market data, the beginning and end of market bust used in this analysis were determined visually from the historical Dow Jones Industrial Average price series. This approach is consistent with standard practice in financial-history research, where human judgment remains necessary to distinguish broad market cycles from short-term noise. The 13 Anxiety-Free Periods are shown in Appendix N with their prior and post low price points.

Study C has two parts.

Part 1 analyzes the difference in cumulative market returns prior to and after the peak in market prices taking place within each of the eleven Anxiety-Free Periods (excluding the 1937 and 1987 episodes).

Part 2 assesses the probability of finding by chance the pre- and post-peak return patterns of the thirteen Anxiety-Free Periods since 1933.

Year of Price Peak	Date of Prior Low Price	Date of Beginning of First 90-Degree Event	Peak Market Price Date	Date of End of Last 90-Degree Event	Date of Post Low Price	Pre-Peak Cumulative Return	Post-Peak Cumulative Return
1937	1935-05-31	1935-11-22	1937-03-05	1937-05-14	1937-11-19	75%	-39%
1948	1947-05-23	1947-11-21	1948-06-11	1948-06-11	1948-11-26	16%	-10%
1954	1953-09-18	1953-10-16	1954-03-05	1954-03-05	1954-03-26	15%	0%
1963	1962-06-22	1962-11-16	1963-05-31	1963-06-28	1963-07-26	35%	-5%
1967	1966-10-07	1967-03-10	1967-03-24	1967-03-31	1967-04-07	18%	-3%
1973	1973-08-24	1973-09-07	1973-09-28	1973-09-28	1973-12-14	10%	-14%
1978	1978-03-03	1978-03-24	1978-09-08	1978-11-24	1978-12-29	21%	-11%
1987	1986-09-12	1986-11-14	1987-08-21	1987-10-09	1987-12-04	54%	-35%
1993	1992-10-09	1993-04-09	1993-11-19	1993-11-19	1994-04-01	18%	-2%
2002	2001-09-21	2001-10-26	2002-03-15	2002-04-05	2002-10-04	29%	-29%
2006	2005-10-21	2006-03-24	2006-03-24	2006-04-07	2006-07-14	10%	-5%
2012	2011-09-23	2012-02-24	2012-09-07	2012-09-07	2012-11-16	24%	-5%
2017	2016-11-11	2017-05-12	2018-01-26	2018-04-20	2018-03-23	41%	-12%
					Avg	***28%***	***-13%***

Figure 19. All Anxiety-Free Periods Since 1934. Sources: CPM Investing LLC calculations using data from NASA, MeasuringWorth, and public market sources. 'U.S. stocks' and 'U.S. stock market' refer to the DJIA, S&P 500, or related ETFs depending on the period.

Study C Part 1 – Eleven Anxiety-Free Periods Since 1933

The early 1930s saw extreme stock market gains and losses that, when combined, can overshadow results from other periods and distort statistical tests. In the 1937 episode, the market rose 75 percent before the peak and then declined by 34 percent. This pattern aligns with our hypothesis but is unusually large. To be conservative, we exclude it from the statistical test. We also exclude the 1987 Anxiety-Free Period because the quantitative models were influenced by that episode. Thus, Study C Part 1 considers the remaining 11 Anxiety-Free Periods.

We calculated cumulative gains from the subjectively determined low price prior to prior to the first 90-degree configuration event, through the market peak taking place between the beginning of the first event and end of the last event. We calculated cumulative losses from the market peak through the subjectively determined low price. As mentioned, the subjectively determined low prices are shown in Appendix N.

The average gains and losses across the 11 episodes are shown in Figure 20 below.

	26 weeks Prior to the First 90-Degree Event through to the Peak of Market	Peak of Market through to 26 weeks After the Last 90-Degree Event
Average	22%	-9%
Maximum	41% (2017)	-29% (2002)
Minimum	10% (1974)	- 0% (1954)

Figure 20. Cumulative Return of 11 Anxiety-Free Periods from 1940 through 2023 (excluding 1987). This figure also shows the average, maximum, and minimum cumulative returns for two sets of weeks. First, gains from the market's low price within a 26-week horizon from the beginning of the Anxiety-Free Period through the peak in market prices. Second, the peak of market price within the Anxiety-Free Periods through the market's lowest price with a 26-week horizon after the Anxiety-Free Period. Sources: CPM Investing LLC calculations using data from NASA, MeasuringWorth, and public market sources. 'U.S. stocks' and 'U.S. stock market' refer to the DJIA, S&P 500, or related ETFs depending on the period.

To test the returns for the pre-peak and post-peak periods in a way that accommodates the different lengths of the Anxiety-Free Periods, we calculated the weekly returns for each across all episodes.

The difference in average weekly returns between the pre-peak and post-peak periods is significantly different ($p < 0.001$).[23] These are important results because the 90-degree configuration, which induces the Anxiety-Free Period, is fixed and determined solely by orbital geometry.

Study C Part 1: Market Return Patterns Around Anxiety-Free Periods

Purpose:
To test whether market returns differ significantly before and after the peak price within Anxiety-Free Periods, as defined solely by orbital geometry.

Key Results:
– Eleven Anxiety-Free Periods from 1933–2023 analyzed (1937 and 1987 excluded)
– Average pre-peak cumulative gain: 22% (range: 10% to 41%)
– Average post-peak cumulative loss: –9% (range: 0% to –29%)
– Difference in average weekly returns: $p < 0.001$.

Interpretation:
Market returns are significantly higher before the Anxiety-Free Period peak than after, consistent with the hypothesis that orbital geometry influences investor sentiment. This is statistical evidence of association, not proof of causation; other market and economic forces may contribute to these return patterns.

Study C Part 2 – Rarity of Return Profiles Across All Thirteen Anxiety-Free Periods Since 1933

There were 13 Anxiety-Free Periods from 1933 to 2023. We conducted a second analysis to evaluate the rarity of the return profiles of the 13 Anxiety-Free Periods in stock market history over this period. We systematically searched the history of the U.S. stock market for all periods that matched the return profiles of each Anxiety-Free Period. This provided a gauge for how rare a given profile is. The intent is not only to quantify rarity but to illustrate that the patterns tied to the 90-degree orbital geometry condition are far from common occurrences in market history.

For each Anxiety-Free Period, we construct a candidate set of 572,800 peak-anchored windows from the stock market's 1933–2023 history. Each candidate window has its own pre-peak gain and post-peak loss values calculated in the same way as the Anxiety-Free Period's actual profile. We then compare the Anxiety-Free Period's observed gain/loss pair to every candidate's pair, recording a match if both values are within ±0.025 of the Anxiety-Free Period's numbers.

The results show that return profiles (the percentage gain before the peak and the percentage loss after the peak) of most Anxiety-Free Period profiles are rare, and some are extraordinarily so. Two episodes (1937 and 1987) have zero matches in their candidate sets. Five others have match rates below 0.2%. The 2002 Anxiety-Free Period's +29% gain followed by –29% loss is matched in just 0.1% of candidates (736 out of 572,800). At the other end of the spectrum, the 1954 episode's +15% gain with no loss is far more common, appearing in 9.3% of candidate windows, which is a reminder that not all Anxiety-Free Period profiles involve an extreme bust. The lack of a meaningful loss during this period may have been affected by the strong economic growth of the post-war period or other sentiment factors that are not reflected in

[23] Note: The two sets of weekly returns—pre-peak and post-peak—were compared using a two-sample t-test with unequal variances (Welch's t-test). The difference in mean returns was found to be highly statistically significant ($p < 0.001$).

the Anxiety-Free Period metric. However, the 1954 case still fits the overall pattern: a geometry-defined period in which returns differ meaningfully before and after the peak, even if the post-peak movement is flat rather than negative. Political and other world events can affect the strength of the returns during Anxiety-Free Periods, but the overall matching of orbital geometry conditions results in statistically significant returns during Anxiety-Free Periods across all 13 cases.

These differences underscore that Anxiety-Free Periods are not interchangeable; each has its own unique return signature. Yet, taken together, the set of return profiles is extraordinarily unlikely to arise by chance. The profiles tied to Anxiety-Free Period timing are collectively more unusual than we would expect from random market fluctuations.

Year	Pre-Peak Gain (%)	Post-Peak Loss (%)	Match Rate (%)
1937	75	-34	0.0
1948	16	-10	2.4
1954	15	0	9.3
1963	35	-5	1.2
1967	18	-3	0.9
1973	10	-14	0.4
1978	21	-12	0.1
1987	54	-35	0.0
1993	18	-2	1.1
2002	29	-29	0.0
2006	10	-5	1.5
2012	24	-5	0.2
2017	41	-12	0.0
Mean	—	—	**1.3%**

Figure 21. Match Counts and Match Rates for Pre-/Post-Peak Return Profiles of 13 Anxiety-Free Periods (Match search: DJIA daily closes 1933–2023, ±0.025 tolerance on cumulative returns. Notes: Each Anxiety-Free Period's return profile was matched against 572,800 candidate ±40-week windows anchored to its own unique peak date. Across all 13 Anxiety-Free Periods, a total of 7,446,400 candidate windows were evaluated. Match Rate = Matches ÷ Candidate Windows × 100. Two Anxiety-Free Periods (1937 and 1987) had zero matches; five Anxiety-Free Period's had match rates below 0.2%. Sources: CPM Investing LLC calculations using data from and MeasuringWorth and public market sources. 'U.S. stocks' and 'U.S. stock market' refer to the DJIA, S&P 500, or related ETFs depending on the period.

Study C Part 2: Rarity of Anxiety-Free Periods Return Profiles

Purpose:
To measure how often each Anxiety-Free Period's specific pre- and post-peak return pattern occurs in the U.S stock market record and assess the collective rarity of all 13 profiles tied to the 90-degree orbital geometry condition.

Key Results:
– Each signature is compared to 572,800 candidate ±40-week windows (1933–2023)
– Two episodes (1937, 1987): zero matches
– Five episodes: match rate below 0.2%
– 2002 episodes (+29%, –29%): 0.1% match rate (736 matches)
– 1954 episodes (+15%, 0%): 9.3% match rate
– Average match rate across Anxiety-Free Periods: 1.3%
– Joint probability (independence assumption): ~3×10^{-33}

Interpretation:
Anxiety-Free Period return profiles are collectively very rare in the historical record. While individual vary, all share the signature of returns shifting markedly between pre- and post-peak periods. The rarity is consistent with a repeatable market rhythm tied to orbital geometry, though not proof of causation.

It is important to note that this analysis covers every 90-degree orbital geometry event that took place between 1933 and 2024. Each such event corresponded to one of the 13 Anxiety-Free Periods listed. This full-population approach removes the possibility of a selection bias and strengthens confidence in the statistical conclusions.

The next logical statistical analysis would be to determine the likelihood of finding all 13 periods by chance in actual market history *and* that all 13 periods are associated with the same measure of orbital geometry, the 90-degree angle between the two Orbital Centers. We did not do this analysis because the probability of seeing the events is already sufficiently low to be meaningful.

These analyses are important because:

- They show that the 90-degree configuration is correlated to boom-and-bust cycles of market performance.
- The relationships tested are statistically significant.
- We can have higher confidence in these tests because every 90-degree event over the last 90 years has been included.

V. Element 2: Solar Emissions Affect Earth's Ionosphere

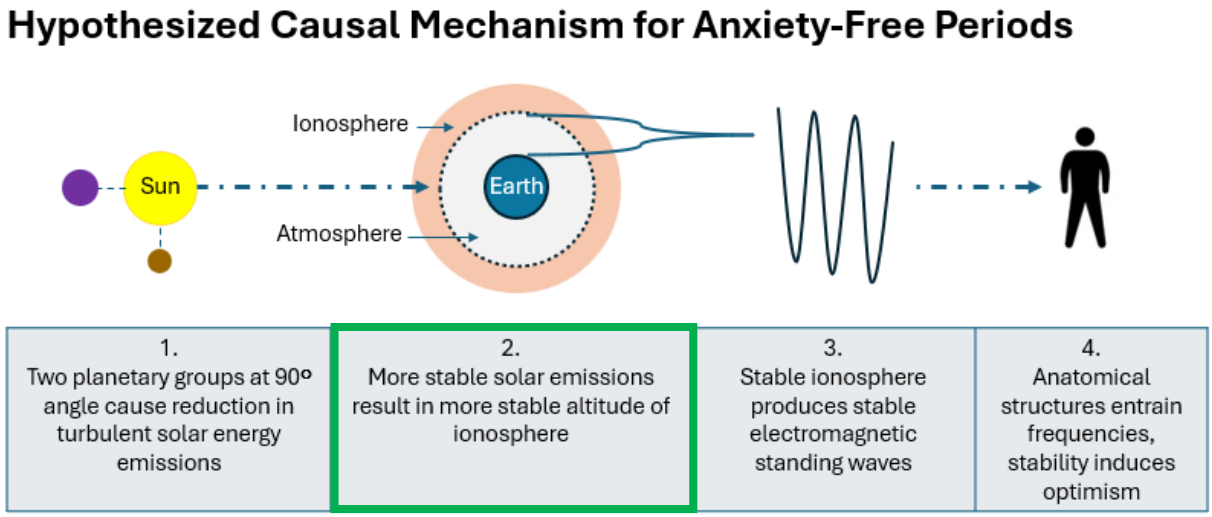

Figure 22. Hypothesized causal mechanism for Anxiety-Free Periods. The diagram outlines the proposed sequence linking solar system geometry, solar emissions, ionospheric stability, global electromagnetic standing waves, and human physiological entrainment. This figure highlights Element 2. Source: CPM Investing LLC.

Overview

This section explains why extremely low frequency solar emissions, particularly those in the 7 to 50 Hz range, are important to this report's hypothesis. Unlike higher-frequency solar radiation, extremely low frequency solar waves can pass through Earth's magnetosphere with relatively little interference due to their very long wavelengths, making them strong candidates for influencing the ionosphere and, indirectly, the stability of the global electromagnetic standing waves. Although difficult to measure directly, extremely low frequency solar waves can be tracked indirectly using magnetometers. Their more subtle influence on Earth systems than their higher frequency counterparts may explain why they are less well-researched compared to higher frequency waves.

This section also explains how reduced turbulence in low frequency electromagnetic waves during a 90-degree configuration event may lead to a more stable ionospheric waveguide, which supports more stable global electromagnetic standing waves. Turbulence typically alters the height and structure of the Earth–ionosphere cavity, shifting resonance frequencies by compressing or expanding the waveguide. During Anxiety-Free Periods, the 90-degree configuration of the Orbital Centers appears to calm solar emissions, stabilizing the cavity and its resonant frequencies. These changes support the broader hypothesis that orbital geometry configurations can modulate solar emissions, which in turn affect Earth's electromagnetic environment.

Many are familiar with the idea that the Earth's magnetic field protects the Earth from many types of solar energy emissions. There are, however, certain types of emissions that can move more easily through that magnetic shield. The Sun emits a wide range of electromagnetic energy with varying characteristics, many of which are described in Appendix O.

To be consistent with our hypothesized mechanism, solar emissions need to exhibit two qualities:

- They must be able to pass through Earth's protective magnetosphere with minimal interference.
- They must be capable of affecting the density of Earth's ionosphere and therefore its altitude.

Solar-generated electromagnetic waves in the extremely low frequency range (below 45 Hz) propagate through Earth's magnetosphere with minimal distortion or reflection, in part because their wavelengths (6,700 km to 100,000 km for 0.03–45 Hz) far exceed the thickness of the Earth's magnetopause (~500–1,000 km), the thin outer boundary of the magnetosphere. However, these waves can still affect the Earth's ionosphere via field-aligned currents and particle precipitation.[24] These properties make extremely low frequency waves strong candidates for transmitting solar influence to Earth's ionosphere.

The durability of low frequency electromagnetic waves offers a mechanism by which solar emissions could maintain enough structure to affect the Earth's ionosphere. While harder to measure directly than higher frequencies, the influence of extremely low frequency waves on the ionosphere makes global electromagnetic standing waves serve as a measurable proxy for their presence and strength.

Measurement Challenges of Low Frequency Electromagnetic Waves

Measuring extremely low frequency electromagnetic waves poses substantial technical and logistical difficulties. The primary issue stems from the relationship between frequency and wavelength: lower frequencies correspond to longer wavelengths. For example, a 30 Hz wave has a wavelength of approximately 10,000 kilometers. To detect such waves directly using conventional antenna technology would require antennas that span a significant fraction of the wavelengths, something entirely impractical for Earth-based and space-based platforms.[25]

As a result, researchers rely primarily on indirect measurement methods. Magnetometers, which measure fluctuations in magnetic field strength, have become the dominant instrument for detecting extremely low-frequency signals. These devices can identify the presence and characteristics of extremely low frequency wave activity based on the magnetic field disturbances they cause, even without a physically large antenna.[26]

In addition to measurement challenges, another reason for the limited focus on extremely low frequency wave detection is their generally benign interaction with human health and global infrastructure. Unlike higher-frequency waves that can induce currents or interfere with electronics, extremely low frequency waves tend to pass through materials with minimal absorption or disruption. This relatively low level of technological and biological interference compared to higher frequency waves has meant that extremely low frequency waves have not been prioritized in defense, communication, or biomedical research.[27]

[24] Yahnin AG, Yahnina TA, Raita T, Manninen J, Manninen M, Engebretson MJ, et al. Simultaneous observations of EMIC waves, ELF/VLF waves, and energetic particle precipitation during magnetic storms. Geomagn Aeron [Internet]. 2020;59(6):753-64.
https://link.springer.com/article/10.1134/S0016793219060148

[25] Burrows, M. L. (1978). ELF Communications Antennas. P. Peregrinus Ltd. (Cited by > 140 studies as of 2025).

[26] Price, C.; Pechony, O.; Greenberg, E. (2006). "Schumann resonances in lightning research". Journal of Lightning Research. 1: 1–15.

[27] World Health Organization (WHO). (2007). Extremely Low Frequency Fields: Environmental Health Criteria *238*. Geneva: WHO Press.
https://www.who.int/publications/i/item/9789241572385

Ionosphere Height Affects Frequency of Standing Waves in Atmosphere

The Earth–Ionosphere cavity is formed between the conductive surface of the Earth and the lower boundary of the ionosphere, typically between 60 and 90 kilometers above sea level. This cavity forms a channel that creates a guide in which electromagnetic waves in the atmosphere resonate. These waves are energized primarily by lightning, while the dimension of the guide determines the frequency of the standing waves. The resulting global electromagnetic standing waves have a main, or fundamental, frequency of approximately 7.83 Hz. In addition to the fundamental frequency (Mode 1), four harmonics can often be detected. The range of electromagnetic standing waves in the atmosphere is shown below.

Standing Wave Modes in the Earth–Ionosphere Cavity	
Mode	**Approximate Frequency**
Fundamental (Mode 1)	7.83 Hz
2nd Mode	14.3 Hz
3rd Mode	20.8 Hz
4th Mode	27.3 Hz
5th Mode	33.8 Hz

Figure 23. Global Electromagnetic Standing Wave Modes in the Earth–Ionosphere Cavity. Approximate frequencies of the first five standing-wave modes generated between Earth's surface and the ionosphere.[28] [29] [30] These resonances arise from the extremely low frequency electromagnetic cavity formed by the planet's conductive surface and its upper atmospheric boundary.[31]

The properties of the waveguide are dynamic, responding to changes in atmospheric structure, ionospheric charge density, and electromagnetic activity from both terrestrial and solar sources.

Turbulent Solar Emissions Affect Ionosphere Height

The waveguide is not globally uniform. Its structure varies with solar illumination, geomagnetic latitude, and space weather. As solar low frequency turbulence interacts with this spatially variable ionospheric boundary, it can produce region-specific alterations in wave transmission.

In this context, turbulence refers to short-term, erratic fluctuations in the low frequency electromagnetic environment. Such disturbances influence the density of the ionosphere and therefore its altitude. Turbulence can deform the electron density profile through localized heating or compression, which shifts the effective reflection height and alters how low frequency waves propagate within the Earth-Ionosphere cavity.

[28] Schumann WO. Über die strahlungslosen Eigenschwingungen einer leitenden Kugel, die von einer Luftschicht und einer Ionosphärenhülle umgeben ist. Z Naturforsch A. 1952;7a:149-154. https://doi.org/10.1515/zna-1952-0202

[29] Schumann WO. Über die Dämpfung der elektromagnetischen Eigenschwingungen des Systems Erde–Luft–Ionosphäre. *Z* Naturforsch *A.* 1952;7a:250-252. https://doi.org/10.1515/zna-1952-0301

[30] Balser M, Wagner C. Observations of Earth–ionosphere cavity resonances. *Nature.* 1960;188:638-641. https://doi.org/10.1038/188638a0

[31] Note: Although often described as harmonics, the Schumann resonances are not exact integer multiples of the fundamental. Their quasi-harmonic spacing reflects the non-ideal structure of the Earth–ionosphere cavity, including ionospheric conductivity and day–night variability.

A lower waveguide height compresses the cavity, which leads to shorter resonance wavelengths and an upward shift in observed frequencies. Conversely, an expanded cavity supports longer wavelengths and slightly lower resonance frequencies. This relationship between cavity height and resonance behavior is well-documented in the literature and allows researchers to infer changes in the waveguide structure by monitoring frequency variation. These changes are especially pronounced during geomagnetic storms or solar proton events, which can modify the conductivity and altitude of the lower ionosphere.[32]

These changes appear as shifts in resonance frequency and intensity that reflect real-time deformation of the cavity boundaries. By observing low frequency wave dynamics, especially in response to turbulent drivers, researchers can monitor subtle changes in the structure of the lower ionosphere with global coverage and continuity across time.[33]

VI. Element 3: Earth's Ionosphere Affects Stability of Global Standing Waves

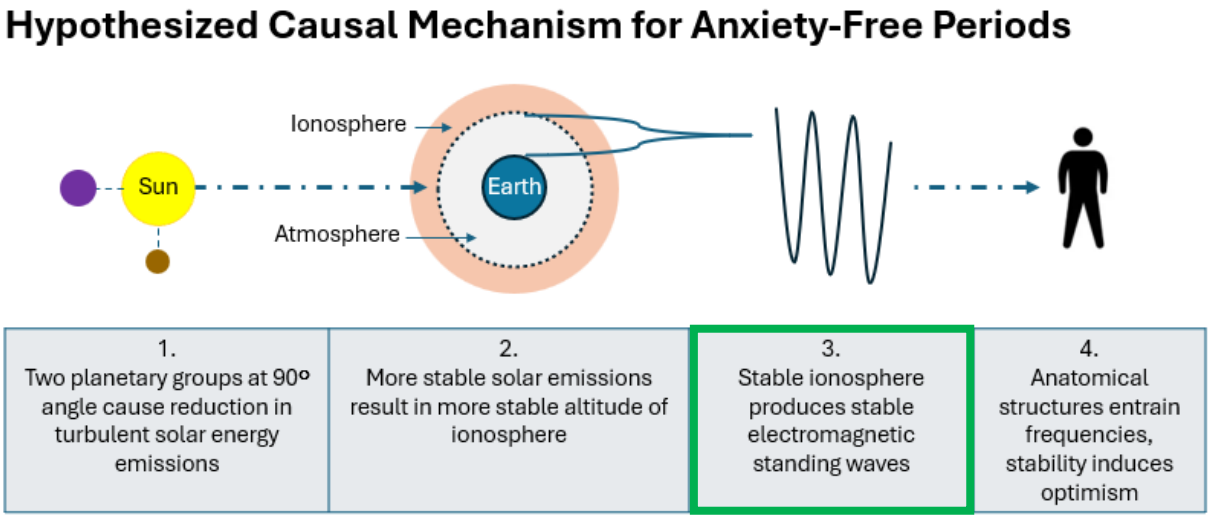

Figure 24. Hypothesized causal mechanism for Anxiety-Free Periods. The diagram outlines the proposed sequence linking solar system geometry, solar emissions, ionospheric stability, global electromagnetic standing waves, and human physiological entrainment. This figure highlights Element 3. Source: CPM Investing LLC.

Overview

In this section, Study D provides compelling evidence that orbital geometry configurations, specifically the 90-degree configuration that typically gives rise to Anxiety-Free Periods, correspond to both increased stability of the global electromagnetic standing waves and strong market returns. The 2017 Anxiety-Free

[32] Barr R, Jones DL, Rodger CJ. ELF and VLF radio waves. J Atmos Sol Terr Phys [Internet]. 2000;62(17-18):1689-718.
https://doi.org/10.1016/S1364-6826(00)00121-8

[33] Nickolaenko AP, Hayakawa M. Resonances in the Earth–ionosphere cavity. Springer; 2014.
https://doi.org/10.1007/978-4-431-54358-9

Period coincided with peaks in both frequency stability and stock market price. M-Spikes also align with patterns seen in the global electromagnetic standing waves.

To determine if the solar calm associated with the Anxiety-Free Periods could be detected in other metrics of solar emissions, Study E analyzes the sunspot number series and the Oulu NM data across nine Anxiety-Free Periods from 1965 to 2023. Although these indicators do not directly track low frequency electromagnetic waves, their consistent behavior near Anxiety-Free Periods suggests a shared underlying mechanism.

Study D – Global Standing Wave Frequency Stability and the 2017 Anxiety-Free Period

Our analysis of the global electromagnetic standing waves supports the hypothesized relationships among orbital geometry configuration, frequency stability, and stock market behavior. We obtained global electromagnetic standing wave data from the British Geological Survey from their Eskdalemuir monitoring site in Scotland. The raw data consisted of magnetometer readings every millisecond. We converted those observations into data describing the means and standard deviations of electromagnetic frequencies for two periods each day, daytime (lasting from 8 am to 4 pm local time) and nighttime.[34] The frequency range covered by this dataset is in the range of 7 Hz (cycles per second) to 50 Hz.

Our focus is not on the frequencies detected but on the variability of those frequencies, or in other words, the frequency stability.[35] We assume that a higher level of frequency stability over these short periods is a good proxy for lower turbulence.

Figure 25 below shows the price level of the US stock market as the brown line for the period covered by usable global electromagnetic standing wave data, June 5, 2015, through December 31, 2021. This period encompasses the steep market price rise of 2017, a price decline at the beginning of 2018, a price decline at the end of 2018 related to trade tariff tensions, and the major price decline in March of 2020 related to the COVID pandemic.

Predicted Episodic Series

Two predicted episodic (as opposed to cyclic) series are represented by the yellow dotted line and light purple dotted line in the middle of the figure. The yellow dotted line shows the predicted 90-degree configuration events associated with the 2017 Anxiety-Free Period. This episode has three 90-degree events or columns with the second being the highest, representing when we expect the highest level of investor optimism (lowest level of anxiety). The light purple dotted line shows the predicted M-Spike episode. Five M-Spikes are shown,[36] gaining in intensity over this period.

Both the 90-degree events related to the Anxiety-Free period and M-Spikes can overwhelm cyclic physics-based drivers. The Micro Driver, which influences the path of the cyclic Micro Market Resilience Index during times of stress, is shown as a darker dotted purple across the bottom of the figure.

[34] Note: For modes two and three of modes associated with the global electromagnetic standing wave frequencies.
[35] Note: Frequency stability is calculated as the standard deviation of standing wave modes two and three, averaged them together, and then inverted the result (multiply by –1). Higher values reflect greater stability, and lower values reflecting more volatility.
[36] Note: There is a small M-Spike at the end of 2016.

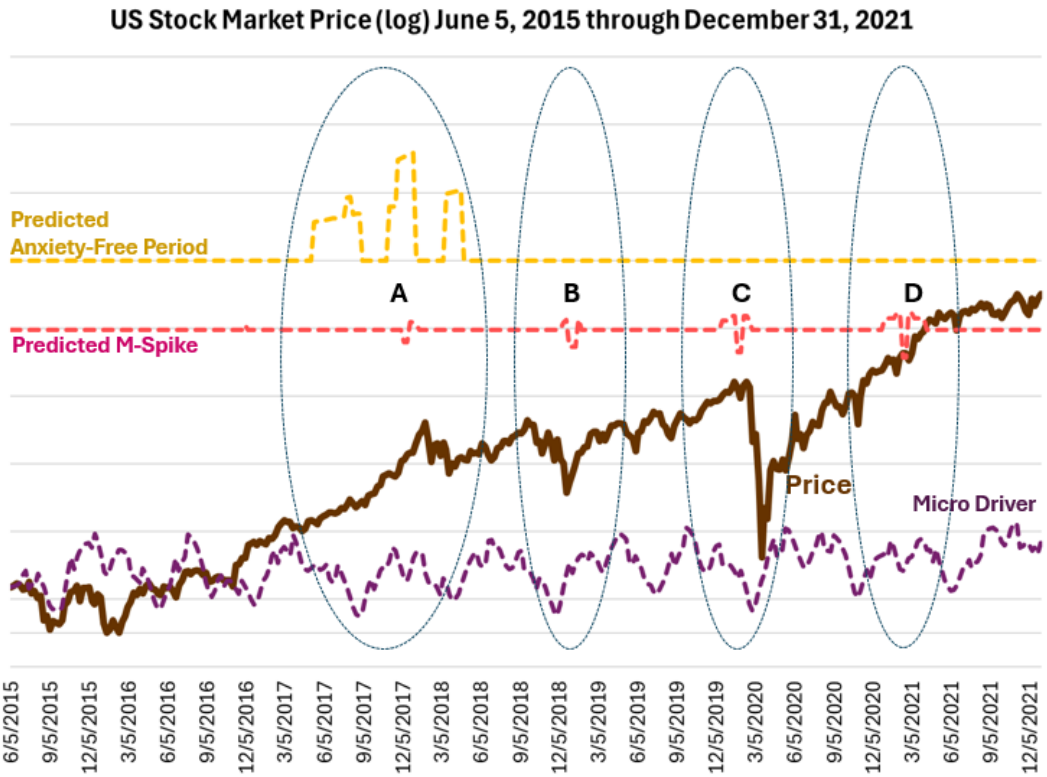

Figure 25. U.S. Stock market price and the indicators for the 2017 Anxiety-Free Period and the M-Spike episodes from June 5, 2015 through December 31, 2021. This chart shows the market price level and the indicators for these two types of episodes along with ellipses A through D, which indicate noteworthy relationships between patterns in stock price movement and the episodic indicators. Sources: CPM Investing LLC calculations using data from NASA, the British Geological Survey, MeasuringWorth, and public market sources. 'U.S. stocks' and 'U.S. stock market' refer to the DJIA, S&P 500, or related ETFs depending on the period.

Figure 26 below shows the same data with the addition of the global electromagnetic standing wave stability metric at the top of the figure. The most important observation from this analysis is that both the stock market level and prominent features in the global electromagnetic standing wave stability series coincide with the 90-degree events as shown below, specifically in ellipse A.

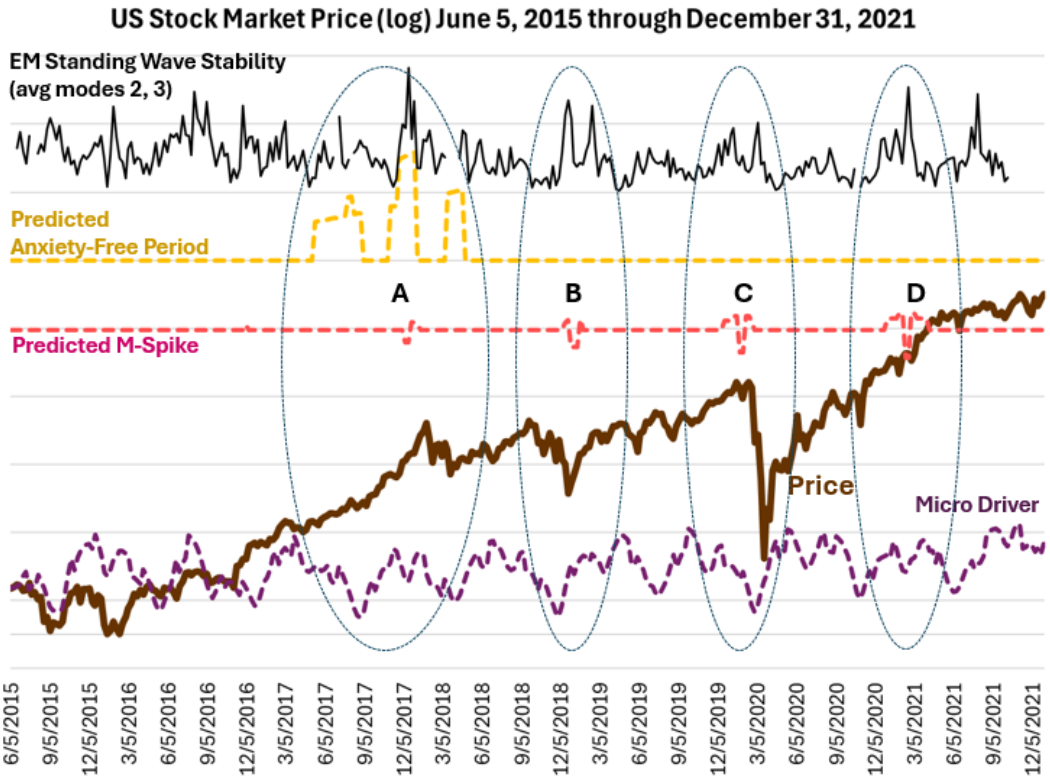

Figure 26. U.S. Stock market price and the indicators for the 2017 Anxiety-Free Period and the M-Spike episodes from June 5, 2015 through December 31, 2021. This chart shows the market price level and the indicators for these two types of episodes along with ellipses A through D, which indicate noteworthy relationships between patterns in stock price movement and the episodic indicators. This chart also shows the stability of the electromagnetic standing waves for modes 2 and 3 observed on weekends between the hours of 8 am and 4 pm local time, lagged approximately two weeks (described in Appendix P). Sources: CPM Investing LLC calculations using data from NASA, the British Geological Survey, MeasuringWorth, and public market sources. 'U.S. stocks' and 'U.S. stock market' refer to the DJIA, S&P 500, or related ETFs depending on the period.

Ellipse A shows that the highest point in the stability of the global electromagnetic standing wave series over the five-year period is close to the high point of the 2017 Anxiety-Free Period. Both are close to the top of the market taking place at the end of 2017.

The M-Spikes in ellipses B, C, and D are the strongest and clearly correspond to similar shifts in the global electromagnetic standing wave stability series. The M-Spike in ellipse A coincides with the second 90-degree configuration event.

The relationship between the stock market and the M-Spike at the end of 2018 (B) appears to have been magnified or perhaps overwhelmed by trade tensions.

Figure 27 below is the same as the prior figure with the addition of a blue "X," which indicates a temporary decrease then increase in electromagnetic standing wave stability. This pattern appears in other solar energy-related metrics, as shown Appendix P. We will investigate this pattern in Study E.

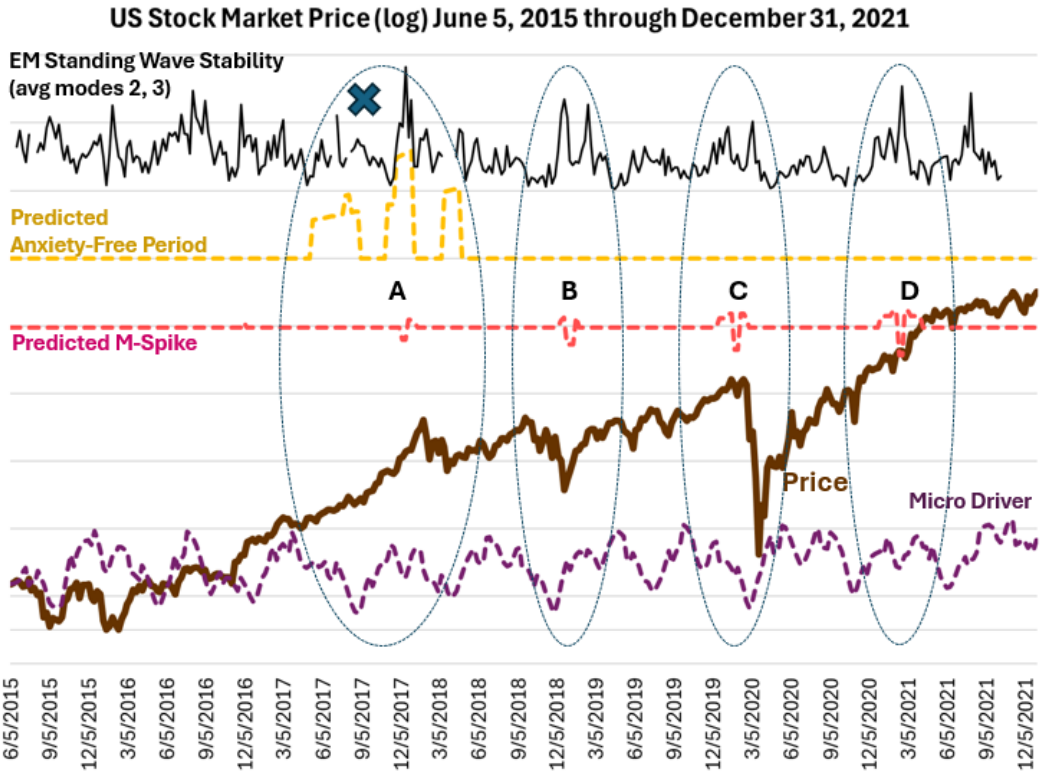

Figure 27. Same as prior figure with the addition of a blue "X" indicating a dip in the standing wave stability after the end of the first column of the Anxiety-Free Sources: CPM Investing LLC calculations using data from NASA, the British Geological Survey, MeasuringWorth, and public market sources. 'U.S. stocks' and 'U.S. stock market' refer to the DJIA, S&P 500, or related ETFs depending on the period.

In a regression of the electromagnetic standing wave stability and the two predicted series, the Predicted Anxiety-Free Period is a significant factor in explaining the variability of the global electromagnetic standing wave stability ($p < 0.001$).[37] It is gratifying to see an alignment of physics-based predictions with actual physical metrics because a connection between planetary positions and objective physical measurements has been elusive.

In Figure 27 above, M-Spike-related global electromagnetic standing wave stability seems to begin earlier than the predicted M-Spike and end later. Thus, while they are visually similar, our statistical tests indicate that the relationship is not significant over this period. The calculations behind M-Spikes are more complicated than those for the 90-degree configurations, and the more complex orbital geometry dynamics may result in less abrupt shifts in physical metrics.[38]

[37] Note: The *p*-value is 0.001, indicating strong statistical evidence against the null hypothesis of no relationship. This supports the view that 90-degree configuration is associated with the stability of the electromagnetic standing waves in the atmosphere.

[38] Note: Our longer-term studies of market behavior near M-Spikes confirms this view. Their statistical significance is about 0.18, which means that we can expect an M-Spike-like market pattern about 18 percent of the time simply by chance. We view the 18% probability of seeing this outcome by chance as sufficiently low to call the M-Spikes noteworthy because the variables of market performance and orbital geometry are disparate.

VI. Element 3: Earth's Ionosphere Affects Stability of Global Standing Waves

Study D: Relationship of Electromagnetic Standing Waves to the 90-Degree Configurations
To test whether two orbital geometry–derived factors help explain variation in electromagnetic standing waves modes 2 and 3.

Key Results:
– Intercept: 140.48, EM Standing Waves value
– Predicted Anxiety-Free Period series: +0.2348 ($p < 0.001$) —significant positive relationship
– M-Spike series: –0.2957 ($p = 0.190$) — not statistically significant
– R^2: 0.052 — low explanatory power

Interpretation:
The Predicted Anxiety-Free Period series shows a statistically significant positive association with EM Standing Wave, while M-Spike series' influence is inconclusive.

Appendix Reference:
See Appendix P for detailed regression specifications, diagnostics, and data definitions.

The results of this study are important, even if the period analyzed is short. First, they support our hypothesis that the stability of global electromagnetic standing waves is affected by orbital geometry configuration as represented by the 90-degree configuration event series and, to a lesser extent, the M-Spike series.

Second, the study provides empirical evidence for solar energy variation in a physical phenomenon (electromagnetic standing waves) that are plausibly linked in independent research to human emotion. Sunspot counts, Oulu NM, F10.7 flux, and Ap index show correlation to human health and emotion (as shown in Appendix B, mentioned earlier), but research indicating how humans are affected by the electromagnetic standing waves has been limited.

Third, in conjunction with the extremely low probability of the 2017 return profile occurring by chance from Study C (indicated as 0.0% in Figure 21), these findings support our hypothesis that investor sentiment is affected by global electromagnetic standing waves.

These figures also illustrate other important points:

1. Real-world issues and events matter. The tariff tensions at the end of 2018 had a negative impact on stock market sentiment and appear to have overwhelmed the initial optimism represented by the first upleg of the M-Spike (ellipse B).
2. Episodic drivers have a strong but temporary impact. As shown by the M-Spike just prior to the COVID Crash (ellipse C), the market appears to have been supported by the M-Spike prior to the Crash. But then that support ended abruptly. We see this pattern in other periods – the end of Anxiety-Free Periods and M-Spikes can be associated with sharp market declines.
3. Not all shifts in solar energy and investor sentiment follow familiar sine waves. Some patterns are angular and abrupt, as we see with episodic events.
4. The two major market declines of the period (B and C) took place at a time when the cyclic (as opposed to episodic) physics-based Micro Driver (purple dotted line at bottom) indicated the greatest naturally occurring short-term pessimism. This supports our general view that, while the magnitude of market price movements up and down is determined by economic and market fundamentals, the timing of the market moves is determined by naturally occurring shifts in sentiment.

However, the coverage of the global electromagnetic standing wave data is short, encompassing only one Anxiety-Free Period. An element contributing to the importance of Study C is that all 13 Anxiety-Free Periods since 1933 are included in the analysis. While this study, Study D, highlights an extremely important physical link between solar energy variation and market behavior, it is just one episode. The single Anxiety-Free Period makes us less confident about there being a broader relationship, despite the high explanatory power of the factor. Confidence can increase if we observe the relationship described in this study with other periods with other 90-degree configuration events. This is why the expected 2026 Anxiety-Free Period will be important to monitor.

Our Focus on Frequency Stability

We focus our research on frequency stability as opposed to the frequency levels of electromagnetic standing waves in this analysis because of our prior research on the Oulu Neutron Monitor readings. That research demonstrated the possible importance of the turbulence-stability dynamic related to human mood and investor sentiment. Appendix Q has additional information on this research.

Study E – Anxiety-Free Periods and Two Solar Emission Metrics

This study is designed to compensate for the narrow coverage of 90-degree configuration events and Anxiety-Free Periods in Study D. Study E investigates whether 90-degree configurations correspond to changes in solar emissions by evaluating two long-term datasets: the sunspot number series and the Oulu NM count rate.[39] These data series provide complementary perspectives on solar activity. The sunspot series reflects solar surface magnetic activity and serves as a proxy for direct electromagnetic emissions from the Sun. Oulu NM data serves as a proxy for solar energy affecting Earth, reflecting the net electromagnetic effect of solar wind, cosmic ray shielding, and geomagnetic conditions at Earth.

Figure 28 below displays the full historical record common to both series (the Oulu data begins in 1964) across all nine Anxiety-Free Periods occurring in this period. The yellow vertical columns indicate the 90-degree configuration events. The price of the U.S. stock market is shown in brown, the sunspot series in orange, and the Oulu NM series in green. Along the bottom of the figure, blue markers indicate when the two Orbital Geometry Centers form 0-degree (the tallest marker) and 180-degree angles with the Sun at the vertex.

[39] Note: Both series are normalized to range from 0.0 to 1.0. The scale for the sunspot series has been inverted to align with the Oulu series. See Appendix G for a description of how we transformed these series.

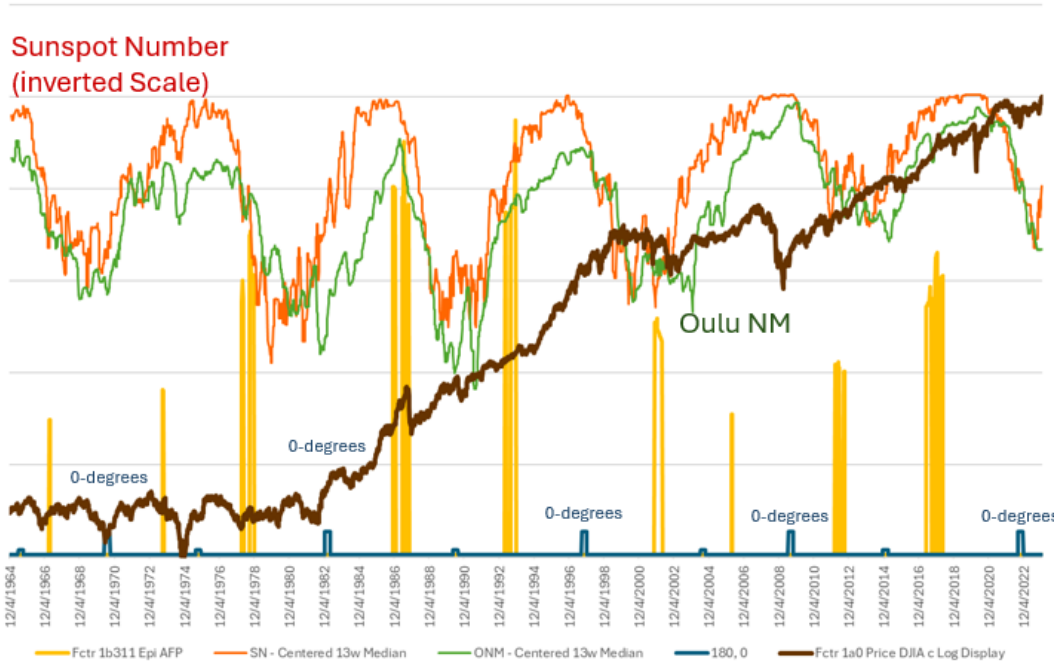

Figure 28. Patterns in the Sunspot and Oulu series covering the last nine Anxiety-Free Periods. Sources: CPM Investing LLC calculations using data from GFZ, Oulu NM, and MeasuringWorth and public market sources. 'U.S. stocks' and 'U.S. stock market' refer to the DJIA, S&P 500, or related ETFs depending on the period.

The sunspot and Oulu series have similar long-term cyclical patterns, likely driven by the Sun's internal dynamics, as referenced in physics literature. Notably, the 90-degree configuration events do not consistently align with a specific phase or position in this cycle.

The 90-degree configuration events occur during the following:

- Ascending or descending legs of the internal cycles: 1966, 1974, 1978, 1993, 2006
- At or near the tops: 1987 and 2017
- At or near the bottoms: 2001, 2012

Figure 29 below shows the most recent three clusters of 90-degree events representing Anxiety-Free Periods.

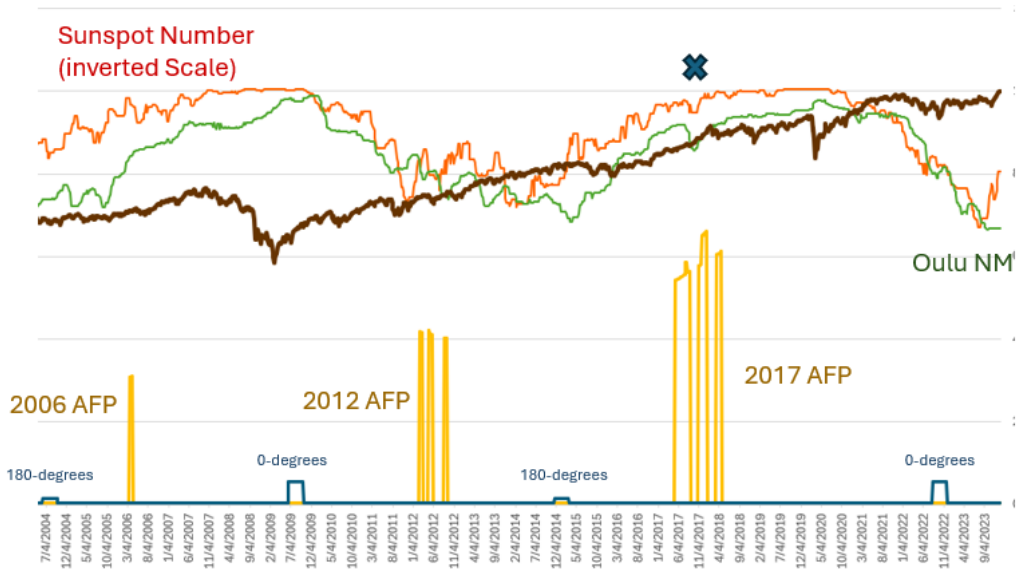

Figure 29. Patterns in the Sunspot and Oulu series covering the last three Anxiety-Free Periods. Sources: CPM Investing LLC calculations using data from GFZ, Oulu NM, and MeasuringWorth and public market sources. 'U.S. stocks' and 'U.S. stock market' refer to the DJIA, S&P 500, or related ETFs depending on the period.

Study D (previously discussed) showed a dip in the electromagnetic standing waves and a decrease in our sunspot series shortly after the first column of the 2017 Anxiety-Free Period, marked as "X" in Figure 22. A visual examination suggests the Oulu series also tracks that pattern closely.

Study E is divided into two parts. Part 1 investigates whether the end of a 90-degree configuration event is associated with systematic changes in the sunspot series, noted by "X" above. Systematic changes would support our view that orbital geometry affects the Sun itself. As mentioned in Appendix G, the sunspot series represents a count of visible conditions of the solar surface that are related to the Sun's energy output. The count is not affected by Earth's atmosphere, its magnetic field, or solar wind. Since our metric has an inverse scale, a drop in our sunspot metric indicates an increase in sunspot count and the Sun becoming more active after a 90-degree configuration event. Part 2 investigates how closely the Oulu series tracks the sunspot series in the period around and during each cluster of 90-degree configuration events.

Study E Part 1 – Dip in Sunspot Series

We compared the directional changes in our sunspot metric in the weeks following the end of the Anxiety-Free Period events from 1935, the inception of our sunspot series, through 2023. Since many of the 13 Anxiety-Free Periods have multiple 90-degree configuration events, this test evaluates 26 90-degree configuration events. If orbital geometry had no impact on solar activity, we would expect approximately 50% of four-week periods to be higher and 50% to be lower over all the horizons evaluated below, from one week after the end of the 90-degree configuration events to 12 weeks after the end.

The results indicate a noticeable increase in our sunspot series four weeks after the end of 90-degree configuration event. Figure 30 below shows the change in the sunspot series over one- to 12-week horizons from 1935 through 2023.

Over a four-week horizon, 77% of the periods ended with a higher reading in our sunspot series. Because our scale is inverted, this means that sunspot number decreased by the end of 77% of the four-week periods. The probability of this occurring by chance from the data is less than 1% ($p < 0.01$). This finding is consistent with the view that the end of the 90-degree angle between the Inner and Outer Centers Anxiety-Free Period has an impact on the Sun as indicated by the sunspot series. The four-week horizon had the highest level of weeks with a one- through 12-week horizon.

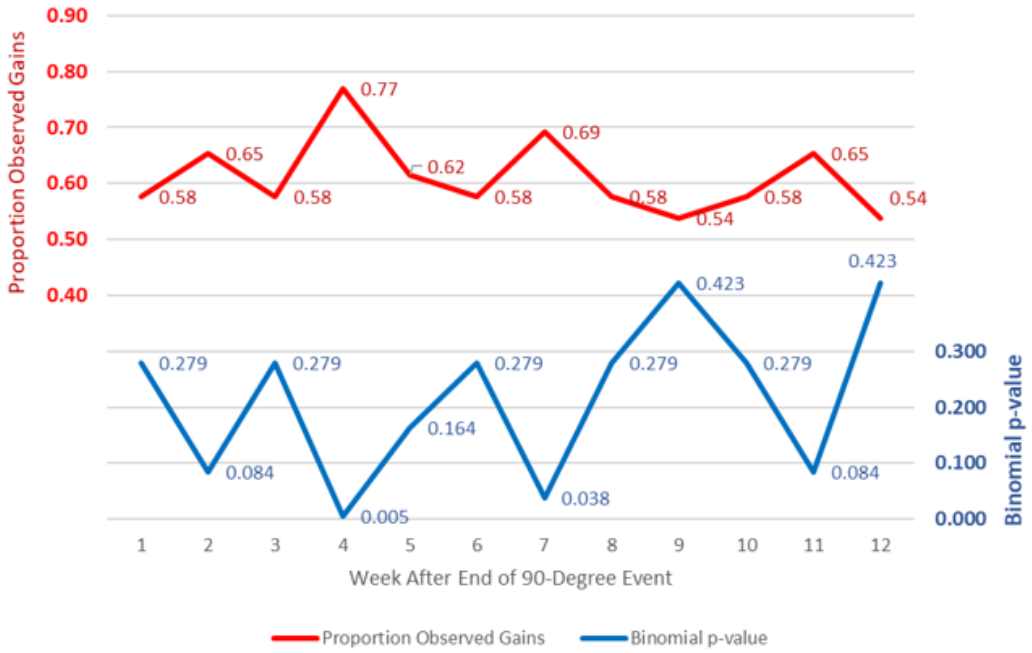

Figure 30. Patterns in the sunspot series covering 26 90-degree configurations 1935 through 2023. Sources: CPM Investing LLC calculations using data from GFZ.

Of all the 4,692 four-week periods possible over this same period, 49.6% were higher at the end of the four weeks, 50.4% were lower. For all windows (1 week through 12 weeks) the ratios are all within a range of 50.6% to 49.4%. This pattern is consistent with expectations and is a strong contrast to the 77% rate associated with four weeks after the end of 90-degree configuration events.

Study E Part 2 – Oulu Series Tracking the Sunspot Series

Study E Part 2 evaluates how closely the Oulu NM series tracks the sunspot series. Part 1 of Study E, described above, focused narrowly on the weeks after the end of 90-degree configuration events. While the Oulu NM series does not show the statistically significant behavior over this period that we see in sunspot activity, we tested to see if a relationship exists if we broaden the time period of our analysis. The impetus for doing this is the visual patterns seen in the nine Anxiety-Free Periods that have occurred since the inception of the usable Oulu data in April 1964 through December 2024. In Appendix R, we can see in the figures for each of these periods that the alignment of the 90-degree configuration events, sunspot series, and the Oulu series could be improved by leading or lagging the data, which we have not done in this analysis. This analysis seeks to determine if there may be a relationship without doing a fitting process to align the series.

Thus, Part 2 analyzes a horizon that begins 16 weeks before the beginning of the first 90-degree configuration event to 16 weeks after the end of the last 90-degree configuration event. The objectives are to determine if a) the sunspot series is more volatile near an Anxiety-Free Period, and b) if the Oulu NM series tracks closely the variability of the sunspot number.

This approach measures sunspot series volatility over a longer window around each cluster of 90-degree configuration events than was used in Part 1, in order to detect rapid increases and decreases in energy emissions that may be associated with the beginning and ends of the 90-degree configuration events within the clusters.

Close tracking of the Oulu series with the sunspot series would support the view that the 90-degree configuration influences both the Sun itself and the solar emissions that reach Earth. We compared two groups of weeks:

1. Weeks during the cluster of 90-degree configuration events and an additional buffer of 16 weeks before and after each cluster, totaling 518 weeks across all nine Anxiety-Free Periods between 1964 and 2024.
2. All other weeks, totaling 2,555 weeks.

We computed a centered seven-week rolling standard deviation of the sunspot series, comparing the two groups identified above. The cluster of 90-degree configuration events and additional buffer weeks exhibited significantly higher sunspot volatility compared to all other weeks ($p < 0.05$).

We then assessed the tracking deviation (i.e., root mean square deviation) between weekly readings of the Oulu and sunspot series, again comparing the two defined groups of weeks. The deviation between Oulu and Sunspot readings during Anxiety-Free Periods was significantly lower than in all other weeks ($p < 0.01$).

VI. Element 3: Earth's Ionosphere Affects Stability of Global Standing Waves

Study E: Solar Activity and Oulu Neutron Monitor Behavior After Anxiety-Free Periods

Purpose:
To test whether the end of 90-degree configuration events is associated with measurable changes in solar activity (sunspot series) and Earth-based measures of cosmic ray flux (Oulu Neutron Monitor series), and to evaluate whether these two metrics track more closely near Anxiety-Free Periods.

Part 1 – Sunspot Behavior Immediately After 90-Degree Configuration Events
– Tested 26 90-Degree Configuration events (1933–2023) for a directional change four weeks following the event.
– Sunspots: After 77% of the events our sunspot metric moved higher, meaning an actual de*crease* in sunspot counts (*binomial* $p < 0.01$).
– Interpretation: Supports the view that orbital geometry affects the Sun's surface activity.

Part 2 – Broader Volatility and Tracking Analysis
– Time window: 16 weeks before the clusters of 90-degree events begin, between the events, and 16 weeks after last one ends (518 weeks related to 90-degree events, 2,555 other weeks).
– Sunspot Volatility: Significantly higher during 90-degree event-related weeks than in unrelated weeks ($p < 0.05$).
– Oulu–Sunspot Tracking: Tracking deviation (RMS difference) significantly lower during 90-degree event-related weeks ($p < 0.01$), indicating closer alignment between Earth-based Oulu readings and sunspot activity.
– Interpretation: Over a longer horizon than used in Part 1, 90-degree configuration event-related weeks coincide with greater variability in solar emissions and tighter coupling between Sun-based and Earth-based measurements, consistent with the hypothesis that orbital geometry affects both.

These results indicate that sunspot volatility increases (which means that movements higher and lower are larger) near a 90-degree configuration and that the Oulu series tracks the sunspot series more closely during these events. Thus, these findings are consistent with the hypothesis that the 90-degree configuration affects the Sun, and the effects can be detected on Earth.

However, Study E is done because of the limited availability of data on the electromagnetic standing waves used in Study D. Sunspot activity and Oulu readings may share similar underlying sources as the low frequency perturbation activity that we suspect is an important part of the proposed mechanism linking solar activity (and orbital geometry) to investor sentiment. We do not have evidence that suggest sunspot activity and Oulu readings directly measure a key element of the proposed mechanism.

VII. Element 4: Electromagnetic Standing Waves Affect Investor Sentiment

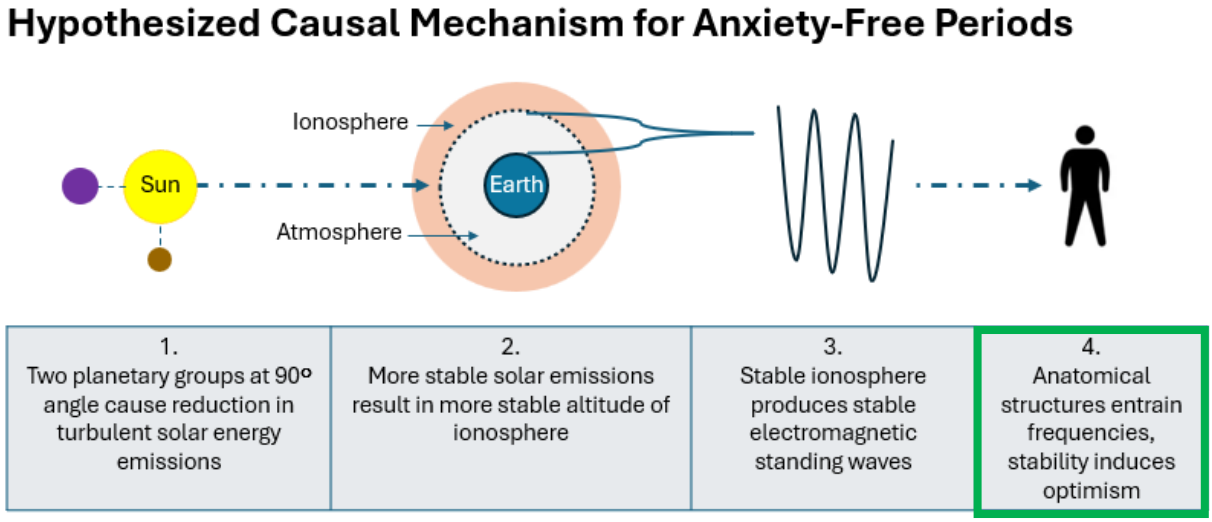

Figure 31. Hypothesized causal mechanism for Anxiety-Free Periods. The diagram outlines the proposed sequence linking solar system geometry, solar emissions, ionospheric stability, global electromagnetic standing waves, and human physiological entrainment. This figure highlights Element 4. Source: CPM Investing LLC.

Overview

This section covers two topics - first, how humans might detect global electromagnetic standing waves and how this could influence investor sentiment, and second, the relationship between the frequencies of the global electromagnetic standing waves and the cognitive and decision-making styles of a large sample of professional investors.

Human Sensitivity to Global Electromagnetic Standing Waves

Entrainment is the process by which one rhythmic system synchronizes with another. In biological and physical systems, it refers to developing an alignment of timing or frequency between two oscillating entities due to mutual influence or an external driver. For example, if the brain's electrical activity begins to oscillate in phase with a rhythmic external signal (e.g., 7.83 Hz), it is said to be entrained to that frequency.

Both global electromagnetic standing waves and brain waves involve electrical activity, but they arise from fundamentally different processes. Electromagnetic standing waves are physical energy fields that travel through space, typically generated by external sources like lightning or electronic equipment. In contrast, brain waves are patterns of electrical activity produced by neurons communicating through electrochemical signaling. This neural activity is initiated by ion exchanges across cell membranes and mediated by neurotransmitters, making it deeply embedded in the brain's biological and chemical architecture. While both involve electricity, brain waves are intrinsically tied to the body's chemical environment, whereas electromagnetic waves are independent physical phenomena.

Electromagnetic Entrainment of Brain Activity

The fundamental mode of the Earth's global electromagnetic standing waves, commonly referred to as Schumann resonance, occurs at approximately 7.83 Hz, a frequency close to the lower end of the human alpha brainwave range (8–12 Hz) and overlapping with the upper theta range (4–8 Hz). Alpha rhythms are typically associated with relaxed but alert states, while theta rhythms are linked to meditative and drowsy conditions. Controlled laboratory and observational studies have suggested that exposure to oscillating magnetic fields at electromagnetic standing wave frequencies can influence brainwave activity, potentially leading to entrainment effects in the alpha or theta bands.[40] [41]

Experimental electroencephalography studies have reported transient synchronization between brain electrical activity and natural electromagnetic standing waves signals, particularly during periods of elevated resonance amplitude variability.[42] These coupling events are not constant but appear to occur during specific environmental conditions.

Global Electromagnetic Standing Wave Variability and Human Function

Evidence from physiological research indicates that short-term variability in electromagnetic standing waves frequencies and amplitudes, rather than static exposure, may exert stronger effects on human neurophysiology. For example, a controlled study using simulated magnetic fields at electromagnetic standing wave frequencies found that microvariations designed to mimic natural fluctuations produced greater reductions in systolic blood pressure and improvements in mood compared to fixed-frequency exposure.[43]

Correlational analyses have shown that daily variations in electromagnetic standing wave power and frequency are associated with concurrent changes in heart rate variability, a marker of autonomic nervous system activity.[44] This relationship suggests that the human cardiovascular system may be sensitive to short-term shifts in global electromagnetic field dynamics.

Clinical Trials and Observational Studies

In a randomized controlled trial, patients with insomnia exposed to weak, oscillating magnetic fields at electromagnetic standing wave frequencies reported improved sleep quality and mood scores.[45] Other electroencephalography-based studies have documented transient coherence between electromagnetic

[40] Pobachenko SV, Kolesnik AG, Borodin AS, Kalyuzhin VV, Kolesnik SB. The effect of weak electromagnetic fields of Schumann resonances on the human EEG. Neurosci Behav Physiol [Internet]. 2006;36(3):311-4.
[41] Hori T, et al. Alpha-like EEG activity in humans induced by Schumann resonance magnetic fields. Int J Biometeorol [Internet]. 2021;65(6):1003-14.
[42] Mulligan BP, Persinger MA. Experimental simulation of the effects of sudden increases in Schumann resonance power on human brain activity. Neurosci Lett [Internet]. 2012;516(1):82-6.
https://doi.org/10.1016/j.neulet.2012.03.077
[43] Saroka KS, Vares DE, Persinger MA (2016) Similar Spectral Power Densities Within the Schumann Resonance and a Large Population of Quantitative Electroencephalographic Profiles: Supportive Evidence for Koenig and Pobachenko. PLoS ONE 11(1): e0146595.
https://doi.org/10.1371/journal.pone.0146595
[44] Alabdulgader A, McCraty R, Atkinson M, Dobyns Y, Vainoras A, Ragulskis M, et al. Long-term study of heart rate variability responses to changes in the solar and geomagnetic environment. Sci Rep [Internet]. 2018;8:2663.
https://doi.org/10.1038/s41598-018-20932-x
[45] Hunziker MH, et al. Effects of weak magnetic fields at Schumann resonance frequencies on sleep: a randomized controlled trial. J Sleep Res [Internet]. 2020;29(6):e12954.
https://doi.org/10.1111/jsr.12954

standing wave variations and activity in brain regions involved in emotional regulation and decision-making.[46]

Collectively, these electroencephalography studies, cardiovascular correlations, and clinical trials support the plausibility that global electromagnetic standing waves may influence human emotional states, potentially including investor sentiment. Nonetheless, causal pathways remain to be established, and further controlled studies are warranted.

Human Exposure and Apparent Response to a Wide Range of Orbital Dimensions

As mentioned in our demonstration in the simulated long-term forecast of the Predicted 14-week RSI for the U.S. stock market, sentiment can be affected by many different measures of orbital geometry. Let's assume that each is related to a global electromagnetic standing wave, its frequency, stability, or some other measure. This broad range of tracks introduces a range of questions:

- How could humans detect and process all these at the same time?
- Are all people sensitive to all these frequencies?
- Are some people more sensitive to certain frequencies and less to others?
- What are the anatomical structures in humans that are sensitive to these frequencies?

While this section does not provide concrete answers to these questions, it describes the current understanding of human sensitivity to global electromagnetic standing waves, the anatomical structures considered prime potential detection structures, and an elaboration of the rationale for bone marrow in the skeleton playing a role.

Cited Anatomical Structures as Candidates for Entrainment

The biological pathways by which electromagnetic standing wave patterns might affect mood or cognition remain under investigation. As listed below, researchers have proposed several mechanisms, many grounded in electromagnetic field biology.

1. **Pineal Gland and Melatonin Rhythms**
   The pineal gland, which regulates melatonin production, is sensitive to geomagnetic and electromagnetic changes. Shifts in standing wave amplitude or frequency may affect melatonin secretion, which in turn modulates sleep cycles, mood, and emotional reactivity. Although indirect, this pathway provides a hormonal link between environmental electromagnetic fields and affective regulation.[47]
2. **Cryptochrome-Based Magnetosensitivity**
   Cryptochromes are photoreceptor proteins known to mediate magnetic sensitivity in migratory animals via quantum spin interactions. In humans, cryptochrome 2 (CRY2) is expressed in the retina and brain. Laboratory experiments have demonstrated that human CRY2 can act as a magnetosensor when expressed in transgenic Drosophila, producing measurable behavioral

[46] Pobachenko SV, et al. EEG changes during exposure to natural and artificial Schumann resonance fields. Neurosci Behav Physiol [Internet]. 2015;45(7):745-54.
https://doi.org/10.1007/s11055-015-0131-1

[47] Burch, J.B., Reif, J.S., Yost, M.G. (2008). Geomagnetic disturbances are associated with reduced nocturnal excretion of melatonin metabolite in humans. https://www.sciencedirect.com/science/article/abs/pii/S0304394099003080

responses to weak magnetic fields.[48] Reviews of the radical-pair mechanism—a quantum biological process—identify cryptochromes as the most likely molecular candidates for magnetoreception across species, including a possible but unconfirmed role in humans.[49] A search of PubMed and major journal databases reveals that there are more than 150 peer-reviewed papers in reputable journals discussing cryptochromes in the context of magnetoreception, with at least 25 directly examining mammalian or human cryptochromes and magnetic field sensitivity. If confirmed in humans, cryptochrome-mediated radical-pair mechanisms could represent a quantum biological pathway for detecting environmental magnetic fields, potentially including extremely low frequency variations such as the Earth's fundamental standing wave frequencies.

3. **Phase-Locked Neural Entrainment**
   Building on earlier evidence of electroencephalography coherence with natural extremely low frequency fields, several researchers have proposed that neural circuits may exhibit phase-locking behavior—synchronizing their internal oscillations with external extremely low frequency signals when those fields display sufficient coherence. Controlled and observational studies have reported transient electroencephalography synchrony[50] with global electromagnetic standing wave signals, particularly during periods of elevated resonance variability.[51] These findings suggest that entire neural networks, rather than only isolated brainwave bands such as alpha or theta, may respond adaptively to global electromagnetic patterns. The mechanism most often discussed involves phase alignment between intrinsic neural oscillations and external extremely low frequency fields, consistent with broader principles of neural entrainment. A survey of literature in PubMed and other major journal databases identified more than 40 peer-reviewed papers addressing electroencephalography coherence or phase-locking with extremely low frequency fields, including at least 15 studies specifically linking global electromagnetic standing wave variations to human electroencephalography measures.

Beyond these candidates, we propose that bone marrow in the medullary cavities in the skeleton could serve as a distributed system of electromagnetic sensors. These structures may help translate low frequency solar emissions into physiological responses, offering a biological basis for how environmental rhythms could shape sentiment across different timescales.

Bone Marrow and Medullary Cavities a Potential Structure

Much of the current research on electromagnetic entrainment has emphasized the brain as the principal sensing and processing organ. However, this focus overlooks a large, highly vascularized, chemically active, and electrically responsive tissue: bone marrow.

[48] Fedele G, Green EW, Rosato E, Kyriacou CP. Human cryptochrome exhibits light-dependent magnetosensitivity. Nat Commun [Internet]. 2014;5:4391.
https://doi.org/10.1038/ncomms5391

[49] Hore PJ, Mouritsen H. The radical-pair mechanism of magnetoreception. Annu Rev Biophys [Internet]. 2016;45:299-344.
https://doi.org/10.1146/annurev-biophys-032116-094545

[50] Pobachenko SV, Kolesnik AG, Borodin AS, Kalyuzhin VV, Kolesnik SB. The effect of weak electromagnetic fields of Schumann resonances on the human EEG. Neurosci Behav Physiol [Internet]. 2006;36(3):311-4.
https://yadda.icm.edu.pl/baztech/element/bwmeta1.element.baztech-5c33c1e5-853d-421c-b368-28f8b076240b

[51] Saroka KS, Persinger MA. Quantitative evidence for direct effects between Earth–ionosphere Schumann resonances and human cerebral cortical activity. Neurosci Lett [Internet]. 2014;560:126-30.
https://doi.org/10.1016/j.neulet.2013.12.055

Medullary cavities are marrow-filled regions within bones such as the femur, tibia, humerus, clavicle, and vertebrae. Many are geometrically long, narrow, and fluid-filled, conditions that make them structurally well-suited to interacting with electromagnetic fields through mechanisms that may include dielectric resonance, capacitive coupling, or field entrainment. Classical cavity resonance modeling shows that these structures would resonate at frequencies much higher than global electromagnetic standing waves, making them unsuitable as resonant cavities for extremely low-frequency fields. However, resonance is not the only pathway for sensitivity. The ionic and dielectric properties of the marrow itself provide alternative routes for weak-field coupling, allowing it to act as a field-sensitive medium.

Thus, bone marrow is not merely a blood-forming organ located deep within bones. It possesses a unique combination of biological, chemical, physical, and anatomical features that makes it a compelling candidate for environmental electromagnetic entrainment. Among these features are its documented sensitivity to extremely low frequency electromagnetic fields, its complex ionic and lipid chemistry, its dense innervation and two-way communication with the central nervous system, its anatomical distribution throughout the body, and its surprisingly large volume and mass, both of which exceed those of the brain.

Bone Marrow Responds to Low-Frequency Electromagnetic Fields

Experimental studies have shown that bone marrow-derived stem cells, particularly mesenchymal stem cells (which can develop into bone, cartilage, and fat cells) and hematopoietic progenitors (which give rise to all types of blood cells), respond to low frequency electromagnetic fields in the range of 1 to 50 Hz. These responses include measurable shifts in cell differentiation and proliferation. For instance, exposure to sinusoidal electromagnetic fields has been found to promote the development of bone-forming cells (osteoblasts) and suppress the formation of fat-storing cells (adipocytes). This suppression of adipogenic pathways (that is, the cellular processes leading to fat cell development) is frequency-dependent and reversible, indicating a form of biological sensitivity or tuning to particular frequencies of electromagnetic input.[52]

The observed effects on stem cell differentiation in marrow suggest not only that marrow can respond selectively to weak electromagnetic fields, but also that it may encode and amplify biologically meaningful information carried by them. These findings are consistent with models in which extremely low frequency fields influence signal transduction pathways and gene expression, even when the field strengths are orders of magnitude below the level of random molecular agitation caused by thermal motion of ions and electrons in biological tissue. Such results imply a form of biological resonance or field sensitivity that is embedded in the cellular and molecular architecture of the marrow.

Chemical and Physical Conditions in Marrow Favor Entrainment

Bone marrow occupies the medullary cavities of bones and contains a rich mixture of ions, lipids, water, proteins, and connective tissue. These components form a gel-like matrix with both dielectric and conductive properties, meaning they can support the formation of electric polarization fields and the movement of ions in response to external stimuli. The ionic content of the marrow, particularly calcium,

[52] Ross CL. Mechanisms of extra-low frequency electromagnetic field (ELF-EMF) on human bone marrow mesenchymal stem/stromal cell differentiation. JSM Biotechnol Bioeng. 2016;3(2):1055.
https://www.researchgate.net/profile/Christina-Ross/publication/306032304_Central_Bringing_Excellence_in_Open_Access_Mechanisms_of_Extra_Low_Frequency_Electromagnetic_Field_ELF-EMF_on_Human_Bone_Marrow_StemStromal_Cell_hBM-MSC_Differentiation/links/57ab7

potassium, sodium, and chloride, provides a pool of charged particles that can interact with oscillating electric fields.

Further, the presence of lipid bilayers, charged membranes, and water-structured regions within marrow tissues makes them suitable for capacitive effects. These effects occur when biological membranes act like tiny capacitors, storing and discharging charges in response to voltage changes across their surfaces. Such behavior supports the idea that marrow could entrain in response to oscillating external fields at frequencies similar to those found in the bands of the global electromagnetic standing waves.

Marrow Communicates with the Central Nervous System

Unlike most peripheral organs, bone marrow is extensively connected to the autonomic nervous system, receiving input from both its sympathetic ("fight or flight") and parasympathetic ("rest and digest") branches. Nerve fibers pass through the hard outer bone and extend into the marrow cavity, where they influence critical functions such as blood cell formation and the release of immune-regulating molecules. At the same time, bone marrow sends chemical signals, including cytokines, hormones, and growth factors, into the bloodstream, which can affect other organs and may also feed back into the central nervous system.

This bidirectional communication suggests that bone marrow is not a passive reservoir of stem cells, but an active participant in neural regulation. If marrow can detect and respond to external electromagnetic fields, those responses could be transmitted through autonomic or hormonal pathways to other physiological systems. This would create a feedback loop in which marrow not only receives environmental signals but also converts them into neural or hormonal responses that influence the body's physiology.[53]

A Distributed and Rigid Structure Enhances Sensory Range

The anatomical distribution of marrow throughout the human skeleton may further amplify its role in environmental sensing. Marrow is present not only in the spine and pelvis but also in the sternum, ribs, skull, and long bones of the limbs. This gives bone marrow a spatial distribution across nearly the entire skeleton. Unlike localized organs such as the brain, the marrow is distributed along multiple axes of the body and can interact with fields from various directions and polarizations.

The rigid cortical bone surrounding marrow also serves a physical function that may support resonance. Bones may act as waveguides or resonators for certain mechanical and electromagnetic vibrations. Enclosing marrow within such structures could focus or amplify certain frequencies, especially those with wavelengths comparable to the size of medullary cavities or trabecular spacing. Because electromagnetic standing wavelengths at the fundamental mode (7.8 Hz) are extremely long (on the order of thousands of kilometers), it is unlikely that the marrow resonates mechanically with these wavelengths. However, the ability of smaller anatomical structures to serve as receivers of local field fluctuations or turbulence – not waves in the traditional sense – remains a plausible and testable idea.

Greater Mass and Volume Than the Brain

In an average adult, marrow mass (2.6 to 3.7 kilograms) and volume (3.5 to 5.0 liters) exceed those of the brain by a factor of two to three. If electromagnetic entrainment depends in part on the amount of responsive biological material, then size matters. More tissue mass provides additional molecules,

[53] Aerts-Kaya F, et al. Neurological regulation of the bone marrow niche. Adv Exp Med Biol. 2019;1212:127-153. https://dlib.scu.ac.ir/bitstream/Hannan/687568/1/9783030328221.pdf#page=133

membranes, and ionic gradients that may interact with weak fields. Combined with marrow's widespread distribution throughout the skeleton, this scale increases the likelihood of detecting fluctuations in global electromagnetic standing waves and allows their effects to be integrated over time and across many sites.[54]

Conclusion

Bone marrow possesses a unique combination of properties that make it an anatomically plausible and biophysically credible organ for electromagnetic entrainment at electromagnetic standing wave frequencies. It is known to respond to low frequency fields in a frequency-specific manner, contains the ionic and lipid structures needed for field interaction, communicates directly with the central nervous system, exists in a distributed form throughout the body, and exceeds the brain in both mass and volume. These properties challenge the prevailing brain-centered view of environmental field sensing and suggest that marrow may play a primary role in mediating biological responses to global electromagnetic rhythms.

If entrainment or field-sensitivity occurs in distributed tissues such as marrow, its most immediate effects would be expected in arousal and stress-regulation systems that influence cognitive style and risk appraisal. In financial markets, these physiological shifts can appear as changes in attention span, tolerance for uncertainty, and preference for rapid action. These dimensions are precisely the kinds of patterns described in decision-style frameworks, making investor profiles a practical way to study whether environmental rhythms align with measurable changes in judgment.

Study F – Professional Investors are More Analytical Than General Population

Since the mid-1980s, we have profiled 831 investment professionals using the Rowe decision-style framework, with 197 profiles confirmed in interviews. The framework allocates a total of 300 points to Directive, Analytical, Conceptual, and Behavioral styles. In our sample, Analytical averaged a score of 99 compared to 90 in the general United States population ($p < 0.001$); the other three styles were modestly lower (all $p < 0.001$). See Appendix S for methodology and statistical tests.

[54] Tavassoli M. Bone marrow: structure and function. In: Stamatoyannopoulos G, et al., editors. The Molecular Basis of Blood Diseases. 3rd ed. Philadelphia: W.B. Saunders; 2001. p. 1-20.

Study F: Decision Styles of Investment Professionals vs. U.S. Population

Purpose:
To evaluate whether investment professionals differ from the general U.S. population in cognitive decision-style biases, based on four dimensions: Directive, Analytical, Conceptual, and Behavioral.

Key Results:
– Sample: 831 investment professionals from global investment firms, directly involved in managing several trillions of dollars.
– Analytical: Professionals average a score of 99 vs. 90 for the general population ($p < 0.001$), indicating stronger emphasis on logic, structure, and data-driven decision-making.
– Directive: Professionals average 71 vs. 75 ($p < 0.001$).
– Conceptual: Professionals average 78 vs. 80 ($p < 0.001$).
– Behavioral: Professionals average 52 vs. 55 ($p < 0.001$).
– All four differences are statistically significant at $p < 0.001$.

Interpretation:
Investment professionals show a distinctive cognitive profile, scoring substantially higher in Analytical style while lower in the other three dimensions. This pattern reflects the analytical rigor and structured reasoning emphasized in professional investing, with trade-offs in directive, conceptual, and behavioral tendencies due to the fixed 300-point allocation across styles.

Appendix Reference:
See Appendix S for methodology, descriptive statistics, and significance tests.

This profile helps explain why short-horizon price changes, which provide an abundance of quantifiable signals, can be over-weighted during emotionally charged periods. The two styles that tend to be dominant in this sample are Analytical and Conceptual. Directive is an important secondary style. In the next section, we associate this style with brainwave activity, and then electromagnetic standing wave frequencies.

Brain Waves

Research on brain electrical activity indicates that different decision styles may correspond to characteristic brainwave ranges. The associations below are supported by prior literature, though the precise relationships remain under investigation:

- Theta (frontal-midline), 4 to 8 Hz → working memory, creativity, learning[55]
- Alpha, 8 to 12 Hz → relaxed alertness, inhibition of irrelevant information[56]
- Beta, 13 to 30 Hz → analytical reasoning, sustained attention[57]

[55] Mitchell DJ, McNaughton N, Flanagan D, Kirk IJ. Frontal-midline theta from the perspective of hippocampal "theta." Prog Neurobiol. 2008;86(3):156-85. https://doi.org/10.1016/j.pneurobio.2008.09.005

[56] Klimesch W. Alpha-band oscillations, attention, and controlled access to stored information. Trends Cogn Sci. 2012;16(12):606-17. https://doi.org/10.1016/j.tics.2012.10.007

[57] Engel AK, Fries P. Beta-band oscillations—signaling the status quo? Curr Opin Neurobiol. 2010;20(2):156-65. https://doi.org/10.1016/j.conb.2010.02.015

Some authors have speculated about parallels with naturally occurring global electromagnetic standing wave frequencies.[58] Figure 32 below illustrates possible relationships. These are not presented as causal, but as a way of organizing data around three observations from our research:

- First, successful investors tend to exhibit a strong analytical bias.
- Second, independent research shows that analytical individuals display active brainwaves in the frequency range of modes 2 and 3.
- Third, modes 2 and 3 of the global standing waves correspond to the 90-degree configuration events described in Study D and shown in Figure 33 on the next page.

Decision-Making Style	Profile of Typical Investment Manager*	Related Dominant Brainwave Type	Brainwave Frequency Range (Hz)	Cognitive State Associated with Brainwave Frequency Range	Electromagnetic Standing Wave Matching Brainwaves
CPM Investing		Various sources			CPM Investing
Conceptual	Secondary style	Theta	4-8	Deep thinking, creativity, memory integration	Fundamental mode (7.83 Hz)
Reference	--	Alpha	8-12	Relaxed alertness, inhibition of irrelevant information	
Analytical	Primary style	Beta (low–mid)	12-20	Logical thinking, complex problem-solving	Modes 2 and 3 (14.3, 20.8 Hz)
Directive[59]	Tertiary style	Beta–Gamma	20-35	Decisiveness, stress reactivity, active attention	Modes 4 and 5 (27.3, 33.8 Hz)

Figure 32. Dominant brainwave frequency range, related decision style, and matching electromagnetic standing wave frequency. Sources: CPM Investing LLC calculations using data from a range of sources. * Relative dominance, based on CPM Investing data on 831 professional investors.

[58] Note: Some researchers, such as Persinger [1], Koenig [2], Nickolaenko and Hayakawa [3], and Cherry [4], have speculated about conceptual parallels between Schumann resonances and human brainwave activity, though these ideas remain untested and are not widely accepted in mainstream neuroscience.

[1] Persinger MA. Religious and mystical experiences as artifacts of temporal lobe function: A general hypothesis. Percept Mot Skills. 1983;57(3):1255-62. https://doi.org/10.2466/pms.1983.57.3f.1255

[2] König HL. Biological effects of extremely low frequency electromagnetic fields. Berlin: Springer; 1974. https://link.springer.com/book/10.1007/978-3-642-65823-4

[3] Nickolaenko AP, Hayakawa M. Resonances in the Earth–ionosphere cavity. Dordrecht: Springer; 2002. https://link.springer.com/book/10.1007/978-94-010-0375-4

[4] Cherry NJ. Schumann resonances, a plausible biophysical mechanism for the human health effects of solar/geomagnetic activity. Nat Hazards. 2002;26(3):279-331. https://doi.org/10.1023/A:1015637127504

[59] Note: Analytical and Conceptual styles show electroencephalography oscillatory correlates. Directive style is linked to rapid neural responsiveness (e.g., P300, beta/gamma bursts) rather than a stable oscillatory band.

Similar conceptual overlaps are suggested for the Conceptual and Directive decision styles. The alpha brainwave range has also been included as a reference for completeness. Again, these parallels should be regarded as conceptual overlaps rather than established empirical correlations. Thus, these decision styles may be aligned, at least conceptually, with modes of global electromagnetic standing waves.

Figure 33 below charts the stability readings of the modes of the global electromagnetic standing wave frequencies. At the top is the main or "fundamental" frequency mode associated with the Conceptual style. The middle panel is the average of the second and third modes and is associated with the Analytical style. The lower panel is the average of the fourth and fifth modes associated with Directive investors.

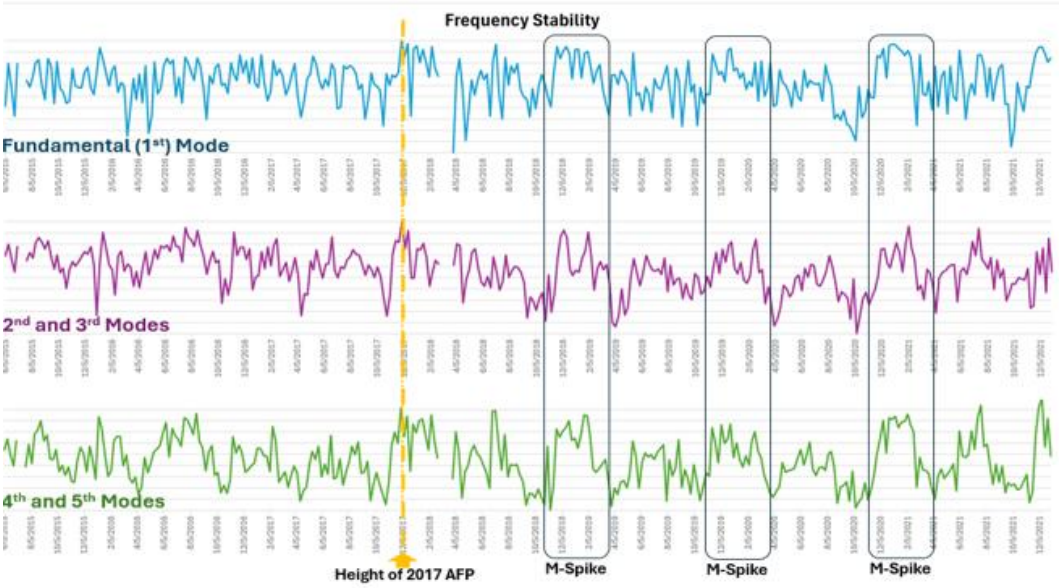

Figure 33. Electromagnetic atmospheric standing wave modes from 2015 through 2021. This graph shows three panels. The upper panel shows the frequency stability of the fundamental frequency (mode 1). The middle panel shows the stability of modes 2 and 3. The lower panel shows the stability of modes 4 and 5. Source: CPM Investing LLC calculations using data from the British Geological Survey.

In Study D, we reported the middle panel, the average of the second and third modes, because that was the series that showed the point of greatest stability as coinciding with the highest column of the Anxiety-Free Period (shown as the vertical dashed yellow line), as well as showing three M-Spikes. The upper and lower panels show the same high stability reading for the Anxiety-Free Period but do not reflect as clearly the middle V-pattern of the M-Spikes, although they still show them as being periods of high frequency stability.

VIII. The Mega Sentiment Cycle

Overview

This section introduces the Mega Sentiment Cycle, a long-term sentiment pattern defined by the angular relationship between the Inner Orbital Center and Outer Orbital Center with the Sun at the vertex. As discussed earlier, when these centers form a 90-degree angle, an Anxiety-Free Period typically occurs. However, the full Mega Sentiment Cycle spans the entire angular journey from 0-degrees to 180 degrees and back to 0, with eight such cycles identified since 1900.

This orbital geometry-derived cycle is purely physical in origin but shows strong alignment with market price movements. The cycle can be divided into four phases, each marked by different investor sentiment tendencies that have significantly different characteristics.

Figure 34 below shows the Mega Cycle since 1900.

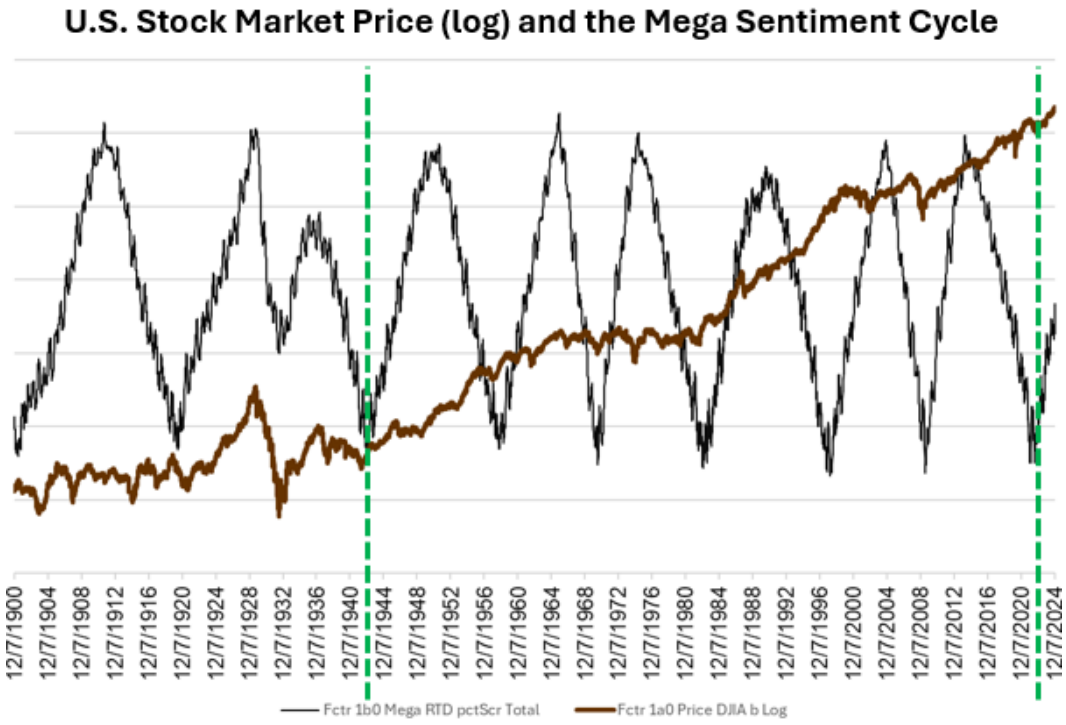

Figure 34. U.S. stock market price level (log) and Mega Sentiment Cycle from 1900 through December 2024. This graph shows the price level of the U.S. stock market and the Mega Sentiment Cycle. Sources: CPM Investing LLC calculations using data from NASA, MeasuringWorth, and public market sources. 'U.S. stocks' and 'U.S. stock market' refer to the DJIA, S&P 500, or related ETFs depending on the period.

Between January 1943 and September 2022 (bordered by the dashed green vertical lines), there have been six full cycles, meaning the average length over this period was about 13 years. The shortest cycle over that period was from October 1997 through August 2009, which lasted 11.8 years. The longest was from January 1943 through May 1948, lasting 15.3 years.

Figure 35 below shows five complete cycles since the late 1950s. The Inner Orbital Center-Sun-Outer Orbital Center degree points are marked. The vertical lines midway between the 0-degree and 180-degree marks are the 90-degree configuration events associated with the Anxiety-Free Periods.

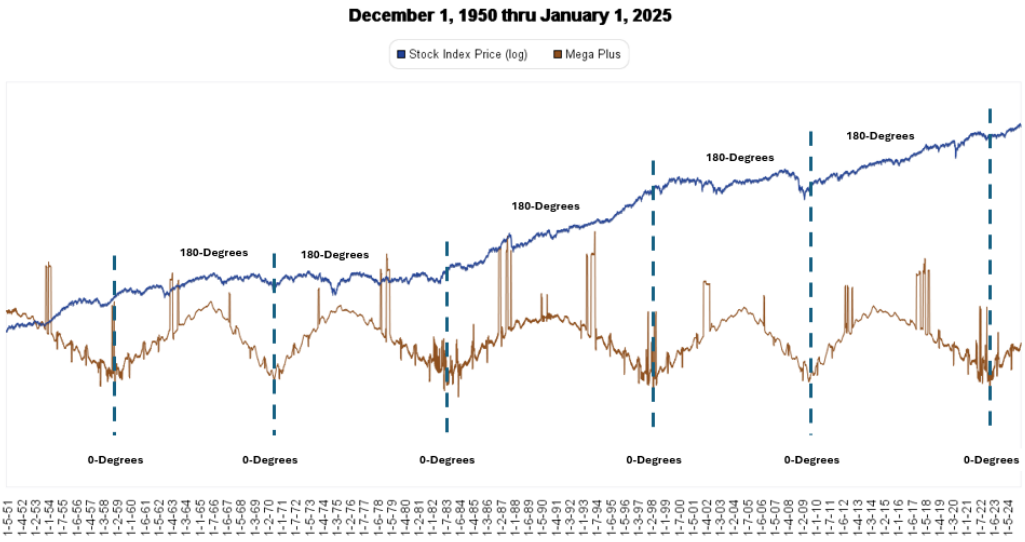

Figure 35. U.S. stock market price level (log) and Mega Sentiment Cycle from 1950 through 2024. This graph shows the price level of the U.S. stock market and the Mega Sentiment Cycle. The angle of the Inner Center-Sun-Outer Center are shown. Sources: CPM Investing LLC calculations using data from NASA, MeasuringWorth, and public market sources. 'U.S. stocks' and 'U.S. stock market' refer to the DJIA, S&P 500, or related ETFs depending on the period.

It is important to keep in mind that the Mega Sentiment Cycle establishes the context for short- and medium-term physics-based sentiment cycles such as those used in the twenty-year forecast of the 14-week RSI for the U.S. stock market discussed in Study A. These shorter cycles have a large impact on the month-to-month direction of the stock market. The shorter cycles are also crucial for determining market tops and bottoms. But there are some notable observations about the four phases of the Mega Sentiment Cycle.

The next set of figures focus only on these four phases, excluding the Anxiety-Free Periods, in order to more effectively characterize those periods. So, in the figures, we omit the Anxiety-Free Periods as well as the 16 weeks before and after each period, in order to exclude the market's reaction to the lead up and the end of the Anxiety-Free Period. We also exclude the eight weeks before and after the 0- and 180-degree marks, resulting in 17 weeks excluded at each of these major inflection points. We omit these weeks to get a more accurate sense of the market phases between these points.

The different phases of the cycle have characteristics that are consistent with our hypothesis of how orbital geometry affects investor sentiment. Figure 36 below shows the four phases of the Mega Sentiment Cycle.

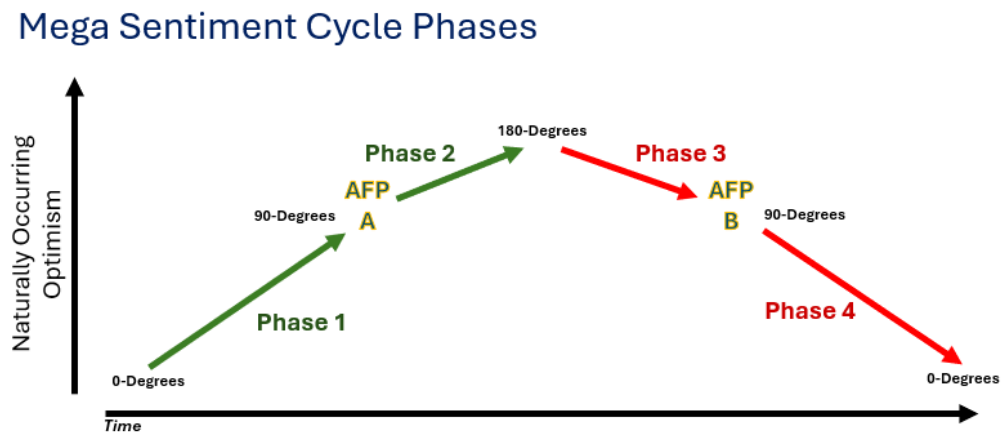

Figure 36. Diagram of the Mega Sentiment Cycle phases. This graph shows the four phases of the Mega Sentiment Cycle and the timing of two Anxiety-Free Periods. The angle of the Inner Center-Sun-Outer Center is shown. Source: CPM Investing LLC.

Notable characteristics are summarized in Figure 37 below.

Phases 1 through 4 Over Six Cycles (1943-2022) – 16w Buffer on AFPs

	Phase 1	Phase 2	Phase 3	Phase 4
Length – yrs (begin 1/1943)	3.4	1.9	1.8	3.4
Percentage of Weeks vs Four-Phase Total	32%	18%	17%	33%
Average Weekly Return [A]	0.18%	0.24%	0.06%	0.12%
Standard Deviation of Weekly Returns [B]	1.9%	2.1%	1.7%	2.3% [C]
Total Net Gains	498%	253%	32%	157%
Share of Net Gains of All Phases	53%	27%	3%	17%
S&P 500 P/E, average	17.5	13.7	15.2	15.7
GDP-Nominal Growth/Week (b April 4,1947)	0.13%	0.11%	0.13%	0.11%
GDP-Real Growth/Week (b April 4, 1947)	0.08%	0.06%	0.08%	0.04%
Implied Inflation/Week (GDP-N less GDP-R)	0.05%	0.05%	0.05%	0.07%

Figure 37. Statistics for the Mega Sentiment Cycle phases, January 1943 – September 2022. The table summarizes four phases of the Mega Sentiment Cycle, including average length, cumulative gains, price-to-earnings (P/E) ratio, and average nominal GDP growth rate.[60] [61]

Unfortunately, data that would provide more complete profiles of these phases, such as corporate profitability, are not readily available for this lengthy period.

[60] CPM Investing LLC calculations using:
U.S. Bureau of Economic Analysis. National Income and Product Accounts.
https://www.bea.gov/data/economy/national;
Shiller RJ. Online Data—Robert Shiller.
http://www.econ.yale.edu/~shiller/data.htm;
MeasuringWorth and public market sources.
https://www.measuringworth.com/datasets/DJA/

[61] Note: A. Higher values indicate better performance. B. Lower values indicate better outcomes. C. Phase 4 standard deviation of returns is significantly higher than Phase 1's (bootstrap test, $p < 0.05$).

Observations

- Phase 1 begins when the Inner Orbital Center-Sun-Outer Orbital Center angle is zero degrees. From this point to when the Anxiety-Free Period occurs is the most optimistic phase outside of an Anxiety-Free Period. Segment 1 has lasted an average of 3.4 years.
- Phase 2 begins at the end of the Anxiety-Free Period (A) (90 degrees) and lasts until the Inner Orbital Center-Sun-Outer Orbital Center angle is 180 degrees. Since 1943, Phase 2 has lasted an average of 1.9 years.
- Phase 3 begins as the Inner Orbital Center-Sun-Outer Orbital Center angle moves past 180 degrees toward the next Anxiety-Free Period (B) at the 90-degree position. Since 1943, Phase 3 has lasted an average of 1.8 years.
- Phase 4 begins after the Anxiety-Free Period (B) and lasts until the Inner Orbital Center-Sun-Outer Orbital Center angle returns to zero degrees. Since 1943, Phase 4 has lasted an average of 3.4 years.

Study G – Difference Among Phases of the Mega Sentiment Cycle

Phase 1 stands out as especially favorable for the stock market. It accounts for only 32% of all weeks in the four phases between January 1943 and October 2022 yet produces 53% of total net investment returns. Perhaps most important, it also has a higher average S&P 500 P/E ratio[62] and the difference is significant: the likelihood that the four groups would exhibit this distribution of average P/E ratios by chance is less than 0.1% ($p < 0.001$), highlighting the heightened investor optimism during Phase 1.

By contrast, Phase 4 makes up the largest share of weeks (33%) but delivers only 17% of the total gains. While the average weekly returns across the phases are not significantly different, the variability of returns is: Phase 4's standard deviation is significantly higher ($p = 0.011$) than Phase 1's, which indicates that investors in Phase 4 face considerably greater volatility without proportionate gains.

Taken together, these results highlight why Phase 1 of the Mega Sentiment Cycle is a critical period of long-term market growth. Over the sample period, Phase 1 produced a cumulative net investment gain of nearly 500 percent, far exceeding the more modest returns observed in the other phases (253 percent in Phase 2, 32 percent in Phase 3, and 157 percent in Phase 4). Importantly, this strong performance was achieved with relatively low volatility: the standard deviation of weekly returns in Phase 1 was 0.0198, the second-lowest of the four phases and statistically lower than the higher-volatility environments of Phases 2 and 4. This combination of high cumulative gains and comparatively lower risk shows that being invested during Phase 1 has been essential to capturing long-term market gains.

Further demonstrating their emotion-based origin, these differences in return and valuation, however, are not matched by differences in real economic growth. Both nominal and real GDP growth are statistically indistinguishable across the four phases ($p = 0.99$), indicating that investor sentiment, rather than accurate foresight about economic conditions, likely drives much of the observed variation in market outcomes. Thus, while there are major differences in stock market returns and investor expectations over the four phases as indicated by the P/E ratios, actual economic growth is similar across the four phases. This

[62] Source for the Standard & Poor's 500 Index (S&P 500) price-to-earnings ratio: Multpl.com. "S&P 500 P/E Ratio." Available at: https://www.multpl.com/

supports our view that we are discussing emotion-based sentiment as opposed to investors being able to collectively intuit economic growth in the "wisdom of crowds" sense. [63]

Study G: Market Performance Across Four Orbital Geometry Phases (1943–2022)

Purpose:
To examine how stock market performance, valuation, and economic growth vary across the four angular phases formed by the cyclic positions of the Inner and Outer Orbital Centers.

Key Results:
– Phase 1: Only 32% of all weeks between Jan 1943 and Oct 2022 yet produced 53% of total net investment gains. Highest average S&P 500 P/E ratio. Probability of observing this P/E distribution by chance: < 0.01%, indicating heightened investor optimism.
– Phase 4: Largest share of weeks (33%) but contributed only 17% of total gains.
– Real economic growth (nominal and inflation-adjusted GDP) is statistically indistinguishable across all four phases ($p = 0.99$).

Interpretation:
Major differences in market returns and valuations occur across the four orbital geometry phases, despite similar real economic growth. This pattern suggests that shifts in investor sentiment, rather than differences in actual economic fundamentals, are likely responsible for the observed variations in market outcomes.

Appendix Reference:
See Appendix T for methodology, phase definitions, and statistical tests for returns, valuations, and economic growth.

These Shifts May Affect the Economic Cycle

Considering the long duration of the Mega Sentiment Cycle, we believe physics-induced sentiment conditions may also affect the underlying business cycle and economic growth. Business leaders are likely affected by the same physics-based sentiment drivers. If they have an optimistic bias, they may invest more in their business, thereby inducing economic growth. In contrast, it seems most plausible that the shifts in sentiment that occur every few weeks relate mostly to emotion as opposed to real economic changes. For simplicity, we discuss all naturally occurring shifts as affecting only investor sentiment and being independent of economic considerations.

Recent Phases of the Mega Sentiment Cycle

Figure 38 below shows the last full Mega Cycle that started in early 2009 and continued until the fall of 2022. We are currently in Phase 1 of the next Mega cycle, which began afterward, in fall 2022. This phase will continue until the Anxiety-Free Period that begins mid-2026.

[63] Surowiecki, J. (2004). The wisdom of crowds: Why the many are smarter than the few and how collective wisdom shapes business, economies, societies, and nations. New York, NY: Doubleday.

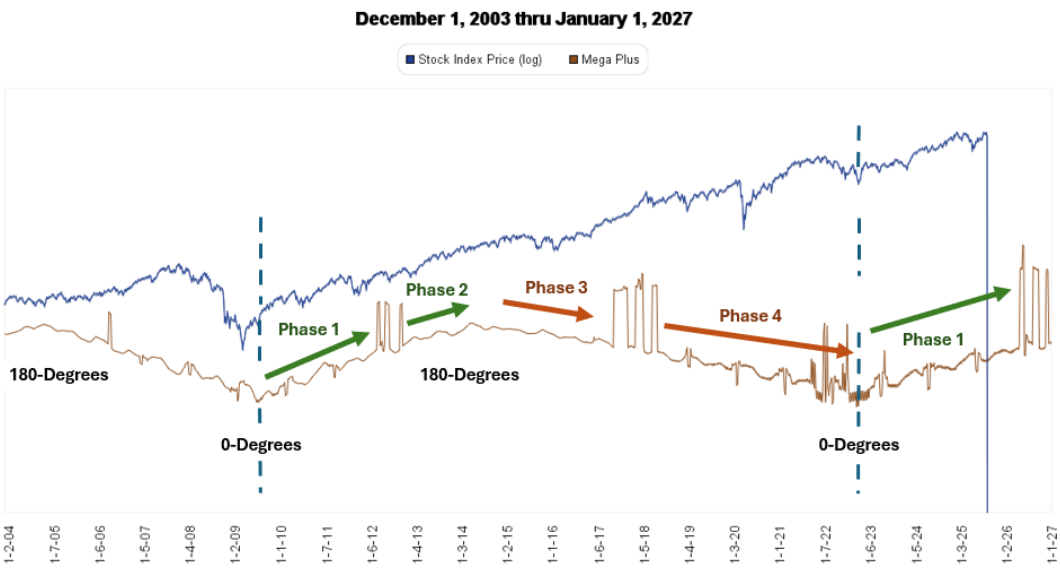

Figure 38. Diagram of the Mega Sentiment Cycle phases from 2004 to 2027. This graph shows the four phases of the Mega Sentiment Cycle and the timing of Anxiety-Free Periods. The angle of the Inner Center-Sun-Outer Center are shown. Sources: CPM Investing LLC calculations using data from NASA, MeasuringWorth, and public market sources. 'U.S. stocks' and 'U.S. stock market' refer to the DJIA, S&P 500, or related ETFs depending on the period.

The statistics on Phase 1 described earlier suggest that, compared to other phases of the stock market, investors currently have the following biases:

- They will tolerate high valuations (suggesting that high valuation ratios alone are unlikely to trigger a broad market downturn),
- React less negatively to negative economic and market news and events, and
- Not easily panic.

These biases will remain in place to at least the first 90-degree configuration event of the 2026 Anxiety-Free Period expected to begin in mid-2026.

IX. Estimating the Likelihood of Widespread Panic

Much of our early work on physics-based sentiment drivers was centered on identifying the forces that affect our custom measures of market resilience for each major stock market index (Market Resilience Indexes). These indexes are based entirely on price action and are designed to reflect the changes in price acceleration. While we believe our acceleration metrics are superior to commonly used metrics, they are conceptually like Wilder's RSI first mentioned in the introduction of this paper. Figure 39 below shows a simplified diagram of the relationship between a U.S. stock market index and our two main Market Resilience Indexes.

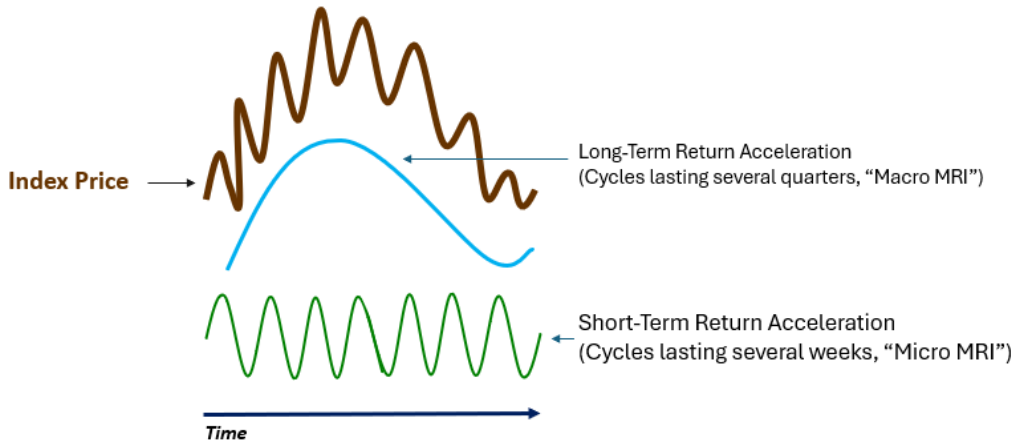

Figure 39. Diagram of the Market Resilience Indexes. This graph shows the market price level and the Macro and Micro Market Resilience Indexes. Source: CPM Investing LLC.

A key advantage of our Market Resilience Indexes is that, although they are calculated solely using market prices, they exhibit inflection points that correspond with solar energy metrics, especially the Oulu NM series. This linkage suggests that our Market Resilience Indexes are aligned with the physical influences that affect the Oulu NM series.

During the development of our price acceleration indexes, we drew inspiration from the Technology Adoption Cycle, a model that helps explain how new ideas spread through a population of decision-makers. The cycle was popularized by Geoffrey Moore in his 1991 book *Crossing the Chasm: Marketing and Selling High-Tech Products to Mainstream Customers*.[64] According to Moore, adoption follows a sequential pattern through segments of the population, each with distinct decision criteria that includes the actions of the prior group.

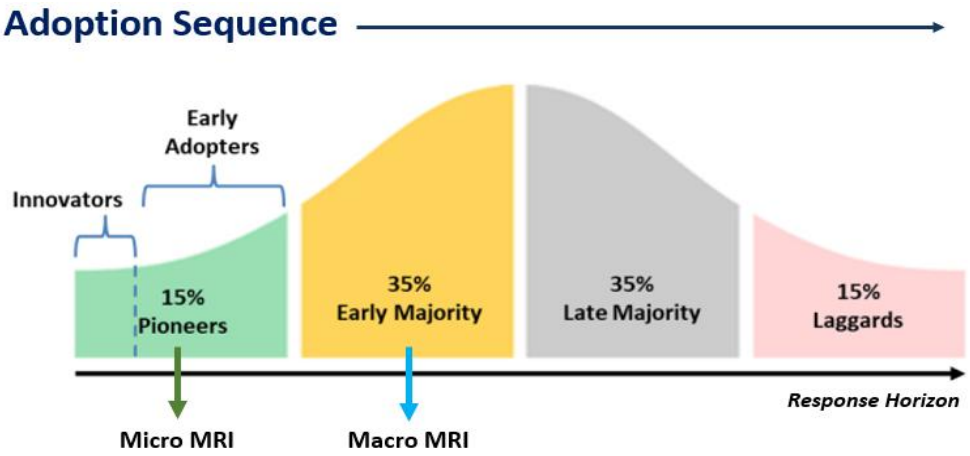

Figure 40. Diagram of the Technology Adoption Cycle. This graphic shows the four investor groups associated with the Technology Adoption Cycle. Source: CPM Investing LLC.

[64] Moore GA. Crossing the chasm: marketing and selling high-tech products to mainstream customers. New York: HarperBusiness; 1991.

For simplicity, we combine Moore's Innovators and Early Adopters into a single group, which we call *Pioneers*. Guided by the Technology Adoption Cycle framework, the relative size of investor groups and their typical behavior in response to the adoption of new investment outlooks are as follows:

- The Pioneers, those most likely to adopt a new economic outlook first, comprise approximately 15% of active investors.
- The Early Majority, based on market validation they believe to be driven by the Pioneers, is next to adopt a new outlook – comprise approximately 35%.
- The Late Majority, based on market validation they believe to be driven by the Early Majority, is next to adopt a new outlook – comprise approximately 35%.
- The Laggards, those who are slowest to adopt new outlooks, make up the remaining 15%.

This framework emphasizes the importance of an integrated marketplace in which investor groups do not operate in isolation. The actions of one group influence the perceptions and decisions of other groups, creating a dynamic environment where market movements are continuously interpreted through the lens of market price. We can think of new investment outlooks – perhaps a pessimistic one replaces an optimistic one – moving sequentially through these groups.

Misinterpreting Physics-Driven Price Moves

Among professional investors, this new outlook could refer simply to a reweighting of known factors influencing the stock market rather than an entirely new outlook. Most professional portfolio managers maintain, either formally or informally, a broad mental model of the economy and markets composed of many interrelated factors. These factors are continually re-evaluated as new information becomes available. The importance, or weight, assigned to each factor is largely subjective, and market action plays a key role in shaping those judgments. When the market moves in line with expectations, these weights tend to remain stable. But when the market moves more dramatically than anticipated, portfolio managers often reassess the weights given to the positive and negative factors they are already closely monitoring.

This process of reweighting known factors based on market action is consistent with longstanding theories in financial economics. Scholars have argued that financial market prices are rich in information, reflecting the aggregation of knowledge, beliefs, and expectations across all participants. Stephen Ross,[65] for example, emphasized that prices are not simply the outcome of trades, they are signals that convey information about risk, return, and value. In this framework, market prices reflect the collective assessment of all currently available information. When prices change, it typically signals either the arrival of new information or a reassessment of the relevance or weight of existing factors.

When price movements are driven not by new or revised economic data, but by sentiment shifts that occur naturally and independently of fundamentals, investors make inaccurate inferences about other investor groups and economic and market conditions. They may conclude that an adjacent investor group has new or better information. In such cases, investors may mistakenly treat the physics-induced shifts as meaningful signals. As they revise their probabilities and weights based on physics-driven price moves, their decision-making becomes increasingly decoupled from economic reality. If one group adjusts this

[65] Ross SA. The arbitrage theory of capital asset pricing. J Econ Theory. 1976;13(3):341-60. https://doi.org/10.1016/0022-0531(76)90046-6

outlook, other investor groups will be influenced. This dynamic can magnify stock market price movement independent of economic considerations.

Sizing the Impact of the Drivers

The Technology Adoption Cycle gives guidelines for the sizes of the different investor groups. We believe the longer-term sentiment cycles associated with the Mega Sentiment Cycle are more relevant to the Late Majority and Laggard groups, whose reactions shape broader market moves over time. In contrast, short-term physics-based drivers, such as the Micro Driver, tend to influence the rapidly responding Pioneers. Figure 41 below shows various physics-based drivers, their associated investor groups and their proportion of the likely stock traders, and the market price metrics that track market movements. The predicted Anxiety-Free Periods and M-Spike episodes are not in this figure because they supersede the dynamics it describes.

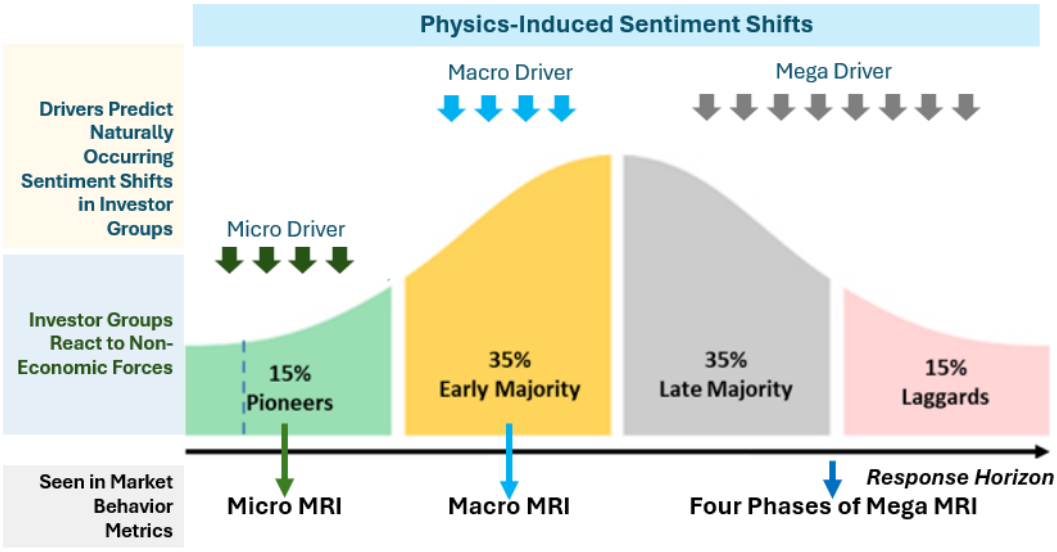

Figure 41. Diagram of the Technology Adoption Cycle. This graphic shows the four investor groups associated with the Technology Adoption Cycle along with the related physics-based drivers. Source: CPM Investing LLC.

To determine the total proportion of investors predisposed to pessimism at a given time, we can calculate the proportions of the investor groups affected by pessimistic physics-based drivers. If both the Micro and Macro Drivers are predisposed to pessimism, this framework implies that approximately 50% of market participants (the Pioneers and Early Majority) share that stance. If the phase of the Mega Cycle is Phase 1 (as it is as of this writing), then the other half of market participants is predisposed to optimism. With these conditions, a stock market decline may occur if there is an economic need for a price decline, but a meaningful downturn (e.g., a loss greater than 30%) has a low probability of occurring compared to other phases.

The sentiment environment in early 2020 before the COVID Crash is another useful example. At that time, the Mega Sentiment Cycle was in Phase 4, which indicates a predisposition toward pessimism for the Late Majority and Laggards representing about half of the likely stock trading population. The Macro physics-based driver representing the Early Majority also indicated pessimism for another 35%. Under these conditions, approximately 85% of likely traders were predisposed to pessimism. When the COVID-19 pandemic created a genuine economic shock, markets responded with a sharp decline, consistent with

the dynamics predicted by the condition of the physics-based drivers. As noted earlier, there was an M-Spike just before the COVID Crash. Had there been no economic catalyst (i.e., no pandemic), it is conceivable that the stock market might have gone through that period with only a modest drop in prices.

This framework also implies that if the Micro Driver alone indicates a predisposition to pessimism, only 15% of the investing population has this bias. As such, it is typically insufficient to trigger a major market decline. Shifts in the Micro Driver occur with high regularity over time.

While the percentage estimates are approximations, the framework offers a structured way to assess the likelihood of widespread investor panic.

X. Upcoming 2026 Anxiety-Free Period

From now until the first 90-degree configuration event of the 2026 Anxiety-Free Period, we expect the market will avoid mass panic across multiple investor groups. The optimism associated with Phase 1 of the Mega Sentiment Cycle, which began in the fall of 2022, should continue to the beginning of the first 90-degree configuration in April of 2026. The first 90-degree event will begin in early May, with the highest level of physics-induced euphoria expected in late May when the Inner and Outer Orbital Centers are 90 degrees apart. Appendix U gives the dates for the upcoming Anxiety-Free Period and M-Spike.

Broad Context

Phase 1 of the current Mega Sentiment Cycle runs from October 2022 until the first 90-degree configuration event of the 2026 Anxiety-Free Period. If historical patterns are held, this phase will have low likelihood of widespread investor panic and losses greater than 30 percent. Investors are unlikely to be concerned about high stock valuations, and economic imbalances are likely to build, creating the economic need for a price decline that will later be precipitated by a shift in orbital geometry.

Structure of the 2026 Episode

The 2026 Anxiety-Free Period will have three 90-degree configuration events. Based on the changes observed in 2017, during these events and especially the first, the electromagnetic standing waves (modes 2 and 3) will become more stable. The first event, shown as the first column in Figure 42 below begins in late April, suggesting that late February may be a good time to become fully invested in the stock market. This first event ends in May, marking the highest peak across all three events of naturally occurring optimism. By early August, optimism should return, although not at the peak levels reached in late May. The third event ends in early December.

Influence of an M-Spike

The first column of the 2026 Anxiety-Free Period also coincides with a moderate M-Spike. Its downward leg falls in May, the same time the first event concludes, reinforcing the risk that June 2026 will be unstable. Volatility is therefore likely to rise in April and May, with a sharp decline in optimism at the end of the first column.

Strategy Guidance

A successful strategy for navigating an Anxiety-Free Period is to be positioned in the market a several weeks before the period begins, remain invested through its highest point shown for cluster, and then follow the Micro Market Resilience Index (or its driver) out of the market.

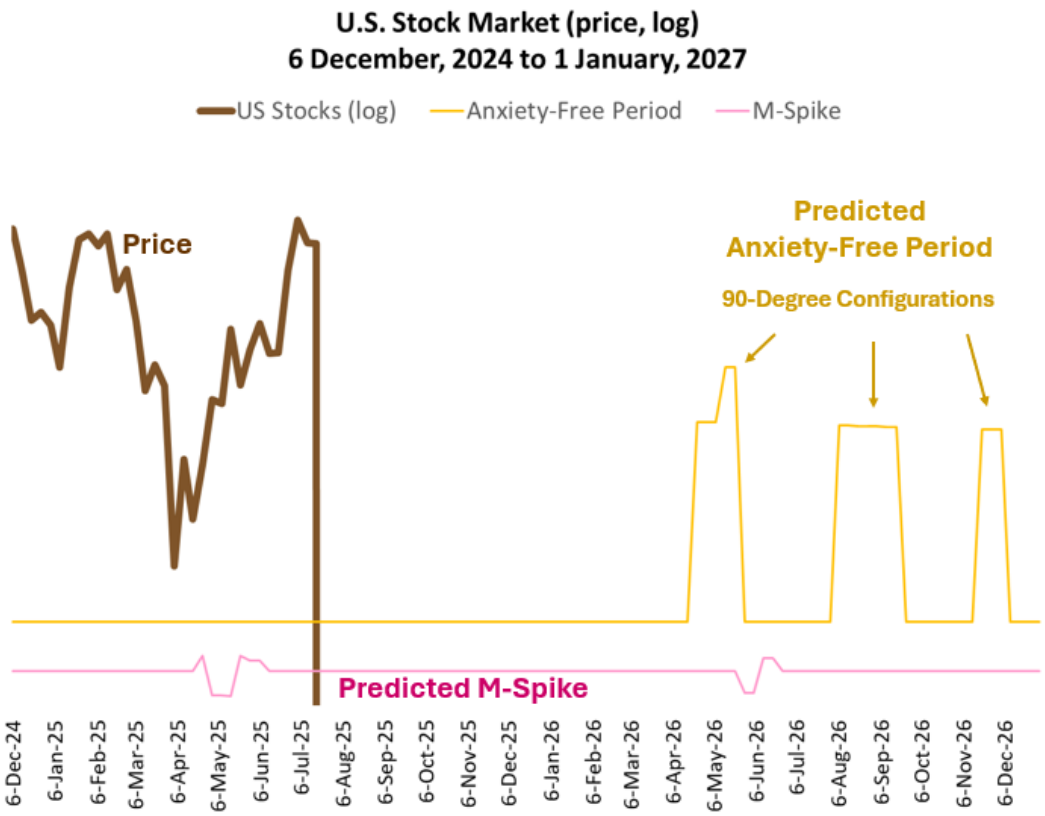

Figure 42. U.S. stock market price level (log) from December 6, 2024, to January 1, 2027. The chart shows the market through July 18, 2025, along with the drivers for the three 90-degree configuration events of the 2026 Anxiety-Free Period and the M-Spike. Sources: CPM Investing LLC calculations using data from NASA, MeasuringWorth, and public market sources. 'U.S. stocks' and 'U.S. stock market' refer to the DJIA, S&P 500, or related ETFs depending on the period.

XI. Conclusion

There is no question that economic and market conditions influence stock prices. However, the emotional biases that investors have when interpreting new information also have a meaningful and measurable impact. Our studies reveal statistically significant, and highly predictable, relationships between orbital geometry (i.e. the 90-degree configuration between the Inner and Outer Orbital Centers that give rise to Anxiety-Free Periods), and several key metrics associated with investor sentiment.

The null hypothesis underlying our various studies is that orbital geometry has no effect on solar energy emissions, and that solar energy emissions, in turn, have no influence on investor sentiment. The statistical evidence presented across multiple independent studies supports rejecting this null hypothesis.

Each study is grounded in the same causal framework: the distribution of mass and electromagnetic forces in the solar system influences solar energy dynamics, which subsequently affects investor sentiment via biologically plausible intermediaries. The following empirical observations support this framework:

Study A: Predicted 14-week RSI for the U.S. Stock Market from 2000 to 2024

a) Short-term changes in orbital geometry are associated with short-term changes in sentiment as measured by the 14-week RSI.
b) Predicted RSI is a useful benchmark for evaluating Actual RSI. Underperformance of the Actual compared to the Predicted suggests investors may hold a negative view of market conditions, even during rising markets.

Study B: The Intensity of 90-Degree Configurations and Anxiety-Free Periods Varies Over Time

a) Conceptually, intensity fluctuates with the tightness of clustering of the members of the Outer Orbital Group. For computational simplicity, we use the distance between the Sun and the Outer Orbital Center as a proxy for the tightness of clustering.
b) Our findings suggest that the impact of orbital geometry on human behavior changes over time, complicating detection and confirmation of any relationship between them.
c) This helps explain why some 90-degree configuration events appear to exhibit strong market influence and Anxiety-Free Periods (e.g., 1987, 1937), while others show little impact (e.g., 2006).

Study C: Eleven 90-Degree Configuration Clusters and Anxiety-Free Periods Since 1933

a) The eleven 90-degree configuration clusters correspond to statistically significant differences in market performance before and after the peak in market prices. These define the Anxiety-Free Periods and the abrupt price declines after them.
b) This indicates that changes in orbital geometry are related to important boom-and-bust market patterns.

Study D: Patterns in Global Electromagnetic Standing Waves Correspond to Predicted 90-Degree Configuration Events in the 2017 Anxiety-Free Period

a) The 90-degree configuration events during this period are significantly aligned with changes in electromagnetic standing wave frequency stability.
b) The M-Spike events also correspond to changes in electromagnetic standing wave patterns, although not reaching a level of statistical significance.
c) These observations support our hypothesis that electromagnetic standing wave stability acts as a transmission pathway between solar variation and human sentiment.

Study E: Twenty-six 90-Degree Configuration Events and Two Solar Energy Metrics

a) The 90-degree configurations are associated with measurable shifts in the energy dynamics of the Sun itself, as indicated by sunspot activity.
b) These shifts can be detected on Earth in Oulu NM readings.

Study F: Professional Investors Have an Analytical Bias:

a) Our analysis of 831 professional investors indicates they are significantly more analytical than the general U.S. population.
b) Independent electroencephalography studies suggest that analytical decision making is centered in the brainwave rage of 13-30 Hz, which overlaps with the electromagnetic waves displaying similar patterns to the physics-based drivers in Study D.

XI. Conclusion

Study G: Four Phases of the Mega Sentiment Cycle

a) The same orbital geometry that leads to Anxiety-Free Periods also maps to four distinct long-term sentiment phases.
b) Phase 1 of the cycle has high cumulative returns and high market valuation ratios compared to the other three phases. Yet there is no discernable difference in economic growth across the four phases.
c) We are currently in Phase 1. It began in late 2022 and will end with the 2026 Anxiety-Free Period.

The naturally occurring shifts in sentiment are additive to the economic and market forces affecting stock prices. Generally speaking, the magnitude of market declines is determined primarily by the condition of economic and market fundamentals, but the timing of any needed price adjustment is determined by naturally occurring sentiment shifts.

The naturally occurring shifts in sentiment we observe are not affected by actual economic or market conditions. Because of this, we have mixed thoughts about the implications of our findings. The patterns are consistent, and the statistical evidence is strong enough to conclude that we as investors allow systematic and highly predictable non-economic influences to shape our economic decisions. This is an undesirable situation.

These sentiment shifts can be mitigated, if we recognize their existence. Understanding when these dynamics are most likely to arise allows us to shift focus toward a stronger foundation grounded in economic and market fundamentals. A useful analogy is the way solar eclipses once triggered collective fear. Today, with understanding and predictive tools, eclipses no longer provoke irrational reactions. We believe investor sentiment can be similarly stabilized by increasing awareness of its environmental drivers.

In summary, we demonstrated that orbital geometry of the solar system can serve as predictive markers of physics-based influences on sentiment. By refining our understanding of these subtle forces, we may improve both investment performance and systemic stability by reducing the impact of misattributed emotions in financial decision-making.

This paper aims to logically outline both the observed relationships and the mechanisms that may underlie them. While the causal chain remains early in its development, we hope this research provides a foundation for deeper exploration.

Philosophical Implications

Looking back over the last 12 decades of stock market behavior, two broader thoughts emerge. First, the two great market crashes of 1929 and 2008—each correcting profound economic excesses—were preceded by an absence of naturally occurring pessimism. We note the late 1920s case in Appendix M. The 2006 Anxiety-Free Period was among the weakest since 1920, as shown in Figure 16. Taken together, these observations and our review of other periods suggest that the market—and perhaps the economy—are healthier when investors pass through alternating phases of optimism (aspirational thinking) and pessimism (critical thinking).

When optimism is not periodically checked by doubt, it drifts into ungrounded speculation; when pessimism is not lifted by hope, it hardens into paralysis. Enduring progress seems to depend on balance—something like walking a middle path through the extremes of human sentiment. Similar

recognition arose in the Vienna School of Economics during the late 19th and early 20th centuries. Ludwig von Mises, for example, emphasized that recessions and downturns, while often painful, are necessary stages that clear distortions and make way for genuine and lasting growth.[66]

Second, we should consider how this response might be beneficial from an evolutionary perspective. Restated for the hypothesized mechanism: how could humans collectively benefit from being sensitive to a change in standing wave stability across a particular threshold? The Sun's energy emissions are always turbulent, but only less so at times. Why would we have developed a sensitivity to that threshold? Perhaps because it reinforced the same kind of balance required in markets. As a species, we may have gained an evolutionary advantage in making better collective decisions by operating near the cusp between optimism and pessimism. Extended periods of either bias—unbroken optimism or unyielding pessimism—create real imbalances. But the alternation, the middle way of moving through both, may have helped us not only to survive but also to thrive, by keeping our choices rooted in reality while still leaving room for aspiration and possibility.

[66] Mises L. The Theory of Money and Credit. London: Jonathan Cape; 1934 (orig. 1912). https://mises.org/library/theory-money-and-credit

Appendices

Appendix A - Key Figures in Research on Solar Energy Variation and Economic Patterns

A number of researchers since the early 19th century have proposed that solar activity cycles, particularly the ~11-year sunspot cycle, may relate to patterns in commodity prices, economic recession, or broader human behavior. Although these ideas remain outside mainstream economic science, they form a thread of interdisciplinary inquiry suggesting that natural cycles may resonate with collective human systems.

William Herschel (1801)

In 1801, Herschel, better known for his astronomical discoveries, published an analysis linking variations in sunspot frequency to English wheat prices. Observing fewer sunspots over several decades (during the Dalton Minimum), he reported that wheat prices peaked precisely when solar activity was low. Though his methods were later criticized, he initiated the idea of a solar, climate, and economy connection.
Why it matters: Herschel was the first to suggest a statistical link between solar variation and economic indicators, laying the groundwork for later hypotheses about solar-economic rhythms.
Seminal work: Herschel W. *Observations tending to investigate the nature of the Sun…* Philosophical Transactions of the Royal Society of London, 1801.[1]

William Stanley Jevons (1875/1878)

British economist Jevons proposed that "commercial crises" recur with a periodicity similar to the sunspot cycle, approximately 10 to 11 years. He noticed that financial panics often coincided with solar maxima and theorized that solar-induced climate variations affected agricultural output, which in turn influenced economic conditions. Though cautious about drawing definitive conclusions, he introduced the solar cycle hypothesis into the framework of academic economics.
Why it matters: Jevons brought the sunspot and market connection into mainstream economic discourse, influencing future economic and sociological analysis.
Seminal work: Jevons WS. Commercial Crises and Sunspot Periodicity. Journal of the Royal Statistical Society, 1878 (and earlier pamphlet versions).[2]

Samuel Benner (1875)

Samuel Benner, an Ohio farmer impacted by the Panic of 1873, published *Benner's Prophecies of Future Ups and Downs in Prices*, in which he mapped commodity and business cycles of approximately 8 to 11 years. These patterns coincided with the rise and fall of sunspot activity. While Benner did not propose a mechanistic explanation, his charts forecast "panic years" and "good times" based on natural cycles.
Why it matters: Benner helped popularize cycle forecasting, associating recurring economic phases with solar-linked periodicity.

[1] Herschel W. Observations tending to investigate the nature of the sun in order to find the causes or symptoms of its variable emission of light and heat. Philos Trans R Soc Lond. 1801;91:265-318. https://royalsocietypublishing.org/doi/10.1098/rstl.1801.0015
[2] Jevons WS. Commercial crises and sun-spots. J R Stat Soc. 1878;41(2):350-72. https://www.jstor.org/stable/2338849

Seminal work: Benner S. Benner's Prophecies of Future Ups and Downs in Prices. Wooster, OH: The Author, 1875.[3]

Alexander L. Chizhevsky (1922–1938)

A Soviet heliobiologist, Chizhevsky linked sunspot cycles to collective human behavior. In *Physical Factors of the Historical Process* (translated edition, 1938), he analyzed centuries of revolutions, wars, and epidemics, finding that peaks in solar activity coincided with periods of major social unrest. Though he did not focus on markets directly, he proposed that solar cycles modulate group dynamics on a mass scale.
Why it matters: Chizhevsky produced one of the first large-scale, cross-disciplinary empirical studies connecting solar cycles to social upheaval.
Seminal work: Chizhevsky AL. Physical Factors of the Historical Process. Paris: Imprimerie de Navarre, 1938.[4]

W.D. Gann (1927–1941)

W.D. Gann was an early 20th-century trader and theorist who developed forecasting techniques based on the idea that price and economic trends followed natural, repeating cycles. In his 1927 book *The Tunnel Thru the Air*, written as a fictional narrative, Gann embedded references to planetary cycles, solar angles, and cosmic rhythms, which he believed had predictive value in financial markets. He elaborated these ideas in *How to Make Profits in Commodities* (1941), introducing time cycles and geometric methods rooted in his belief that markets were governed by external natural laws.
Why it matters: Gann's work kept interest in planetary and solar influences alive within practitioner circles during a time when such views were being dismissed by academic economics.
Seminal works:
Gann WD. The Tunnel Thru the Air: Or, Looking Back from 1940. New York: W.D. Gann, 1927.[5]
Gann WD. How to Make Profits in Commodities. New York: W.D. Gann, 1941.[6]

Edward R. Dewey (1930s–1971)

As founder of the Foundation for the Study of Cycles, Dewey compiled global time-series data across economic, biological, sociological, and astronomical domains to show recurring 11-year cycles. In *Cycles: The Science of Prediction* (1971), he documented correlations between sunspot activity and a range of economic indicators. While avoiding direct causal claims, he emphasized the empirical regularity of these patterns and advocated for serious interdisciplinary research.
Why it matters: Dewey established the formal institutional framework for cycle research and brought statistical rigor to solar-economic correlations.

[3] Benner S. Benner's prophecies of future ups and downs in prices. Wooster (OH): The Author; 1875. https://archive.org/details/bennerprophecies00benn
[4] Chizhevsky AL. Physical factors of the historical process. Paris: Imprimerie de Navarre; 1938. https://archive.org/details/ChizhevskyPhysicalFactors1938
[5] Gann WD. How to make profits in commodities. New York: Lambert-Gann Publishing Co.; 1941. https://archive.org/details/HowToMakeProfitsInCommodities1941
[6] Gann WD. How to make profits in commodities. New York: Lambert-Gann Publishing Co.; 1941. https://archive.org/details/HowToMakeProfitsInCommodities1941

Seminal work: Dewey ER. Cycles: The Science of Prediction. New York: Holt, Rinehart and Winston, 1971.[7]

Theodor Landscheidt (1974–1989)

A German solar physicist, Landscheidt investigated how planetary-induced variations in solar angular momentum might influence solar cycles and, by extension, terrestrial climate and economic rhythms. In *Sun–Earth–Man: A Mesh of Cosmic Oscillations* (1989), he argued that planetary alignments govern the timing of solar minima and maxima, which in turn coincide with multi-decade economic and environmental fluctuations.
Why it matters: Landscheidt helped bridge astrophysical modeling with long-term social and economic cycle theory, inspiring new investigations into solar and planetary harmonics.
Seminal work: Landscheidt T. Sun–Earth–Man: A Mesh of Cosmic Oscillations. Cycles Research Institute reprint, 1989.[8]

Ray Tomes (1990s–present)

Tomes extended Dewey's work by proposing a unified harmonic theory of cycles. His models suggest that patterns in economics, solar activity, and geophysical systems arise from shared harmonic structures. He posits that financial market behavior reflects resonant frequencies derived from planetary and solar motion, observable through mathematical analysis of time-series data.
Why it matters: Tomes advanced cycle theory by framing solar and economic patterns within a larger harmonic structure that unifies seemingly disparate systems.
Seminal work: Tomes R. Towards a Unified Theory of Cycles. Conference paper, 1990s.[9]

Paul Macrae Montgomery (late 20th century)

Montgomery was a financial commentator known for his work on sentiment-based contrarian indicators, including the well-known "magazine cover" signal. He speculated that investor mood and market psychology might also reflect deeper environmental or cosmic cycles, including solar and lunar influences, though he did not formalize these ideas into academic theory.
Why it matters: Montgomery introduced cycle-based speculation into professional finance, offering intuitive bridges between environmental rhythms and investor behavior.
Seminal reference: Montgomery PM. Various commentary pieces, including "Beware the Ides of March," published throughout the late 20th century.

Comment

These researchers represent a lineage beginning in the early 19th century, when solar activity was first linked to agricultural yields and market behavior. That lineage continued through institutional cycle research in the mid-20th century and into more recent approaches that explore either external cycle periodicity or biological sensitivity to environmental variation. Their collective work indicates that speculation about solar-cycle influence on economic behavior has a long, though unconventional,

[7] Dewey ER. Cycles: the science of prediction. New York: Holt, Rinehart and Winston; 1971. https://archive.org/details/cycles-the-science-of-prediction
[8] Landscheidt T. Sun–Earth–man: a mesh of cosmic oscillations. Pulheim: Cycles Research Institute; 1989. http://www.john-daly.com/solar/landscheidt/secm.htm
[9] Tomes R. Interplanetary cycles and their terrestrial effects. Cycles. 1990;41(4):149-58. https://ray.tomes.biz/cycles.html

historical pedigree. Broad acceptance of this reasoning, however, has been limited by the absence of a plausible, physically observable mechanism supported by empirical data.

Interest in solar and natural cycle theories reached its institutional peak during the mid-20th century, particularly through the work of Edward Dewey and the Foundation for the Study of Cycles. Over time, mainstream economics and finance shifted toward models grounded in mechanistic clarity and statistically robust outcomes.

Bibliometric surveys of academic databases show that very few peer-reviewed articles—likely fewer than ten per decade—examined a direct connection between solar activity and human mood, behavior, or economic sentiment from the 1940s through the 1990s. The number of studies declined over time: several exploratory papers appeared in the 1940s and 1950s, but by the 1960s through the 1980s, only one or two papers per decade addressed the topic, and none gained lasting recognition in mainstream journals. This drop in publication reflects a broader decline in institutional support for solar-sentiment research during that era.

More recent work has followed two general arenas of research. Some researchers emphasize harmonic interpretations, which propose that recurring cycles in economic or financial behavior arise from mathematically resonant structures tied to planetary and solar motion. These approaches often assume that natural systems, including markets, respond to long-term harmonic waveforms and that predictive power lies in detecting frequency alignment over time. Ray Tomes is one of the most visible current proponents of this view and has developed a unified theory of cycles based on harmonic principles across multiple domains.

In contrast, sentiment-based interpretations focus on the possibility that short-term variation in solar energy, such as changes in solar irradiance, geomagnetic activity, or electromagnetic field structure, can influence neurobiological systems that regulate mood, motivation, and judgment. In this view, economic behavior may be modulated not by memory of past cycles but by current environmental inputs that affect collective risk tolerance and decision-making. While memory and path dependence may shape long-term economic cycles, real-time physiological responses are likely more relevant to short-term sentiment shifts. Our work is primarily in this arena, although we see evidence of a memory of resonant structures as well.

Appendix B – Studies Linking Solar Energy Variation to Biology and Emotion

- Biological stress responses, including elevated heart rate, have been linked to increases in solar wind intensity, suggesting a direct impact on the autonomic nervous system.[1]
- There is an increased incidence of alterations in blood flow, such as elevated systolic and diastolic blood pressure and epileptic seizures, associated with solar activity.[2]
- Heart attack rates and coronary disease events have been observed to rise during periods of geomagnetic disturbance.[3] [4]
- Neurological and psychiatric conditions, including depression and other mental illnesses, are also reported to increase during periods of elevated solar and geomagnetic activity.[5]
- Suicide attempts have been statistically linked to monthly variations in solar energy metrics such as Kp10.[6] Additional earlier findings point to increases in suicides and homicides during geomagnetic disturbances.[7]
- Behavioral outcomes such as the frequency of car accidents have shown temporal correlations with geomagnetic activity.[8]

[1] Alabdulgader A, McCraty R, Atkinson M, Dobyns Y, Vainoras A, Ragulskis M, Stolc V. Long-term study of heart rate variability responses to changes in the solar and geomagnetic environment. Sci Rep. 2018;8(1):2663. https://doi.org/10.1038/s41598-018-20932-x

[2] Babayev ES, Allahverdiyeva AA. Effects of geomagnetic activity variations on the physiological and psychological state of functionally healthy humans: Some results of Azerbaijani studies. Adv Space Res. 2007;40(12):1941–1951. https://doi.org/10.1016/j.asr.2007.02.099

[3] Palmer SJ, Rycroft MJ, Cermack M. Solar and geomagnetic activity, extremely low frequency magnetic and electric fields and human health at the Earth's surface. Surv Geophys. 2006;27(5):557–595. https://doi.org/10.1007/s10712-006-9010-7

[4] Vencloviene J, Babarskiene R, Slapikas R. The association between solar particle events, geomagnetic storms, and hospital admissions for myocardial infarction. Nat Hazards. 2013;65:1–12. https://doi.org/10.1007/s11069-012-0310-6

[5] Gordon C, Berk M. The effect of geomagnetic storms on suicide. South African Psychiatry Review. 2003 Aug 1;6(3):24-7. https://hdl.handle.net/10520/EJC72999

[6] Nishimura T, Tsai IJ, Yamauchi H, Nakatani E, Fukushima M, Hsu CY. Association of geomagnetic disturbances and suicide attempts in Taiwan, 1997–2013: A cross-sectional study. Int J Environ Res Public Health. 2020;17(4):1154. https://doi.org/10.3390/ijerph17041154

[7] Gordon C, Berk M. The effect of geomagnetic storms on suicide. South African Psychiatry Review. 2003 Aug 1;6(3):24-7. https://hdl.handle.net/10520/EJC72999

[8] Alania MV, Gil A, Wieliczuk R. Statistical analysis of the influence of solar and geomagnetic activity on car accident events in Poland in the period of 1990–1999. Acta Phys Pol A. 2001;100(Suppl):199–207. https://doi.org/10.1016/S0273-1177(01)00377-5

Appendix C – Recent Studies Linking Orbital Geometry to Solar Activity

Researchers have explored the possibility that the gravitational interactions of planets, most notably Venus, Earth, and Jupiter, may influence the Sun's magnetic activity, manifesting as the approximately 11-year sunspot cycle. A 2016 study conducted by researchers at the Helmholtz-Zentrum Dresden-Rossendorf (HZDR) in Germany suggests that the tidal forces exerted by these planets could synchronize with the Sun's internal magnetic processes, potentially modulating solar activity.[1]

The researchers propose that the alignment of Venus, Earth, and Jupiter every 11.07 years tends to coincide with the solar minimum, a period of reduced sunspot activity. They hypothesize that even the relatively weak tidal forces from these planetary alignments might influence the Tayler instability—a magnetic phenomenon within the solar interior—thereby affecting the solar dynamo responsible for magnetic field generation.

Supporting this general hypothesis, a 2007 NASA technical report by Ching-Cheh Hung analyzed solar flare and sunspot data and found a statistically significant correlation between large solar flare events and the alignments of Venus, Earth, and Jupiter.[2] The report noted that 25 of the 38 largest known solar flares occurred when one or more of the tide-producing planets were nearly aligned with the solar event locations—either within ±10° longitude or directly opposite the Sun. The probability of this alignment pattern happening by chance was calculated to be only 0.039 percent, suggesting a potential causal link between planetary alignment and heightened solar activity.

A recent study extends this discussion beyond gravitational effects to direct magnetic coupling. Using *TESS* and *CHEOPS* observations, Ilin et al. (2025) reported that the close-in planet HIP 67522 b induces recurring stellar flares by perturbing its host star's magnetic field. The authors found that the flare rate increased roughly six-fold when the planet was near transit, demonstrating a persistent phase-locked interaction between orbital position and stellar magnetic activity.

Although the HIP 67522 system differs from the Sun in scale and geometry, the finding offers the clearest empirical evidence yet that planetary motion can modulate magnetic energy release in a star. This lends support to the broader premise that orbital geometry can influence magnetic coherence and flare production, even if the mechanism—electromagnetic rather than tidal—differs from that proposed for the Sun.[3]

Nevertheless, the broader scientific community remains skeptical. Critics argue that planetary gravitational influences are many orders of magnitude weaker than the internal forces governing solar dynamics. According to the prevailing view, the Sun's magnetic behavior is predominantly driven by internal mechanisms such as differential rotation, toroidal and poloidal magnetic fields, and convective

[1] Stefani F, Giesecke A, Weber N, Weier T. Synchronized Helicity Oscillations: A Link Between Planetary Tides and the Solar Cycle? Solar Physics. 2016;291(8):2197–2212.
https://doi.org/10.1007/s11207-016-0968-0. [Cited by 133 studies as of 2015].

[2] Hung C-C. Apparent Relations Between Solar Activity and Solar Tides Caused by the Planets. NASA Technical Reports Server (NTRS); 2007. NASA/TM-2007-214817.
https://ntrs.nasa.gov/api/citations/20070025111/downloads/20070025111.pdf. [Widely circulated, cited in follow-up observational analyses]

[3] Ilin E, Vedantham H K, Poppenhäger K, et al. Close-in planet induces flares on its host star. Nature. 2025 Jul 17; 643: 645–648.
https://doi.org/10.1038/s41586-025-09236-z

turbulence—processes which underpin the solar dynamo and are thought to operate largely independently of planetary alignments.[4] These views are discussed in Appendix D.

[4] Charbonneau P. Dynamo Models of the Solar Cycle. Living Reviews in Solar Physics. 2010;7(3). https://doi.org/10.12942/lrsp-2010-3. [Cited by over 950 articles]

Appendix D – Views on Orbital Geometry Affecting Solar Energy Emissions

The consensus among solar physicists is that planetary influences on the Sun, via gravitational or magnetic effects, are too weak to produce significant changes in solar output or magnetic variability. The dominant drivers of solar activity, including the 11-year Schwabe cycle, are explained by internal magnetohydrodynamic (MHD) processes, especially the solar dynamo within the convection zone and tachocline.

The Standard Solar Model describes the structure and energy generation of the Sun as governed by four key processes: hydrostatic equilibrium, thermonuclear fusion, radiative transfer, and convection. This model successfully explains the Sun's luminosity, size, and temperature profile, and its predictions have been confirmed by observations such as helioseismology and solar neutrino measurements.[1] According to the model, the amount of solar energy reaching each planet (known as solar irradiance) depends only on the planet's distance from the Sun, following the inverse square law:

$$I = L / (4\pi r^2)$$

where I is the irradiance, L is the Sun's total luminosity, and r is the distance from the Sun. This equation implies that irradiance decreases with the square of the distance, and there is no mechanism in the model for the planets to influence or feed back into the Sun's behavior.

Charbonneau's widely cited review outlines the theoretical and empirical basis for internally generated solar cycles, making no allowance for external (planetary) forcing.[2] Planetary tidal forces are minuscule compared to internal forces. For example, Callebaut et al. demonstrates quantitatively that tidal effects from planets such as Jupiter are many orders of magnitude too weak to affect solar convection or magnetic field generation.[3]

Minority View: Planets May Modulate Solar Variability

A smaller body of literature argues that planetary gravitational or magnetic alignments may weakly modulate solar cycles. These models often involve harmonic analysis or hypothesize mechanisms by which small external perturbations could resonate with solar processes. This is analogous to resonant phenomenon such as a singer hitting the exact pitch as the natural resonant frequency of a crystal wine glass, causing it to shatter despite the sound waves being much weaker than the strength of glass.

Scafetta has proposed that planetary harmonics can synchronize solar cycles though "both gravitational and electro-magnetic planet-sun interactions and internal non-linear feedbacks."[4]

[1] Bahcall JN, Serenelli AM, Basu S. New solar opacities, abundances, helioseismology, and neutrino fluxes. Astrophys J Lett. 2005;621(1):L85–L88. (Cited by ~1,300 studies as August 2025).
https://doi.org/10.1086/428929

[2] Charbonneau P. Dynamo models of the solar cycle. Living Rev Sol Phys. 2010;7(3). (Cited by >1,000 studies as August 2025).
https://link.springer.com/article/10.12942/lrsp-2010-3

[3] Callebaut D, de Jager C, Duhau S. The influence of planetary attractions on the solar tachocline. J Atmos Sol Terr Phys. 2012;80:73–78. (Cited by ~50 studies as August 2025).
https://www.sciencedirect.com/science/article/abs/pii/S1364682612000892

[4] Scafetta N, Willson RC. Empirical evidences for a planetary modulation of total solar irradiance and the TSI signature of the 1.09-year Earth-Jupiter conjunction cycle. Astrophysics and Space Science. 2013 Nov;348(1):25-39.

Another example is Abreu et al., who presented a statistical link between planetary torques and long-term solar activity proxies like cosmogenic radionuclides.[5] However, their methodology and causality claims have been disputed in later studies (e.g., Poluianov et al.).[6]

[5] Abreu JA, Beer J, Ferriz-Mas A, McCracken KG, Steinhilber F. Is there a planetary influence on solar activity? Astron Astrophys. 2012;548:A88. (Cited by ~250 studies as August 2025).
https://doi.org/10.1051/0004-6361/201219997

[6] Poluianov SV, Usoskin IG, Arlt R, Leussu R. Critical analysis of a hypothesis of the planetary tidal influence on solar activity. Astron Astrophys. 2018;618:A44. (Cited by ~40 studies as August 2025).
https://arxiv.org/pdf/1401.3547

Appendix E – Geometry-Driven Sentiment Shifts Have Become More Prominent

We can measure naturally occurring shifts in sentiment and actual market conditions beginning in 1920 using our measure of short-term index price acceleration, the Micro Market Resilience Index (MRI). The short-term trends in price acceleration typically last several weeks. We show that the Micro MRI more closely tracks physics-induced sentiment shifts now than it did in the early decades of this period.

Figure D-1 below shows the period beginning in Sep 2019 and ending in May 2022, which includes the COVID crash in March 2020. Only our measure of index price acceleration, the Micro MRI, is shown as the green line. The purple line shows the Micro Driver, which predicts the path of the Micro MRI and is based on orbital geometry.

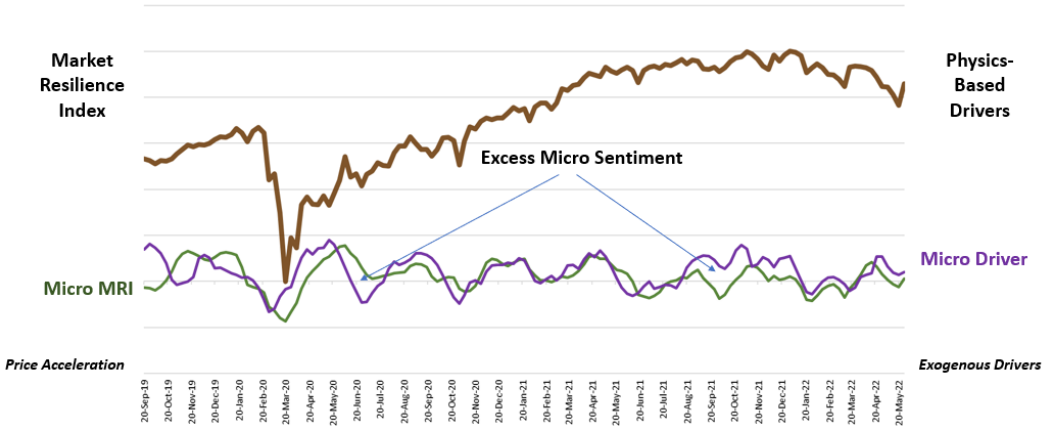

Figure D-1 Market price shown as a brown line and the Micro Driver (purple) that predicts the path of the Micro MRI under economic and market stress from 2019 through 2022. Sources: CPM Investing LLC calculations using data from NASA, MeasuringWorth, and public market sources. 'U.S. stocks' and 'U.S. stock market' refer to the DJIA, S&P 500, or related ETFs depending on the period.

The peaks and troughs of the Micro MRI line align with those of the Micro Driver, even though this chaotic period in the market. Figure D-1 above also shows the difference between the predicted path of the Micro MRI and its actual path, which we label *Excess Micro Sentiment*.

Figure D-2 below shows the Excess Micro Sentiment from 1920 through 2022.

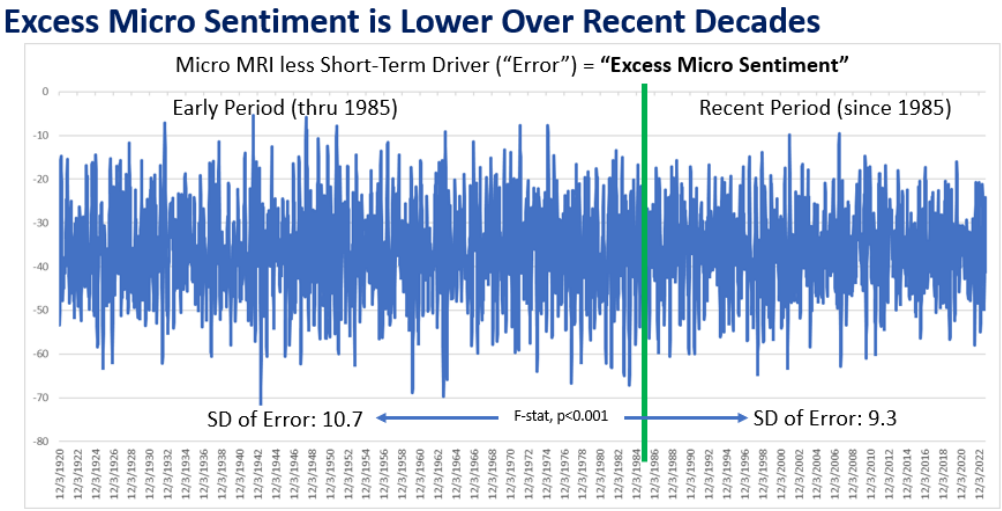

Figure D-2. Excess Micro Sentiment from 1920 through 2022. Geometry of the Inner Orbital Center and the Outer Orbital Center. Sources: CPM Investing LLC calculations using data from NASA, MeasuringWorth, and public market sources. 'U.S. stocks' and 'U.S. stock market' refer to the DJIA, S&P 500, or related ETFs depending on the period.

One can see that Excess Micro Sentiment appears to be decreasing over the last several decades.

This trend is supported by a statistical analysis of the Excess Micro Sentiment in both periods. We evaluated the standard deviation of the Micro MRI, its driver, and Excess Micro Sentiment in two periods. The Early Period covers from 1920 to 1985. The second is from 1985 through 2022.

The selection of 1985 as the boundary is based on when institutional investment managers began to make extensive use of large databases of fundamental and market data, computers for processing that data, and algorithms for making initial trading decision about a wide range of U.S. stocks. This development was marked by the Rusell Investment Group establishing a practice group focused on the assessment of quantitative investment processes in 1985. Figure D-3 below shows the results of the analysis.

	Early Period 1920-1985	Recent Period 1985-2022	Significance of Difference
1. Number of Weeks	3397	1968	n/a
2. Std Dev of Micro Driver Levels (%)	7.23	7.20	No difference
3. Std Dev of Micro MRI Levels (%)	7.62	6.48	$p < 0.01$
4. Std Dev of Excess Micro Sentiment (%)	10.7	9.3	F-Stat, $p < 0.001$

Figure D-3. Statistics related to the "early period" from 1920-1985 and the "recent period" from 1985-2022. Source: CPM Investing LLC calculations using data from MeasuringWorth and public market sources. 'U.S. stocks' and 'U.S. stock market' refer to the DJIA, S&P 500, or related ETFs depending on the period.

Given that the Micro Driver is based on normalized physical measures of orbital geometry, we would expect the standard deviation to be the same in the two samples. Row 2 in Figure D-3 above supports this view.

Row 3 shows the standard deviation of the Micro MRI in the two samples. The standard deviation in the Early Period is significantly higher than in the Recent Period.

Row 4 shows that the Excess Micro Sentiment was significantly larger during the Early Period.

These results support our view that the market is becoming more efficient with respect to company-specific, economic, and market conditions, but is not getting more efficient in pricing these physics-induced sentiment shifts. As the market becomes more efficient regarding economic variables, physics-induced investor sentiment shifts play an increasingly dominant role in market volatility.

Appendix F – Market Resilience Indexes and Wilder's RSI

In order to monitor the resilience of the stock market, in 2007 we developed proprietary metrics based on the acceleration of price changes in the US Stock market. The indexes are:

1. **Micro MRI** - shows periods of positive price acceleration that last about 13 weeks.
2. **Macro MRI** - shows periods of positive price acceleration lasting several years.
3. **Exceptional Macro MRI -** indicates (on its appearance) when the Macro MRI may develop a steeper positive slope, or (on its disappearance) a less steep slope.

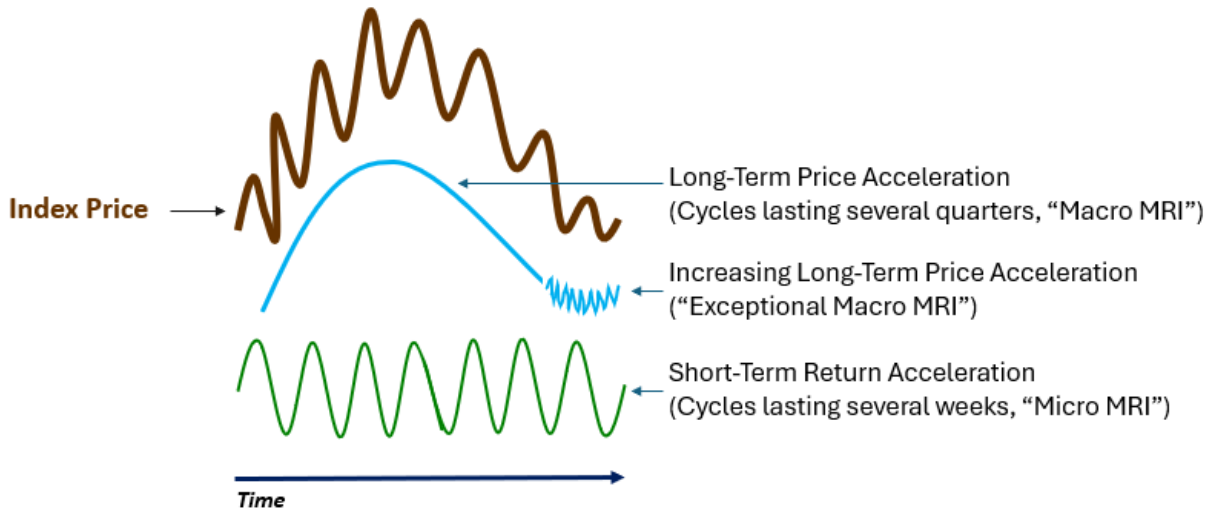

Figure F-1. Diagram of the Market Resilience Indexes. Source: CPM Investing LLC

Wilder's Relative Strength Index (RSI) is widely used in the investment industry and is used extensively in this report. The Market Resilience Indexes are conceptually similar to RSI but are more sensitive to price-movement inflection points. Both are derived from successive slopes of price over time: RSI approximates the price change gradient (slope), while MRI approximates price change acceleration. For simplicity in this report, we describe both as being measures of price acceleration.

Physics Analogy

Market Concept	Physics Analogy	Description	Formula	Described in this Report As
Price	Position	Market index price level *Shortened: Price*	Price	Price
Wilder's RSI	Velocity	Price change gradient (slope)	Change in price ÷ Change in time	Price acceleration
MRI	Acceleration	Price change acceleration	Change in the price change gradient ÷ (Change in time × Change in time)	Price acceleration

Figure F-2. Table describing the market concepts of price, RSI, and MRI along with their physics analogies, descriptions and formulas. Source: CPM Investing LLC.

The RSI reflects the price change gradient (slope), showing how steadily prices are moving upward or downward over time. Unlike a true mathematical slope, RSI is bounded between 0 and 100. It approaches 100 when all closing prices of the market in the lookback period are positive and approaches 0 when all are negative, compressing potentially unbounded slopes into a fixed, interpretable scale.

The MRI reflects the acceleration of that gradient, showing whether the steepness of price movement is itself increasing or decreasing. Like RSI, MRI is also bounded.

Appendix G –Solar Energy Metrics, Sources and Our Adjustments

This appendix describes the sources, transformation steps, and analytical roles of key solar energy metrics used in this study.

Metric	Start Date	Primary Use	Detection Method	Inferred or Measured EMF Frequency Range
Sunspot Number	1700s	Measures long-cycle solar magnetic activity and solar cycle intensity.	Visual counting of dark spots on the photosphere.	None
Ap Index	1932	Proxy for disturbances of Earth's magnetic field; tracks magnetospheric turbulence.	Derived from global K-index readings over 3-hour intervals of primarily ULF/ELF (0.001–30 Hz) waves.	None
F10.7 cm Solar Radio Flux	1947	Proxy for UV/EUV output and coronal magnetic complexity.	Ground-based antennas detect radio emission at 2800 MHz (10.7 cm wavelength).	Close to 2800 MHz
Oulu NM Raw Count Rate (uncorrected)	1964	Raw galactic cosmic ray count without pressure correction.	Ground-level secondary particle counts from galactic cosmic rays.	None
Oulu NM Air Pressure	1964	Contextual variable affecting neutron count detection.	Local barometric pressure at neutron monitor station.	None
Oulu NM Count Rate (corrected for air pressure)	1964	Measures solar shielding effect against galactic cosmic rays.	Neutron monitor counts secondary particles at ground level.	Not directly inferred

Figure G-1. Table showing six metrics related to solar energy, their inception dates, primary uses, detection methods, and electromagnetic frequency ranges they encompass. Sources: See Appendix V for data sources.

1. Sunspot Number (Inverted Scale)

The international sunspot number (SSN) is a standardized count of sunspot groups and individual spots on the solar surface. Higher values correspond to stronger solar magnetic activity and increased solar emissions. For this analysis, the SSN is inverted and normalized to align with market sentiment models, since periods of lower solar activity tend to coincide with higher investor confidence. Data are obtained from the Solar Influences Data Analysis Center (SILSO) and distributed by the GFZ German Research Centre for Geosciences. The GFZ sunspot number is the same as the International Sunspot Number (Rz), republished alongside long-term geomagnetic indices such as the aa and Ap indices (both of which measure variations in the Earth's magnetic field; the aa index extends back to 1868 and serves as a long-term proxy for solar wind activity), providing a uniform dataset widely used in solar–terrestrial research.

2. Ap Index (Inverted Scale)

The Ap Index quantifies geomagnetic activity and is derived from planetary K-index data. Higher Ap values signify more geomagnetic disturbance. Feynman shows how geomagnetic activity contains a baseline component that correlates closely with sunspot number, providing a widely cited framework for SSN–Ap relationships.[1] For modeling, we apply the following transformation steps:

- Calculate the 7-day trailing median.
- Take the log of the value and multiply by −1.
- Compute the 7-day moving average.
- Normalize to a 0.0 to 1.0 scale.

In this form, lower Ap values (indicating stability) are associated with higher stock prices. The Ap Index Stability Level is derived from the 7-day standard deviation of Ap values. We use Ap data from the GFZ German Research Centre for Geosciences.[2]

3. F10.7 cm Solar Radio Flux (Inverted Scale)

The F10.7 index measures solar radio flux at 2800 MHz and serves as a proxy for solar UV and EUV radiation. Higher values indicate increased solar radiation and complexity. Tapping establishes the strong cycle-to-cycle correlation between sunspot number and the F10.7 solar radio flux, now the standard reference.[3] We use F10.7 data from the GFZ German Research Centre for Geosciences and process the raw data by:

- Calculating the 7-day trailing moving average
- Normalizing to a 0.0 to 1.0 scale
- Scale inversion (1-normalzed level)

The stability level is determined from the 7-day standard deviation of these values. This proxy is distinct in that it directly measures solar emissions at a specific radio frequency, providing insight into coronal and ultraviolet output.

4. Oulu Neutron Monitor Count

The Oulu series reflects galactic cosmic ray influx and is used as a contra-indicator of solar activity. These readings are provided by the University of Oulu in Finland.[4] The Oulu NM readings represent the number of galactic cosmic rays reaching the Oulu monitor in Finland. Because the Sun's magnetic field modulates cosmic-ray flux—shielding Earth when strong and allowing more through when weaker—these readings act as an inverse proxy for solar electromagnetic activity. Assuming a relatively constant incoming cosmic-ray rate, a higher Oulu count implies weaker solar shielding and lower solar activity.

[1] Feynman J. Geomagnetic and solar wind cycles, 1900–1975. Journal of Geophysical Research. 1982;87(A8):6153-6162.
https://agupubs.onlinelibrary.wiley.com/doi/10.1029/JA087iA08p06153

[2] GFZ German Research Centre for Geosciences. GFZ Data Services: Solar and Geomagnetic Indices.
https://dataservices.gfz-potsdam.de

[3] Tapping KF. The 10.7 cm solar radio flux (F10.7). Space Weather. 2013;11(7):394-406.
https://agupubs.onlinelibrary.wiley.com/doi/10.1002/swe.20064

[4] University of Oulu, Sodankylä Geophysical Observatory. Cosmic Ray Station.
https://cosmicrays.oulu.fi

Higher neutron counts imply lower solar shielding. This index is distinct because it indirectly captures solar energy levels by measuring the flux of galactic cosmic rays, which are modulated by solar wind and magnetic shielding. Kane quantifies the anti-correlation between sunspot number and neutron monitor counts, a benchmark for Oulu NM studies of cosmic-ray modulation.[5] We include three measures: uncorrected count (raw), local atmospheric pressure (pres), and corrected (pressure-adjusted) count (cor).

Oulu calculates the corrected count based on the uncorrected count and local atmospheric pressure. The corrected count is a proxy for net solar energy reaching Earth. It reflects the combined effect of solar wind and magnetic shielding.

We use the reported values for each Friday. Readings of zero are replaced with the average of the three Friday values before and after the zero reading. All three series are normalized to a 0.0 to 1.0 range.

Orientation

Each of these solar metrics captures a distinct aspect of solar-terrestrial interaction. Inversion and normalization are used to align them with sentiment data. Except for the techniques mentioned above, we did not apply time lags to artificially enhance correlation with market sentiment.

Figure G-2 below shows the series from December 3, 1965 through December 29, 2023.

[5] Kane RP. Solar modulation of galactic cosmic rays during solar cycles 19–23. Advances in Space Research. 2011;47(9):1578-1583.
https://ui.adsabs.harvard.edu/abs/2011NewA...16..430C/abstract

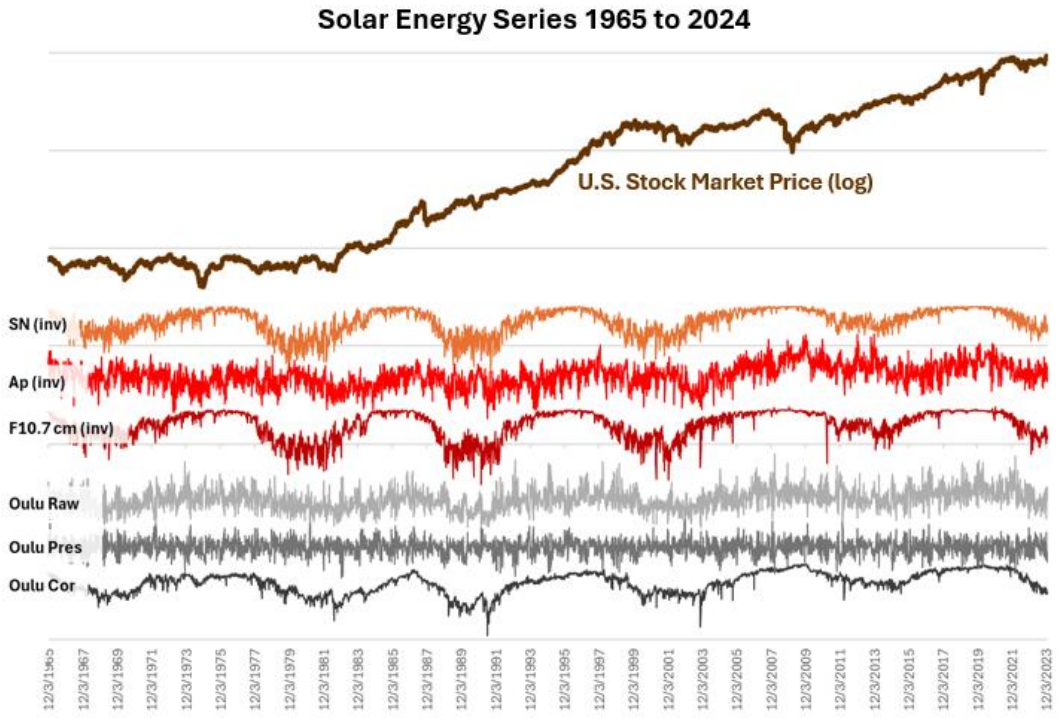

Figure G-2. Graph showing the U.S. stock market on a log scale from 1964 through 2023 and six metrics related to solar energy, their inception dates, primary uses, detection methods, and electromagnetic frequency ranges they encompass. Sources: solar data sources listed in Appendix V and MeasuringWorth and public market sources. 'U.S. stocks' and 'U.S. stock market' refer to the DJIA, S&P 500, or related ETFs depending on the period.

Appendix H - Market Resilience Indexes Correspond to The Oulu Series

Figure H-1 below shows the logarithmic price of the stock market as the dark blue line, spanning from 1961 through the end of 2022. In the middle portion of the figure, the Oulu NM (air pressure corrected) readings appear in red (starting in 1964). See Appendix G for a description of the Oulu NM readings. At the top of the figure, our measure of long-term market price acceleration, the Macro Market Resilience Index, is shown in light blue.

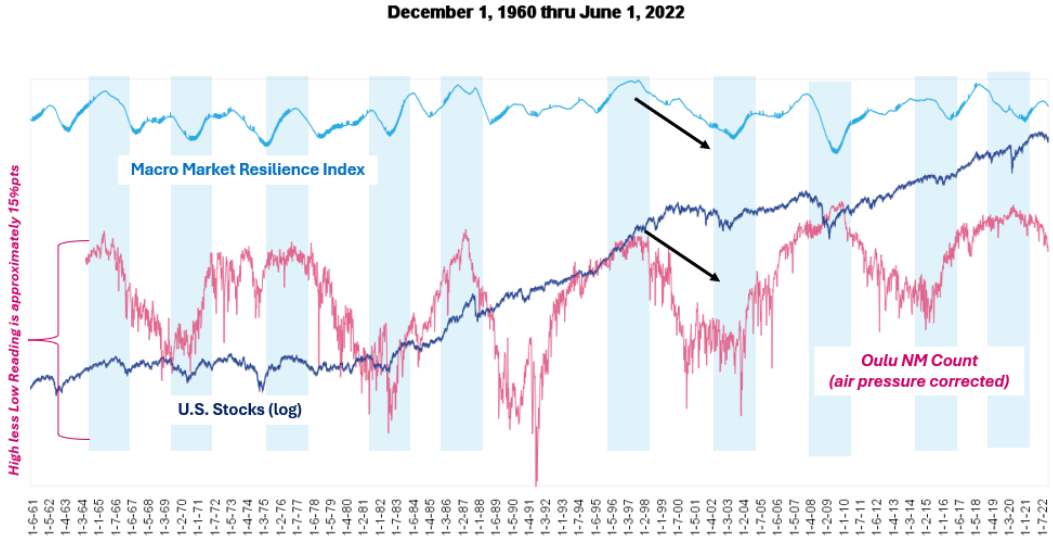

Figure H-1. Graph showing the SU.S. stock market as a dark blue line on a log scale from 1964 through 2022 and the Macro Market Resilience Index and the Oulu NM count (air pressure corrected). Sources: Oulu NM and MeasuringWorth and public market sources. 'U.S. stocks' and 'U.S. stock market' refer to the DJIA, S&P 500, or related ETFs depending on the period.

Many of the patterns in the two data series are similar, and these are highlighted by the shaded bands. Changes in Oulu NM readings often correspond to inflection points in our Macro Market Resilience Index. Perhaps more interesting is that the Macro Market Resilience Index corresponds to the Oulu readings even when the price of the stock market moves in a different direction, as was the case indicated by the two black arrows from 1997 through 2003.

Changes in Short-Term Trends

A similar relationship is visible between our Micro Market Resilience Index and the weekly Oulu readings that have not been corrected for air pressure. The figure below shows the Friday Oulu readings, represented by the yellow line, and the Micro Market Resilience Index as the green line.

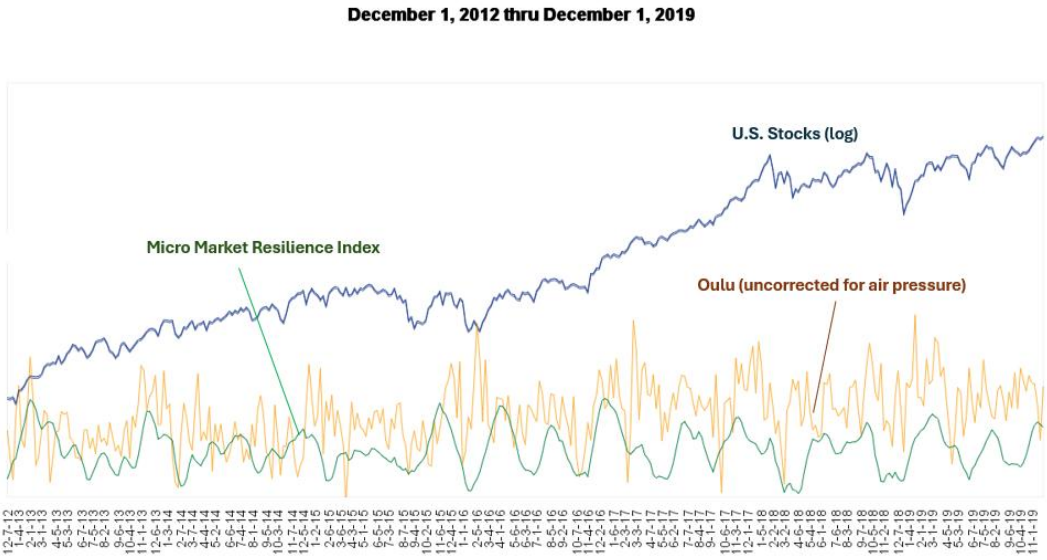

Figure H-2. Graph showing the U.S. stock market price on a log scale from 2012 through 2019 and the Macro Market Resilience Index and the Oulu NM count (air pressure corrected). Sources: Oulu NM and MeasuringWorth and public market sources. 'U.S. stocks' and 'U.S. stock market' refer to the DJIA, S&P 500, or related ETFs depending on the period.

Short-term price patterns in the stock market are reflected in both the Micro Market Resilience Index and the Oulu readings that have not been corrected for air pressure. The following figure shows the same data but uses a centered 56-day moving average of the Friday Oulu readings to smooth out week-to-week variability, which makes it easier to see the relationship described.

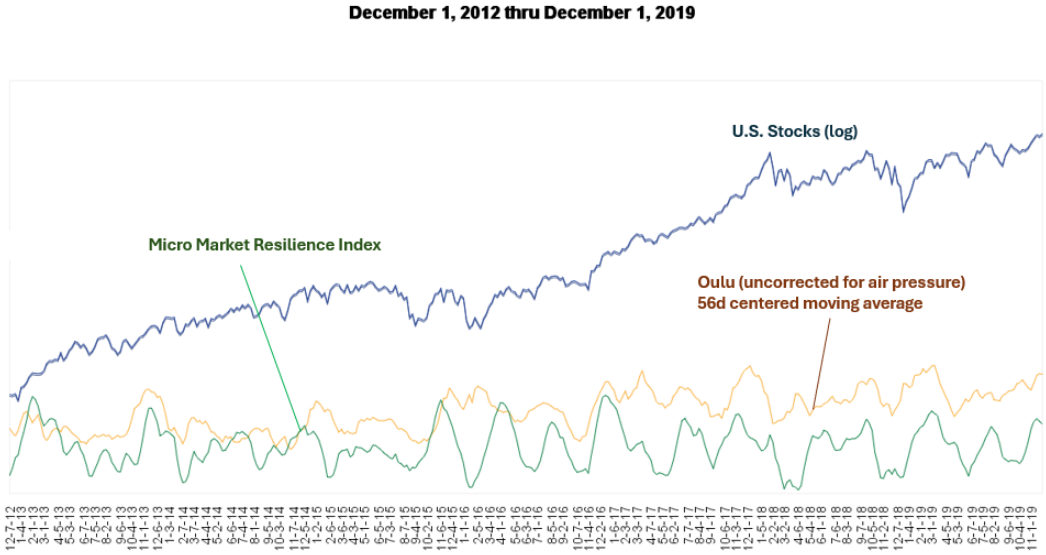

Figure H-3. Graph showing the U.S. stock market price on a log scale from 2012 through 2019 and the Micro Market Resilience Index and a 56-day centered moving average of the Oulu NM count (uncorrected for air pressure). Sources: Oulu NM and MeasuringWorth and public market sources. 'U.S. stocks' and 'U.S. stock market' refer to the DJIA, S&P 500, or related ETFs depending on the period.

The relationship between short-term price acceleration and the Oulu readings is apparent. The interesting feature of this Oulu series is that it includes the effect of atmospheric air pressure at the monitoring site in

Finland. This suggested that air pressure fluctuations may be an element in the mechanism linking environmental forces (measured by Oulu) and the Micro Market Resilience Index.

Some research has identified a relationship between air pressure oscillation and emotional responses in humans, which we describe in Appendix Q. During our research we concluded, however, that air pressures is not likely to be the primary pathway affecting humans. However, it may be a confirming signal that reinforces the changes in in the global electromagnetic atmospheric standing waves.

Appendix I – Macro Market Resilience Index and Oulu NM Series

We tested whether Oulu NM readings move in step with long-term shifts in investor sentiment. To do this, we compared the Oulu NM series with our measure of long-term price acceleration, the Macro Market Resilience Index. The data for this analysis ranged from April 24, 1964 to December 27, 2024, the period during which continuous and usable Oulu data is available.

Rolling Four-Year Window Correlations

The statistical tests show that the Oulu series has a measurable relationship with the Macro MRI. In rolling four-year windows, Oulu explains between 30% and 70% of the variance in Macro MRI. These results are consistently well beyond what could happen by chance and are visible across multiple decades. This indicates that the connection is not confined to a single solar cycle or isolated market period but persists as a long-term feature of the data.

Rolling Four-Year Window Correlations Using Smoothed Data

When both series are smoothed to highlight long-term movements, their trends rise and fall together, with a correlation of 0.74**.** The smoothing was done using a 56-week centered moving average, which provides a symmetrical window of 28 weeks before and 28 weeks after the center point.

Inflection Point Match Rate Using Smoothed Data

We next examined whether turning points in the smoothed series coincided. The Macro MRI produced 42 major inflection points over the study period, while the Oulu series had 39. Of these, 21 occurred within ±8 weeks of each other. A permutation test—where one series is randomly shifted thousands of times to estimate the chance distribution of match rates—confirmed that this alignment is highly unlikely to be random ($p = 0.008$). In other words, the timing of major shifts in Oulu and in the Macro MRI series is statistically synchronized.

Adjusting for the Approximately 11-Year Solar Cycle

Finally, spectral (frequency-domain) analysis confirmed that the two series share a common rhythm in the 8–13-year band**,** corresponding to the solar cycle. The presence of shared power in this frequency range strengthens the interpretation that the relationship is not accidental but reflects a deeper connection between cosmic-ray modulation, as captured by Oulu NM counts, and long-term patterns in investor sentiment.

Summary of Results

Figure I-1 summarizes the main findings across the different tests. The relationship between Oulu and the Macro MRI is evident in the variance explained, the strength of long-term correlations, the weak residual correlation, and the statistically significant alignment of inflection points.

Rolling R^2 Range (4-year windows)	Long-Term Trend Correlation (r)	Correlation of Residuals (r)	Turning Points (Macro, Oulu)	Matches (±8 weeks)	Permutation *p*-value
0.30 – 0.70	0.74	0.05	42, 39	21	0.008

Figure I-1. Table showing the results of regression analysis of the smoothed Macro Market Resilience Index and the Oulu NM (corrected for air pressure) series. Sources: CPM Investing LLC calculations using Oulu NM. Note: "Correlation of Residuals" measures the correlation between the short-term fluctuations of the two series after subtracting the 56-week moving average trend. A value near zero (0.05) indicates that the relationship between Oulu and the Macro MRI is concentrated in long-term cycles rather than short-term noise.

Together, these findings provide evidence that the Macro MRI is systematically linked to changes in Oulu NM readings. The relationship is evident in three complementary dimensions: the variance explained in rolling windows, the alignment of inflection points, and the shared multi-year rhythm tied to the solar cycle.

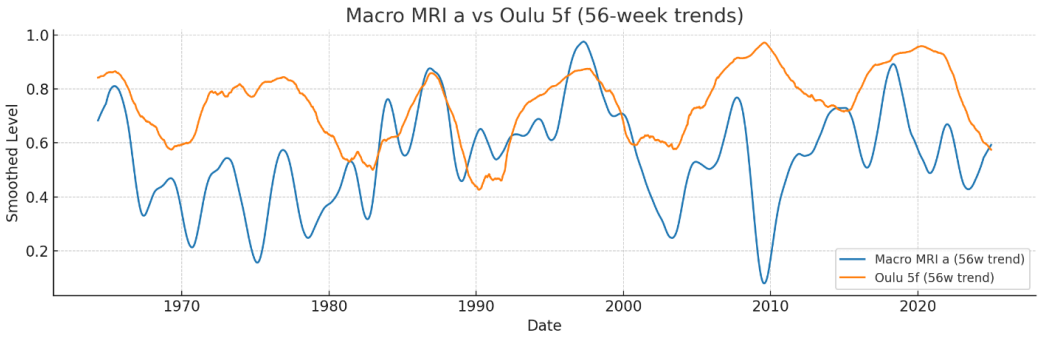

Figure I-2. Graph showing the smoothed Macro Market Resilience Index and the 56-week moving average of the Oulu NM (corrected for air pressure) series. Sources: CPM Investing LLC calculations using data from NASA, Oulu NM, MeasuringWorth, and public market sources. 'U.S. stocks' and 'U.S. stock market' refer to the DJIA, S&P 500, or related ETFs depending on the period.

Appendix J – Outer Planets Deserve Greater Weight Than Traditional Models Suggest

We did not begin our modeling with a view about the impact of any planet on solar energy emissions. Instead, we derived the current weights assigned to the planets based on standard formulas, such as that for tidal attraction, which were explanatory of observed cyclic shifts in investor sentiment. This process revealed notable correlations involving all four outer planets, Jupiter, Saturn, Uranus and Neptune. Like many historical studies in heliophysics and astrophysics, this portion of our work rests on empirical correlations rather than deterministic models.

The results of our studies are more consistent with a minority view in solar physics: that Uranus and Neptune may exert meaningful influences on solar activity. As discussed in Appendix D, the prevailing view holds that changes in the Sun's energy output stem from internal dynamo processes and magnetic cycling, without significant planetary input. However, several researchers have challenged this view, arguing that the outer planets—particularly Uranus and Neptune—may exert gravitational or electromagnetic effects that modulate solar behavior.

Minority Views Supporting Outer Planet Influence

Jose (1965) proposed that the Sun's motion around the solar system barycenter, driven largely by the gas giants, could produce mechanical perturbations to solar activity. This idea was foundational in linking planetary motion to solar variability.[1]

Charvátová (2000) argued that regularities in the Sun's path around the barycenter correlate with prolonged solar minima, such as the Maunder Minimum. Her analysis implicated the massive outer planets in modulating long-term solar quiet periods.[2]

Sharp (2010) proposed a speculative link between angular momentum exchanges from the outer planets and the timing of historical solar minima. Though not formally modeled, this work contributed to a broader body of literature associating planetary dynamics with solar variability.[3]

Steinhilber et al. (2009) reconstructed total solar irradiance over the Holocene and found multidecadal to millennial-scale fluctuations, some of which may reflect periodic influences consistent with long-term planetary cycles.[4]

Hannes Alfvén, the Nobel laureate and pioneer of magnetohydrodynamics, argued that planetary magnetic fields, particularly those of Jupiter and Saturn, should not be understood as isolated cavities bounded only by solar wind pressure. In his view, the solar wind is a conducting plasma

[1] Jose, P.D. Sun's Motion and Sunspots. Astronomical Journal. 1965;70:193–200. doi:10.1086/109714
[2] Charvátová, I. Can origin of the 2400-year cycle of solar activity be caused by solar inertial motion? Ann. Geophys. 2000;18(3):399–405.
https://doi.org/doi:10.1007/s00585-000-0399-x
[3] Sharp, G.J. Long Term Sunspot Cycle Phase Coherence with Periodic Phase Disruptions. arXiv:1610.03553 [astro-ph.SR]. 2010 (preprint; not peer reviewed).
[4] Steinhilber, F.; Beer, J.; Fröhlich, C. Total solar irradiance during the Holocene. Geophys. Res. Lett. 2009;36:L19704.
https://doi.org/doi:10.1029/2009GL040142

in which magnetic fields can remain connected to their sources over large distances, forming extended electromagnetic circuits that conventional pressure-balance models do not capture.[5] [6]

Alfvén emphasized the role of field-aligned currents (often called Birkeland currents) and plasma coupling across vast regions of space.[7] From this perspective, the magnetospheres of Jupiter and Saturn are not cleanly delimited at the subsolar standoff distance but are instead embedded in a larger system of currents that can extend over tens of astronomical units. These extended field structures may not provide the strong shielding of the near-planet magnetosphere but can influence charged-particle motion, wave propagation, and electromagnetic connectivity on interplanetary scales.[8]

Spacecraft observations support part of this picture. Pioneer and Voyager missions detected plasma and magnetic perturbations at large distances from Jupiter and Saturn, showing that their magnetic influence extends well beyond simple pressure-balance boundaries.[9] Jupiter's magnetotail, in particular, has been observed to stretch outward past Saturn's orbit.[10] While there is no firm evidence that Jupiter's field measurably perturbs the solar wind inward at Earth's orbit (1 AU), Alfvén's framework allows for such long-range electromagnetic coupling under certain plasma conditions.[11] [12]

In summary, Alfvén's views expand the notion of planetary magnetospheres beyond pressure-limited cavities to include long-range electromagnetic coupling through plasma. From this standpoint, the magnetic fields of Jupiter and Saturn could extend farther inward toward the Sun than conventional models suggest, potentially influencing solar wind structure and particle dynamics across much of the inner solar system. These ideas are controversial and have not been widely accepted, yet they highlight the possibility that outer-planet magnetic fields introduce structure to the interplanetary medium that helps preserve electromagnetic turbulence as it propagates to Earth's orbit.[13] [14]

[5] Alfvén H, Fälthammar C-G. Cosmical electrodynamics. 2nd ed. Oxford: Clarendon Press; 1963. https://archive.org/details/cosmicalelectrod0000alfe

[6] Alfvén H. Cosmic plasma. Dordrecht: D. Reidel; 1981. https://archive.org/details/cosmicplasma0000alfv

[7] Alfvén H. Double layers and circuits in astrophysics. IEEE Trans Plasma Sci. 1986;14(6):779–93. https://doi.org/10.1109/TPS.1986.4316626

[8] Peratt AL. The legacy of Hannes Alfvén. IEEE Trans Plasma Sci. 2010;38(6):1234–9. https://ieeexplore.ieee.org/document/5505985

[9] Acuña MH, Ness NF. The magnetic field of Jupiter: Pioneer 10 observations. Science. 1973;182(4111):343–6. https://doi.org/10.1126/science.182.4111.343

[10] Ness NF, Acuña MH, Behannon KW, Burlaga LF, Connerney JEP, Lepping RP, et al. Magnetic field studies by Voyager 1: Preliminary results at Jupiter. Science. 1979;204(4396):982–7. https://doi.org/10.1126/science.204.4396.982

[11] Alfvén H. Cosmic plasma. Dordrecht: D. Reidel; 1981. https://archive.org/details/cosmicplasma0000alfv

[12] Alfvén H. Double layers and circuits in astrophysics. IEEE Trans Plasma Sci. 1986;14(6):779–93. https://doi.org/10.1109/TPS.1986.4316626

[13] Alfvén H, Fälthammar C-G. Cosmical electrodynamics. 2nd ed. Oxford: Clarendon Press; 1963. https://archive.org/details/cosmicalelectrod0000alfe

[14] Peratt AL. The legacy of Hannes Alfvén. IEEE Trans Plasma Sci. 2010;38(6):1234–9. https://ieeexplore.ieee.org/document/5505985

Lack of Acceptance of Alfven's Views

Alfvén's circuit model of plasmas[15] differs from the Parker magnetohydrodynamic framework, which forms the basis of modern heliophysics. [16] Although Alfvén's local field-aligned currents have been empirically confirmed, [17] Alfvén's broader idea of heliosphere-wide electric circuits remains unproven and is generally considered outside mainstream astrophysics. [18]

[15] Alfvén H. Double layers and circuits in astrophysics. IEEE Trans Plasma Sci. 1986;14(6):779-93. https://ntrs.nasa.gov/api/citations/19870010655/downloads/19870010655.pdf

[16] Parker EN. Dynamics of the interplanetary gas and magnetic fields. Astrophys J. 1958;128:664–76. https://ui.adsabs.harvard.edu/abs/1958ApJ...128..664P/abstract

[17] Iijima T, Potemra TA. The amplitude distribution of field-aligned currents at northern high latitudes observed by TRIAD. J Geophys Res. 1976;81(13):2165–74. https://earthref.org/ERR/25830/

[18] Peratt AL. The legacy of Hannes Alfvén. IEEE Trans Plasma Sci. 2010;38(6):1234–9. https://ieeexplore.ieee.org/document/5505985

Appendix K – Emission Preservation Zone

We propose that when the magnetic environments of the outer planets—Jupiter, Saturn, Uranus, and Neptune—are clustered within a confined sector of the solar system, they contribute to the preservation of low-frequency electromagnetic emissions. In such a configuration, the overlapping planetary magnetospheres create an Emission Preservation Zone between the Sun and the cluster. This zone reduces the usual damping and scattering of extremely low-frequency perturbations, allowing them to remain coherent over greater distances and reach Earth more intact.

Introduction

The heliosphere contains a spectrum of electromagnetic and plasma (magnetohydrodynamic, or MHD) fluctuations generated by solar activity. As these disturbances travel outward, small high-frequency ripples typically dissipate quickly through nonlinear cascade and heating. In contrast, large-scale, low-frequency fluctuations are more resilient and can persist well beyond the orbit of Saturn, more than ten astronomical units from the Sun.[1]

These low-frequency waves are particularly sensitive to large-scale plasma and magnetic structures. Unlike high-frequency radiation such as X-rays, which travels through the heliosphere largely unaffected, extremely low-frequency waves (below ~100 Hz) interact with the charged plasma environment. Their survival depends on the structure of the interplanetary medium they traverse.[2] [3]

Emission Preservation Zone

When Jupiter, Saturn, Uranus, and Neptune cluster together, their combined magnetic fields may form a structured pathway in space. This environment can preserve extremely low-frequency perturbations by reducing phase distortion and scattering, enabling them to propagate coherently over long distances. The effect is not amplification but conservation: solar-origin signals that would normally decay before reaching Earth remain measurable at 1 AU.

By contrast, when the outer planets are more widely dispersed, the guiding effect weakens. In such periods, emissions scatter more readily, lose coherence, and dissipate before reaching Earth. This implies a geometry-dependent preservation of emissions: coherence is enhanced during clustering and diminished during dispersion.

An Antipodal Region of Greater Damping

This hypothesis also suggests a corresponding antipodal region—opposite the planetary cluster—where no such preservation occurs. In this sector, the absence of organized magnetic structures increases damping and scattering, producing a more chaotic propagation environment.

[1] Richardson JD, Paularena KI, Lazarus AJ, Belcher JW. Radial evolution of the solar wind from IMP 8 to Voyager 2. Adv Space Res. 1996;18(1–2):17–26.
[2] Tu C, Marsch E. MHD structures, waves and turbulence in the solar wind: observations and theories. Space Sci Rev. 1995;73(1-2):1-210.
[3] Goldstein ML, Roberts DA, Matthaeus WH. Magnetohydrodynamic turbulence in the solar wind. Annu Rev Astron Astrophys. 1995;33:283-325.
https://doi.org/10.1146/annurev.aa.33.090195.001435

Magnetic Field Topology and Planetary Differences

Jupiter and Saturn possess strong, largely dipolar magnetic fields aligned with their rotation axes. These stable magnetospheres, along with structures such as Jupiter's Io plasma torus, inject plasma and support extended magnetotails that interact persistently with the solar wind.[4] By contrast, Uranus and Neptune display highly tilted, multipolar magnetic fields that vary in orientation and coupling with the solar wind.[5] [6] Voyager observations confirm that these environments are sources of localized turbulence and wave activity. When clustered, the combined influence of these diverse magnetospheres may reinforce the preservation of solar-origin low-frequency perturbations.

Analogies and Modeling Considerations

The Emission Preservation Zone can be likened to acoustic resonance in cathedrals, where architectural geometry sustains sound waves instead of damping them.[7] In electromagnetic terms, it is similar to a waveguide or resonant cavity, where constructive interactions with boundary conditions allow certain frequencies to persist.[8] These analogies highlight how geometry and structure can sustain energy transmission without amplification.

From a modeling standpoint, the outer planets should be treated as dynamic, spatially extended magnetic scatterers. Global MHD simulations that incorporate realistic planetary field geometries and heliospheric turbulence may clarify how clustering configurations alter the propagation of low-frequency waves.

Empirical Support

Our Study B shows that during outer-planet clustering, correlations among weekly solar activity indicators—including the Sunspot Number, Ap Index, and F10.7 flux—are elevated. This suggests that the interplanetary medium may offer less distortion in such periods. The Oulu Neutron Monitor, while not a direct measure of solar wind turbulence, also shows increased coherence with solar indicators, consistent with changes in heliospheric structure during clustering episodes.

Limitations and Uncertainties

Uncertainties remain in this hypothesis. While magnetospheres clearly shape local plasma structures, their collective effect across interplanetary distances has not been directly observed. Disentangling planetary effects from solar cycle variability poses challenges. The precise angular span defining a clustered state requires refinement, and global simulations capable of integrating planetary magnetospheres with heliospheric turbulence are still in development.

---

[4] Thomas N, Bagenal F, Hill T, Wilson J. The Io neutral clouds and plasma torus. In: Bagenal F, Dowling TE, McKinnon WB, editors. Jupiter: The Planet, Satellites and Magnetosphere. Cambridge University Press; 2004. p. 561–591.

[5] Ness NF, Acuña MH, Burlaga LF, et al. Magnetic field observations near Uranus: Voyager 2 results. Science. 1986;233(4759):85–89.

[6] Connerney JEP, Acuña MH, Ness NF. The magnetic field of Neptune. J Geophys Res. 1991;96(S01):19023–19042.

[7] Blesser B. An acoustical interpretation of classical architecture. J Acoust Soc Am. 2001;109(6):2972.

[8] Howes GG, Dorland W, Cowley SC, Hammett GW, Quataert E, Schekochihin AA, Tatsuno T. A model of turbulence in magnetized plasmas: implications for the dissipation range in the solar wind. J Geophys Res. 2008;113:A05103.
https://doi.org/10.1029/2007JA012665

Appendix L – The Role of Right-Angle Geometry in Astrophysics

The observation that Anxiety-Free Periods occur when the centers of inner and outer planetary orbits are separated by 90 degrees with the Sun at the vertex suggests that right-angle geometries may play a role in solar dynamics. While this specific application has not been previously proposed, astrophysical literature contains multiple contexts in which 90-degree angular relationships produce distinctive physical effects.

Polarization of Light at 90 Degrees: Rayleigh Scattering

Rayleigh scattering occurs when light interacts with particles that are much smaller than its wavelength, such as molecules in Earth's atmosphere. This scattering is stronger for shorter wavelengths, which is why the sky appears blue. Importantly, Rayleigh scattering is not only a change in the direction of light but also in its polarization (the orientation of the light waves). The degree of polarization depends on the angle between the incoming sunlight and the direction in which it is observed.

When this angle is 90 degrees, the polarization of the scattered light reaches its maximum. In practical terms, if one looks at a patch of the sky that is directly overhead when the Sun is on the horizon, the scattered light is highly polarized. This 90-degree geometry is routinely used in astrophysics and atmospheric physics to measure aerosols, detect planetary atmospheres, and study interstellar dust.[1]

This example demonstrates that orthogonal geometries (90 degrees) are not arbitrary but mark special points of physical significance in the behavior of electromagnetic radiation.

Tidal Forcing and Right-Angle Geometry

In celestial mechanics, the 90-degree separation of the Moon and Sun relative to Earth is known as quadrature. At this configuration, the tidal forces of the Sun and Moon act at right angles, partially cancelling one another. The result is a neap tide, a well-documented phenomenon where tidal range is minimized due to orthogonal force vectors.[2] This provides a clear example of how right-angle alignments reduce the coherence of otherwise reinforcing astrophysical forces.

Turbulence and Magnetic Field Orientation

In plasma astrophysics, turbulence and wave–particle interactions are strongly dependent on the angle between motion and magnetic fields. Energy transfer in solar wind turbulence is anisotropic, favoring directions perpendicular to the mean magnetic field. Perpendicular (near 90-degree) orientations can enhance nonlinear interactions, leading to altered transport and dissipation of energy.[3] [4] Similarly,

[1] Coulson KL. Polarization and Intensity of Light in the Atmosphere. Hampton, VA: A. Deepak Publishing; 1988. NASA Technical Report Server entry available: https://ntrs.nasa.gov/citations/19880015415

[2] Cartwright DE, Tayler RJ. New computations of the tide-generating potential. Geophys J R Astron Soc. 1971;23(1):45–74. https://doi.org/doi:10.1111/j.1365-246X.1971.tb01803.x

[3] Tu C, Marsch E. MHD structures, waves and turbulence in the solar wind: observations and theories. Space Sci Rev. 1995;73(1-2):1-210.

[4] Bruno R, Carbone V. The solar wind as a turbulence laboratory. Living Rev Sol Phys. 2013;10(1):2. https://doi.org/10.12942/lrsp-2013-2

cyclotron resonance occurs when charged particles interact with electromagnetic waves at pitch angles near 90 degrees, a geometry that maximizes wave–particle coupling in some regimes.[5]

Dynamo Symmetry and Orthogonal Forcing

The solar dynamo, which underlies sunspot formation, is highly sensitive to changes in boundary conditions and symmetry breaking. External gravitational or electromagnetic influences that act at right angles to existing field structures may perturb the coherence of the dynamo in ways that differ qualitatively from in-line alignments (0° or 180°). Although direct evidence is limited, models of magnetic field evolution emphasize the role of symmetry and angular orientation in maintaining or disrupting coherent magnetic structures.[6]

Relevance to Anxiety-Free Periods

Taken together, these examples highlight that right-angle geometries are not neutral but often associated with reduced coherence, enhanced cross-field interaction, or distinct dynamical states. By analogy, when the inner and outer orbital centers form a 90-degree angle with the Sun, the orthogonal geometry may act to redistribute or dampen turbulence in the solar wind. Such changes could propagate into the solar dynamo, manifesting as altered sunspot numbers. This interpretation provides a physics-based framework linking orbital geometry to solar variability, consistent with the empirical correlation of AFPs and sunspot changes.

[5] Smith CW, Hamilton K, Vasquez BJ, Leamon RJ. Dependence of the dissipation range spectrum of interplanetary magnetic fluctuations on the rate of energy cascade. Astrophys J Lett. 2006;645(1):L85-8.
[6] Charbonneau P. Dynamo models of the solar cycle. Living Rev Sol Phys. 2010;7(3). https://doi.org/10.12942/lrsp-2010-3

Appendix M – Assessing the Intensity of Anxiety-Free Period Episodes

We hypothesize that the intensity of an Anxiety-Free Period depends on how tightly the members of the Outer Orbital Group (Jupiter through Neptune) cluster around their calculated center. Tighter clustering amplifies an orbital center's influence on the distribution of solar energy.

Interestingly, the best proxy for clustering is its distance from the Sun. As the Outer Orbital Center moves farther away from the Sun, its influence becomes more directionally focused, increasing the intensity of solar perturbations intersecting Earth's orbit. When the Outer Orbital Center is near or within the Sun's circumference, its apparent intensity is weakest. In this configuration, low-frequency perturbations directed toward the Outer Orbital Center are less likely to cross Earth's path. Conversely, when the Outer Orbital Center is more distant, Earth is more likely to be swept by a concentrated band of these perturbations.

Figure M-1 below shows two configurations of the Outer Orbital Center. The Sun is represented by the yellow circle, Earth's orbit is the dotted line around the Sun. The members of the Outer Orbital Center are shown. Since 1900, the closest the Outer Orbital Center has been to the Sun was in late 1929, which is shown in the left panel. The farthest was in 1984, which is shown on the right.

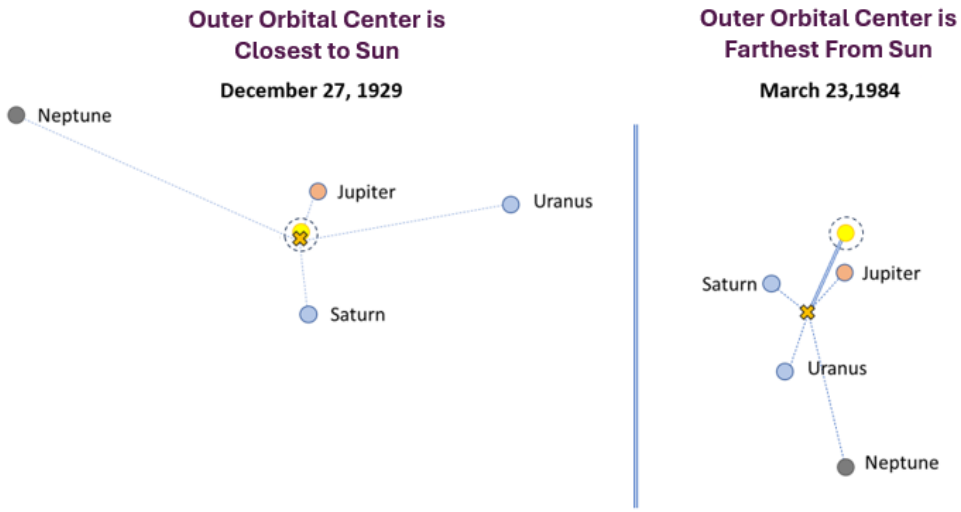

Figure M-1. Graph showing the location of the Outer Orbital Center on to dates. On December 27, 1929, the Outer Orbital Center was its closest to the Sun since 1900. At that time, the members of the Outer Orbital Group are spread throughout the solar system. On March 23, 1984, the Outer Orbital Center was the farthest from the Sun since 1900. At this time, the member of the group are tightly clustered. Sources: CPM Investing LLC calculations using NASA data.

It is interesting to note that these dates correspond to noteworthy periods in market history. Late 1929 was close to the end of the roaring '20s. Our hypothesis is that close proximity of the Outer Orbital Center to the Sun would induce little pessimism to investors, and this is consistent with the late Roaring '20s period. We don't include the solar dynamics of the pre-1933 because the returns of the 1900 to 1933 period are so extreme they would sway the analyses. The year 1984 was close to the end of the long period of pessimism of the 1970s and early 1980s, which is also consistent with our hypothesis.

The figure below shows the two intensity-related metrics, a) distance between the Sun and the Outer Orbital Center, and b) our measure of the tightness, which is the average standard deviation of the members' distance from the Outer Orbital Center.

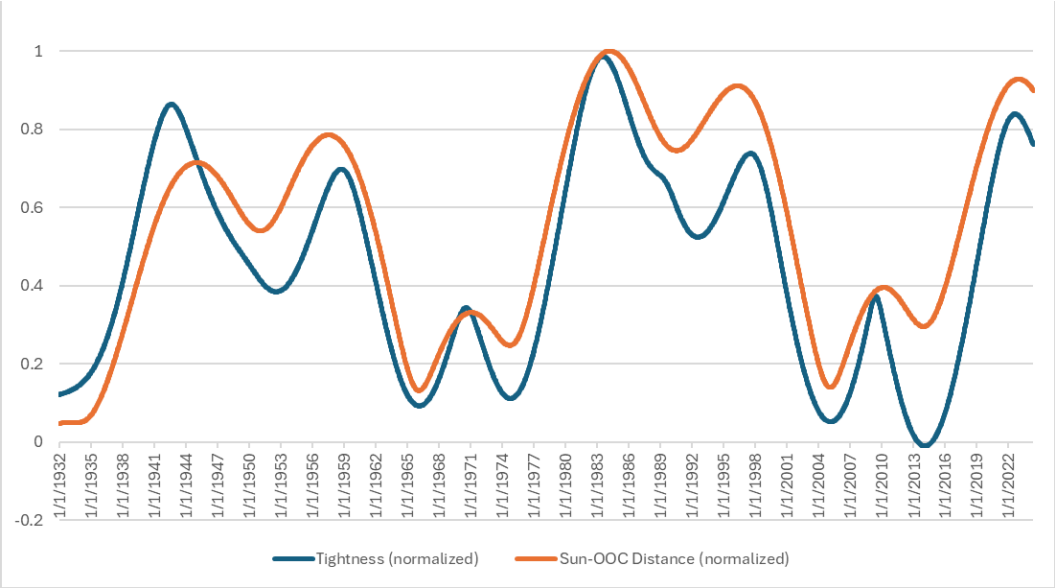

Figure M-2. Graph showing two measures, which have been normalized, related to the Outer Orbital Center from 1932 to 2024. Tightness is determined by the standard deviation of the distances of the members of the Outer Orbital Group to the Outer Orbital Center. Sun-OOC Distance is the distance between the Sun and the Outer orbital Center. Sources: CPM Investing LLC calculations using NASA data.

The correlation between these two metrics is 0.89. We favor using the distance related metric because of its simplicity, its relative stability, and its ease of calculation.

Appendix N – Thirteen Anxiety-Free Periods and Prior and Post Market Lows

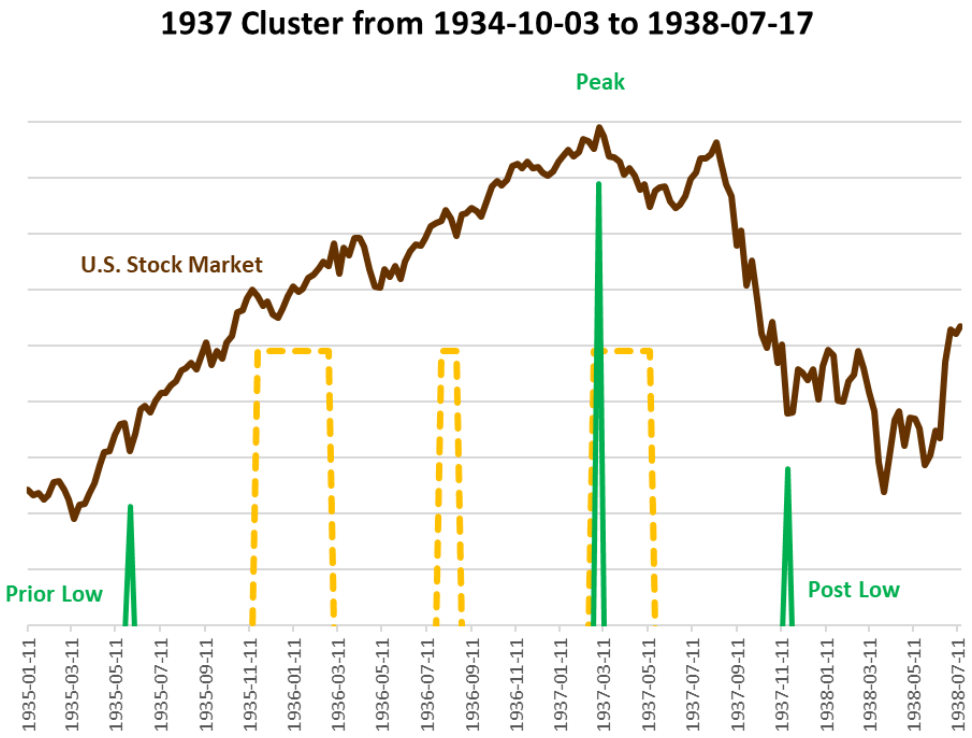

Figure N-1. Graph showing the 1937 Anxiety-Free Period, the related peak in market price and the prior- and post-low price points. Sources: CPM Investing LLC calculations using data from NASA, MeasuringWorth, and public market sources.

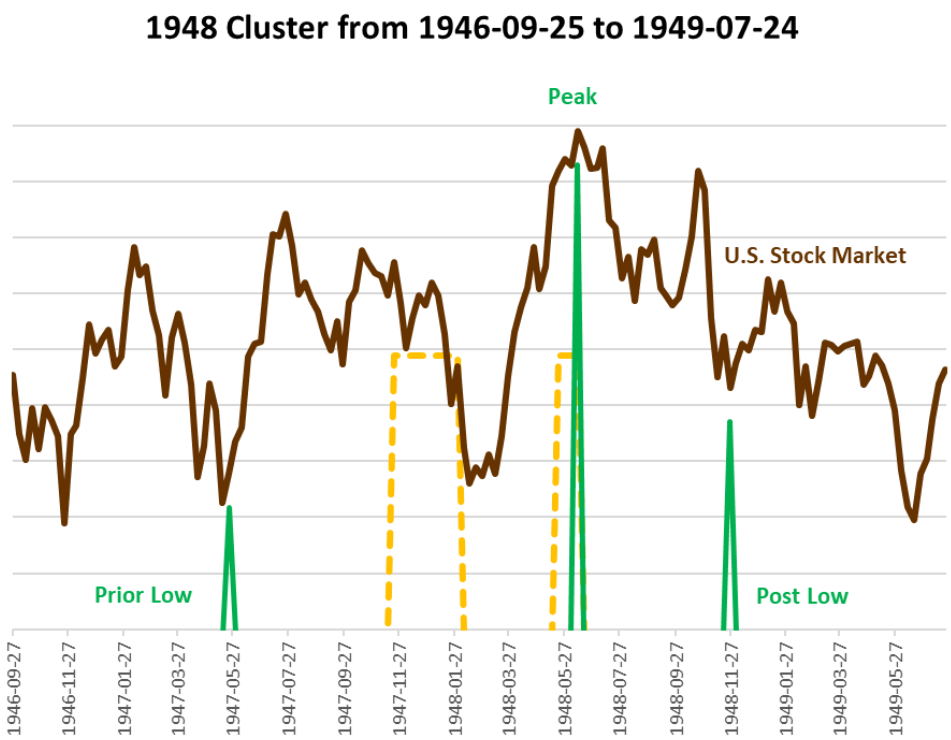

Figure N-2. Graph showing the 1948 Anxiety-Free Period, the related peak in market price and the prior- and post-low price points. Sources: CPM Investing LLC calculations using data from NASA, MeasuringWorth, and public market sources.

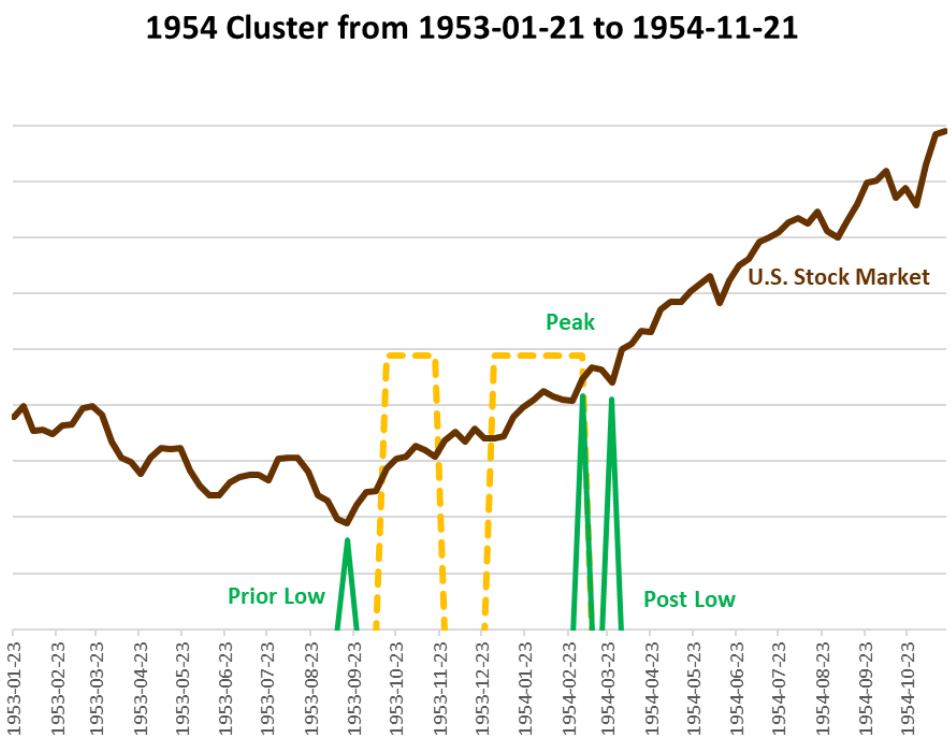

Figure N-3. Graph showing the 1954 Anxiety-Free Period, the related peak in market price and the prior- and post-low price points. Sources: CPM Investing LLC calculations using data from NASA, MeasuringWorth, and public market sources.

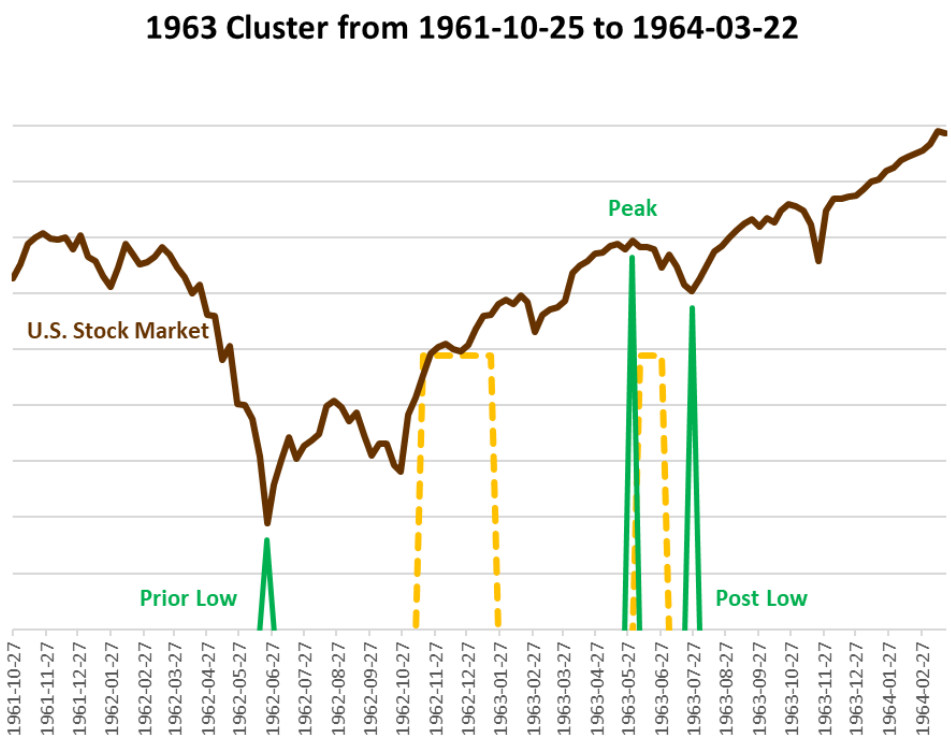

Figure N-4. Graph showing the 1963 Anxiety-Free Period, the related peak in market price and the prior- and post-low price points. Sources: CPM Investing LLC calculations using data from NASA, MeasuringWorth, and public market sources.

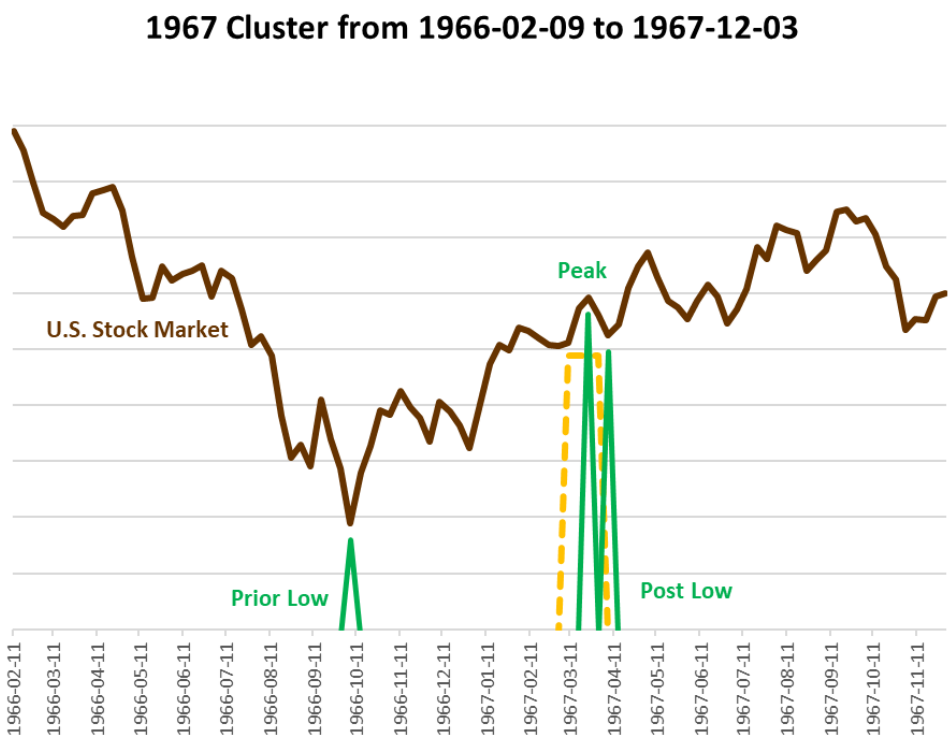

Figure N-5. Graph showing the 1967 Anxiety-Free Period, the related peak in market price and the prior- and post-low price points. Sources: CPM Investing LLC calculations using data from NASA, MeasuringWorth, and public market sources.

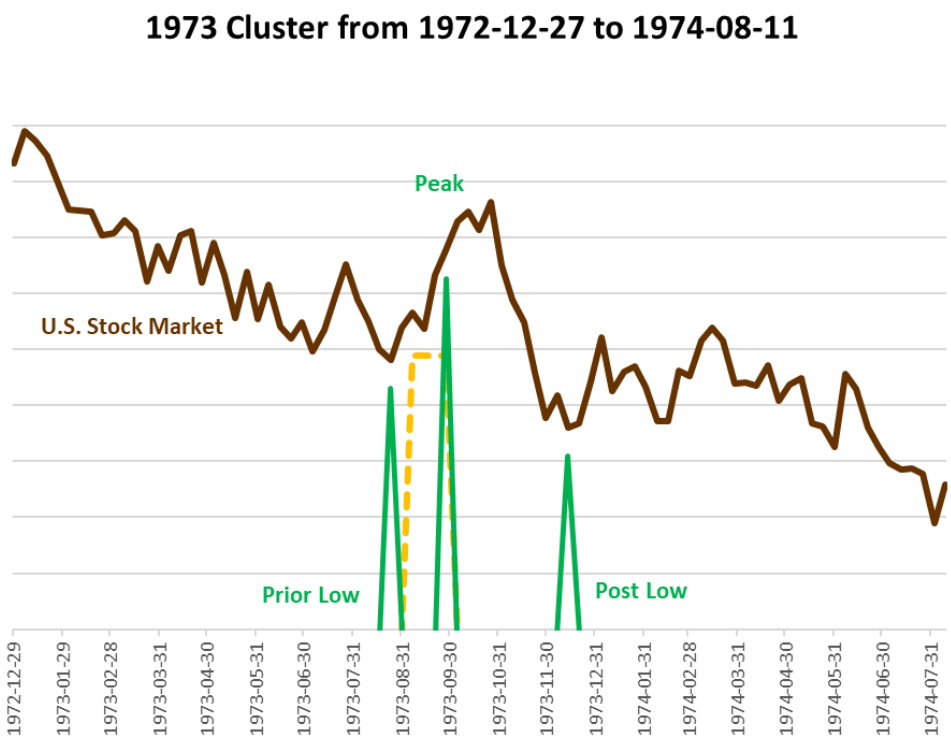

Figure N-6. Graph showing the 1937 Anxiety-Free Period, the related peak in market price and the prior- and post-low price points. Sources: CPM Investing LLC calculations using data from NASA, MeasuringWorth, and public market sources.

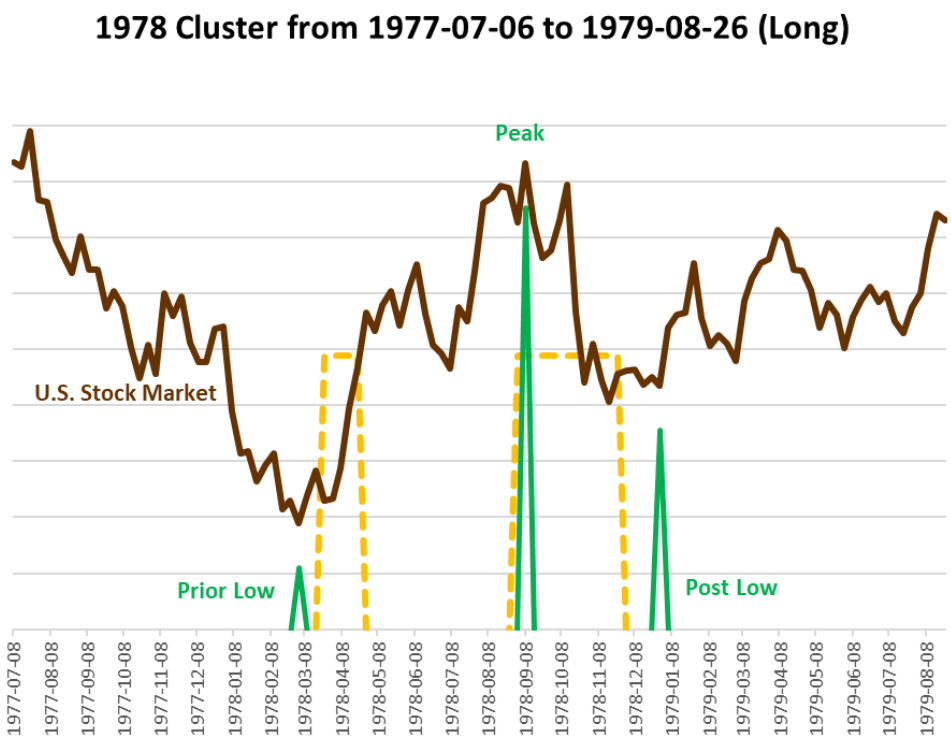

Figure N-7. Graph showing the 1978 Anxiety-Free Period, the related peak in market price and the prior- and post-low price points. Sources: CPM Investing LLC calculations using data from NASA, MeasuringWorth, and public market sources.

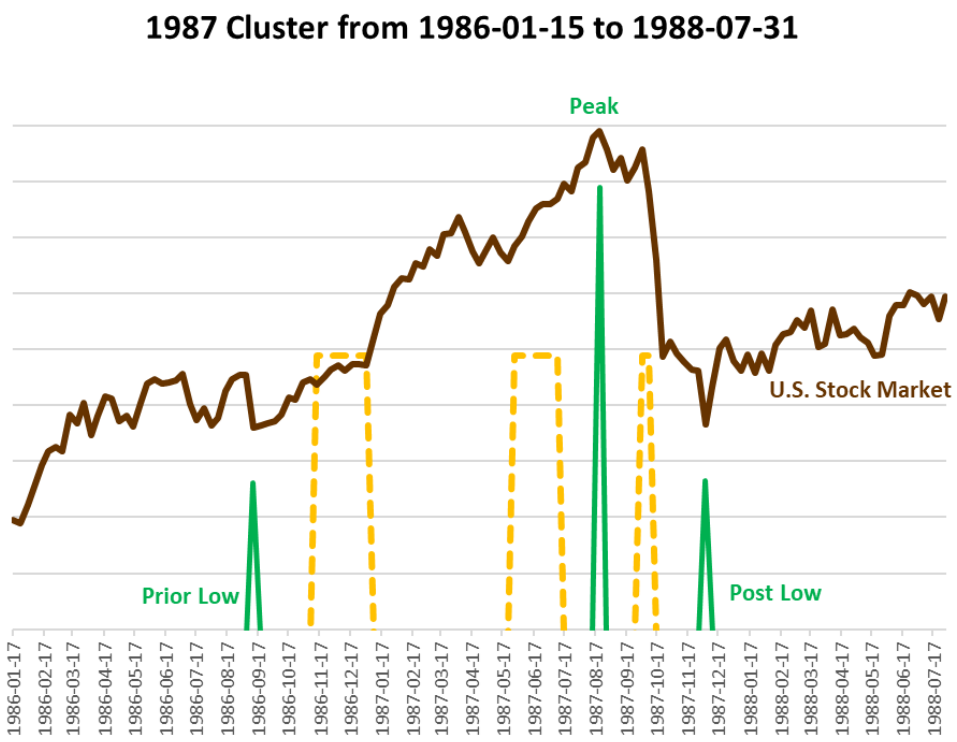

Figure N-8. Graph showing the 1987 Anxiety-Free Period, the related peak in market price and the prior- and post-low price points. Sources: CPM Investing LLC calculations using data from NASA, MeasuringWorth, and public market sources.

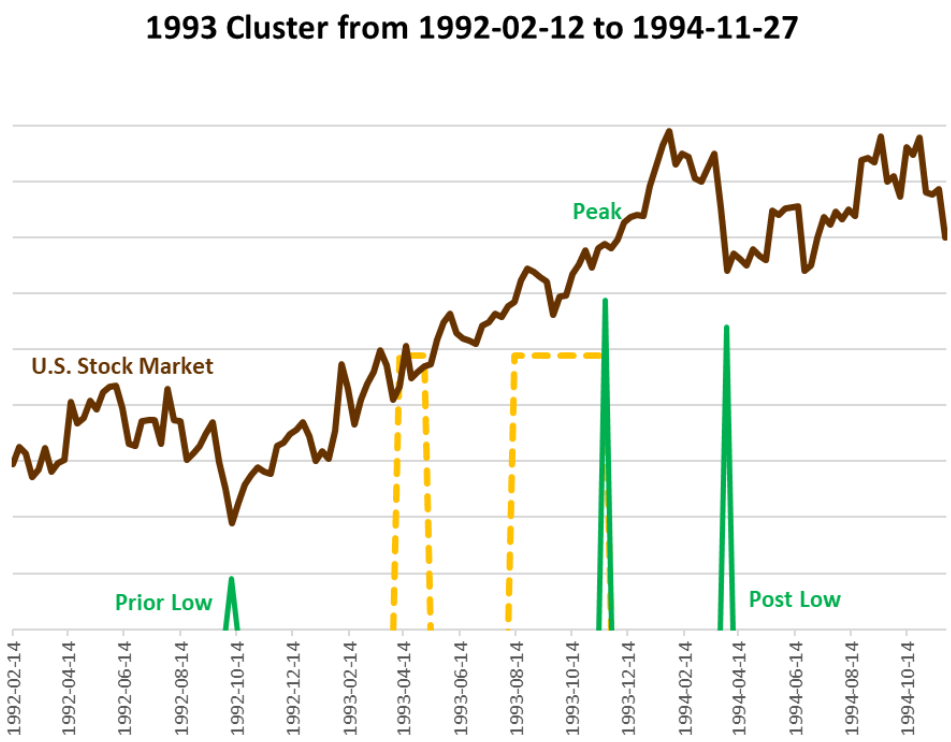

Figure N-9. Graph showing the 1993 Anxiety-Free Period, the related peak in market price and the prior- and post-low price points. Sources: CPM Investing LLC calculations using data from NASA, MeasuringWorth, and public market sources.

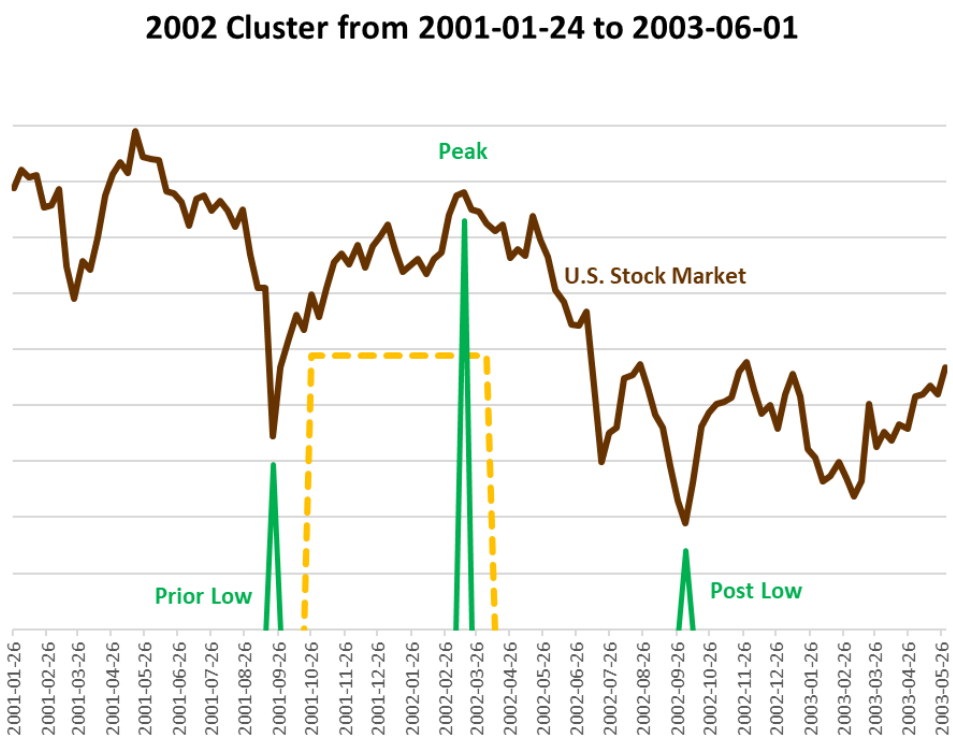

Figure N-10. Graph showing the 2002 Anxiety-Free Period, the related peak in market price and the prior- and post-low price points. Sources: CPM Investing LLC calculations using data from NASA, MeasuringWorth, and public market sources.

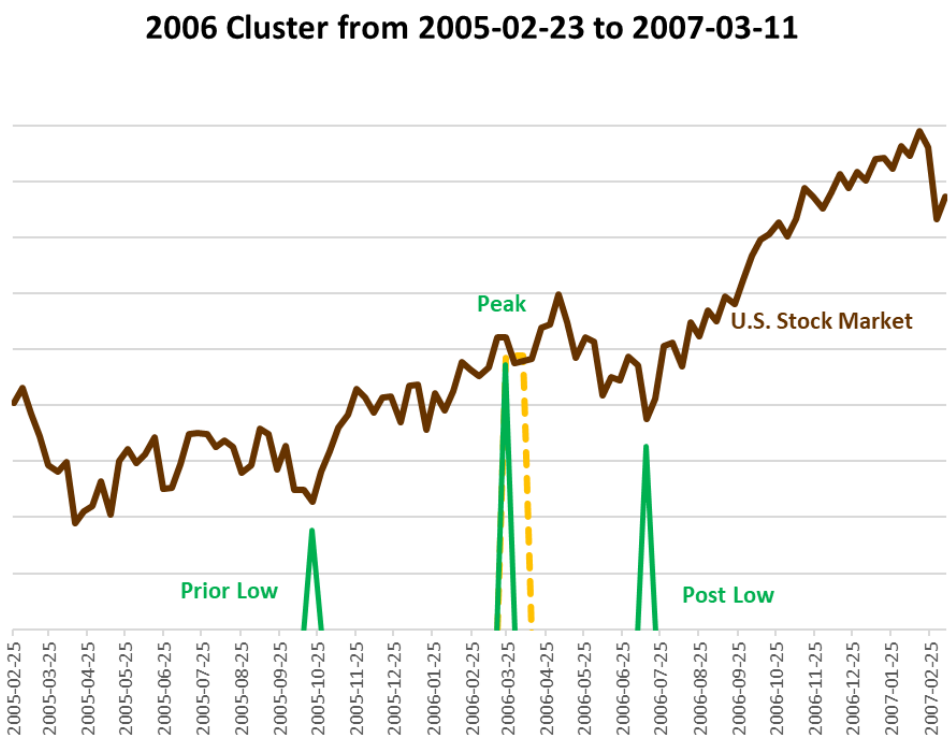

Figure N-11. Graph showing the 2006 Anxiety-Free Period, the related peak in market price and the prior- and post-low price points. Sources: CPM Investing LLC calculations using data from NASA, MeasuringWorth, and public market sources.

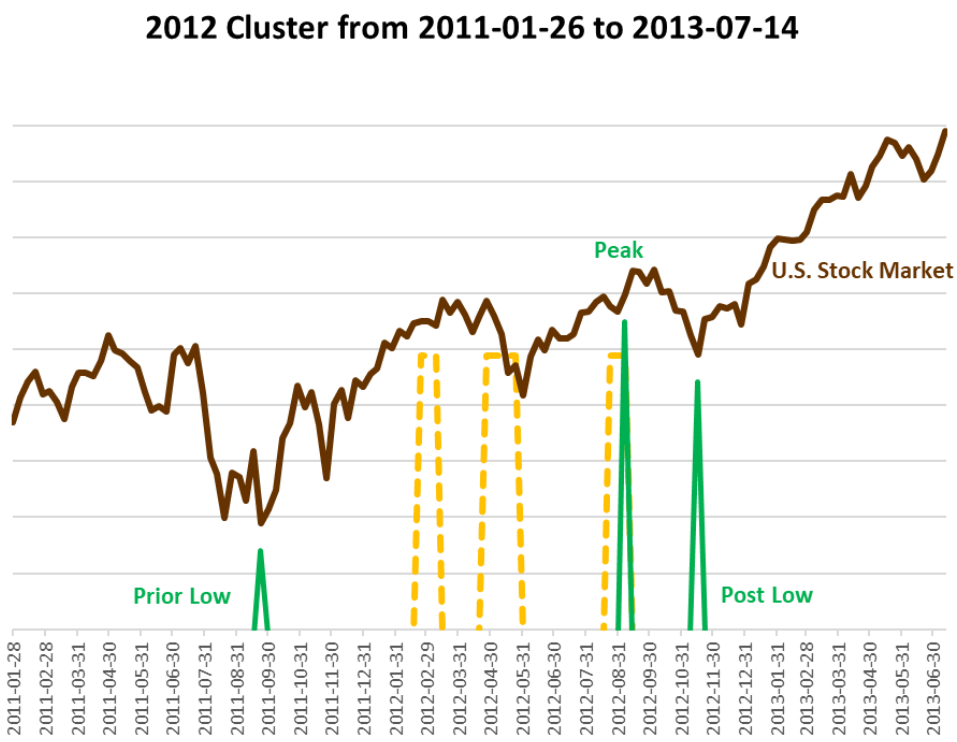

Figure N-12. Graph showing the 2012 Anxiety-Free Period, the related peak in market price and the prior- and post-low price points. Sources: CPM Investing LLC calculations using data from NASA, MeasuringWorth, and public market sources.

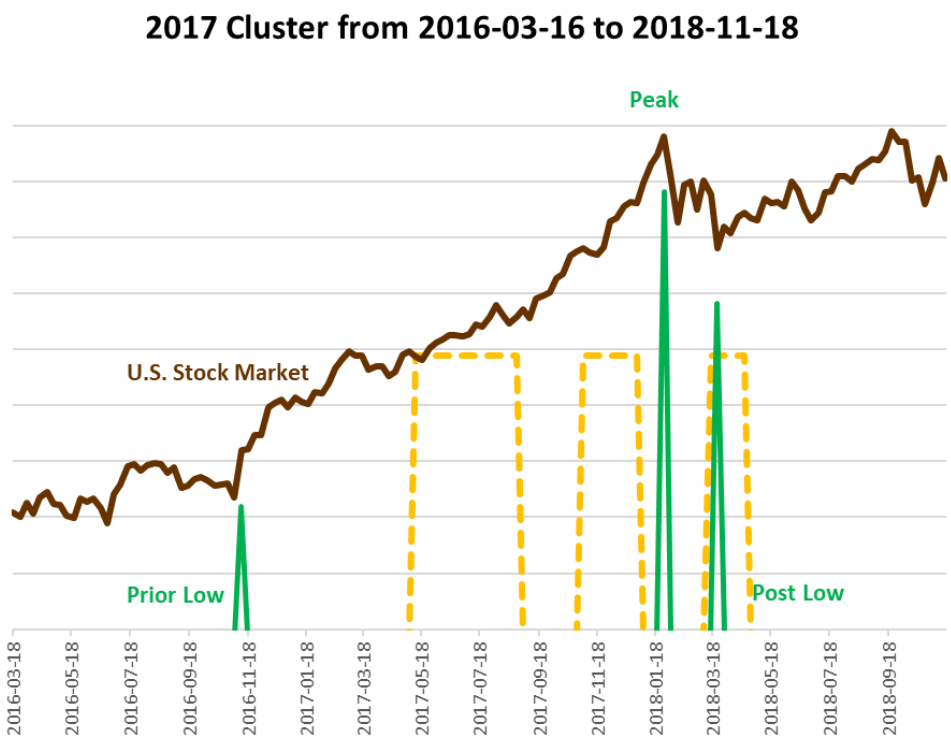

Figure N-13. Graph showing the 2017 Anxiety-Free Period, the related peak in market price and the prior- and post-low price points. Sources: CPM Investing LLC calculations using data from NASA, MeasuringWorth, and public market sources.

Appendix O - Electromagnetic Emissions and the Solar Convection Zone

The Sun's convective zone plays a critical role in the hypothesized mechanism described in this paper. Plasma motion and evolving magnetic fields originate here, and gravitational forces from compact planetary groupings may distort these flows—particularly near the solar equator, where toroidal magnetic fields are strongest.[1] These distortions may enhance magnetic twisting, buckling, or reconnection, leading to the release of turbulent, low-frequency electromagnetic energy, referred to here as low-frequency perturbations.[2] [3]

The structure of the toroidal field may also act as a waveguide, channeling Alfvén waves, which are magnetic oscillations that travel along field lines, and other magnetohydrodynamic fluctuations.[4] Although the Parker spiral, which is the spiral-shaped pattern of the Sun's magnetic field in the solar system that is created as the solar wind carries field lines outward while the Sun rotates about once every 27–28 days, generally distorts wave paths over long distances, emissions generated within toroidal magnetic corridors near the Sun may retain structure long enough to affect Earth's space environment.[5]

Observations from missions like the Parker Solar Probe support this possibility. They reveal that solar wind turbulence is spatially structured and varies by angular position, suggesting that some low-frequency emissions maintain their configuration during propagation.[6]

Analogies from plasma physics, astrophysical accretion disks, and Earth's geodynamo provide further support. In all these systems, small, persistent directional forces can induce large-scale magnetic instabilities.[7] [8] These parallels support the plausibility that gravitational influences on the Sun may contribute to directional turbulence and structured electromagnetic emissions.

A Wide Frequency Range

Solar and heliospheric activity generate electromagnetic radiation across the full spectrum, from gamma rays to extremely low frequencies (ELF). Perturbations—defined as irregular or transient fluctuations—can arise in any band. However, their ability to propagate through the heliosphere, interact with Earth's magnetic boundaries, and influence near-Earth systems varies by frequency.

---

[1] Miesch MS. Large-scale dynamics of the convection zone and tachocline. Living Rev Sol Phys. 2005;2(1):1. https://doi.org/10.12942/lrsp-2005-1

[2] Priest ER, Forbes TG. Magnetic reconnection: MHD theory and applications. Cambridge University Press; 2000.

[3] Yamada M, Kulsrud R, Ji H. Magnetic reconnection. Rev Mod Phys. 2010;82(1):603. https://doi.org/10.1103/RevModPhys.82.603

[4] Alfvén H. Existence of electromagnetic-hydrodynamic waves. Nature. 1942;150:405–406. https://doi.org/10.1038/150405d0

[5] Jokipii JR, Kota J. The polar heliospheric magnetic field. Geophys Res Lett. 1989;16(1):1–4. https://doi.org/10.1029/GL016i001p00001

[6] Bale SD et al. Highly structured slow solar wind emerging from an equatorial coronal hole. Nature. 2019;576(7786):237–242. https://doi.org/10.1038/s41586-019-1818-7

[7] Balbus SA, Hawley JF. Instability, turbulence, and enhanced transport in accretion disks. Rev Mod Phys. 1998;70(1):1. https://doi.org/10.1103/RevModPhys.70.1

[8] Glatzmaier GA, Roberts PH. A three-dimensional self-consistent computer simulation of a geomagnetic field reversal. Nature. 1995;377(6546):203–209. https://doi.org/10.1038/377203a0

This section outlines the theoretical and observational rationale for focusing on ELF perturbations (below 30 Hz, with a practical upper bound of 45 Hz). Although the electromagnetic spectrum is continuous, we emphasize three frequency bands—high frequency (X-ray and microwave), radio (10 kHz to 300 MHz), and ELF (0.1 to 100 Hz)—because they correspond to distinct mechanisms, propagation characteristics, and terrestrial effects. Intermediate bands, such as VLF to HF (3 kHz to 30 MHz), do contain solar signals, but they are harder to isolate by source and more heavily distorted by the Earth's ionosphere, which can reflect or absorb them depending on solar conditions and time of day.[9] For this reason, observational tools and theoretical models tend to prioritize frequencies where signal integrity, source attribution, and Earth impact are more readily measured.[10]

The Electromagnetic Spectrum

Solar EM waves emerge from diverse processes across the solar atmosphere, driven by magnetic reconnection, plasma instabilities, and pressure gradients. The following subsections describe the origins and behaviors of selected frequency bands in relation to their ability to carry low-frequency perturbations to Earth.

High Frequencies (X-ray, Microwave)

These emissions originate mainly from magnetic reconnection in the solar corona and upper chromosphere. When twisted magnetic field lines snap and reconnect, they release intense bursts of energy that heat plasma to tens of millions of degrees, emitting short-duration radiation in the X-ray and ultraviolet range.[11]

Perturbations: Often impulsive and burst-like, these emissions are tightly tied to flare activity.

- *Loss in the heliosphere:* Rapid geometric spreading and absorption in surrounding plasma dissipate these emissions quickly.
- *Directionality:* Initially directional due to localized flare regions but generally lose structure due to scattering.
- *Magnetospheric interaction:* These high-frequency waves are absorbed or scattered by Earth's upper atmosphere and rarely penetrate the magnetosphere.

Radio Bursts (10,000 Hz–300,000,000 Hz)

These bursts stem from coronal mass ejections, flares, and high-speed solar wind shocks. They span tens of kilohertz to hundreds of megahertz. The F10.7 Solar Flux (at 2.8 GHz), while outside this range, is often used as a proxy for solar activity.[12]

[9] Schunk RW, Nagy AF. Ionospheres: Physics, Plasma Physics, and Chemistry. Cambridge University Press; 2009.
[10] Gurnett DA, Bhattacharjee A. Introduction to Plasma Physics: With Space and Laboratory Applications. Cambridge University Press; 2005.
[11] Benz AO. Flare observations. Living Rev Sol Phys. 2017;14(1):2. https://doi.org/10.1007/s41116-016-0004-3
[12] Tapping KF. The 10.7 cm solar radio flux (F10.7). Space Weather. 2013;11(7):394–416. https://doi.org/10.1002/swe.20064

Perturbations: Appear as noisy, fluctuating signatures in frequency-time space.

- *Loss in the heliosphere:* Plasma dispersion, scattering, and magnetic refraction reduce signal structure during propagation.
- *Directionality:* Initial emissions may be directional, but most become diffuse.
- *Magnetospheric interaction:* Frequencies below ~30 MHz are generally reflected by the ionosphere. Higher frequencies may reach the upper atmosphere but are often absorbed or redirected before reaching deeper layers.[13]

Extremely Low Frequency (ELF) Waves (0.1–100 Hz)

ELF waves emerge from large-scale solar dynamics, including pressure gradients between solar wind streams, solar magnetic field rotation, and internal convective shearing. These processes can produce Alfvénic turbulence, which are random, wave-like fluctuations in magnetized plasma, and generate low-frequency EM perturbations detectable across the heliosphere.[14]

Perturbations: May appear as broad, irregular fluctuations or smoother wave patterns.

- *Loss in the heliosphere:* ELF waves attenuate very slowly due to their long wavelengths (thousands of kilometers), maintaining their integrity across great distances.
- *Directionality:* Often guided by large-scale solar structures like coronal holes or magnetic sector boundaries, lending them some directional bias.
- *Magnetospheric interaction:* ELF emissions couple well to Earth's ionosphere and magnetosphere, where they influence plasma density and modulate electromagnetic behavior. These frequencies also resonate with field line oscillations, increasing their impact.[15]

Conclusion

While perturbations occur throughout the solar spectrum, ELF waves stand out for their persistence, efficient transmission, and ability to influence Earth's near-space environment. Their propagation properties and strong coupling to geophysical boundaries make them uniquely suited to act as long-range carriers of solar energy. For these reasons, ELF perturbations are a central focus of our investigation into solar influence on market behavior.

[13] Hargreaves JK. The Solar-Terrestrial Environment. Cambridge University Press; 1992.
[14] Tu C, Marsch E. MHD structures, waves and turbulence in the solar wind: observations and theories. Space Sci Rev. 1995;73(1-2):1-210.
[15] Glassmeier KH, Othmer C, Cramm R, Stellmacher M, Engebretson M. Magnetospheric field line resonances: A comparative planetology approach. Surveys in Geophysics. 1999 Jan;20(1):61-109. https://doi.org/10.1023/A:1006659717963

Appendix P – 2017 Anxiety-Free Period and Global Electromagnetic Standing Waves

This appendix describes our analysis of the global electromagnetic standing wave (commonly described as Schumann resonance) frequency stability during the 2017 Anxiety-Free Period (AFP).

Calculation of the Schumann Resonance Series

We obtained electromagnetic standing wave data from the British Geological Survey from their Eskdalemuir monitoring site in Scotland. The raw data consisted of readings of every millisecond. We converted those observations into data describing the means and standard deviations of frequencies for each day. The Eskdalemuir dataset we analyzed consists of daily values for the North-south channel and modes one through five in the range 7–45 Hz for metrics such as mean frequency and standard deviation. We filtered the daily-level statistics by excluding days in the top 2.5% of daily average integrated power (total energy contained within a specific frequency band over a given time period). These filtering steps help reduce the influence of days with frequencies that are potentially affected by electric storms and other extreme events.

Figures O-4 and O-6 below show the data for the weekends lagged by approximately 12 days. Our analysis uses weekly data, and we selected weekend electromagnetic standing wave values to minimize the impact of industrial interference on the signal. Each week, electromagnetic standing wave values from Saturday and Sunday were averaged and assigned to the Friday immediately before the weekend. We then lagged the series by two weeks, meaning that each weekend's Schumann resonance values are compared to market behavior approximately two weeks later. This approach is motivated by research showing that investors often respond slowly to changes. In particular, limited attention and distraction, especially around weekends, can delay market reactions until the following week or later.[1] [2] Moreover, the well-documented phenomenon of post-earnings announcement drift shows that investor underreaction can persist for several weeks after news becomes public, reinforcing the relevance of testing lags in the range we apply.[3]

This two-week data lag helps align physical signals with the likely timing of investor response. This lag allows people to notice, interpret, and act on those signals, and for those actions to show up in market or sentiment data. Our physics-based drivers, including the AFP and M-Spike, are calibrated to the stock market making the lag important for assessing the alignment between the Schumann resonance data and the drivers.

Focus on Stability

Our focus is on the variability of the frequencies. We calculated the standard deviation of modes two and three, averaged them together, and then invert the result (multiply by –1) to create a stability score—with

[1] Hirshleifer D, Teoh SH. Limited attention, information disclosure, and financial reporting. J Account Econ. 2003;36(1–3):337–386.
https://doi.org/10.1016/j.jacceco.2003.10.002

[2] DellaVigna S, Pollet JM. Investor inattention and Friday earnings announcements. J Finance. 2009;64(2):709–749.
https://doi.org/10.1111/j.1540-6261.2009.01448.x

[3] Bernard VL, Thomas JK. Post-earnings-announcement drift: Delayed price response or risk premium? J Account Res. 1989;27:1–36.
https://doi.org/10.2307/2491062

higher values reflecting more stability, and lower values reflecting more volatility. We assume that a higher level of stability over these short periods is a good proxy for lower turbulence.

Various Metrics Tested

Figure P-1 below shows the US stock market (log scale) from June 5, 2015, through December 31, 2021 along with two lines indicating our predicted physics-based episodes. The predicted AFP shows the 2017 AFP represented as three columns. The predicted M-Spike shows five M-Spikes beginning with a small one in 2016. The ellipses shows that these drivers correspond to distinct market dynamics.

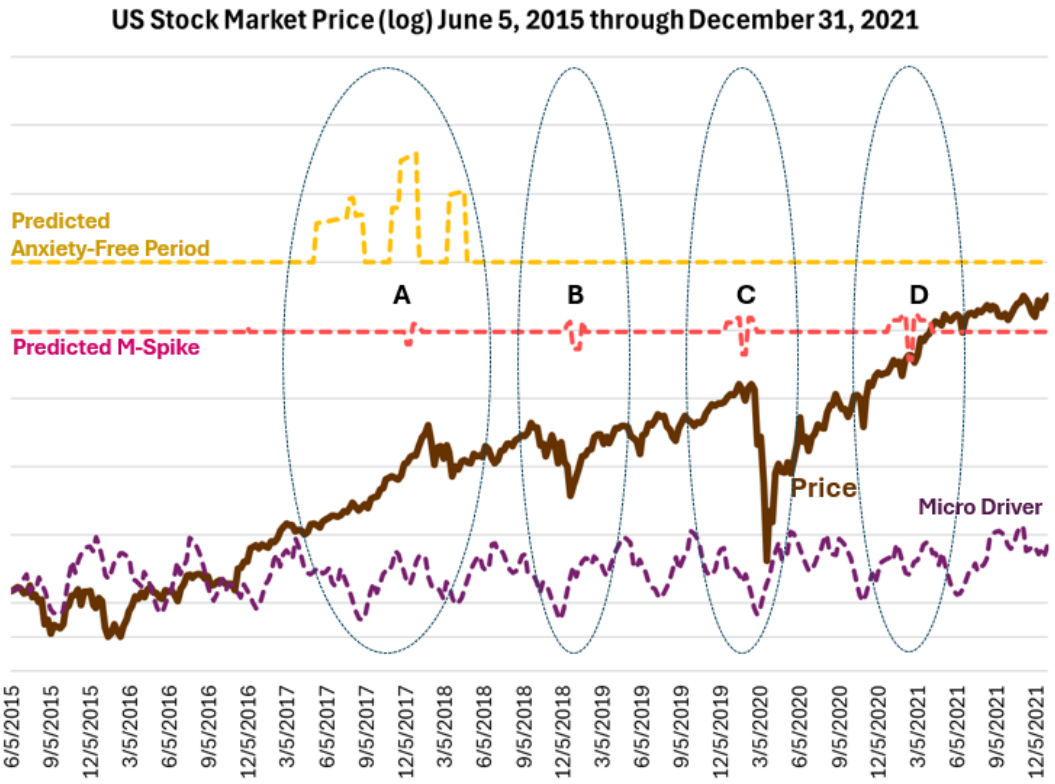

Figure P-1. Graph showing the price of the U.S. stock market from 2015 through 2021 along with the Predicted Anxiety-Free Period, M-Spoke, and Micro Driver series, which are based entirely on orbital geometry. Four ellipses (A-D) highlight periods of noteworthy market dynamics. Sources: CPM Investing LLC calculations using NASA, MeasuringWorth, and public market sources. 'U.S. stocks' and 'U.S. stock market' refer to the DJIA, S&P 500, or related ETFs depending on the period.

Ellipse A shows the several month period of strong stock market gains, ending with a peak in the market at the end of 2017. This period coincides with the columns of the 90-degree configuration events. Ellipses B through D highlight market episodes that correspond to the M-Spikes shown in the drivers. Both predicted series are determined by planetary influence distribution, so these corresponding patterns imply a relationship between planetary influence distribution and these particular market dynamics.

In Figure P-2 below, we add the integrated power (inverted) reading for the Shuman resonance frequencies. These are trailing 7-day averages.

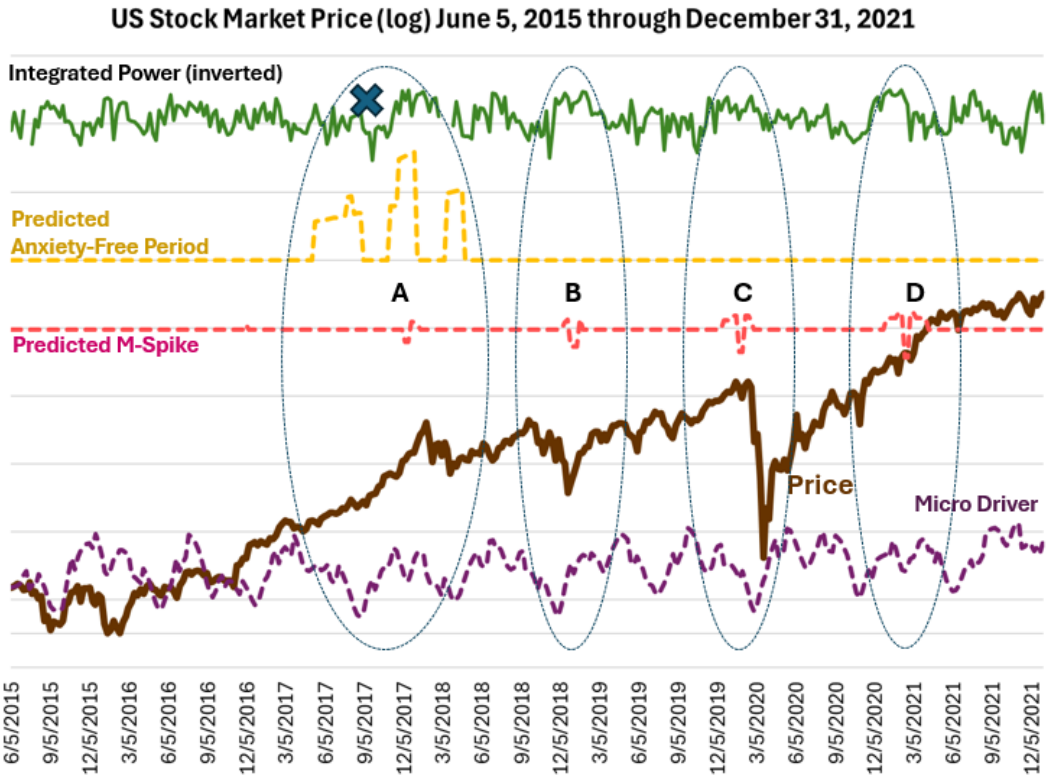

Figure P-2. Graph showing the price of the U.S. stock market from 2015 through 2021 along with the Predicted Anxiety-Free Period, M-Spoke, and Micro Driver series, which are based entirely on orbital geometry. Four ellipses (A-D) highlight periods of noteworthy market dynamics. It also shows the Integrated Power (inverted) of the magnetometer readings designed to detect the global electromagnetic standing waves coving the daytime (8 am to 4 pm local time) period of all days (weekday and weekend) in the period. Sources: CPM Investing LLC calculations using data from NASA, British Geological Survey, MeasuringWorth, and public market sources. 'U.S. stocks' and 'U.S. stock market' refer to the DJIA, S&P 500, or related ETFs depending on the period.

Changes in integrated power appear to correspond to the AFP driver. The patterns in the integrated power readings appear moderately similar to those of the M-Spike driver.

Figure P-3 below shows the change in the mean frequency of Mode 3 of the Schumann resonance frequencies.

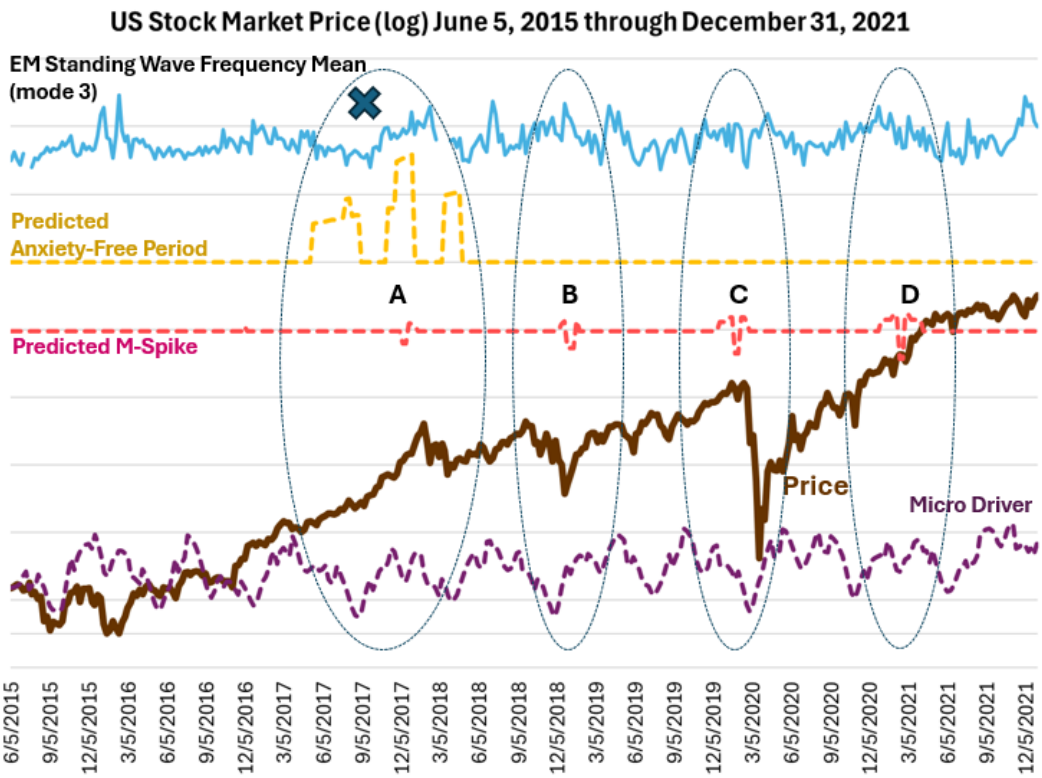

Figure P-3. Graph showing the price of the U.S. stock market from 2015 through 2021 along with the Predicted Anxiety-Free Period, M-Spoke, and Micro Driver series, which are based entirely on orbital geometry. Four ellipses (A-D) highlight periods of noteworthy market dynamics. It also shows the mean of the global electromagnetic standing wave frequency (modes 3) coving the daytime (8 am to 4 pm local time) period of weekend days in the period. Sources: CPM Investing LLC calculations using data from NASA, the British Geological Survey, MeasuringWorth, and public market sources. 'U.S. stocks' and 'U.S. stock market' refer to the DJIA, S&P 500, or related ETFs depending on the period.

There are corresponding patterns. Figure P-4 below shows the frequency stability of modes 2 and 3.

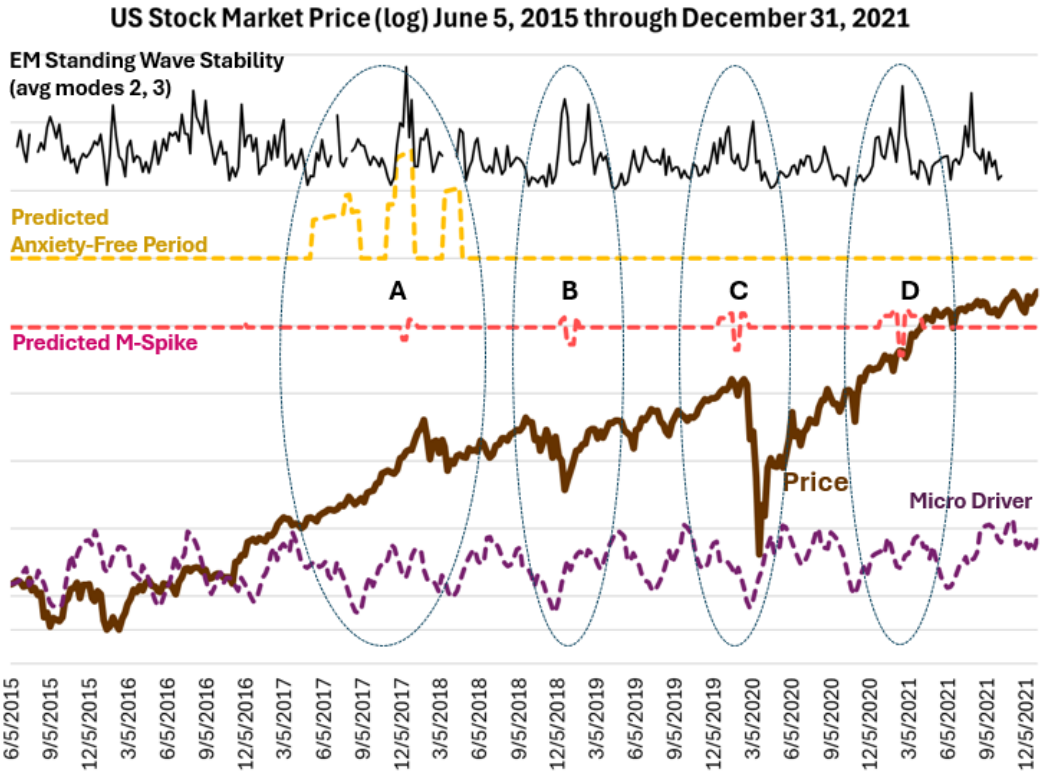

Figure P-4. Graph showing the price of the U.S. stock market from 2015 through 2021 along with the Predicted Anxiety-Free Period, M-Spoke, and Micro Driver series, which are based entirely on orbital geometry. Four ellipses (A-D) highlight periods of noteworthy market dynamics. It also shows the stability of the global electromagnetic standing waves (modes 2 and 3) coving the daytime (8 am to 4 pm local time) period of weekend days in the period. Sources: CPM Investing LLC calculations using data from NASA, the British Geological Survey, MeasuringWorth, and public market sources. 'U.S. stocks' and 'U.S. stock market' refer to the DJIA, S&P 500, or related ETFs depending on the period.

We focus on the variability/stability relationships of the dependent and independent variables. The results of this analysis support that focus.

These readings best show that stability is highest at the peak of the AFP. The M-Spikes are also clearly visible. Our regression analyses over this short period with relatively few episodes show statistical significance in the two episodic drivers shown.

Regression of Standing Wave and Orbital Geometry Factors

This section details an ordinary least squares (OLS) regression examining the relationship between electromagnetic standing wave Modes 2 and 3 and two orbital geometry–derived factors: 90-degree factor and M-Spike factor. The goal is to determine whether variations in electromagnetic standing waves can be statistically explained by these two predictors, allowing the regression to estimate an intercept term.

Data

- Source: Electromagnetic standing wave - British Geological Survey
- Dependent variable: Electromagnetic standing wave stability (average of modes 2 and 3)

- Independent variables:
  - 90-degree factor — orbital geometry factor tied to anxiety-free periods.
  - M-Spike factor — orbital geometry factor tied to short-term M-Spike.

Method

An OLS regression was run with global electromagnetic standing wave stability as the dependent variable and the predicted AFP and M-spike factors as independent variables. A constant term was included to allow the intercept to be estimated from the data. No variable transformations were applied. Multicollinearity was tested using the variance inflation factor (VIF) and found to be negligible (VIF ≈ 1.00 for both predictors).

Results

Variable	Coefficient	Std. Error	t-Statistic	p-Value
90-Degree Factor	0.23	0.06	3.8	< 0.001
M-Spike Factor	–0.30	0.23	–1.3	0.19

Figure P-5. Table showing the results of a regression of the global electromagnetic standing wave stability and the predicted AFP and M-spike factors as independent variables from 2015 through 2021. Sources: CPM Investing LLC calculations using data from NASA, the British Geological Survey, MeasuringWorth, and public market sources. 'U.S. stocks' and 'U.S. stock market' refer to the DJIA, S&P 500, or related ETFs depending on the period.

Interpretation

The model suggests that 90-degree factor has a measurable positive association with electromagnetic standing waves, while M-Spike factor's effect is not distinguishable from zero in this sample. The intercept (~140.5) represents the baseline electromagnetic standing waves value when both factors are zero. The R^2 is low (0.05), which indicates that most of electromagnetic standing wave variation is not explained by these two predictors, suggesting other factors are also at play.

The M-Spike has more episodes during this period, but the M-Spike does not show as a statistically significant predictor at conventional levels, despite the visual correspondence between M-Spike fluctuations and electromagnetic standing wave stability. The M-Spike is calibrated to the market, and the driver does correspond to similar patterns in the market, but the patterns in the electromagnetic standing wave stability metric are broader. There could be many reasons for this, but the calculation for the M-Spike is more complicated and the effects of planetary influence distribution associated with them may be more diffuse than the expected sharp boundaries of the AFP.

Despite the limitations of this analysis, the peak of stability occurring when it is expected and similar patterns in the M-Spikes make the connection between electromagnetic standing wave stability and planetary influence distribution intriguing.

An Expanded Dataset

The global electromagnetic standing wave frequences and their detection are influenced by environmental and atmospheric factors including power equipment close to the instruments used to detect them, as well as by lightning globally. Figure P-4 above shows readings from the available data that we believe are relatively free from these interferences. That data series:

- Excludes daily readings that have the strongest 2.5% of power readings in order to reduce the impact of lightning,
- Includes readings from daylight hours (from 8 am to 4 pm) to fully detect the electromagnetic standing waves without being affected by the ionosphere boundary changes associated with the transitions between day and night, and
- Includes readings only from weekends to avoid commercial activity that might introduce interference at the detection site.

Figure P-6 below shows the same information as Figure P-4 above with the addition of series that do not meet the same stringent criteria. It includes series recorded during the workweek as well as nighttime readings.[4] We did this to determine whether our efforts to clean the data might have affected the results described above.

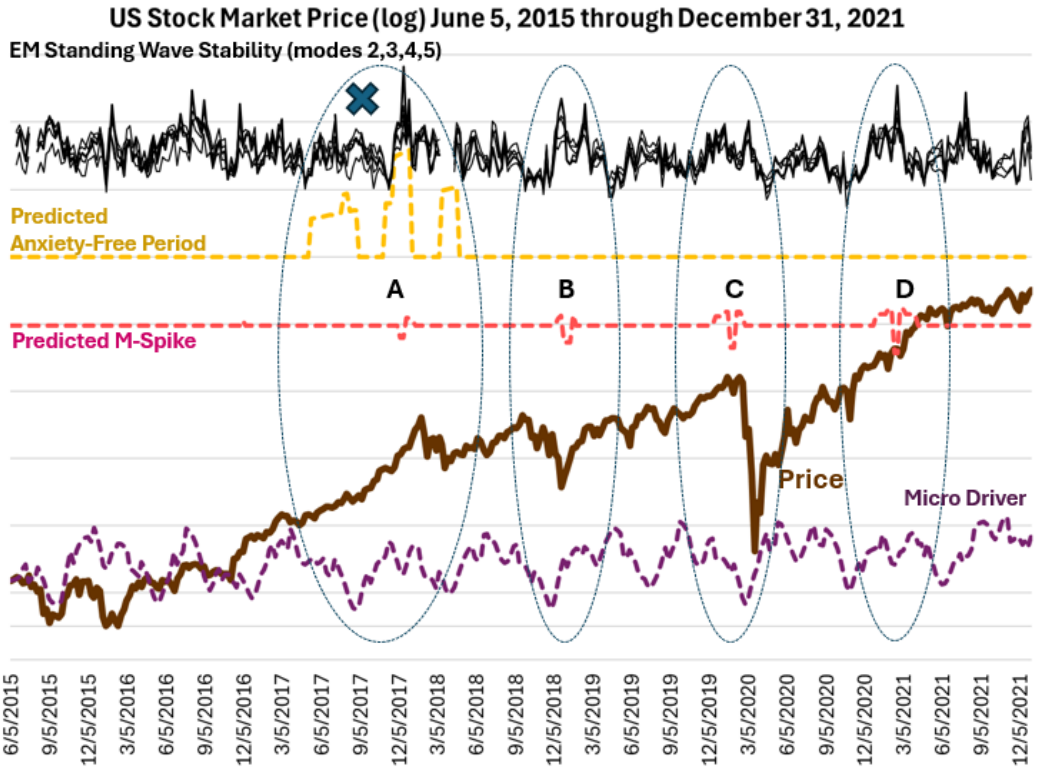

Figure P-6. U.S. Stock market price and the indicators for the 2017 Anxiety-Free Period and the M-Spike episodes from June 5, 2015 through December 31, 2021. This chart shows the market price level and the indicators for these two types of episodes along with ellipses A through D, which indicate noteworthy relationships between patterns in stock price movement and the episodic indicators. This chart also shows the stability of the electromagnetic standing waves for modes 2 through 5 observed on all days between the hours of 8 am and 4 pm local time. Sources: CPM Investing LLC calculations using data from NASA, the British Geological Survey, MeasuringWorth, and public market sources. 'U.S. stocks' and 'U.S. stock market' refer to the DJIA, S&P 500, or related ETFs depending on the period.

While a noisier picture, the same noteworthy patterns are present in the stability data for the global electromagnetic standing waves. The highest level of stability continues to correspond to the highest

[4] Note: This figure shows the stability metric for standing wave modes four and five, daytime readings, and for seven days a week.

column of the Anxiety-Free Period (ellipse A). In addition, the M-Spike patterns are still visible in the noisier patterns.

Other Solar Energy Metrics

The following slides show other series related to solar energy. The "X" highlights an anomaly that will be investigated in Study E. Figure P-7 below shows the Oulu NM (corrected for air pressure) series.

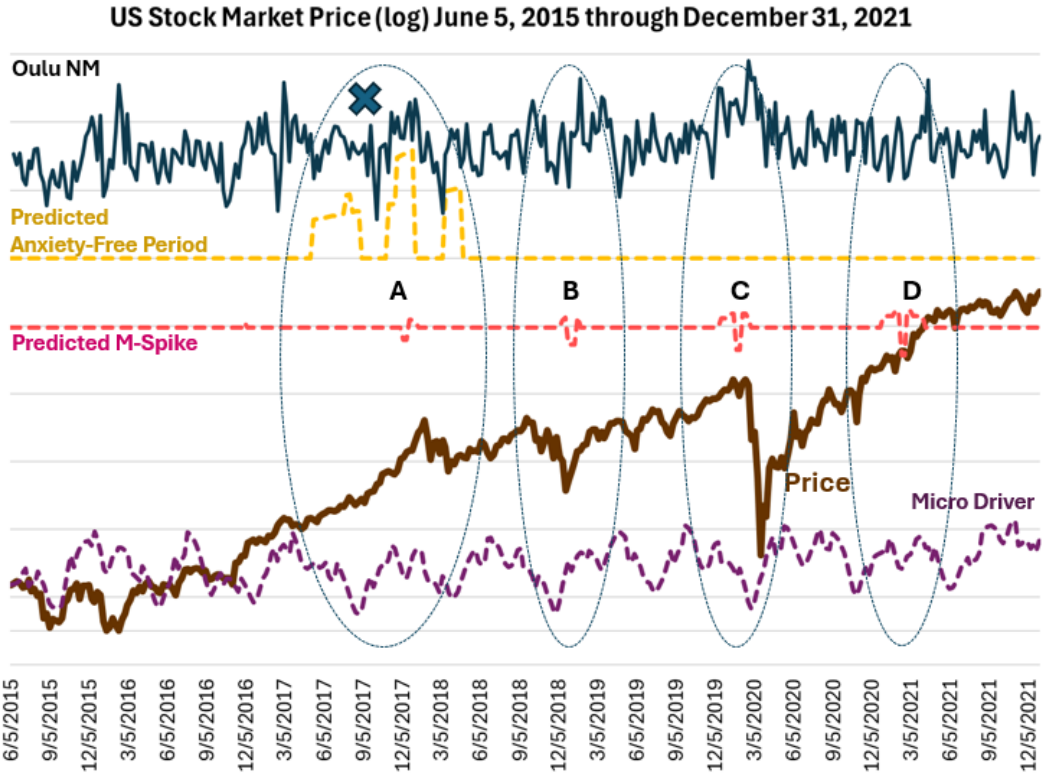

Figure P-7. Graph showing the price of the U.S. stock market from 2015 through 2021 along with the Predicted Anxiety-Free Period, M-Spoke, and Micro Driver series, which are based entirely on orbital geometry. Four ellipses (A-D) highlight periods of noteworthy market dynamics. It also shows the Oulu NM readings (corrected for air pressure) covering the daytime (8 am to 4 pm local time) periods for weekdays and weekend days in the period. Sources: CPM Investing LLC calculations using data from NASA, the British Geological Survey, MeasuringWorth, and public market sources. 'U.S. stocks' and 'U.S. stock market' refer to the DJIA, S&P 500, or related ETFs depending on the period.

Figure P-8 below shows the sunspot count series (inverted) series.

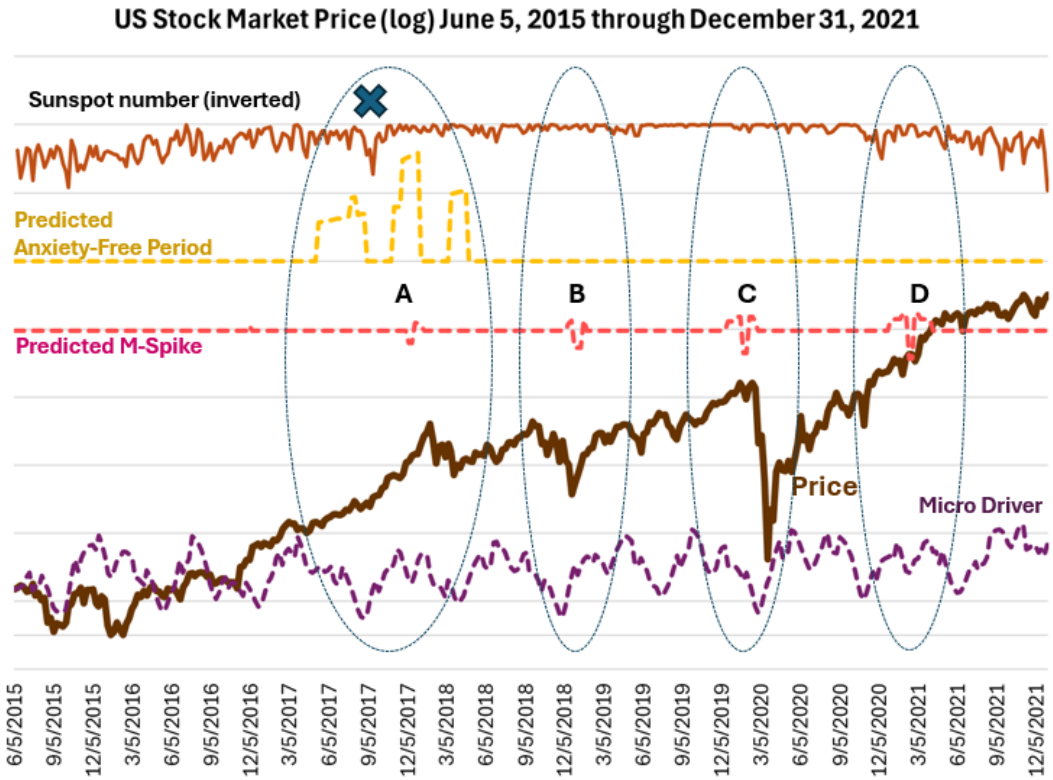

Figure P-8. Graph showing the price of the U.S. stock market from 2015 through 2021 along with the Predicted Anxiety-Free Period, M-Spoke, and Micro Driver series, which are based entirely on orbital geometry. Four ellipses (A-D) highlight periods of noteworthy market dynamics. It also shows the sunspot count series (inverted). Sources: CPM Investing LLC calculations using data from NASA, the British Geological Survey, MeasuringWorth, and public market sources. 'U.S. stocks' and 'U.S. stock market' refer to the DJIA, S&P 500, or related ETFs depending on the period.

Appendix Q – Air Pressure Oscillations and Delyukov

When analyzing the electromagnetic standing wave data, we looked for a shift in the turbulence–stability dynamic because of our research into the Oulu galactic cosmic ray readings. In our search for a plausible pathway linking solar activity to human mood, we identified intriguing correlations between readings from the Oulu Neutron Monitor (Oulu NM) and investor sentiment. The Oulu NM readings function as inverse proxies for solar electromagnetic activity: when solar output is high, the solar wind and heliospheric magnetic field more effectively shield Earth from galactic cosmic rays, resulting in lower neutron counts at ground-based detectors like Oulu. Conversely, elevated Oulu NM counts typically indicate lower solar activity and reduced shielding. [1] [2] [3]

Oulu has maintained continuous observations since the mid-1960s, offering three data series: the raw galactic cosmic ray count, the atmospheric pressure as measured at the monitoring site in Finland, and the galactic cosmic ray count corrected for atmospheric pressure. Pressure correction is essential because increased atmospheric pressure raises the air column above the detector, which reduces the number of secondary cosmic ray particles that reach ground level. While the pressure-corrected cosmic ray counts revealed patterns aligning with longer-term sentiment indicators, it was the uncorrected counts and local atmospheric pressure metrics that showed stronger correlations with shorter-term fluctuations in mood and investor behavior.

This observation led us to examine whether atmospheric pressure itself might influence human sentiment. We found controlled experimental studies demonstrating that low-frequency atmospheric pressure oscillations—especially quasi-chaotic or irregular fluctuations—can impair attention, disrupt short-term memory, and reduce task performance in healthy individuals.[4] These effects are thought to arise from the mechanical influence of external air pressure variations on baroreceptors, sensory structures in the aortic arch and carotid sinuses that regulate cardiovascular responses.

We ultimately determined that air pressure oscillations are unlikely to be the primary vector linking solar activity to sentiment because our more detailed analysis suggested that pressure readings lagged changes in sentiment during some periods. We also questioned the global reach of measured air pressure oscillations. However, the line of inquiry helped direct our attention to the broader turbulence-versus-stability dynamic as an early organizing principle in our research.

[1] Forbush SE. World-wide cosmic-ray variations, 1937–1952. J Geophys Res. 1954;59(4):525–542. https://doi.org/10.1029/JZ059i004p00525

[2] O'Brien KP, Burke GW. The analysis of cosmic-ray records. Rev Geophys. 1973;11(1):87–112. https://doi.org/10.1029/RG011i001p00087

[3] Usoskin IG, Kovaltsov GA, Mishev A, Gil A. Heliospheric modulation of cosmic rays during the neutron monitor era: Unified data set. J Geophys Res Space Physics. 2017;122(4):3875–3887. https://doi.org/10.1002/2016JA023819

[4] Delyukov A, Didyk L. The effects of extra-low-frequency atmospheric pressure oscillations on human mental activity. Int J Biometeorol. 1999;43:31–37. https://doi.org/10.1007/s004840050113

Atmospheric Pressure Fluctuations and Self-Doubt in Mental Performance

In a controlled study on ultra-low-frequency air pressure changes, Anatoly Delyukov and Lyudmila Didyk examined how subtle atmospheric pressure oscillations (APO) influence human mental activity.[5] The researchers exposed volunteers to different types of artificially generated pressure waves, simulating natural fluctuations that occur during turbulent or stormy weather. One specific condition—quasi-chaotic atmospheric pressure oscillations, which mimicked naturally disordered, low-frequency pressure noise—stood out for its disruptive effects on attention and task performance.

Participants exposed to these chaotic pressure changes showed a statistically significant decline in attention and a concurrent rise in heart rate, while failing to improve on short-term memory or performance rate tasks. Some even reported a vague but telling sensation that "something prevented them from performing the task better".[6] In contrast, rhythmic or periodic APO (with 30- to 90-second cycles) improved attention, slowed heart rate, and enhanced performance for many participants, especially those with lower baseline mental activity.

These findings suggest that irregular atmospheric pressure changes may subtly disrupt focused mental effort. While the study did not directly measure self-doubt, the subjective reports—combined with measurable declines in attention—support the idea that individuals may mistakenly interpret these lapses as personal failings, rather than responses to an invisible environmental force. This interpretation aligns with other research on infrasound, which has been shown to impair concentration, mood, and perceived cognitive control even when not consciously heard.[7]

In a later paper, Delyukov offered a detailed hypothesis for why APO affect mental function. He argued that baroreceptors—small pressure-sensitive structures in the carotid sinus and aortic arch—are directly influenced by external air pressure changes.[8] These baroreceptors normally regulate blood pressure through a feedback loop involving the medulla oblongata. However, if the external air pressure oscillates, as it does in natural or artificial APO, the baroreceptors may feed false information into this control system, generating physiological changes that extend beyond cardiovascular regulation. In his experiments, Delyukov found that APO exposure significantly altered systolic pressure, cardiac output, and even synchronized heart rate variability with the oscillation frequency. Crucially, baroreceptor signals also reach the hypothalamus and may influence emotional state and cognitive performance—a pathway that helps explain why these subtle pressure waves can affect mental activity, even in otherwise healthy individuals.

Together, these studies support the idea that disordered atmospheric pressure fluctuations can destabilize focus and trigger unexplained cognitive lapses, which may be experienced as doubt, fatigue, or inefficacy.

[5] Delyukov A, Didyk L. The effects of extra-low-frequency atmospheric pressure oscillations on human mental activity. Int J Biometeorol. 1999;43:31–37.
https://doi.org/10.1007/s004840050113

[6] Delyukov A, Didyk L. The effects of extra-low-frequency atmospheric pressure oscillations on human mental activity. Int J Biometeorol. 1999;43:31–37.
https://doi.org/10.1007/s004840050113

[7] Zhang, W., Yin, J., Gao, BY. et al. Inhibition of astroglial hemichannels ameliorates infrasonic noise induced short-term learning and memory impairment. Behav Brain Funct 19, 23 (2023).
https://doi.org/10.1186/s12993-023-00226-7

[8] Delyukov A, Höppe P, Tsybenko V. To the mechanism of physiological effects of atmospheric pressure fluctuations. Presented at: AMS Conference on Biometeorology and Aerobiology; 2004.
https://ams.confex.com/ams/pdfpapers/78836.pdf

Because these changes are silent and omnipresent, especially during weather shifts or high turbulence, they may represent a hidden influence on workplace performance, mental well-being, and environmental safety.

Appendix R – Nine Anxiety-Free Periods Since 1964 and Two Solar Emission Metrics

Visual inspection of the data suggests that the lower deviation observed inside the broad AFP window may result from those periods often falling on the rising or falling phases of the broader solar cycles.

The statistical relationships and the observed patterns support our assertion that orbital geometry of the solar system affects the Sun's energy emissions.

In the figures below, the height of the vertical columns marking the AFPs has been adjusted to highlight their relationships to the sunspot and Oulu time series. The tallest portion of each column typically corresponds to the peak of optimism, with the sharp spike at the top indicating the moment of greatest optimism.

1973 Anxiety-Free Period

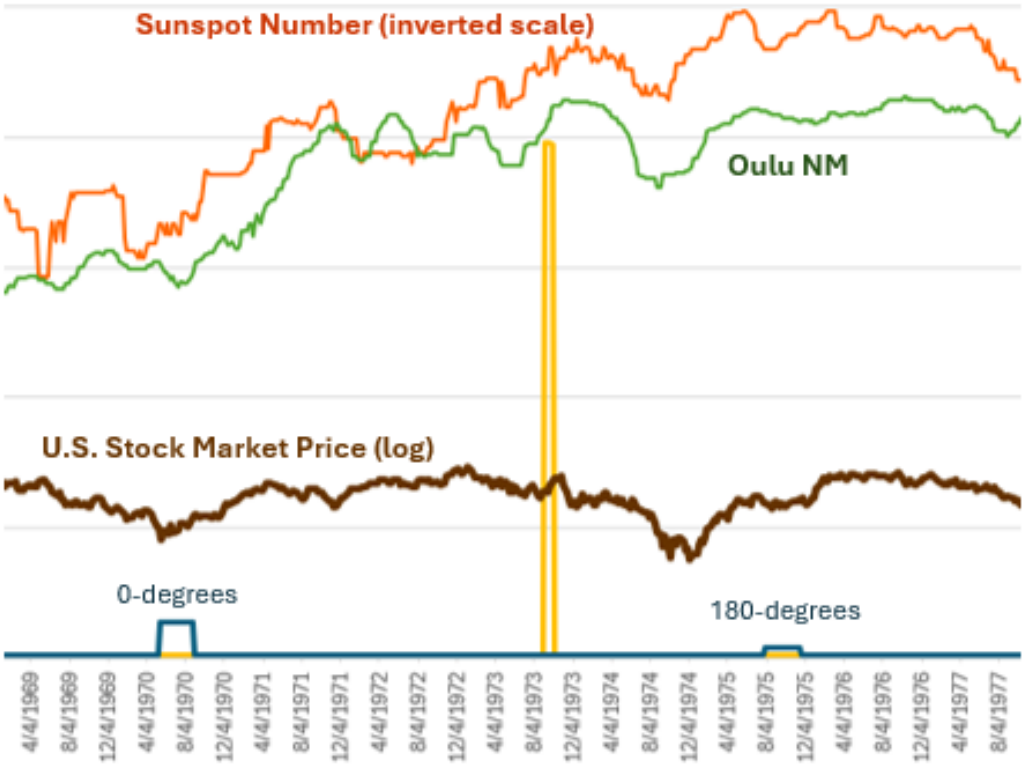

Figure R-1. U.S. Stock market price shown as the brown line (log scale) before and after the 1974 Anxiety-Free Period. The 90-degree configuration begins when the yellow line moves higher from its base line and ends when the line moves back to the base line. The orange line is the sunspot count number (normalized on an inverted scale). The green line is the Oulu NM readings (corrected for air pressure). The 0-degree configuration between the Inner and Outer Orbital Centers is indicated by the shorter of the two blue-line columns. The 180-degree configuration is indicated by the taller of the two columns. Sources: CPM Investing LLC calculations using data from NASA, Oulu NM, MeasuringWorth, and public market sources. 'U.S. stocks' and 'U.S. stock market' refer to the DJIA, S&P 500, or related ETFs depending on the period.

The AFP occurs while the Sunspot and Oulu series are ascending, and at the beginning of the upward movement of the market. The decline of the sunspot, Oulu, and the market in 1974 are noteworthy.

1978 Anxiety-Free Period

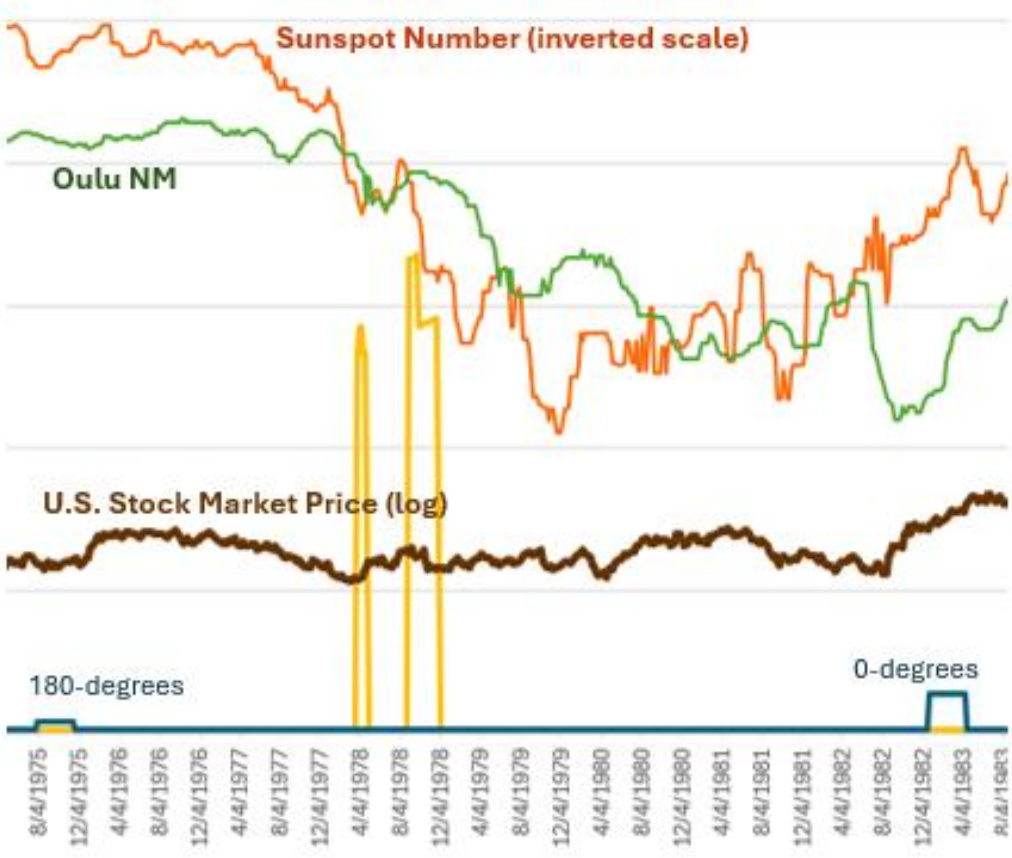

Figure R-2. U.S. Stock market price shown as the brown line (log scale) before and after the 1978 Anxiety-Free Period. A 90-degree configuration begins when the yellow line moves higher from its base line and ends when the line moves back to the base line. The orange line is the sunspot count number (normalized on an inverted scale). The green line is the Oulu NM readings (corrected for air pressure). The 0-degree configuration between the Inner and Outer Orbital Centers is indicated by the shorter of the two blue-line columns. The 180-degree configuration is indicated by the taller of the two columns. Sources: CPM Investing LLC calculations using data from NASA, Oulu NM, MeasuringWorth, and public market sources. 'U.S. stocks' and 'U.S. stock market' refer to the DJIA, S&P 500, or related ETFs depending on the period.

The highest point in the AFP, which occurs at the beginning of the second column, corresponds with a similar pattern in the sunspot series, although the sunspot series pattern takes place well before the AFP's pattern. This suggests that the calibration of the AFP is not completely accurate.

1987 Anxiety-Free Period

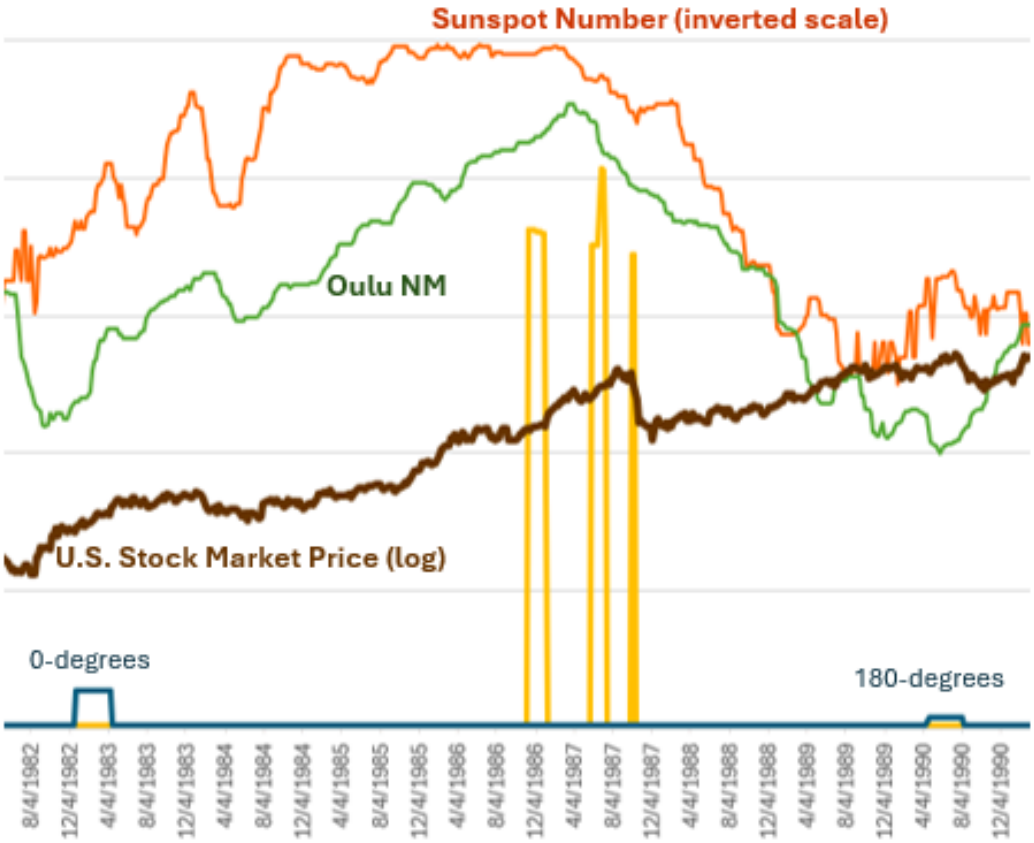

Figure R-3. U.S. Stock market price shown as the brown line (log scale) before and after the 1987 Anxiety-Free Period. A 90-degree configuration begins when the yellow line moves higher from its base line and ends when the line moves back to the base line. The orange line is the sunspot count number (normalized on an inverted scale). The green line is the Oulu NM readings (corrected for air pressure). The 0-degree configuration between the Inner and Outer Orbital Centers is indicated by the shorter of the two blue-line columns. The 180-degree configuration is indicated by the taller of the two columns. Sources: CPM Investing LLC calculations using data from NASA, Oulu NM, MeasuringWorth, and public market sources. 'U.S. stocks' and 'U.S. stock market' refer to the DJIA, S&P 500, or related ETFs depending on the period.

The highest point in the AFP (at the end of the second column) takes place just before the peak in the market. The peaks in the sunspot count and Oulu series take place earlier and coincide with an intermediate peak in market prices taking place between the first two columns of the AFP.

1993 Anxiety-Free Period

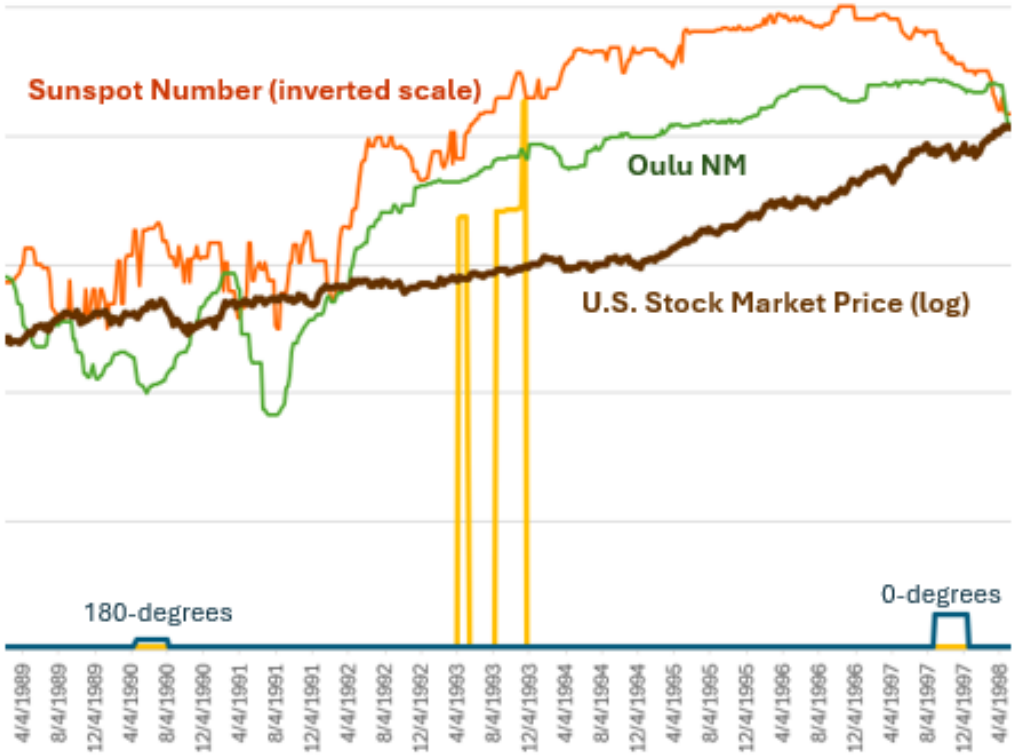

Figure R-4. U.S. Stock market price shown as the brown line (log scale) before and after the 1993 Anxiety-Free Period. A 90-degree configuration begins when the yellow line moves higher from its base line and ends when the line moves back to the base line. The orange line is the sunspot count number (normalized on an inverted scale). The green line is the Oulu NM readings (corrected for air pressure). The 0-degree configuration between the Inner and Outer Orbital Centers is indicated by the shorter of the two blue-line columns. The 180-degree configuration is indicated by the taller of the two columns. Sources: CPM Investing LLC calculations using data from NASA, Oulu NM, MeasuringWorth, and public market sources. 'U.S. stocks' and 'U.S. stock market' refer to the DJIA, S&P 500, or related ETFs depending on the period.

The highest point in the AFP at the end of the second column occurs shortly after a brief peak in the Sunspot series, again suggesting a calibration issue.

2001 Anxiety-Free Period

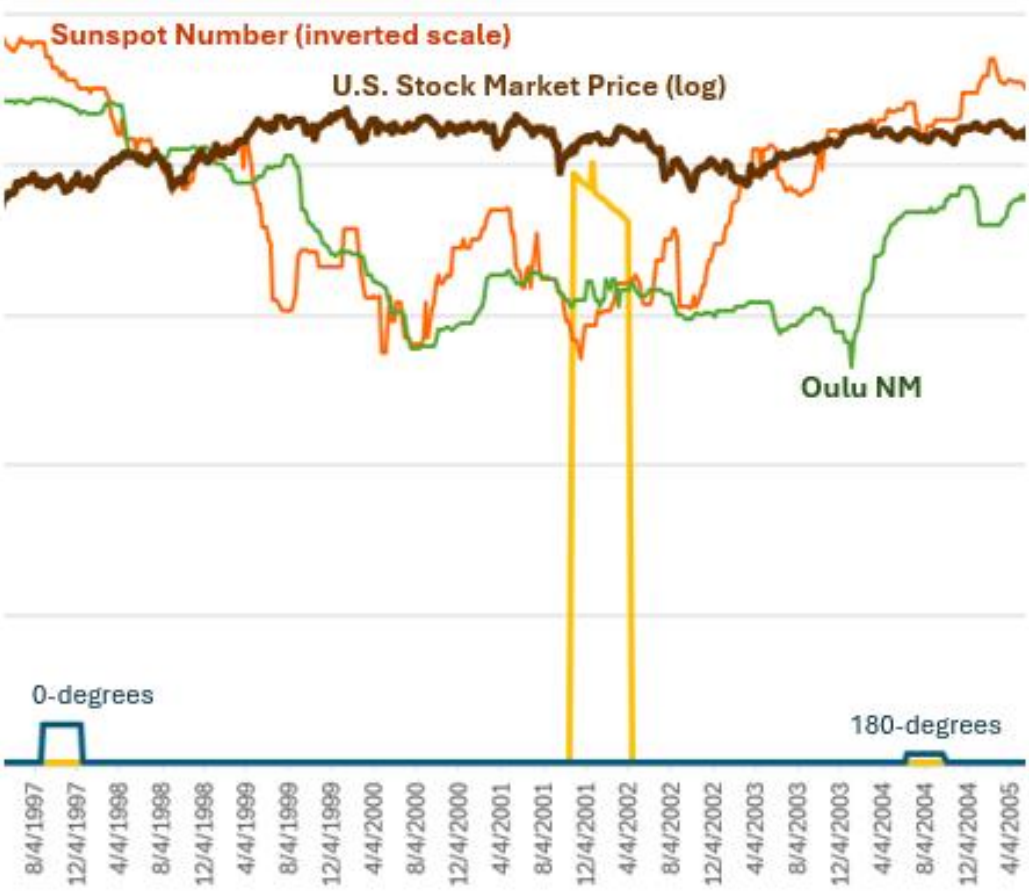

Figure R-5. U.S. Stock market price shown as the brown line (log scale) before and after the 2001 Anxiety-Free Period. A 90-degree configuration begins when the yellow line moves higher from its base line and ends when the line moves back to the base line. The orange line is the sunspot count number (normalized on an inverted scale). The green line is the Oulu NM readings (corrected for air pressure). The 0-degree configuration between the Inner and Outer Orbital Centers is indicated by the shorter of the two blue-line columns. The 180-degree configuration is indicated by the taller of the two columns. Sources: CPM Investing LLC calculations using data from NASA, Oulu NM, MeasuringWorth, and public market sources. 'U.S. stocks' and 'U.S. stock market' refer to the DJIA, S&P 500, or related ETFs depending on the period.

2006 Anxiety-Free Period

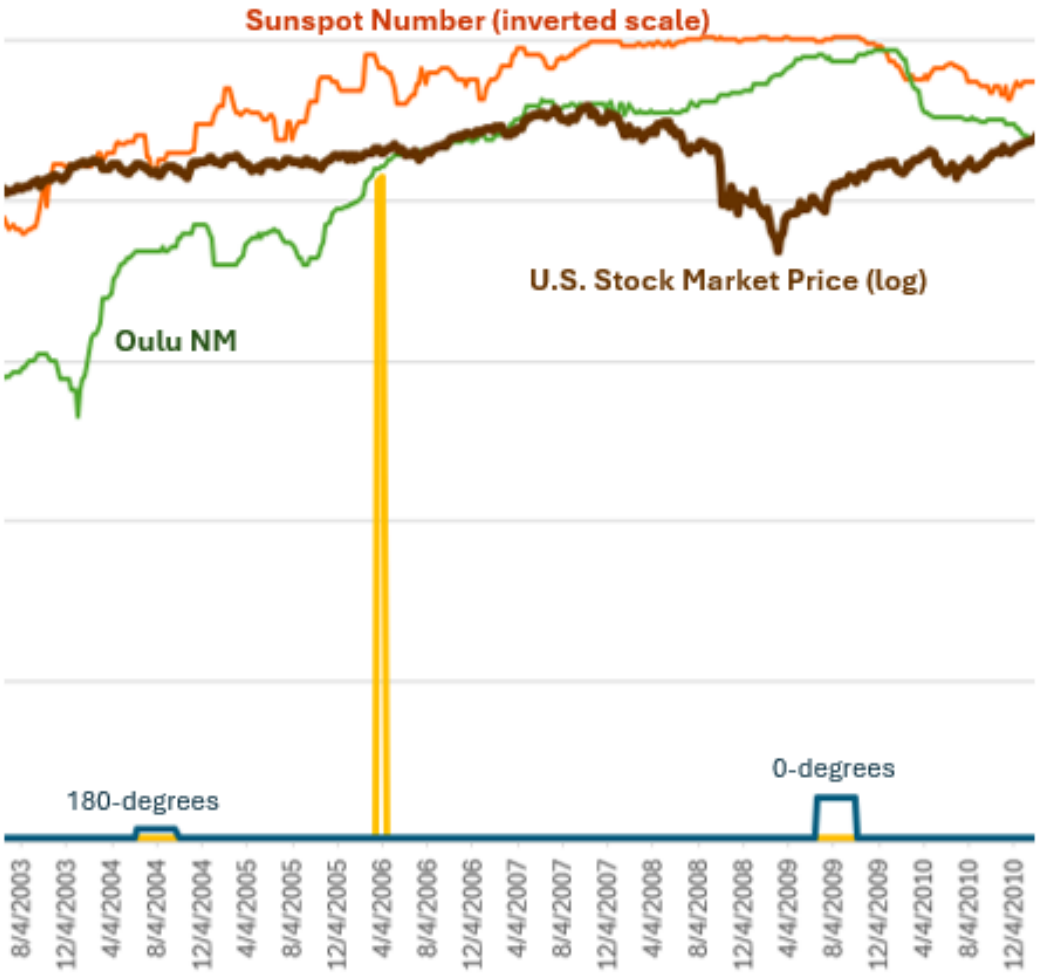

Figure R-6. U.S. Stock market price shown as the brown line (log scale) before and after the 2006 Anxiety-Free Period. A 90-degree configuration begins when the yellow line moves higher from its base line and ends when the line moves back to the base line. The orange line is the sunspot count number (normalized on an inverted scale). The green line is the Oulu NM readings (corrected for air pressure). The 0-degree configuration between the Inner and Outer Orbital Centers is indicated by the shorter of the two blue-line columns. The 180-degree configuration is indicated by the taller of the two columns. Sources: CPM Investing LLC calculations using data from NASA, Oulu NM, MeasuringWorth, and public market sources. 'U.S. stocks' and 'U.S. stock market' refer to the DJIA, S&P 500, or related ETFs depending on the period.

The AFP occurs at approximately the same time as a peak in the sunspot series.

2012 Anxiety-Free Period

Figure R-7. U.S. Stock market price shown as the brown line (log scale) before and after the 2012 Anxiety-Free Period. A 90-degree configuration begins when the yellow line moves higher from its base line and ends when the line moves back to the base line. The orange line is the sunspot count number (normalized on an inverted scale). The green line is the Oulu NM readings (corrected for air pressure). The 0-degree configuration between the Inner and Outer Orbital Centers is indicated by the shorter of the two blue-line columns. The 180-degree configuration is indicated by the taller of the two columns. Sources: CPM Investing LLC calculations using data from NASA, Oulu NM, MeasuringWorth, and public market sources. 'U.S. stocks' and 'U.S. stock market' refer to the DJIA, S&P 500, or related ETFs depending on the period.

The short-term high point in the Sunspot series occurs just before the highest point in the AFP.

2017 Anxiety-Free Period

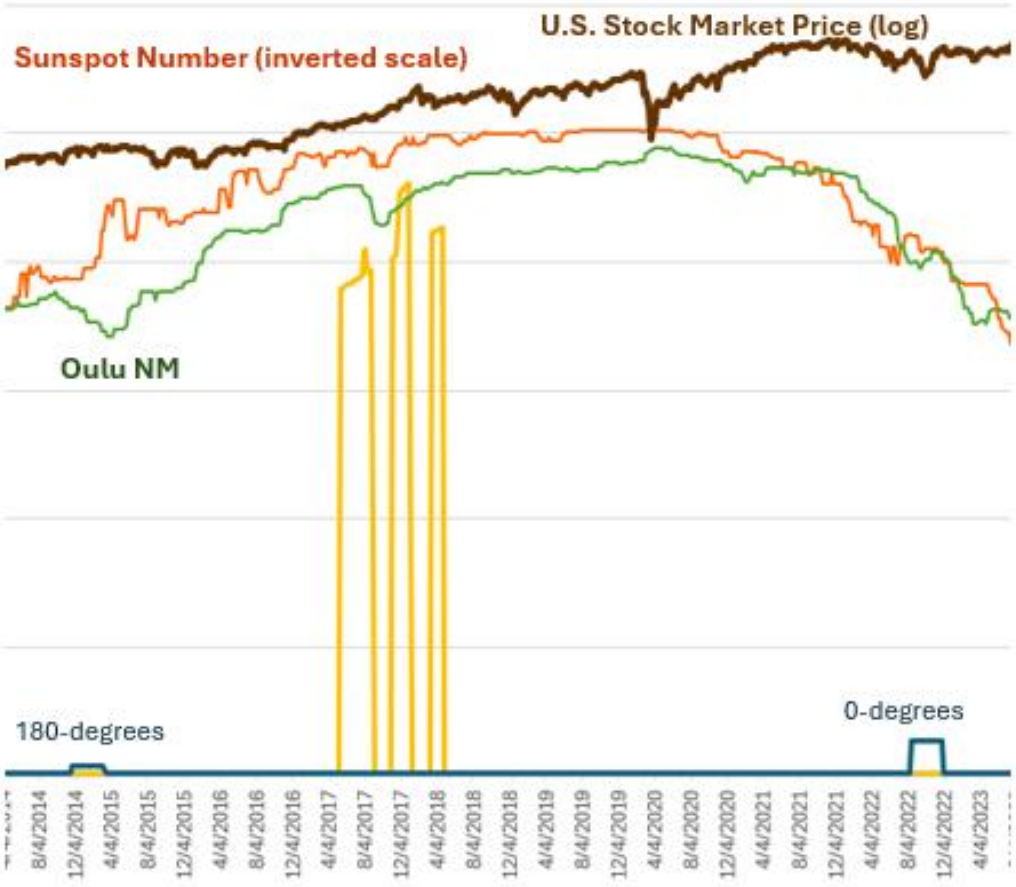

Figure R-8. U.S. Stock market price shown as the brown line (log scale) before and after the 2017 Anxiety-Free Period. A 90-degree configuration begins when the yellow line moves higher from its base line and ends when the line moves back to the base line. The orange line is the sunspot count number (normalized on an inverted scale). The green line is the Oulu NM readings (corrected for air pressure). The 0-degree configuration between the Inner and Outer Orbital Centers is indicated by the shorter of the two blue-line columns. The 180-degree configuration is indicated by the taller of the two columns. Sources: CPM Investing LLC calculations using data from NASA, Oulu NM, MeasuringWorth, and public market sources. 'U.S. stocks' and 'U.S. stock market' refer to the DJIA, S&P 500, or related ETFs depending on the period.

The sunspot and Oulu series dip between the first two columns of the AFP.

Appendix S – Decision Style Biases of Investment Professionals

Investment professionals tend to develop and use investment processes that have core processes that fit their own decision-making styles. The most successful in terms of investment performance and commercial success augment these core processes with disciplines and practices that accentuate the strengths and compensate for the weaknesses inherent in that core process. In the institutional investment industry, there are innumerable ways to generate positive return, and we see a wide range of processes implemented by people with a range of decision styles, but that range is centered on the Analytical decision style.

Over many years, we collected 831 profiles of investment professionals worldwide that are directly involved in managing several trillions of dollars. This dataset, while biased toward U.S. stock market investing, also reflects global decision-making practices.

Decision-Style Scores

All Investment Professionals				
n=831	Directive	Analytical	Conceptual	Behavioral
Average	71	99	78	52
Std Dev	12.9	14.1	13.6	13.4
General US Population				
Average	75	90	80	55
Std Dev	15	15	15	15

Figure S-1. Decision style biases of investment professionals compared to the general U.S. population. This table shows the average scores and standard deviations for Directive, Analytical, Conceptual, and Behavioral decision styles for 831 investment professionals and for the general U.S. population. Source: CPM Investing LLC.

These results confirm the distinctive analytical bias of professional investors summarized in the main body (see Study F).

Thus, people who are successful investors use a process that fits their style of decision making. Two observations stand out. First, professional investors generally do not operate successfully long term in processes that conflict with their decision-style biases. It is not simply that they are unwilling to change; they find it extremely difficult to succeed outside their natural style. For example, individuals with a Conceptual bias often struggle to be effective long term in a Directive framework, and vice versa.

Second, individuals tend to maintain consistent decision-style profiles across different roles and firms. An individual's scores may shift over time, but the relative ranking of styles remains stable. For instance, a person with a primary Directive style and a secondary Analytical style usually retains that ranking years later.

These observations suggest that decision-style biases are largely hard-wired. People cannot make major changes in their styles, nor would they likely be satisfied trying to do so.

Below are generalizations of the types of processes developed and operated by Analytical, Conceptual and Directive investment professionals. They are developed based on the descriptions of the strategies provided by those included in our assessments, and on our experience working with many investment teams.

Typical Investment Processes Used by Analytical Individuals and Teams

According to our research, the typical Analytical investment strategy seeks to produce strong investment gains by doing deeper research on companies to find attractive conditions that others miss and to assemble portfolios of many stock holdings that reflect their research. Analytical individuals prefer to make decisions based on objective data and analysis as opposed to the views of others. Analytical decision-makers tend to reason deductively, relying on structured logic and data to draw conclusions from known principles.

They perform well when the complex relationships they have researched remain stable, which allows them time to do research, discover attractive investment opportunities, and implement those ideas in portfolios. They tend to embed their insights into repeatable processes for researching, aggregating information, and implementing decisions. They adhere to these disciplines and are reluctant to change them. They tend to be most concerned with analytical rigor and price changes and place a secondary emphasis on how well a potential investment fits a broader theme.

Analytical investors can become complacent after building their processes. They tend not to lose sleep wondering if all the elements will come together because immense effort has been devoted to engineering those processes. The vulnerability of highly analytical investment teams is that the complex relationships they seek to exploit can change and render their processes less effective. When instability is moderate and reasonably stationary, learned relationships and factor models keep their edge; when it breaks from that range, processes need recalibration.

Typical Investment Processes Used by Conceptual Individuals and Teams

Investment processes used by Conceptual individuals tend to focus on a few high-impact variables to fully understand and assess the broad investment environment. Conceptual individuals tend to have the ability to see and understand new variables and new relationships. They use the insights they develop about key dynamics to guide their analysis and decision making. Conceptual decision-makers are intuitive, often synthesizing abstract ideas and patterns to envision creative, long-term solutions.

They lose sleep wondering whether there are factors missing from their consideration. They can handle ambiguity but can become bored and then overwhelmed with matters that are complex and tedious.

Among the investment managers with a strong bias to the Conceptual style, many use the terms, “macro,” “macroeconomic research,” or “global stock portfolios” in the descriptions of their roles. At senior levels, conceptual individuals tend to have a relatively big impact on the performance of the portfolios compared to other investment individuals on the team. Of the three biases described here, this one places the highest emphasis on favoring stocks because of an investment theme.

Typical Investment Processes Used by Directive Individuals and Teams

Directive individuals acknowledge the investment world is complex and select a narrow slice of that world to exploit. Directive decision-makers operate instinctively, drawing on experience and gut-level judgment to act quickly and decisively. They review many possible opportunities and look for those that fit a pattern they have determined to be profitable. The more opportunities they review in a day, the better. Their investment bets tend to have short payoff horizons.

Among the investment managers that score high in the Directive style, we see the term “technical investing” and “small cap (company) growth.” For both these strategies, the number of investment

opportunities is large. Technical investors emphasize finding stocks that fit established price patterns that indicate attractive times to buy and sell.

For small cap strategies, volatile prices and more extreme fundamentals of individual small companies means that stocks move in and out of the criteria for "buys" and "sells" quickly. Of the three biases, Directive investors place the highest importance on a stock's price meeting certain specific objective criteria.

If we assume that all individuals have approximately the same level of attention that can be allocated to gathering information and making decisions, Conceptual individuals favor developing a thorough understanding of broad qualitative variables and relationships, making a few high-impact bets, and devoting less attention to deep objective research. Analytical individuals favor thorough research and use systems and objective processes to expand the breadth of possible investment opportunities they consider. Directive individuals favor breadth of coverage using focused and objective selection criteria and give less attention to research depth.

Stability of Global Electromagnetic Standing Wave Modes

Frequency stability is a focus of this analysis. Figure S-2 below shows the stability of the global electromagnetic standing wave modes, the change in stability over time as a percentage of stability, along with the Decision style we believe is most closely related.

A	B	C
Electromagnetic Standing Wave Modes	**Stability (lower means more stable)**	**Change in Stability Over Time**
1	1.8 Hz	45%
2 and 3	4.7 Hz	25%
4 and 5	31.3 Hz	20%

Figure S-2. Table showing electromagnetic standing wave modes and their stability from 2015 through 2022 along with the change in stability over that period. Sources: CPM Investing LLC calculations using data from the British Geological Survey.

If we look at how stability changes over time (column C) and the magnitude of shifts in stability compared to the background level of stability (column B), people with a Conceptual style may be more comfortable with a generally stable environment on a short-term bases (column B) but can tolerate larger relative shifts over time. Operating in this type of situation may afford them the opportunity to focus on understanding the major drivers of future change and making bigger bets.

By contrast, people with a Directive style may have an affinity for more volatile environment (column B) and making smaller investment bets. Perhaps finding success being more responsive to numerous changes. People with the Analytical style mentally engage with a more moderate level of stability and a wider range of bets. With these observations, we find intriguing the role of bone marrow and its possible role in entrainment.

Appendix T – Four Phases of the Mega Sentiment Cycle

The differences among the four orbital geometry phases occur in the absence of any systematic variation in underlying economic growth. Weekly GDP growth averages are tightly clustered across all four segments, ranging from 0.00112 to 0.00132, and exhibit no statistically significant difference when compared using ANOVA ($p = 0.99$). This decoupling of market returns from economic fundamentals implies that segment behavior is not caused by accurate expectations of future GDP growth.

Study G: Valuations and GDP Growth by Phase
To test whether valuation levels vary systematically across the four phases of the orbital geometry cycle, we analyzed weekly S&P 500 price-to-earnings (P/E) ratios for the period covered by the phase dataset. The sample sizes, means, and standard deviations for each phase are:

- Phase 1: n = 1,097 weeks, mean = 17.4, SD = 4.9
- Phase 2: n = 636 weeks, mean = 13.8, SD = 4.7
- Phase 3: n = 610 weeks, mean = 15.3, SD = 4.9
- Phase 4: n = 1,120 weeks, mean = 15.8, SD = 5.4

A one-way ANOVA using these summary statistics shows highly significant differences among the four phases ($F = 74.19$, $p < 0.001$), indicating that mean P/E ratios are not equal across phases.

Pairwise comparisons (two-sample t-tests using pooled standard errors) show that all phase pairs differ significantly at $p < 0.001$, except for Phase 3 vs Phase 4, which is not significant at the 5% level:

Phase Pair	Mean Diff	t-stat	p-value	Significant
1 vs 2	3.6	15.3	< 0.001	Yes
1 vs 3	2.2	8.8	< 0.001	Yes
1 vs 4	1.7	7.7	< 0.001	Yes
2 vs 3	-1.5	-5.4	< 0.001	Yes
2 vs 4	-2.0	-7.9	< 0.001	Yes
3 vs 4	-0.5	-1.9	0.055	No

Figure T-1. Table showing the four phases of the Mega Sentiment Cycle and the significance of the differences between their S&P 500 P/E ratios. Sources: CPM Investing LLC calculations using data from Multpl.com.

Autocorrelation Check
Weekly P/E ratios exhibit high persistence, with lag-1 autocorrelations ranging from 0.986 to 0.995 across phases. This reduces the effective number of independent observations to between approximately 2.6 and 7.6 per phase. While adjusting for this persistence reduces nominal significance levels, the differences remain statistically meaningful and do not alter the conclusion that valuations vary substantially across phases.

GDP Growth Analysis
We also tested whether average GDP growth rates differ meaningfully across the four phases. Using data from April 4, 1947 onward, average weekly GDP growth rates (Nominal and Real) were:

Phase	GDP-Nominal	GDP-Real
1	0.13%	0.08%
2	0.11%	0.06%
3	0.13%	0.08%
4	0.11%	0.04%

Figure T-2. Table showing the four phases of the Mega Sentiment Cycle and the GDP-Nominal and GDP-Real weekly growth rates. Source: CPM Investing LLC calculations using data from U.S. Bureau of Economic Analysis.

Differences in GDP growth rates across phases are not statistically significant (ANOVA $p \gg 0.05$), indicating that the observed variation in P/E ratios is not explained by underlying differences in economic growth.

Interpretation

The pattern of P/E variation is consistent with the hypothesis that investor sentiment, rather than changes in economic fundamentals, drives valuation expansion and contraction across the cycle. Phase 1 exhibits the highest average valuation, Phase 2 the lowest, with Phases 3 and 4 occupying intermediate positions. The lack of significant difference between Phases 3 and 4 suggests that valuation pressures may stabilize in the latter half of the cycle. Taken together, the evidence supports the hypothesis that orbital geometry affects phases of investor sentiment. These shifts in sentiment influence pricing behavior and valuation expectations, leading to observable patterns in return outcomes that are not explained by economic variables alone.

Appendix U –AFP and M-Spike Dates 2017 to 2027

M-Spike Levels are relative to a baseline of zero.

Date Friday	90-Degree Configuration	M-Spike Level
5/12/2017	90-Degree	
5/19/2017	90-Degree	
5/26/2017	90-Degree	
6/2/2017	90-Degree	
6/9/2017	90-Degree	
6/16/2017	90-Degree	
6/23/2017	90-Degree	
6/30/2017	90-Degree	
7/7/2017	90-Degree	
7/14/2017	90-Degree	
7/21/2017	90-Degree	
7/28/2017	90-Degree	
8/4/2017	90-Degree	
8/11/2017	90-Degree	
8/18/2017	90-Degree	
8/25/2017	90-Degree	
9/1/2017		
9/8/2017		
9/15/2017		
9/22/2017		
9/29/2017		
10/6/2017		
10/13/2017		
10/20/2017		
10/27/2017		
11/3/2017	90-Degree	
11/10/2017	90-Degree	
11/17/2017	90-Degree	
11/24/2017	90-Degree	
12/1/2017	90-Degree	
12/8/2017	90-Degree	-0.36
12/15/2017	90-Degree	-0.36
12/22/2017	90-Degree	0.22
12/29/2017	90-Degree	0.22
1/5/2018		0.15
1/12/2018		
1/19/2018		
1/26/2018		
2/2/2018		
2/9/2018		
2/16/2018		
2/23/2018		
3/2/2018		
3/9/2018		
3/16/2018	90-Degree	
3/23/2018	90-Degree	
3/30/2018	90-Degree	
4/6/2018	90-Degree	
4/13/2018	90-Degree	
4/20/2018	90-Degree	
4/27/2018		
5/4/2018		
5/11/2018		
5/18/2018		
5/25/2018		
6/1/2018		
6/8/2018		
6/15/2018		
6/22/2018		
6/29/2018		
7/6/2018		
7/13/2018		
7/20/2018		
7/27/2018		
8/3/2018		
8/10/2018		
8/17/2018		
8/24/2018		
8/31/2018		
9/7/2018		
9/14/2018		
9/21/2018		
9/28/2018		
10/5/2018		
10/12/2018		
10/19/2018		
10/26/2018		
11/2/2018		
11/9/2018		
11/16/2018		
11/23/2018		
11/30/2018		
12/7/2018		

Date Friday	90-Degree Configuration	M-Spike Level
12/14/2018		0.17
12/21/2018		0.25
12/28/2018		-0.42
1/4/2019		-0.42
1/11/2019		-0.43
1/18/2019		0.26
1/25/2019		
2/1/2019		
2/8/2019		
2/15/2019		
2/22/2019		
3/1/2019		
3/8/2019		
3/15/2019		
3/22/2019		
3/29/2019		
4/5/2019		
4/12/2019		
4/19/2019		
4/26/2019		
5/3/2019		
5/10/2019		
5/17/2019		
5/24/2019		
5/31/2019		
6/7/2019		
6/14/2019		
6/21/2019		
6/28/2019		
7/5/2019		
7/12/2019		
7/19/2019		
7/26/2019		
8/2/2019		
8/9/2019		
8/16/2019		
8/23/2019		
8/30/2019		
9/6/2019		
9/13/2019		
9/20/2019		
9/27/2019		
10/4/2019		
10/11/2019		
10/18/2019		
10/25/2019		
11/1/2019		
11/8/2019		
11/15/2019		
11/22/2019		
11/29/2019		
12/6/2019		
12/13/2019		
12/20/2019		0.20
12/27/2019		0.20
1/3/2020		0.20
1/10/2020		0.30
1/17/2020		0.30
1/24/2020		-0.50
1/31/2020		-0.50
2/7/2020		0.30
2/14/2020		0.30
2/21/2020		0.20
2/28/2020		
3/6/2020		
3/13/2020		
3/20/2020		
3/27/2020		
4/3/2020		
4/10/2020		
4/17/2020		
4/24/2020		
5/1/2020		
5/8/2020		
5/15/2020		
5/22/2020		
5/29/2020		
6/5/2020		
6/12/2020		
6/19/2020		
6/26/2020		
7/3/2020		
7/10/2020		

Date Friday	90-Degree Configuration	M-Spike Level
7/17/2020		
7/24/2020		
7/31/2020		
8/7/2020		
8/14/2020		
8/21/2020		
8/28/2020		
9/4/2020		
9/11/2020		
9/18/2020		
9/25/2020		
10/2/2020		
10/9/2020		
10/16/2020		
10/23/2020		
10/30/2020		
11/6/2020		
11/13/2020		
11/20/2020		
11/27/2020		
12/4/2020		
12/11/2020		
12/18/2020		
12/25/2020		
1/1/2021		0.22
1/8/2021		0.22
1/15/2021		0.22
1/22/2021		0.22
1/29/2021		0.33
2/5/2021		0.33
2/12/2021		-0.56
2/19/2021		-0.56
2/26/2021		0.34
3/5/2021		0.34
3/12/2021		0.23
3/19/2021		0.23
3/26/2021		0.23
4/2/2021		0.23
4/9/2021		
4/16/2021		
4/23/2021		
4/30/2021		
5/7/2021		
5/14/2021		
5/21/2021		
5/28/2021		
6/4/2021		
6/11/2021		
6/18/2021		
6/25/2021		
7/2/2021		
7/9/2021		
7/16/2021		
7/23/2021		
7/30/2021		
8/6/2021		
8/13/2021		
8/20/2021		
8/27/2021		
9/3/2021		
9/10/2021		
9/17/2021		
9/24/2021		
10/1/2021		
10/8/2021		
10/15/2021		
10/22/2021		
10/29/2021		
11/5/2021		
11/12/2021		
11/19/2021		
11/26/2021		
12/3/2021		
12/10/2021		
12/17/2021		
12/24/2021		
12/31/2021		
1/7/2022		
1/14/2022		0.23
1/21/2022		0.23
1/28/2022		0.23
2/4/2022		0.23
2/11/2022		0.23

Date Friday	90-Degree Configuration	M-Spike Level
2/18/2022		0.34
2/25/2022		0.34
3/4/2022		-0.57
3/11/2022		-0.57
3/18/2022		0.34
3/25/2022		0.35
4/1/2022		0.23
4/8/2022		0.23
4/15/2022		0.23
4/22/2022		0.23
4/29/2022		
5/6/2022		
5/13/2022		
5/20/2022		
5/27/2022		
6/3/2022		
6/10/2022		
6/17/2022		
6/24/2022		
7/1/2022		
7/8/2022		
7/15/2022		
7/22/2022		
7/29/2022		
8/5/2022		
8/12/2022		
8/19/2022		
8/26/2022		
9/2/2022		
9/9/2022		
9/16/2022		
9/23/2022		
9/30/2022		
10/7/2022		
10/14/2022		
10/21/2022		
10/28/2022		
11/4/2022		
11/11/2022		
11/18/2022		
11/25/2022		
12/2/2022		
12/9/2022		
12/16/2022		
12/23/2022		
12/30/2022		
1/6/2023		
1/13/2023		
1/20/2023		
1/27/2023		
2/3/2023		
2/10/2023		0.24
2/17/2023		0.24
2/24/2023		0.24
3/3/2023		0.23
3/10/2023		0.23
3/17/2023		0.35
3/24/2023		-0.58
3/31/2023		-0.58
4/7/2023		-0.57
4/14/2023		0.34
4/21/2023		0.23
4/28/2023		0.23
5/5/2023		0.23
5/12/2023		0.23
5/19/2023		0.23
5/26/2023		
6/2/2023		
6/9/2023		
6/16/2023		
6/23/2023		
6/30/2023		
7/7/2023		
7/14/2023		
7/21/2023		
7/28/2023		
8/4/2023		
8/11/2023		
8/18/2023		
8/25/2023		
9/1/2023		
9/8/2023		
9/15/2023		

Date Friday	90-Degree Configuration	M-Spike Level
9/22/2023		
9/29/2023		
10/6/2023		
10/13/2023		
10/20/2023		
10/27/2023		
11/3/2023		
11/10/2023		
11/17/2023		
11/24/2023		
12/1/2023		
12/8/2023		
12/15/2023		
12/22/2023		
12/29/2023		
1/5/2024		
1/12/2024		
1/19/2024		
1/26/2024		
2/2/2024		
2/9/2024		
2/16/2024		
2/23/2024		
3/1/2024		
3/8/2024		0.22
3/15/2024		0.22
3/22/2024		0.22
3/29/2024		0.22
4/5/2024		0.34
4/12/2024		-0.56
4/19/2024		-0.56
4/26/2024		-0.56
5/3/2024		0.34
5/10/2024		0.22
5/17/2024		0.22
5/24/2024		0.22
5/31/2024		0.22
6/7/2024		
6/14/2024		
6/21/2024		
6/28/2024		
7/5/2024		
7/12/2024		
7/19/2024		
7/26/2024		
8/2/2024		
8/9/2024		
8/16/2024		
8/23/2024		
8/30/2024		
9/6/2024		
9/13/2024		
9/20/2024		
9/27/2024		
10/4/2024		
10/11/2024		
10/18/2024		
10/25/2024		
11/1/2024		
11/8/2024		
11/15/2024		
11/22/2024		
11/29/2024		
12/6/2024		
12/13/2024		
12/20/2024		
12/27/2024		
1/3/2025		
1/10/2025		
1/17/2025		
1/24/2025		
1/31/2025		
2/7/2025		
2/14/2025		
2/21/2025		
2/28/2025		
3/7/2025		
3/14/2025		
3/21/2025		
3/28/2025		
4/4/2025		
4/11/2025		
4/18/2025		

Date Friday	90-Degree Configuration	M-Spike Level
4/25/2025		0.30
5/2/2025		-0.50
5/9/2025		-0.50
5/16/2025		-0.50
5/23/2025		0.30
5/30/2025		0.20
6/6/2025		0.20
6/13/2025		
6/20/2025		
6/27/2025		
7/4/2025		
7/11/2025		
7/18/2025		
7/25/2025		
8/1/2025		
8/8/2025		
8/15/2025		
8/22/2025		
8/29/2025		
9/5/2025		
9/12/2025		
9/19/2025		
9/26/2025		
10/3/2025		
10/10/2025		
10/17/2025		
10/24/2025		
10/31/2025		
11/7/2025		
11/14/2025		
11/21/2025		
11/28/2025		
12/5/2025		
12/12/2025		
12/19/2025		
12/26/2025		
1/2/2026		
1/9/2026		
1/16/2026		
1/23/2026		
1/30/2026		
2/6/2026		
2/13/2026		
2/20/2026		
2/27/2026		
3/6/2026		
3/13/2026		
3/20/2026		
3/27/2026		
4/3/2026		
4/10/2026		
4/17/2026		
4/24/2026	90-Degree	
5/1/2026	90-Degree	
5/8/2026	90-Degree	
5/15/2026	90-Degree	
5/22/2026	90-Degree	
5/29/2026		-0.44
6/5/2026		-0.43
6/12/2026		0.26
6/19/2026		0.26
6/26/2026		
7/3/2026		
7/10/2026		
7/17/2026		
7/24/2026		
7/31/2026		
8/7/2026	90-Degree	
8/14/2026	90-Degree	
8/21/2026	90-Degree	
8/28/2026	90-Degree	
9/4/2026	90-Degree	
9/11/2026	90-Degree	
9/18/2026	90-Degree	
9/25/2026		
10/2/2026		
10/9/2026		
10/16/2026		
10/23/2026		
10/30/2026		
11/6/2026		
11/13/2026		
11/20/2026	90-Degree	
11/27/2026	90-Degree	
12/4/2026	90-Degree	
12/11/2026		
12/18/2026		
12/25/2026		

Appendix V – Data Sources

The datasets used in this report span solar, geomagnetic, financial, and cosmic ray domains. They were selected for their continuity, scientific credibility, and relevance to understanding heliospheric conditions and investor sentiment.

Solar and geomagnetic indices

GFZ German Research Centre for Geosciences. Kp Index and Ap Index data. Potsdam: GFZ; 2025. https://www.gfz-potsdam.de/en/kp-index.

British Geological Survey. Geomagnetic observatory data (Eskdalemuir, Scotland). Nottingham (UK): BGS Geomagnetism Team; 2025. https://www.bgs.ac.uk/data/service/geophysics/geomagnetism/observatory/.

Royal Observatory of Belgium. International Sunspot Number (Version 2). Brussels: SILSO, World Data Center Sunspot Index and Long-term Solar Observations; 2025. https://www.sidc.be/silso/datafiles.

Natural Resources Canada. Penticton 10.7 cm solar radio flux data. Ottawa: Canadian Space Weather Forecast Centre; 2025. https://spaceweather.gc.ca/forecast-prevision/solar-solaire/solarflux/sx-5-en.php.

Heliospheric particle data

NASA. OMNIWeb database. Greenbelt (MD): NASA Goddard Space Flight Center; 2024. https://omniweb.gsfc.nasa.gov.

Cosmic ray flux

Oulu University. Cosmic Ray Station, Sodankylä Geophysical Observatory, University of Oulu, Finland; 2025. https://cosmicrays.oulu.fi.

S&P 500 valuation data

Multpl (Multpl.com). https://www.multpl.com/.
Note: Multpl compiles historical data from S&P Dow Jones Indices and other public sources.

Financial market and economic data

U.S. Bureau of Economic Analysis. National Income and Product Accounts. Washington (DC): BEA; 2025. https://www.bea.gov/data/economy/national;
MeasuringWorth. Dow Jones Industrial Average, daily, monthly, and annual data, 1896–present; 2025. https://www.measuringworth.com/datasets/DJA/

For the purposes of this paper, “U.S. stocks” and “U.S. stock market” refer to the DJIA, the S&P 500, or related ETFs depending on the time period analyzed. Figures show normalized or transformed representations of performance; raw index levels are not reproduced. All financial data are used solely for research purposes and are not redistributed commercially.